SUPERHUMPS IN AM CANUM VENATICORUM STARS

MARGARET HARROP-ALLIN

Department of Astronomy
University of Cape Town
South Africa

A dissertation submitted to the University of Cape Town in partial fulfilment of the requirements for the degree of Master of Science

March 1996

Abstract

The AM Canum Venaticorum stars are an inhomogeneous group of six stars that are characterised by the absence of hydrogen lines in their spectra. The structure of these stars has been the subject of much debate, and single star models were considered as recently as 1992. The prevailing opinion, however, is that the AM CVn stars are semi-detached binaries which consist of a low-mass, degenerate helium secondary which is transferring mass via an accretion disc to a DB white dwarf. Under this model, the orbital periods of the AM CVn systems are in the range 1000 – 3000 s. The AM CVn systems show many of the accretion disc-related phenomena that are observed in non-magnetic (hydrogen-rich) cataclysmic variables.

Five of the six systems show low-amplitude optical oscillations with periods between 500 and 2000 s. The oscillations have a complex and variable harmonic structure. Since they are consistent with the predictions of the double-degenerate binary model, the oscillations were assumed to correspond to the orbital period in each system. However, the fundamental periods and their harmonics are unstable, showing amplitude and phase drifts on a time scale of weeks to months. The instability of the photometric periods has therefore been an obstacle to accepting that the AM CVn stars are binary systems. An alternative explanation was proposed by O'Donoghue & Kilkenny (1989): the photometric variations in the AM CVn stars are not their orbital periods, but are caused by the same mechanism that produces superhumps in SU UMa dwarf novae. Superhumps are optical variations observed during the superoutbursts of SU UMa stars with periods a few percent in excess of the orbital period. The superhumps usually disappear as the star declines to quiescence after a superoutburst. Superhumps are thought to be the result of periodic enhancements of tidal dissipation in the outer regions of the accretion disc. In addition

to the superhumps in SU UMa dwarf novae, *permanent* superhumps have been observed in other hydrogen-rich cataclysmic variables.

The aim of this dissertation is to present new photometric data and to explore the period structure of four of the six known AM CVn stars to see whether the observations are consistent with a superhump interpretation. The aim is also to draw comparisons between the AM CVn stars and examples of hydrogen-rich cataclysmic variables in which superhumps have been observed, and in this way to strengthen the evidence that similar mechanisms are operating in the hydrogen-rich superhumpers and the multiperiodic AM CVn stars.

Chapter 1 places the AM CVn systems in context among interacting binaries in general and the cataclysmic variables in particular, and reviews their observational properties and the competing models that have been advanced to explain their behaviour. A summary of the known hydrogen-rich superhumping systems is given, and the evidence suggesting that the photometric variations in AM CVn stars are superhumps is presented. Chapter 2 outlines the techniques used in acquiring and reducing CCD photometry. The data acquired specifically for this dissertation was obtained using the UCT Wright high speed CCD photometer, a frame transfer device capable of time resolutions of 10 s with virtually no dead time. A description of the methods used to reduce the CCD frames is given. Chapter 3 presents data of two hydrogen-rich systems which display superhumps: the dwarf nova TY PsA and the nova-like variable V442 Oph. Spectroscopic observations of TY PsA in superoutburst show that there are compelling similarities between the spectra of SU UMa stars in superoutburst and AM CVn star spectra. Photometry of V442 Oph is presented in which the principal photometric period differs from the orbital period, and changes on a time scale of years. Chapters 4 – 7 present and discuss high speed photometry of the AM CVn stars V803 Cen, GP Com, CP Eri and EC 15330-1403 in the context of the superhump model. The dissertation concludes with a Discussion, in which the results of the work are summarised, suggestions for future work are made, and a model is presented which may account for some of the more detailed aspects of the period structure observed in AM CVn.

Contents

List of Figures

List of Tables

Chapter 1

Introduction

1.1 Cataclysmic Variables and the AM CVn stars

1.1.1 Close binary stars: why bother?

It is estimated that at least two-thirds of all stars in the Galaxy occur in multiple systems (e.g. Povenda, Allen & Parrao 1982). The members of some multiple systems are very far apart and may take hundreds or thousands of years to complete a revolution about their common centre of mass. The stars interact only in the sense that they are gravitationally bound, and the evolutionary path of each component star is not affected by the other members of the multiple system. In other systems, the stellar components are sufficiently close that the evolutionary history of each of the components departs appreciably from the evolution of single stars. It is estimated that almost half of the Galactic stellar population occurs in such close binary systems (Sahade & Wood 1978).

Binary stars are our main source of knowledge of the physical parameters of stars. Specifically, *eclipsing* binaries are the only objects in the sky that can provide us with direct information of stellar masses and radii. The study of visual binaries and the determination of their component masses and radii was one of the main fields of astronomical research even before the importance of a star's mass to its evolutionary history was recognised. However, the parameters obtained for the members of binary stars apply to isolated stars only if the binary system is observed before any evolutionary interaction has started. The

evolution of the members of close binary systems are profoundly affected by the other system members. Close binary systems present intriguing problems of their own, and the variety of fascinating phenomena observed in close binaries, which have no counterparts among the single stars, are of major interest in modern astronomical research.

1.1.2 Cataclysmic variables

The cataclysmic variables (CVs) include dwarf novae, recurrent and classical novae, and the nova-like variables. Their name refers to the outbursts that characterize the class — outbursts which are violent, but not fatal to the star. The idea that CVs are close binary systems was a result of the introduction (in the mid-1940s) of the 1P21 photomultiplier, enabling light curves with a time resolution shorter than a minute to be recorded. A.P. Linnell's 1949 study of UX UMa (which was, at the time, the eclipsing binary with the shortest known orbital period) revealed low-amplitude fickering in the light curve, and a complex and variable eclipse profile. A photometric survey of CVs carried out in the early 1950s by M.F. Walker revealed rapid brightness variations in a number of nova remnants, dwarf novae and nova-like variables. During this survey, Walker discovered eclipses in the classical nova DQ Her (Nova Her 1934), and speculated that *all* novae might be binaries (Walker 1954). Soon after this discovery, a number of other CVs were shown to be binary systems following a programme of spectroscopic observations (e.g. Joy 1954a, Joy 1954b, Crawford & Kraft 1956, Kraft 1962, Kraft 1964, Krzeminski & Kraft 1964). For a comprehensive review of the historical development of the study of CVs, see chapter 1 of Warner (1995a). CVs are now known generally to comprise a white dwarf (the primary) and a late-type dwarf star on or near the main sequence (the secondary) in a close binary configuration. Apart from a few exceptions like GK Per (with an orbital period $P_{orb} \sim 2\,\mathrm{d}$) and the T CrB systems (with giant secondaries and $P_{orb} \sim 200\,\mathrm{d}$) the hydrogen-rich CVs have orbital periods between 1.3 and 10 hours, and the separation of the stellar components is very small ($\lesssim 2\mathrm{R}_{\odot}$).

In a binary system, the gravitational and centrifugal potential of the system can be described using equipotential surfaces. Because the secondaries in CVs are similar to main sequence stars and are therefore centrally condensed, the Roche approximation (Kopal

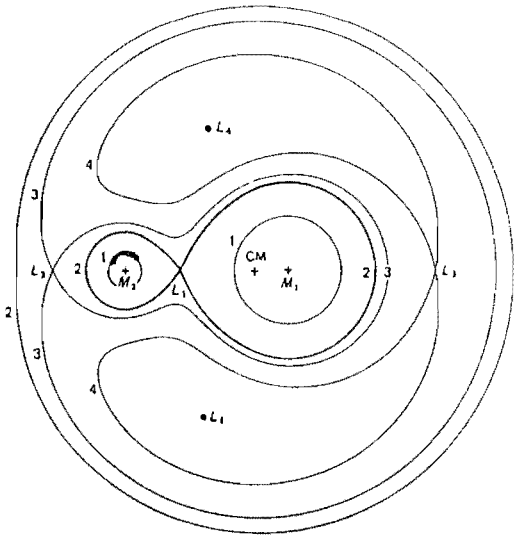

Figure 1.1: Roche equipotentials for a binary with a mass ratio of 0.2, showing the positions of the five Lagrangian points. From Frank, King & Raine (1985).

1959) can be adopted, in which the component stars are treated as point masses. The shapes of the Roche equipotentials are functions only of the mass ratio q of the binary (defined as $q = M_{secondary}/M_{primary}$); the more massive star has the more extensive Roche surface. The scale of the system is determined by a, the separation between the centres of mass of the two stars. Within a certain distance of the centre of each star, the surfaces are closed around that star. Beyond this distance, each equipotential surface encloses both components of the binary. The critical Roche surface is the (unique) double-lobed surface which just encloses both stars. The two lobes are in contact at the inner Lagrangian point (L_1): this is one of the five Lagrangian points (see figure 1.1) where a test particle (one of negligible mass) will remain stationary in the binary frame unless perturbed by an external force. The points L_1, L_2 and L_3 are points of unstable equilibrium.

The concept of a critical Roche surface fixed in the binary frame is only strictly applicable when the binary orbit is circular; an elliptical orbit introduces a time-dependent potential and thus a time-dependent critical surface. However, the effects of tidal interaction on the secondary cause its rotation to synchronize with that of the orbital revolution, and any initial eccentricity of the binary orbit is removed on a time scale much shorter than the lifetime of the CV. Most CVs can be assumed to have circular orbits and synchronously

rotating secondaries (Warner 1995a).

If neither star fills its critical Roche lobe, the system is said to be 'detached'. If both stars fill their respective lobes, the system is a 'contact' binary. When one star fills its Roche lobe, the system is a 'semi-detached' binary. CVs are members of this last category. In CVs, the secondary fills its Roche lobe and matter spills over into the primary's Roche lobe. Because the matter from the secondary possesses angular momentum due to the binary rotation, it cannot accrete directly onto the surface of the white dwarf. If the primary does not have an appreciable magnetic field ($\lesssim 5\,\mathrm{MG}$), the stream flows past the primary and collides with itself at a point well inside the primary's Roche lobe. The relative kinetic energy of the impact is radiated away, and the mass transfer stream forms a ring around the primary which, in the presence of viscous effects, subsequently spreads into a disc. The radius of the initial ring of gas, r_r, is the smallest outer radius any disc can theoretically possess. Approximate expressions for r_r are

$$\frac{r_r}{a} = 0.0859\, q^{-0.426} \tag{1.1}$$

for $0.05 \leq q < 1$, accurate to 1% (Hessman & Hopp 1990), and

$$\frac{r_r}{a} = 0.0883 + 0.04858 \log \frac{1}{q} + 0.11489 \left(\log \frac{1}{q} \right)^2 - 0.020475 \left(\log \frac{1}{q} \right)^3 \tag{1.2}$$

for $0.001 \leq q \leq 0.05$ (Verbunt & Rappaport 1988).

On the other hand, the largest (theoretical) disc radius is determined by tidal limitation. In discs where the radius of the disc approaches the Roche lobe radius of the primary, the outer regions of the disc will be disturbed by the gravitational influence of the secondary. The tidal truncation radius is the radius of the largest single-particle orbit that does not intersect any other orbit. Two-dimensional hydrodynamic modelling shows that the tidal stress and viscous stress become comparable in this region and truncate the disc (Warner 1995a section 2.5.5 and references therein). An approximate expression for the maximum radius of this last non-intersecting orbit, r_{max}, is

$$\frac{r_{max}}{a} = \frac{0.60}{(1+q\ )} \tag{1.3}$$

valid for $0.03 \leq q < 1$ (Warner 1995).

The accretion disc in CVs accounts for a large fraction of the optical and ultraviolet luminosity, particularly during outbursts, when almost all the flux is of accretion origin. Once the accretion disc is fully established, the mass transfer stream will interact with the outer rim of the accretion disc. This creates a shock-heated area (the "bright spot") that can in some cases dominate even the disc emission (at optical wavelengths). It is this bright spot that is the cause of the spectroscopic 'S'-wave, modulated at the orbital period, that is seen in many CV systems (e.g. Honeycutt, Schlegel & Kaitchuck 1987). The ratio of the (visual) bright spot luminosity L_{bs} to that of the disc, L_d, is related to the rate of mass transfer through the disc ($\dot{\mathrm{M}}_d$), the rate of mass transfer from the secondary ($\dot{\mathrm{M}}_2$), and to R_1/r_d , where R_1 is the radius of the primary and r_d is the radius of the accretion disc:

$$\frac{L_{bs}}{L_d} \propto \frac{\dot{\mathrm{M}}_2}{\dot{\mathrm{M}}_d}\frac{R_1}{r_d} \tag{1.4}$$

(for a given binary inclination). Since

$$\frac{R_1}{r_d} \approx \frac{0.40\,q^{2/3}}{{P_{orb}}^{3/2}(\mathrm{h})}, \tag{1.5}$$

the prominence of the bright spot with respect to the disc is expected to increase with decreasing P_{orb} (Warner 1995a chapter 2 and references therein). This is because, for a smaller disc, the material from the mass transfer stream has further to fall into the potential well of the primary before impacting on the outer edge of the disc.

1.1.3 Classication of CVs

The various subclasses of CV are defined as follows (this description follows the definitions of Warner 1995a). Classical novae are novae which have shown only one outburst, with

an amplitude of up to 20 mag. Recurrent novae have more than one nova outburst. The outbursts in novae are probably thermonuclear runaways in the hydrogen-rich material accreted onto the surface of the white dwarf primary. Nova-like variables are an inhomogeneous group of non-eruptive CVs which include pre- and post-novae, stars whose observational baseline is too short for their outbursts to have been observed. The nova-like variables show slow variations in brightness but no outburst behaviour: they are thought to possess steady-state, high $\dot{M}$ discs. Nova-likes also include the VY Scl stars, which show occasional reductions in brightness from an approximately constant maximal magnitude. These reductions in brightness are probably caused by the temporary lowering of $\dot{M}_2$. A mechanism that explains the behaviour of the VY Scl stars is given in Wu, Wickramasinghe and Warner (1995) and Warner (1995d), who explain the brightness variations in the VY Scl stars in terms of irradiation-driven mass transfer in the presence of shielding by the accretion disc. An alternative mechanism, in which the modulation of $\dot{M}_2$ occurs because of star spots on the secondary covering the region around L_1, is proposed by Livio & Pringle (1994).

Dwarf novae (DN) have outbursts of 2 – 5 mag, although a few objects have very large outburst amplitudes of more than 6 mag (see e.g. Howell, Szkody & Cannizzo 1995). At quiescence, dwarf novae show emission line spectra. During the rise to outburst, the emission line spectrum is gradually transformed to an absorption spectrum. The mechanism of the DN outburst was a source of debate for many years, but is now thought to be the result of a thermal instability in the disc which results in an enhancement of the rate of $\dot{M}_d$ (see, for instance, the review by Cannizzo 1993). A number of DN, the SU UMa stars, show (in addition to the normal outbursts) unusually bright and long superoutbursts in which the maximum brightness exceeds the usual outburst maximum by ~ 0.7 mag. The superoutbursts last 5 times as long as the normal outbursts, and occur predominantly in systems with orbital periods less than two hours (i.e. in systems with small mass ratios). A large fraction (0.3 – 0.4 mag) of the extra superoutburst light is modulated as prominent periodic humps — superhumps — with periods a few percent in excess of the orbital period. The current model for superhumps was proposed by Whitehurst (1988), who performed hydrodynamic simulations in which superhumps are produced in systems with $q \lesssim 0.25$ by periodic enancements of tidal dissipation in an eccentric, progradely precessing accretion disc. The precessing disc model was subsequently developed by Osaki

(1989), Hirose & Osaki (1990), Whitehurst & King (1991), Molnar & Kobulnicky (1992), Lubow (1994) and Murray (1996).

The magnetic CVs are those in which the primary has a sufficiently large magnetic field to disrupt, completely or partially, the accretion disc. There are two subclasses of magnetic CV: the polars and the intermediate polars. In polars, the primary's magnetic field is sufficiently strong to prevent a disc from being formed: the mass transfer stream becomes threaded onto the primary's field lines and is channeled towards the magnetic poles. The strength of the magnetic field causes the white dwarf's rotation to synchronize with that of the binary, and the polar rotates essentially as a rigid body. In the intermediate polars the disc is partially disrupted by the primary's magnetic field, but the white dwarf is not in synchronous rotation with the binary.

A small subclass of helium-rich CVs, the six AM CVn stars, are the topic of this dissertation. It is not immediately obvious that the AM CVn stars are CVs, or even that they are binary stars. Sixty years after the discovery of the prototype, there is now some agreement the AM CVn stars are indeed binaries; however, many details of their behaviour remain to be worked out. The AM CVn stars are thought to have orbital periods between 17 and 46 minutes, as will be described later in this chapter. These systems are therefore even more compact and have more extreme mass ratios than their hydrogen-rich counterparts, resulting in a variety of phenomena which are probably caused by the strong tidal interactions between the outer accretion disc and the secondary (as seen in the SU UMa dwarf novae) and by irradiation-driven mass transfer (as observed in the VY Scl stars). A recent review of the AM CVn stars is given by Warner (1995b).

1.1.3.1 Why study CVs?

The usual justification for studying CVs is that they are ready-made laboratories for studying accretion discs. Accretion discs are found in a diverse range of astrophysical settings, and studies of discs in CVs have applications in many other fields of astronomical research. Quasars and active galactic nuclei may be powered by the release of gravitational potential energy as gas is fed into a massive black hole by an accretion disc. Many of the

X-ray sources within our Galaxy are identified with binary stars comprising a neutron star accreting matter, via a disc, from a companion star. Viscous stresses in accretion discs provide a means of removing the angular momentum of material collapsing to form new stars. The Earth may be a remnant of an accretion disc that once surrounded the young Sun. In CVs we find the ideal laboratory to study accretion discs because, in many cases, the optical luminosity of the system is dominated by light from the accretion disc. CVs possess optically thin and optically thick discs, steady-state and non-steady discs, edge-on and face-on discs, and discs with different mass transfer rates.

Another reason why CVs attract such interest is their fascinating behaviour in all parts of the spectrum, and on time scales varying from fractions of a second to millions of years. It is extremely satisfying to observe several orbits of a star (with accompanying flickering, flaring and perhaps eclipse behaviour) during a single observing run. Because of their short orbital periods, CVs lend themselves well to study by exhibiting phenomena within time scales convenient for observation. CVs show interesting properties in almost all parts of the electromagnetic spectrum. The expanding shell in novae and recurrent novae has been resolved in radio waves; radio emission from dwarf novae and magnetic CVs probably originates in the magnetospheres of the secondaries (see e.g. Chanmugam 1987). In the infrared, observations of the cooler components of the system such as the secondary and the faint outer part of the disc can be made (e.g. Dhillon & Marsh 1995). Infrared K-band photometry is used to estimate the distances to CVs: this makes use of the observation that the surface brightness of the cooler M stars is only weakly dependent on the unreddened V-K colour (Bailey 1981, see also Ramseyer 1994). Ellipsoidal variations in IR light curves confirm the highly distorted shape of the secondary, as well as aiding in determining the inclination of the system (e.g. U Gem: Berriman et al. 1983, OY Car: Berriman 1984).

Most of our knowledge of CVs has come from observations in the optical (this is because multi-wavelength astronomical observations are a fairly recent development). The underlying structure of CVs, their rapid variability and their outburst behaviour were all initally studied using optical observations. The radial temperature distribution of CV accretion discs can be determined from broad-band (optical) light curves by treating the eclipse of an accretion disk as a maximum entropy image reconstruction problem. Horne

(1985a,b) has developed techniques for reconstructing the intensity distribution on the face of the disk from broad-band eclipse light curves. The MEM method has also been applied to spectra: Rutten et al. (1993) derived radial flux distributions for each of 110 spectral regions of the disc of UX UMa, allowing spectra to be reconstructed for various disc annuli. The spectral resolution obtained revealed not only the radial dependence of absorption and emission line features with in the disc, but also the spectral details of the bright spot. Another instance of how optical observations have furthered our knowledge of the structure of CVs is in studies of cyclotron harmonics in optical spectra of polars: this provides a means of measuring the strength and geometry of the magnetic field (e.g. Visvanathan & Wickramasinghe 1979, Cropper et al. 1990).

Much of the energy in CVs is radiated shortward of 1200Å (see Warner 1995a chapter 2 and references therein). Observations of CVs in high energy bands has provided a wealth of information about the flux distributions of dwarf novae and novae in outburst (e.g. Gallagher & Code 1974, la Dous 1991). The boundary layer, where material in the inner accretion disc is forced to match the (much slower) rotation rate of the primary, emits in the extreme ultraviolet, soft and hard X-rays (see eg. Warner 1995a chapter 2). Many magnetic CVs were detected in surveys by satellites such as HEAO-1, Einstein, EXOSAT and ROSAT. Most optically bright CVs have been detected in hard ($\gtrsim 1\,\mathrm{keV}$) X-rays (Beuermann & Thomas 1993). The X-ray emission in polars has its origin in the stand-off shock front caused by gas falling supersonically along the field lines of the primary and impacting in the primary's atmosphere. The hard X-ray emission originates in the post shock region where the material cools as it settles onto the surface of the primary. The white dwarf atmosphere in the vicinity of the accreting pole intercepts about half of this radiation and re-radiates it as soft X-rays and UV emission. X-ray emission from non-magnetic CVs could come from the corona of the secondary or the corona of the disc.

Gamma rays have been detected from the threading region in magnetic CVs, and modulated γ-ray signals such as the 33 s rotation modulation in AE Aqr have been observed in TeV γ-rays using ground-based telescopes that detect optical Cerenkov radiation (eg. Meintjies et al. 1992). From radio to TeV gamma rays, CVs continue to provide fascinating new areas of research.

1.1.4 The AM CVn stars

1.1.4.1 Discovery

The six members of the AM CVn star subclass were discovered by a variety of methods. AM CVn was noted as a high Galactic latitude blue star by Malmquist (1936) and Humason & Zwicky (1947), who designated the star HZ 29. Spectral observations by Greenstein & Matthews (1957) revealed broad, shallow absorption lines of He I and a total absence of hydrogen. They classified HZ 29 as a DB white dwarf. GP Com is a high proper motion star and appears in the catalogue of Giclas, Burnham & Thomas (1961) as G61-29. In the catalogue, the star is described as a "possible white dwarf". Spectra obtained by Burbidge & Strittmatter (1971) showed strong emission lines of He I. At the time, G61-29 was the only object known to have a purely helium emission line spectrum. V803 Cen (formerly AE 1) was discovered serendipitously: it happens to lie very near the active radio galaxy Centaurus A (NGC 5128), the most intense continuum radio source in the sky that is identified with a galaxy. During a photometric survey of the region conducted by Elvius & Hall (1964), a star with intense blue colours and large-amplitude intensity variations was noticed. Further investigation by Elvius (1975) revealed variations in V from 14 to 17, and variable spectra of He I. Elvius noted similarities between the spectra of AE 1 and HZ 29, and drew comparisons between AE 1 and the R Coronae Borealis star MV Sgr. CP Eri was listed by Luyten & Haro (1959) as a high galactic latitude object with large brightness variations. The last two members of the AM CVn star subclass, EC 15330 and CR Boo (PG 1346+082), were discovered in surveys searching for blue objects (the Edinburgh-Cape survey: Stobie et al. 1992, and the Palomār-Green survey: Green, Schmidt & Liebert 1986).

1.1.4.2 Observational properties

A detailed account of the discovery and observational history for V803 Cen, GP Com, CP Eri and EC 15330 are given in chapters 4 through 7. The observational characteristics mentioned here are those that identify the stars as belonging to the AM CVn subclass. In addition, those observations that are needed to justify the interacting binary white dwarf (IBWD) model and the case for superhumps, are described. The observational properties

of the AM CVn stars are summarized in table 1.1.

Spectroscopy

The most distinctive common property of the AM CVn stars is the complete absence of hydrogen in their spectra. Optical spectra of AM CVn have been presented by Greenstein & Matthews (1957), Robinson & Faulkner (1975), Williams (1983), Patterson et al. (1992) and Patterson, Halpern & Shambrook (1993). They show broad, shallow He I absorption lines with asymmetric profiles and variable line depths. The line asymmetries cause apparent shifts in the γ-velocity of the lines. Weak He II λ4686Å emission was observed by Patterson et al. (1992) in AM CVn; the line centre is not shifted relative to its rest wavelength as is the case with the asymmetric He I absorption lines. CR Boo has also displayed He II λ4686Å emission (Patterson et al. 1992). The optical spectra of EC 15330-1403 (O'Donoghue et al. 1994) are very similar to those of AM CVn, although He II λ4686Å emission has not been observed. The spectra of CR Boo, V803 Cen and CP Eri, which show distinct high and low photometric states (see table 1.1), are similar to those of AM CVn in the high state. In their low state, the absorption features vanish and are replaced by a plain continuum or weak emission lines (O'Donoghue & Kilkenny 1989, Kepler, Steiner & Jablonski 1989, O'Donoghue et al. 1990). The same He lines appear in the high and low states with some changes in relative strength. The weakness of the emission lines in the low state suggests that the continuum has considerable optical thickness, despite the fact that the continuous opacity of neutral helium in the visible region is two orders of magnitude smaller than that of hydrogen for appropriate temperatures and densities (O'Donoghue & Kilkenny 1989).

GP Com has an emission line spectrum similar to V803 Cen, CP Eri and CR Boo in their low states, except that the lines are much stronger. He I and He II dominate, although lines from heavier elements such as N, O and Mg are present in near-IR spectra (Marsh, Horne & Rosen 1990; for details see chapter 5). Observations by Nather, Robinson & Stover (1981) show an 'S'-wave component in all emission lines with a period of 2790 s. By analogy with the 'S'-waves seen in hydrogen-rich CVs, the periodic radial velocity variation in GP Com demonstrates that this system is an interacting binary with an or-

Table 1.1: Observational properties of the AM CVn stars

Star	Alias	Principal period and harmonics (s)	Other periods (s)	V mag range	He I λ4471Å (FWHM)	References
AM CVn	HZ 29	1051[a], 525, 350	1011, 289, 801, 26	14.1 – 14.2	40	1 – 3
EC 15330		1119, 560		13.6	32	4
CR Boo	PG 1346	1490, 745, 495, 372	1471.4	13.0 – 18.0	45	5, 6
V803 Cen	AE 1	1611, 805, 537, 402, 322, 268	175	13.2 – 17.4	21	7 – 10
CP Eri		1724, 862, 574, 431, 345		16.5 – 19.7		11
GP Com	G61-29	2790[b]		15.8	31	12, 13

Notes:
(a) Not observed in power spectra; the 525 s period and other commensurate periods are harmonics of this unseen fundamental (see text for a discussion).
(b) Spectroscopic period (Nather, Robinson & Stover 1981).

References: 1. Provencal et al. 1995; 2. Patterson, Halpern & Shambrook 1993; 3. Patterson et al. 1993; 4. O'Donoghue et al. 1994; 5. Wood et al. 1987; 6. Provencal 1994; 7. Westin 1980; 8. O'Donoghue, Menzies & Hill 1987; 9. O'Donoghue & Kilkenny 1989; 10. O'Donoghue et al. 1990; 11. Abbott et al. 1992; 12. Nather, Robinson & Stover 1981; 13. Marsh, Horne & Rosen 1991.

bital period of 46.5 min.

Robinson & Faulkner (1975) searched for radial velocity variations at the principal photometric period of AM CVn but found none, to a limit of $K_1 < 30\,\mathrm{km\,s^{-1}}$. Radial velocity variations at the principal photometric periods in V803 Cen are less than $16\,\mathrm{km\,s^{-1}}$ (O'Donoghue & Kilkenny 1989); in EC 15330 the upper limit is $K_1 < 20\,\mathrm{km\,s^{-1}}$ (O'Donoghue et al 1994) and in GP Com the observed amplitude for the 2790s 'S'-wave period is $14.6\,\mathrm{km\,s^{-1}}$ (Nather, Robinson & Stover 1981). These stringent limits on periodic radial velocity variations are strong constraints on models for the AM CVn stars.

The absorption line profile asymmetry in AM CVn varies on a well-defined period of 13.38 h (Patterson, Halpern & Shambrook 1993) (see figure 1.2). Absorption line asymmetry variations have also been observed in EC 15330 (O'Donoghue et al. 1994) although a definite period for the skewness variations could not be obtained because of the weakness of the lines. Asymmetry variations have also been observed in the absorption lines in CR Boo (Wood et al. 1987). The periodic variation in line profile asymmetry observed in AM CVn is of crucial importance in understanding the structure of these systems.

Photometry

The mean brightness of AM CVn and EC 15330 hardly change. EC 15330 has been at $V \sim 13.6$ on every occasion it has been observed. AM CVn *may* show long-term variability with an amplitude of up to 0.1 mag, but this is not a secure result: long-term constancy is also possible (Patterson et al. 1992).

Three of the six AM CVn stars show distinctive photometric high and low states: these are tabulated in table 1.1. The large-amplitude changes occur on time scales of a few days. Wood et al. (1987) used archival data from the Harvard meteor programme to study the large-amplitude variations of CR Boo during the interval 1952 – 1957: the system was brighter than $m_{pg} \sim 14.0$ roughly 74% of the time and had a quasi-period of 4–5 days. The light curve from a WET (Nather 1989) run on CR Boo is shown in figure 1.3 (from Provencal 1994). Two outbursts from $V \approx 18$ with rise times of ~ 0.5 d and duration 1–2

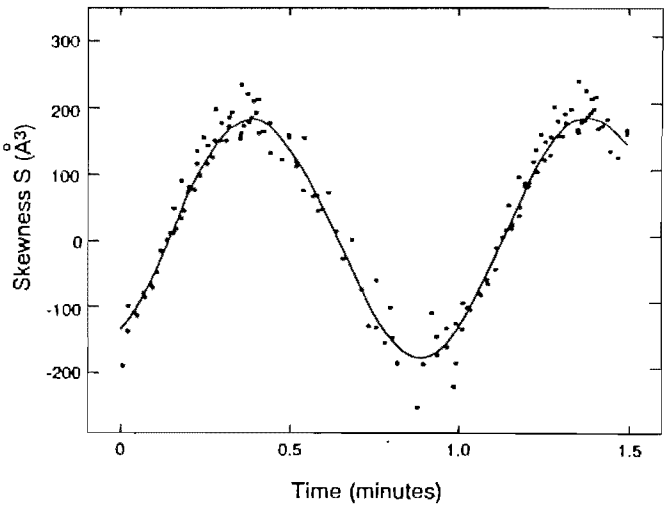

Figure 1.2: The skewness (third moment) of the He I λ4922Å line in AM CVn, folded on the 13.38 h period. From Patterson, Halpern & Shambrook (1993).

days are present. No long-term light curves of CP Eri and V803 Cen are available, but these systems appear to show similar (perhaps somewhat more erratic) behaviour than CR Boo (Westin 1980, O'Donoghue, Menzies & Hill 1987, O'Donoghue & Kilkeny 1989). CP Eri has been observed to drop from $V \approx 16.7$ to $V \approx 18.0$ in ~ 1 day (see chapter 6). The magnitude difference between high and low state in V803 Cen, CP Eri and CR Boo, decreases with increasing principal period: CR Boo has the largest range and CP Eri the smallest.

The light curve of GP Com is dominated by flickering. A photometric period similar to the 46.5 min orbital period is, however, sometimes observed in the light curve (Warner 1972, see also chapter 5). The other five stars are photometric variables with principal periods in the range 1051 – 1725 s (see table 1.1). The rapid variations have amplitudes of a few percent, and show harmonic structure with as many as seven harmonics (e.g. V803 Cen: O'Donoghue & Kilkenny 1989). In AM CVn, the peak frequencies observed in power spectra are all harmonics of an unseen 1051 s period: most of the power is observed at 525 s with a slight asymmetry in the minima suggesting that the true photometric period

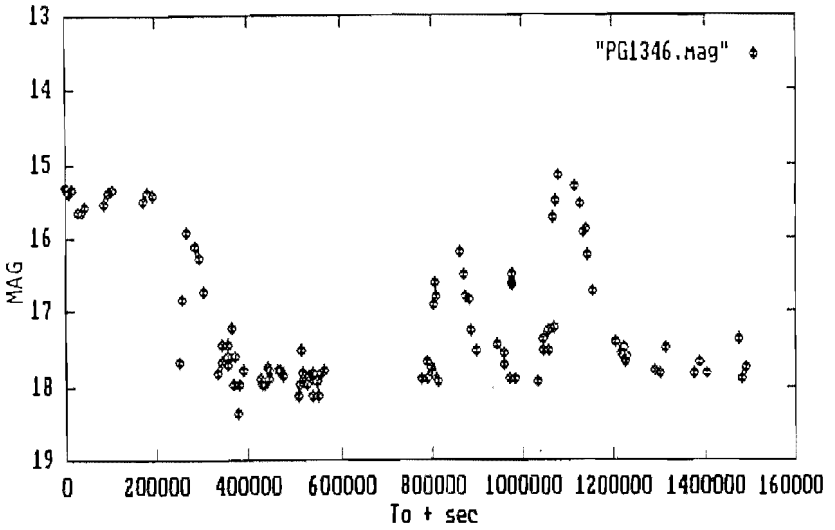

Figure 1.3: The light curve of CR Boo over 18d during a WET run (from Provencal 1994).

is 1051 s (Smak 1967; see also Warner & Robinson 1972). Several non-commensurate periods have been observed in AM CVn, CR Boo and V803 Cen (see table 1.1). The 1011 s variation in AM CVn exhibits strong amplitude variability on a time scale of months, although its frequency does not vary (Provencal et al. 1995). The 1471.4 s variation in CR Boo, observed in low state light curves, appears to be a coherent variation, returning with its original phase after each high state during a WET run over period of about two weeks. The first harmonic of the 1471.4 s period maintains a constant frequency and intensity in all low state runs during the WET run (Provencal 1994).

WET photometry of AM CVn obtained in 1990 (Provencal et al. 1995) revealed fine structure in the power spectrum: low-amplitude sidebands were observed on the high frequency side of the first three harmonic peaks. The frequency splitting between the multiplet components is a constant 20.77μHz. The inverse of this quantity is 13.38 h, precisely the period observed by Patterson, Halpern & Shambrook (1993) in the absorption line profile asymmetry variations.

High-energy observations

The ultra-violet counterpart of the optical 'S'-wave of GP Com was identified in HST UV spectra by Marsh et al. (1995). During 13 h of HST observations, GP Com displayed three large flares in the dominant N V emission line. The observations also revealed C IV emission at a level of 0.094 times the N V flux. Marsh et al. (1995) speculate that the flaring behaviour arises from variable mass loss in a wind, or by irradiation of the accretion disc. UV spectra of AM CVn from IUE show broad absorption features of N V λ1240Å, Si III λ1300Å, Si IV λ1400Å, C IV λ1549Å and He II λ1640Å. There is no evidence for spectral variation in the IUE data (Patterson et al. 1992). Hard X-ray emission from GP Com was detected by the Einstein satellite IPC (Patterson & Raymond 1985): a flux of $9.0 \times 10^{-12}\,\mathrm{erg\,cm^{-2}\,s^{-1}}$ in the range 0.2 – 4.0 keV was deduced. By contrast, AM CVn was detected with the same instrument to have a total X-ray flux of less than $2.0 \times 10^{-13}\,\mathrm{erg\,cm^{-2}\,s^{-1}}$ (Becker 1981). ROSAT observations of GP Com yield X-ray luminosities in the range 1.91×10^{30} – $5.52 \times 10^{31}\,\mathrm{erg\,s^{-1}}$ (for a distance of 160pc) (Ulla 1995). The count rates for GP Com in the broad (0.11 – 2.4 keV), hard (0.52 – 2.4 keV) and soft (0.11 – 0.4 keV) ROSAT PSPC bands are comparable to those for the SU UMa star VW Hyi.

CR Boo was described by Wood et al. (1987) as a weak X-ray source (from EXOSAT observations). Ulla (1994, 1995) derived an X-ray luminosity for CR Boo from ROSAT PSPC images in the range 8.85×10^{28} – $1.18 \times 10^{31}\,\mathrm{erg\,s^{-1}}$ for a distance of 150 pc. The only X-ray information avaiable for V803 Cen is from ROSAT images taken in the region of Centaurus-A by Arp (1994) in the range 1.0 – 2.4 keV. Ulla (1995) calculates a luminosity of between 1.71×10^{29} and $3.92 \times 10^{30}\,\mathrm{erg\,s^{-1}}$ for V803 Cen. CP Eri appears to be the weakest X-ray emitter (of those AM CVn stars measured with ROSAT): only 3σ upper limits to its ROSAT PSPC count rates are available, as the object was not detected. A null detection of CP Eri by the EGRET instrument on the Compton Observatory is reported by Schlegel et al. (1995). It is not yet known whether the large-amplitude optical brightness variations observed in CR Boo, V803 Cen and CP Eri are accompanied by similar changes in the X-rays (Ulla 1995).

Ulla (1995) has compiled observations of AM CVn by the Einstein IPC, ROSAT PSPC,

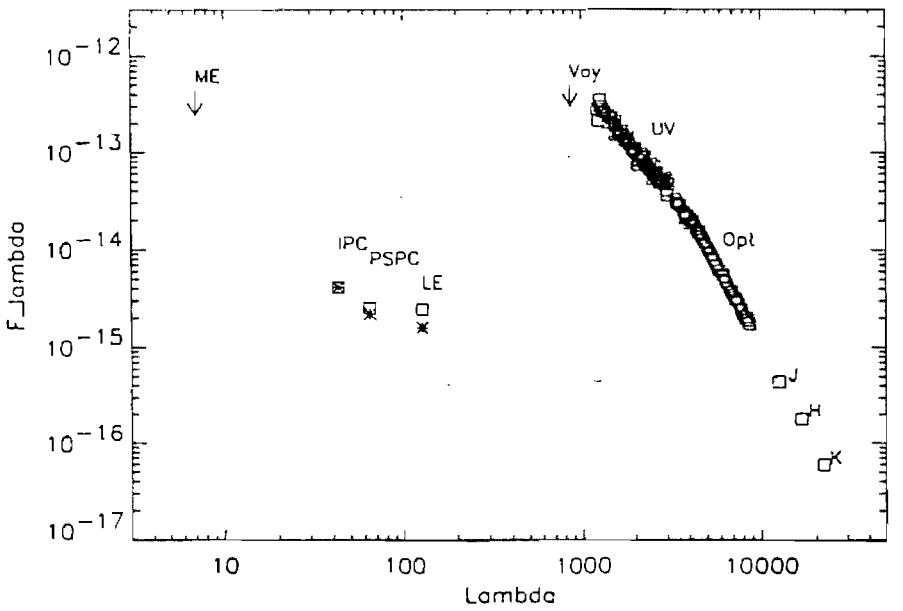

Figure 1.4: Flux distribution of AM CVn from the infrared to hard X-rays, plotted on logarithmic scales (from Ulla 1995). The horizontal axis is in Å and the vertical in erg $cm^{-2} s^{-1} Å^{-1}$. Open squares correspond to brehmsstrahlung and stars to blackbody models for the Einstein IPC, ROSAT PSPC and EXOSAT LE instrument observations. The downward arrows are the upper limits set by Voyager and the ME EXOSAT band. The spectrum shows that the peak flux of AM CVn is emitted in the EUV.

Voyager and in the EXOSAT LE and ME bands and combined these with flux measurements in the UV, optical and infrared to produce a multi-wavelength flux distribution (see figure 1.4). The maximum of the overall flux distribution of AM CVn peaks around EUV wavelengths.

1.1.4.3 Competing models

The model for the AM CVn stars that is the most consistent with observation is that proposed by Faulkner, Flannery & Warner (1972, hereafter FFW). Before 1972, AM CVn had already been the subject of much work and speculation: FFW opened their paper with the words "The peculiar blue object HZ 29 has had a remarkably checkered career in the astronomical literature". Models proposed for AM CVn prior to 1972 included a DB white dwarf (Eggen & Greenstein 1965) and an active galactic nucleus (Burbidge, Burbidge & Hoyle 1967). Rapid variability observed by Smak (1967) convinced him that AM CVn was an interacting binary, although the lack of detectable radial velocity variations (Greenstein & Matthews 1957) was a worry. Models proposed for V803 Cen included a DB white dwarf; Elvius (1975) and Westin (1980) also drew comparisons between V803 Cen and MV Sgr, an R Coronae Borealis star.

Supporting evidence for the interacting binary white dwarf model

FFW proposed that AM CVn is a short-period binary with a low-mass, degenerate helium secondary, transferring mass via an accretion disc to a DB white dwarf. The 17 min period was interpreted as the orbital period. Although some of the fine details of FFW's model are now known to be incorrect (for example, they took the double-humped light curve to imply that the system was an *eclipsing* binary), the essentials of the FFW model have survived. The model is sometimes referred to as the 'interacting binary white dwarf' or IBWD model.

FFW's justification that the secondary in AM CVn is a degenerate helium-rich star is as follows. They derive an expression relating the mean density of a Roche lobe-filling secondary to the orbital period. The mean density of the secondary is

$$\bar{\rho}_2 = \frac{M_2}{\frac{4}{3}\pi {R_2}^3} \tag{1.6}$$

where R_2 is the volume radius of the secondary. An approximate formula for R_2 in terms of the mass ratio q is

$$\frac{R_2}{a} = \frac{0.49q^{2/3}}{0.6q^{2/3} + \ln(1+q^{1/3})} \tag{1.7}$$

(Eggleton 1983: FFW used an earlier, slightly less accurate approximate formula for R_2 from Paczynski 1971). Using Kepler's third law, this gives

$$\bar{\rho}_2\,(\mathrm{g\,cm^{-3}}) = 107 P_{orb}(\mathrm{h}) \tag{1.8}$$

This equation is accurate to 3%, independent of q, over the range $0.01 \leq q \leq 1$.

Figure 1.5 is a logarithmic plot of the radius versus the mass of lobe-filling secondaries together with lines of constant period and equations of state for the zero-age main sequence (ZAMS), the helium ZAMS and for cold degenerate matter. Rough estimates of the mass and radius of a lobe-filling secondary can be obtained by finding the intersection of the equation of state of interest with the period of the binary. An orbital period of 1051 s implies that the secondary of AM CVn cannot be a hydrogen-rich star (this is consistent with the total absence of hydrogen in all AM CVn star spectra). There are two helium-rich candidates for the secondary: a helium ZAMS star with $M_2 \sim 0.4 - 0.5\,\mathrm{M}_\odot$, and a degenerate helium low-mass white dwarf with $M_2 \sim 0.04\mathrm{M}_\odot$. The helium dwarf can immediately be eliminated because it would give large radial velocity variations, unless the binary inclination were close to zero. The stringent upper limits on K_1 for the AM CVn stars prove that the secondary cannot be a helium main-sequence star.

The identification of GP Com as an AM CVn star (first suggested by Warner 1972) lends strong support to the FFW model, because GP Com is *demonstrably* a binary with a short orbital period. The light curve is dominated by flickering, which is indisputable evidence of mass transfer. If the mass transfer is occurring by Roche lobe overflow, equation 1.8 with $P_{orb} = 45.6\,\mathrm{min}$ implies that the mean density of the secondary is $200\,\mathrm{g\,cm^{-3}}$. The

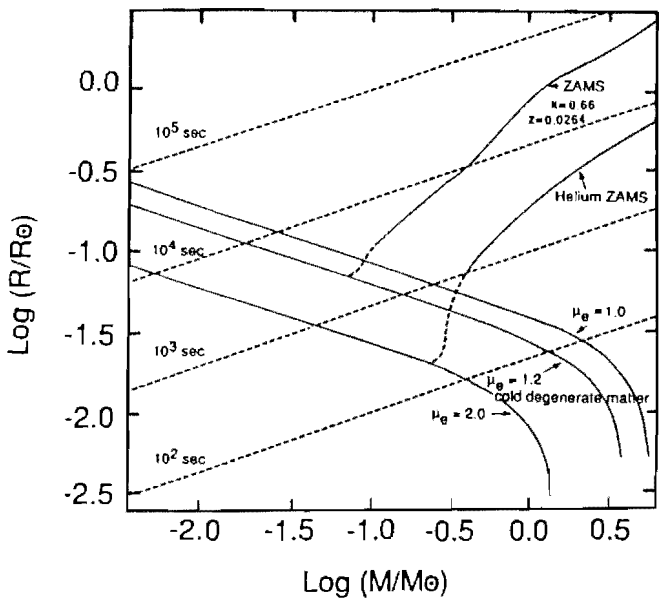

Figure 1.5: Lines of constant period (dashed lines) in a plot of secondary radius versus its mass for lobe-filling secondaries, along with various equations of state. Approximate values for the mass and radius of a secondary can be found by finding the intersection of the equation of state of interest with the orbital period of interest. Because of mass loss, the evolution of the secondary proceeds along to the left along any equation of state curve, and a transition to a degenerate sequence occurs. From Faulkner, Flannery & Warner 1974.

only way in which a star with this density could avoid being degenerate is by being very hot. But, as noted by Burbidge & Strittmatter (1971), the large proper motion of GP Com requires that its distance be less than 200 pc if it is gravitationally bound to the Galaxy. Since its apparent visual magnitude is $\sim$ 15.8, the absolute visual magnitude must be greater than about +9.5 (Nather, Robinson & Stover 1981). This is too faint for a very hot normal star. Therefore, the secondary in GP Com is degenerate.

Strong support for a binary interpretation for the AM CVn stars as a group comes from the three large-amplitude AM CVn stars. The only mechanism that could produce the large brightness changes observed in CR Boo, V803 Cen and CP Eri, without a significant colour change, is mass transfer in an interacting binary. A mechanism that has been pro-

posed for the brightness variations in CR Boo, V803 Cen and CP Eri is variations in $\dot{M}_2$. The long-term light curve of CR Boo (figure 1.3) bears a strong resemblance to the VY Scl star MV Lyr (Warner 1995b), where the changes in brightness are due to fluctuations in the rate of mass transfer from the secondary. Wu, Wickramasinghe & Warner (1995) explain the brightness variations in the VY Scl stars by examining the effects of irradiation of the secondary. Heat released due to the accretion of material onto the white dwarf is absorbed by the atmosphere of the secondary, causing the secondary to expand beyond its Roche lobe. This increases $\dot{M}_2$. However, the disc can shield the secondary from the white dwarf, reducing the heating effect, and a complex feedback process is established. Wu, Wickramasinghe & Warner (1995) find chaotic solutions in the range 3 – 4 h, which is the range of orbital periods inhabited by the VY Scl stars. According to this model, the VY Scl star brightness modulations are due to changes in the heating effect caused by varying degrees of shielding of the secondary by the disc. We would expect the effects of irradiation of the secondary to be important in the AM CVn stars if they are compact binaries. Warner (1995a) calculates that the AM CVn stars should experience the same irradiative flux as the VY Scl stars when their orbital periods are in the range 1280 s $\lesssim P_{orb} \lesssim$ 1520 s. This is fairly close to the observed photometric periods[1] for CR Boo, V803 Cen and CP Eri. However, the secondaries in the AM CVn stars are degenerate, and have much smaller masses than the secondaries in hydrogen-rich CVs, and their response to irradiation has not yet been modelled.

The flux distributions of the AM CVn stars closely approximate single photospheric temperatures. The optical flux gradient in AM CVn is well fitted by a blackbody distribution with $T = 20\,000$ K (Wampler 1967) and V803 Cen has a flux distribution consistent with a blackbody of $T = 26\,000$ K. At first sight, this observation would appear to be a point against an interacting binary model for the AM CVn stars, because an accretion disc is expected to show a characteristic *range* of temperatures. However, under the IBWD model, the AM CVn stars are very compact systems and their accretion disc radii are expected to be small; the disc will thus have a small range of effective temperatures. Patterson et al. (1992) calculate theoretical fluxes for blackbody discs, assuming $M_1 = 0.9\,M_\odot$, a

[1]The principal photometric periods and the orbital periods differ by only a few percent if the photometric modulations are superhumps: see later.

mass transfer rate $\dot{M}_d \sim 3 \times 10^{-9}\,\dot{M}_\odot\,y^{-1}$ and a disc radius $r_d = 1.5 \times 10^{10}$ cm (parameters appropriate for AM CVn) and deduce that the flux distributions of small discs can mimic a single temperature fairly well. The fact that the flux distributions of AM CVn stars are consistent with single temperatures is thus consistent with the IBWD model.

There is no sign of a DB white dwarf absorption spectrum in observations of GP Com, or in low state spectra of CR Boo, V803 Cen and CP Eri. The system brightness must therefore be dominated by disc emission. O'Donoghue & Kilkenny (1989) show that the spectra of AM CVn, CR Boo and V803 Cen can be satisfactorily explained if the line-forming region is in the atmosphere of an accretion disc. The widths of the lines in AM CVn and CR Boo are explicable by Doppler broadening in an accretion disc; the line widths in V803 Cen are consistent with Stark broadening in the disc atmosphere, and V803 Cen is deduced to be at a lower inclination than AM CVn and CR Boo (O'Donoghue & Kilkenny 1989).

Another point in favour of the IBWD model is the observation of rapid quasi- periodic oscillations in the light curve of AM CVn. On four consecutive nights in May 1976, low-amplitude QPOs with periods 26 s were observed (Patterson et al. 1979). Also, Warner & Robinson (1972) present evidence for transient periods in the range 113–121 s. QPOs are seen in a variety of CV subclasses (see chapter 3), and the 26 s period, which is much shorter than anything previously seen in pulsating white dwarfs, is typical of the short-period oscillations seen in hydrogen-rich CVs, known as dwarf nova oscillations (see Warner 1995a, chapter 8).

Alternatives to the IBWD model

Since the IBWD model was proposed, it has been commonly assumed that the 1051 s period in AM CVn (and, by analogy, the principal periods in the other four multiperiodic AM CVn stars) represents the orbital period of a compact binary. An orbital clock, however, should be a stable one, and reliable ephemerides for the principal periods in the AM CVn stars have never been found. The phase wanderings of the principal period in AM CVn coupled with the assumption that the 1051 s period must be an orbital period,

led Patterson et al. (1992) to comment: "The most severe obstacle to accepting AM CVn as a short-period binary is the instability of the photometric period". Several ideas as to how to account for the lack of strict coherence of the 1051 s period have been suggested: a third body was included by Krzeminski (1972) to explain the wanderings in $O-C$ diagrams, and a large $\dot{P}$ term was invoked by Patterson et al. (1979). Neither of these suggestions have led to ephemerides with any predictive power.

Patterson et al. (1992), as a possible alternative to the IBWD model, point out several rather intriguing similarities between AM CVn and DB pulsators. The DB pulsators (Winget et al. 1982, Winget 1988) are similar to AM CVn in their spectra, flux distributions, and the period and amplitude of their photometric variations.

The broad-band flux distribution of AM CVn is very similar to the DB pulsator GD 358: in the wavelength range 1250 – 5000Å, the flux distributions agree within $\sim$ 0.03 mag. However, the detailed optical and ultraviolet spectra are quite different. While the ultraviolet spectrum of GD 358 is largely featureless, AM CVn shows a host of strong absorption features that are much broader and stronger (by a factor of 10 in equivalent width) than the metal lines occasionally seen in the spectra of hot white dwarfs. The dominant ultraviolet light source in AM CVn cannot therefore be subject to the gravitational settling that stratifies white dwarf atmospheres and causes their spectra to be largely monoelemental. There are differences in the optical spectra, too (see figure 1.6). The lines in the pulsating DB white dwarfs have large equivalent widths and sharp cores, and do not show the variable asymmetry of the lines in AM CVn.

O'Donoghue et al. (1994) observe that the spectra of EC 15330 and AM CVn are also very different to the spectra of hot luminous subdwarf He-sdO and He-sdB stars (Moehler et al. 1990) (see figure 1.7). He-sdB stars show prominent absorption lines of C II, C III and He II in the range 4000 – 5000 Å, which are absent from AM CVn star spectra. The He-sdO spectra show strong He II absorption; in the same wavelength range, the only evidence for He II in AM CVn star spectra is the weak emission feature seen occasionally at λ4686Å.

The clock in pulsating white dwarfs is not perfect. The periods in some DB pulsators

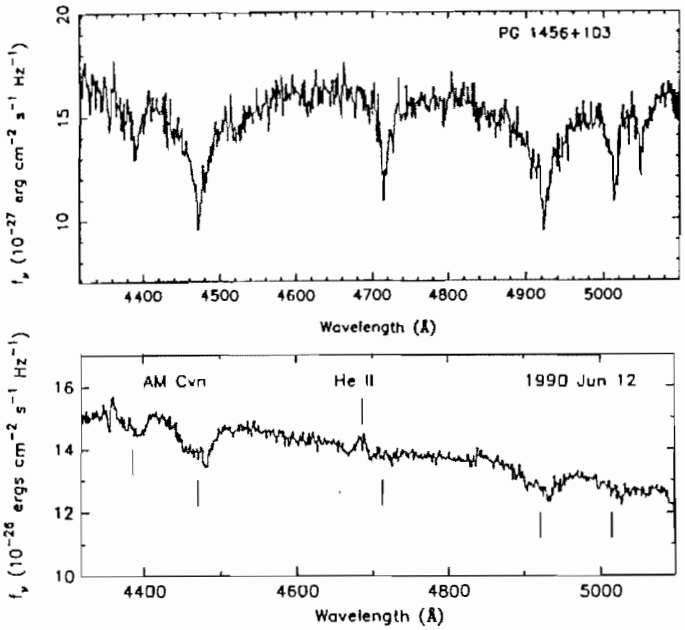

Figure 1.6: The spectrum of the pulsating DB white dwarf PG1456+103 as compared to that of AM CVn. Adapted from Patterson et al. (1992).

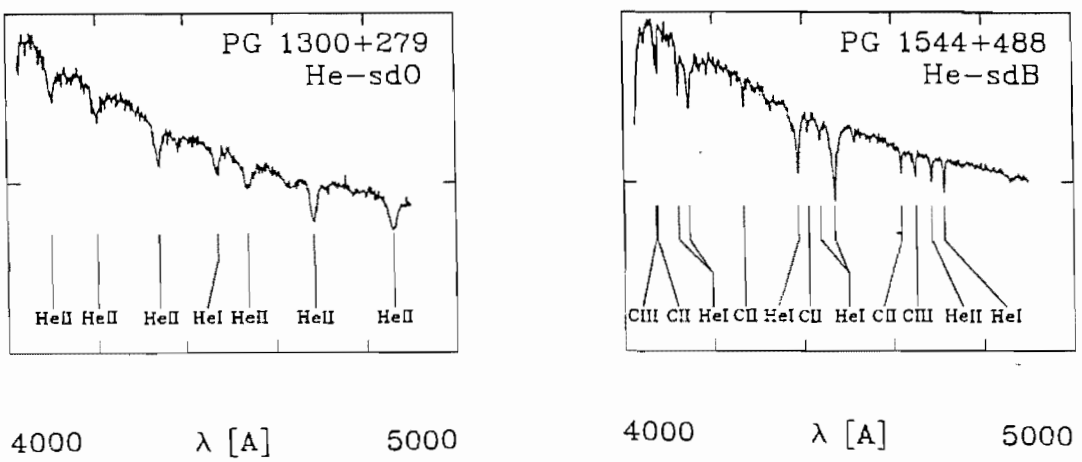

Figure 1.7: Spectra of He-sdO and He-sdB subdwarfs from 4000 – 5000 Å from Moehler et al. (1990).

are very stable, and in others change from night to night (for references see Patterson et al. 1992). One star (G29-38) shows a nearly constant period and amplitude, but with drifts in phase on a time scale of weeks to months: this is reminiscent of what is seen in AM CVn. However, the harmonic structure of DB pulsations is not as complex and variable as that of the AM CVn stars. Also, it has been established that most of the light emitted in AM CVn and EC 15330, and CR Boo, V803 Cen and CP Eri in the high state, originates in an accretion disc (e.g. O'Donoghue & Kilkenny 1989). The white dwarf primary has not been detected in any of these systems. As the principal periods in these stars reach amplitudes of 10% or more, and are most evident in the high state, the brightness variations are most likely to be of disc origin, and not due to white dwarf pulsations.

There is an alternative explanation for the wandering period of AM CVn, one that is consistent with everything else we know about the system, and which is not only allowed by the IBWD model, but is a *natural consequence* of the model. According to this interpretation, the principal periods are not the orbital periods, but differ from the orbital periods by only a few percent. Despite the similarities between AM CVn and the DB pulsators, the fact that AM CVn is almost identical to CR Boo, V803 Cen and CP Eri in their high states eliminates the possibility of a single-star model for AM CVn: CR Boo, V803 Cen and CP Eri must be mass-transferring binaries to achieve their large-amplitude brightness variations, and so, by analogy, must AM CVn.

1.1.4.4 Structure and evolution of the AM CVn stars.

Assuming that the IBWD model is indeed correct (and it is the model most consistent with observation), what can be deduced about the behaviour, structure and evolution of the AM CVn stars?

Mass transfer rates and bright spot luminosities

Equation 1.8 shows that, for $P_{orb} \sim 0.4\,\mathrm{h}$, the secondary will be degenerate, or at least semi-degenerate. In addition, Warner (1995a) shows that $\dot{M}_2$ is large enough to drive

the secondary out of thermal equilibrium. Using the mass radius relation for a semi-degenerate secondary from Savonije et al. (1986) in combination with equation 1.8, the relation between the secondary mass and the orbital period is

$$M_2 = 1.83 \times 10^{-2} {P_{orb}}^{-1.27}(\mathrm{h}). \tag{1.9}$$

Warner (1995a) derives an expression for the rate of mass transfer from the secondary, appropriate for non-equilibrium models:

$$\dot{\mathrm{M}}_2 = \frac{4.4 \times 10^{-12} {M_1}^{2/3}}{(1+q)^{1/3}(0.74-q)} {P_{orb}}^{-5.21}(\mathrm{h})\,\mathrm{M}_\odot\,\mathrm{y}^{-1}. \tag{1.10}$$

Assuming that the principal photometric periods in AM CVn, EC 15330, CR Boo, V803 Cen and CP Eri are close to their orbital periods, this gives a mass transfer rate of $3.9 \times 10^{-9}\mathrm{M}_\odot\,\mathrm{y}^{-1}$ for AM CVn, diminishing to $1.0 \times 10^{-11}\mathrm{M}_\odot\,\mathrm{y}^{-1}$ for GP Com. The rate of mass transfer through the disc used in Patterson et al.'s (1992) blackbody disc model to reproduce the flux distribution of AM CVn, $3.0 \times 10^{-9}\mathrm{M}_\odot\,\mathrm{y}^{-1}$, is very close to the theoretical value for the rate of mass transfer from the secondary: this is consistent with the disc in AM CVn being in a high state. The strong emission line spectrum and hard X-ray emission of GP Com suggests a mass transfer rate of $\sim 3 \times 10^{-12}\mathrm{M}_\odot\,\mathrm{y}^{-1}$ (Patterson & Raymond 1985), in rough agreement with the result obtained using equation 1.10.

The ratio of the bright spot luminosity to disc luminosity is proportional to $\dot{\mathrm{M}}_2/\dot{\mathrm{M}}_d$, proportional to R_1 and inversely proportional to r_d (equation 1.4) for a given orbital inclination. The rate of mass transfer from the secondary for AM CVn is similar to that for nova-like variables (e.g. Warner 1995a chapter 2), so $\dot{\mathrm{M}}_2$ would be roughly the same for AM CVn and the nova-like variables. R_1, the radius of the white dwarf, will also be similar for nova-like and AM CVn star primaries. However, the much smaller disc radius in AM CVn results in a much more prominent bright spot (relative to the disc) than is seen in nova-likes. Taking $r_d \sim 5.0 \times 10^{10}\,\mathrm{cm}$ for a nova-like with $P_{orb} = 4\,\mathrm{h}$, and $r_d \sim 1.0 \times 10^{10}\,\mathrm{cm}$ for an AM CVn star (see section 1.3.1), the ratio of L_{bs}/L_d for an AM CVn system is ~ 5 times larger than that for a nova-like. If the AM CVn stars are observed more face-on than the average nova-like, this number will increase. The bright spot can therefore make a substantial contribution to the total brightness of the

shorter-period AM CVn stars.

Equation 1.10 gives the *secular* mean $\dot{M}_{dot}$ and does not take into account the effects of irradiation of the secondary. The instantaneous $\dot{M}_2$ in the large-amplitude systems may exceed this value. Thus $\dot{M}_2$ in the high state of these systems, and the $\dot{M}_2$ for AM CVn and EC 15330, may exceed the quantity predicted by equation 1.10 by a factor of several.

A classication scheme

AM CVn and EC 15330 show absorption spectra and have stable, high $\dot{M}_d$ discs similar to the hydrogen-rich nova-like variables. The spectra of CR Boo, V803 Cen and CP Eri transform from absorption in their high states to weak emission or plain continua in their low states; this is similar to the VY Scl stars. GP Com is like a dwarf nova in quiescence, with a strong emission line spectrum and a low mass transfer rate from the secondary, and is expected to show dwarf nova outbursts with recurrence intervals of tens of years[2]. AM CVn star spectra are therefore He-rich analogies of the H-rich cataclysmic variables. This classication scheme for the AM CVn stars was proposed by Warner (1995a). The extreme sensitivity of mass transfer rate to orbital period (equation 1.10) supports the classification, assuming that the orbital periods of the AM CVn stars are close to their photometric periods.

1.1.4.5 Origin and evolution of the AM CVn stars

Tutukov & Yungelson (1995) show that the (theoretical) orbital periods of systems with degenerate helium secondaries overlap with the interval of orbital periods of the AM CVn stars. Warner (1995a, chapter 9) describes an evolutionary channel which produces ultra-short period binaries consisting of pairs of degenerate helium stars.

[2]GP Com is similar to the very short-period SU UMa stars (such as WZ Sge, WX Cet, LL And and HV Vir), which show only superoutbursts and have very long outburst recurrence time scales. The secondaries in these stars may be degenerate (Warner 1995c).

Most CVs are thought to start their lives as binaries with orbital periods in the range 0.3 – 165 y and separations between 130 and 2 000 $R_\odot$. The initial mass of the primary lies in the range $0.95 < M_1 \lesssim 10$. The heavier of the two stars (the "initial primary") will evolve off the main sequence first, becoming a giant star. If the mass ratio is very large, mass transfer occurs as a runaway process on a dynamical time scale: the orbital separation shrinks as mass from the heavier component is transferred to the less heavy star, causing the mass transferring star to over-fill its Roche lobe even further, increasing the rate of mass transfer. The accreting secondary cannot adjust its structure at the rate at which mass is arriving. As a result, the transferring gas first fills the outer Roche lobe (this is the equipotential labelled '3' in figure 1.1) and then grows to form a common envelope around both stars. Both stars experience a strong drag force as they revolve around their common centre of gravity within the giant envelope, and the secondary spirals in towards the core of the giant star. The heat deposited in the envelope eventually exceeds its binding energy, and the whole envelope is thrown off as a planetary nebula. The binary now consists of a main sequence secondary orbiting a hot subdwarf primary. The lifetime of the common envelope phase is $\sim 10^3$ y. Astronomers have not yet identified an object which is definitely in the common envelope phase; however, several planetary nebulae are known in which the nuclei are short-period binaries which must have recently emerged from a common envelope (eg. V477 Lyr: Pollacco & Bell 1994).

The nature of the detached binary that emerges from the common envelope is dependent on the stage of internal development of the initial primary when it first fills its Roche lobe. A possible evolutionary route which will lead to a helium-rich secondary transferring mass to a helium white dwarf is as follows. If the initial primary has a mass greater than $\sim 3\,M_\odot$ and has a radiative envelope at the time it evolves and fills its Roche lobe, mass transfer will occur on a thermal time scale, as stars with radiative envelopes shrink as they lose mass. As $q > 1$, the binary separation will decrease, and mass transfer continues on a thermal time scale until the initial primary is less massive than the mass acceptor, and the mass ratio of the binary is reversed. From this point on, mass transfer from the initial primary will result in an *increase* in binary separation. The now secondary (the initial primary) expands on a nuclear time scale. Mass transfer will proceed on a nuclear time scale from the evolved star to the unevolved star until the hydrogen envelope is removed. During this stage, it is the expansion of the evolved star that keeps it in contact with

its Roche lobe. When the hydrogen envelope is removed, the star no longer has a giant structure. The helium core of the initial primary is left as a $0.21 - 0.46\,M_\odot$ helium white dwarf in orbit around a main sequence star.

When this star in turn evolves off the main sequence, the mass ratio is so large that the rate at which the orbital separation decreases results in mass transfer on a dynamical time scale, and the binary enters a common envelope phase. The binary emerging from the common envelope consists of two white dwarfs in a short period binary. Orbital angular momentum then slowly drains away due to gravitational radiation, until the lower mass white dwarf (the larger of the two) fills its Roche lobe and begins transferring matter to the heavier white dwarf. Apart from nova explosions (which cannot occur because the mass donor is not transferring hydrogen), these double degenerate systems are expected to show many of the disc-related phenomena seen in the hydrogen-rich systems.

Once an AM CVn star is born, how does it evolve? Figure 1.5 shows that, as the secondary in a binary loses mass, evolution proceeds to the left along the equation of state curve. At a certain mass and orbital period, a transition occurs to a degenerate sequence. From then on, the secondary will expand as it loses mass. The secondary evolves up the degenerate sequence (to larger radii), and the orbital period of the system increases. The AM CVn stars are double-degenerate binaries, and must therefore be on the orbital period increasing branch. The precise value of the orbital period minimum $P_{orb,min}$ depends sensitively on $\dot{M}_2$ and on the chemical composition of the secondary, decreasing monotonically with X. Calculated values of $P_{orb,min}$ for a hydrogen-rich secondary with moderate $\dot{M}_2$ are $\sim 80\,\mathrm{min}$ (e.g. Rappaport, Joss & Verbunt 1983). This is in agreement with observation: the shortest observed orbital period of a CV with normal hydrogen-rich composition is $\sim 75\,\mathrm{min}$ (Warner 1995a section 2.2). Iben & Tutukov (1991) find that the theoretical $P_{orb,min}$ for helium-rich cataclysmics is $\sim 13\,\mathrm{min}$.

Just after passing the orbital period minimum, an AM CVn star will have a mass transfer rate (equation 1.10) of $\dot{M}_2 \approx 3 \times 10^{-8}\,M_\odot\,\mathrm{y}^{-1}$. The lifetime ($\sim M_2/\dot{M}_2$) at this period is very short, because the high rate of mass transfer causes the secondary to expand and the binary separation to increase to higher P_{orb} very quickly. $\dot{M}_2$ decreases rapidly with increasing P_{orb}, but is supplemented by an irradiation-induced component until P_{orb} ex-

ceeds approximately 1500 s (Warner 1995b). At this stage, an AM CVn star is expected to show behaviour similar to the hydrogen-rich VY Scl stars, as the irradiative flux on the surface of the secondary is comparable to that of the VY Scl stars in this period range. The main difference is that, because the VY Scl star secondaries are non-degenerate, they will evolve to shorter orbital periods, while the AM CVN stars evolve through the range of $\dot{M}_2$ instability with increasing P_{orb}. When the orbital separation is so large that irradiation cannot lift $\dot{M}_2$ into a quasi-stable state, the system will be in a state of very low $\dot{M}_2$: these systems would be like the large outburst amplitude SU UMa stars, showing infrequent dwarf nova outbursts.

1.2 Superhumps in hydrogen-rich systems

The photometric periods in the AM CVn stars are consistent with being a superhump phenomenon. It is for this reason that the principal photometric periods are similar to the orbital periods, and why they do not show strict phase stability. Superhumps were first observed in superoutbursting SU UMa dwarf novae, and it is in these systems that superhumps have been modelled and are now reasonably well-understood. The systematics of superoutbursts in dwarf novae are reviewed by Warner (1995c).

1.2.1 Observations of superhumps in SU UMa dwarf novae

The SU UMa dwarf novae display two distinct types of outburst: normal outbursts which last from 2 to 4 days, during which the system increases in brightness by 2–5 mag, and less frequent but quasi-periodic superoutbursts, which last 5–10 times as long as a normal outburst and reach a peak brightness up to ~ 0.7 mag above the normal outburst peak. Superoutbursts appear to be triggered by normal outbursts (e.g. Vogt 1983, van der Woerd & van Paradijs 1987). The superoutburst light curve has a distinctive shape which is essentially identical from superoutburst to superoutburst in a given system. Following the supermaximum, the superoutburst has an extended plateau of brightness, after which the system returns to quiescence at the same rate of decline as a normal outburst. Warner (1995c) shows that the slope of the plateau phase is a nearly constant 9 d mag^{-1} for all

SU UMa stars.

The SU UMa stars have orbital periods among the shortest of the hydrogen-rich CVs (all but one, TU Men, have orbital periods below the period gap), and this implies that they have small mass ratios. The mass-period relationship for a main sequence secondary can be approximated (Warner 1995a equation 2.100) as

$$M_2 = 0.065 {P_{orb}}^{5/4} (\mathrm{h}) \tag{1.11}$$

where M_2 is in solar masses. The average mass of the primaries in dwarf novae is $0.74 \pm 0.07\,\mathrm{M}_\odot$ (Warner 1995a table 2.5). For $M_1 \gtrsim 0.6\,\mathrm{M}_\odot$ and $P_{orb} \lesssim 2\,\mathrm{h}$, we expect $q \lesssim 0.25$. This is confirmed by observation where values of q have been obtained from detailed photometric studies: mass ratios in the SU UMa stars OY Car (Wood et al. 1989), HT Cas (Horne et al. 1991) and Z Cha (Wood et al. 1986) are less than 0.15.

As yet, no well-observed superoutburst has been seen without accompanying superhumps. Superhumps[3] are well-defined periodic modulations appearing after the supermaximum with amplitudes 0.3–0.4 mag. They were first observed in the December 1972 superoutburst of VW Hyi by Vogt (1974) and Warner (1975). The delay between the time of supermaximum and the onset of superhumps could be a function of P_{orb}, or of the mean normal or superoutburst recurrence times (Warner 1995c). During the plateau phase, the superhump amplitude decreases faster than the system light, and the superhumps disappear roughly at the end of the plateau. In the better-observed systems, the superhump period is seen to decrease during the plateau phase of the superoutburst. Ephemerides for the times of superhump maximum in e.g. VW Hyi (van Amerongen, Bovenschen & van Paradijs 1987), SU UMa (Udalski 1990), T Leo (Lemm et al. 1993) and VY Aqr (Patterson et al. 1993) show statistically significant $\dot{\mathrm{P}}$ around $-(3-10) \times 10^{-5}$.

Superhumps are seen in SU UMa systems of all inclinations, implying an intrinsic flux variation rather than a geometric effect. Even systems which do not have detectable orbital humps during quiescence, show full-amplitude superhumps. Naylor et al. (1987) found that the superhump signal originates in an extended region in the outer part of

[3]The term "superhump" was first used by Brian Warner in 1975

the accretion disc. Simulation of eclipses in Z Cha during superoutburst show that the superhump light source is an extended region of the disc, involving $\sim 1/4$ of its area. In addition, it was found that the superhump light source could be modelled as a non-uniformly bright rim to the disc, modulated in intensity at the superhump period (Warner & O'Donoghue 1988).

Superhumps grow rapidly to maximum and have asymmetric, roughly triangular shapes with a rise steeper than the decline. In the systems with known orbital periods, the superhump period exceeds P_{orb} by 0.8–7.2% (Warner 1995c). As the system fades and the superhump amplitude decreases, the superhump develops a more complex shape. The additional peaks repeat with the superhump period. Figure 1.8 shows the development of these structures during a superoutburst of VW Hyi in October 1978 (Schoembs & Vogt 1980). One of these peaks, the "late superhump", remains pronounced during the decline to quiescence and is shifted by 0.4 – 0.5 in phase with respect to the original superhumps. Late superhumps have been observed in e.g. VW Hyi (van der Woerd et al. 1988), OY Car (Schoembs 1986), SU UMa (Udalski 1990) and V1159 Ori (Patterson et al. 1995). In V1159 Ori, the late superhumps have been observed to persist throughout the decline phase to quiescence, and apparently survive until the next normal outburst. van der Woerd et al. (1988) obtained simultaneous optical, near-IR and EXOSAT X-ray observations of VW Hyi during late superoutburst and deduced that the late superhump light source is an optically thin plasma which covers an area that is a significant fraction of the accretion disc.

Optical spectra of the lower inclination SU UMa stars during superoutburst show broad, shallow absorption lines; weak emission reversals are seen in some systems. In the high-inclination systems, the spectra at supermaximum show emission lines with narrow absorption cores (Warner 1995a section 3.6.5). Large variations from night to night in the γ-velocity of the broad absorption lines have been observed in TY PsA (Warner, O'Donoghue & Wargau 1989), TU Men and VW Hyi (for references see Warner 1995a). In TY PsA, the line asymmetry varies on a period that is consistent with the beat period of the orbital and the superhump period (see chapter 3).

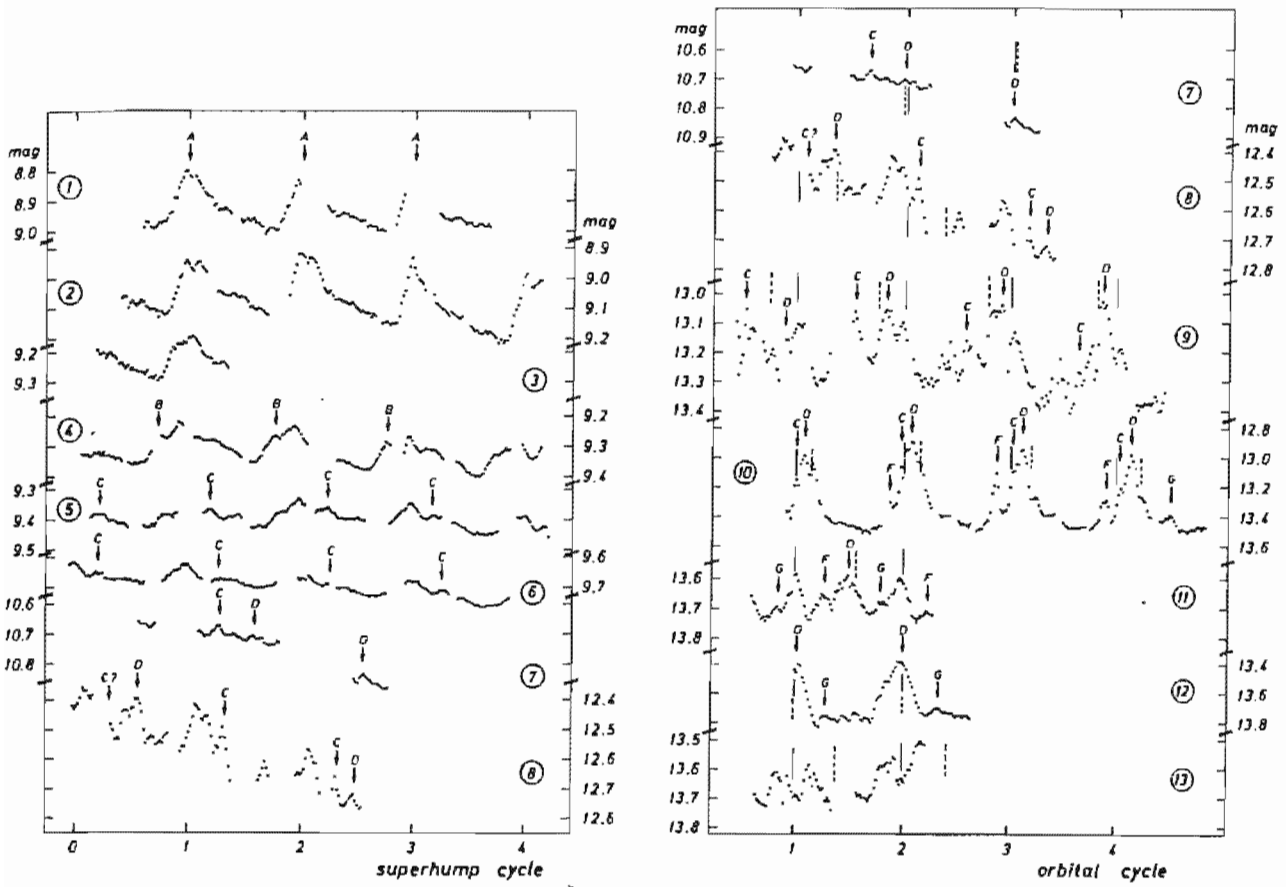

Figure 1.8: Light curves of VW Hyi during superoutburst and during the transition to quiescence. The superhump ('A') dominates during the initial stages. Towards the end of the plateau, periodic secondary structures appear. The late superhump is marked 'D'. From Schoembs & Vogt (1980).

1.2.2 Hydrogen-rich nova-like variables and nova remnants with multiple periodicities

Many nova-like variables and nova remnants show multiple periodicities with photometric periods that differ from their spectroscopic (presumably orbital) periods. The photometric periods are, in general, imperfect clocks. In some cases, systems show photometric periods slightly in excess of their orbital periods, while in other cases the photometric period is less than P_{orb}. These systems are listed in table 1.2. Where more than one photometric period has been reported for a given star, the year of observation is given alongside the period. If the star is a nova remnant, the year of outburst is given.

The term 'superhump' has come to refer to *any* photometric modulation that is slightly displaced from P_{orb}. In the cases where the photometric period is *less* than P_{orb}, the modulation is a 'negative superhump' (e.g. Patterson et al. 1993). It is thought (see the following section) that the negative superhumps originate from a different mechanism than the one producing normal superhumps with positive period excesses.

Warner (1985), to explain the differing photometric and spectroscopic periods in the nova remnant CP Pup, suggested that the observations were consistent with a superhump interpretation, and that CP Pup was in a state of permanent outburst, with a high $\dot{M}_d$. The existence of the Z Cam stars — dwarf novae above the period gap which occasionally get stuck in an outburst state for tens of days to years — shows that there is no clear distinction between the eruptive and the noneruptive stars (or "permanently eruptive", as they are permanently in a luminous state suggestive of large $\dot{M}_d$). Patterson et al. (1993) comment that "it does not strain credulity to suppose that discs accreting at some high rate ... would share common properties, regardless of whether the high rate was planning to endure for a month, a year, or centuries."

O'Donoghue (1990) points out that nova remnants below the period gap would have relatively small mass ratios (because of the large white dwarf masses, e.g. Livio, Shankar & Truran 1988). The discs in nova remnants are thought to have high $\dot{M}_d$: irradiation from the primary, heated by the nova eruption, is expected to heat the secondary and maintain a high rate of mass transfer for a century or more after the explosion. Nova

Table 1.2: Hydrogen-rich nova-like variables and nova remnants with multiple periodicities

Star	Subclass	Orbital period (h)	Photometric period(s) (h)	References
GQ Mus	NR (1983)	?	1.425	12
CP Pup	NR (1942)	1.468	1.587	2,3
BK Lyn	NR? (101 AD)	1.7995	1.8848	15, 16, 20
V348 Pup	NL, IP?	2.444	~ 2.5	19, 1
V795 Her	NL	2.5983	2.796	7, 13
H 0551-819	NL, IP?	2.9518	3.053 (1993)	6
			2.88 (1995)	
V442 Oph	NL (VY Scl)	2.970	2.845 (1983)	4,5
			2.902 (1995)	
MV Lyr	NL (VY Scl)	3.1896	3.312	8
TT Ari	NL (VY Scl)	3.3012	3.192	9, 10
V603 Aql	NR (1916)	3.3157	3.5136	1
T Pyx	RN	3.44	1.825[a]	17, 18
CN Ori	DN[b]	3.917	3.828	14, 21
TV Col	IP	5.487	5.828	11

Notes: NL: nova-like variable; NR: nova remnant; RN: recurrent nova; IP: intermediate polar; DN: dwarf nova.

(a) The photometric period may be the first harmonic of a superhump period (Patterson et al. 1993).

(b) CN Ori is a dwarf nova but *not* a superoutbursting system, so is included here.

References:

1. Patterson et al. 1993; 2. Bianchini, Friedjung & Sabbadin 1985; 3. Warner 1985; 4. Smith & Still, private communication (see chapter 3); 5. This work, chapter 3; 6. Patterson 1995; 7. Shafter et al. 1990; 8. Skillman, Patterson & Thorstensen 1995; 9. Cowley et al. 1975; 10. Udalski 1988; 11. Hellier 1993; 12. Diaz & Steiner 1989; 13. Patterson & Skillman 1994; 14. Schoembs 1982; 15. Skillman & Patterson 1993; 16. Ringwald et al. 1996; 17. Vogt et al. 1990; 18. Schaefer et al. (1992); 19. Tuohy et al. 1990, 20. Warner 1995b; 21. Mantel et al. 1987.

remnants are thus similar to the SU UMa stars in superoutburst in terms of mass ratio and $\dot{M}_d$. The behaviour of nova remnants such as CP Pup and GQ Mus had previously been interpreted as indications of a magnetic white dwarf (e.g. Diaz & Steiner 1989). O'Donoghue (1990) proposed that a superhump interpretation is more likely.

Warner (1995a) suggests that all nova-like variables and nova remnants below the period gap are superhump candidates. The nova remnant GQ Mus, classified as a polar by Diaz & Steiner (1989), is a very good superhump candidate. No circular polarisation was detected in this system by Cropper (1986). Its light curve (figure 1.9) is very similar to that of an SU UMa star in early superoutburst (e.g. TV Crv, see chapter 6). The remnant of the very fast Nova Mus 1983, it is estimated to have a primary mass of $1.2\,M_\odot$ (Warner 1995a section 5.8.3). With a photometric period of 85.5 min that so closely resembles a superhump, it is likely that the orbital period is below the period gap, and consequently that the secondary mass is small. This implies a small mass ratio. In addition, the (irradiation-induced) mass transfer rate is very high: $\sim 1 \times 10^{-7}\,M_\odot\,y^{-1}$ (Warner 1995a section 5.8.6 and references therein). These two criteria — a small mass ratio and a high mass transfer rate — make superhumps a likely option if the system does indeed have a disc. The initial identification of the system as a polar was based largely on the appearance of the light curve. With a mass transfer rate as high as $\sim 1 \times 10^{-7}\,M_\odot\,y^{-1}$, the primary would require a magnetic moment μ_1 greater than $\sim 8 \times 10^{33}\,G\,cm^{-3}$ to prevent a disc from being formed (Warner 1995a equation 7.7). The intermediate polar with one of the strongest magnetic fields (BG CMi) has $\mu_1 \sim 10^{33}\,G\,cm^{-3}$ and polars have $\mu_1 \sim 10^{34}\,G\,cm^{-3}$ (Warner 1995a sections 6.2.1 and 7.2.2). The primary would thus have to have a very substantial field to disrupt the disc completely.

V1500 Cyg was listed as a candidate superhumper by Patterson et al. (1993), on the grounds that it has a polarimetric period which exceeds its photometric period (which is stable, and almost certainly represents the orbital period) by about 2% (Patterson 1979, Stockman, Schmidt & Lamb 1988). However, the primary has a magnetic field strength of ~ 25 MG and is therefore a polar (Stockman, Schmidt & Lamb 1988). The discrepancy between its orbital and polarimetric periods could be the result of the nova eruption in 1975, which may have desynchronised the white dwarf's rotation and the orbital period (Stockman, Schmidt & Lamb 1988). The strong X-ray source V348 Pup (1H 0709-360)

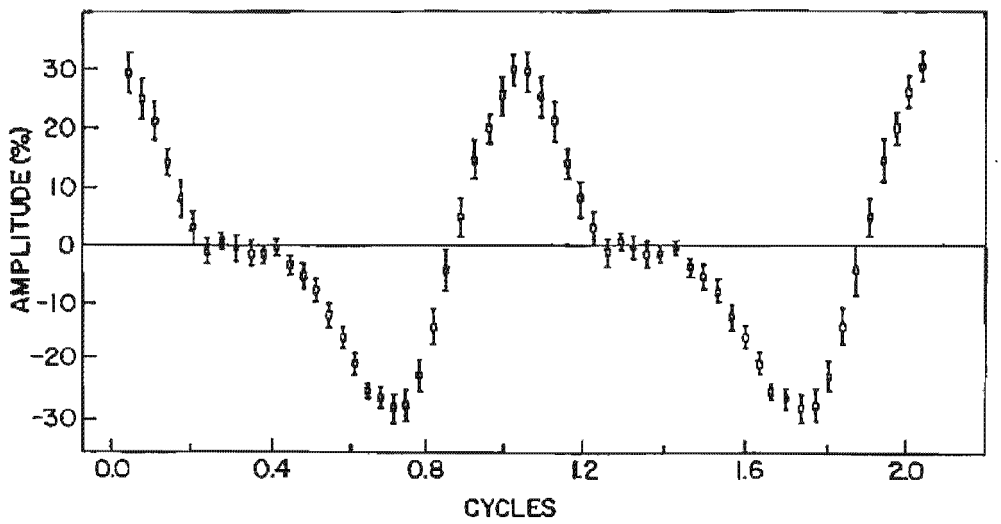

Figure 1.9: Mean light curve of GQ Mus. The pulse shape is strongly suggestive of a superhump – for comparison see figure 6.3 in chapter 6. From Diaz & Steiner (1989).

may also be a desynchronised polar, although Patterson et al. (1993) list it as a superhump candidate. In addition, T Pyx and CP Pup are also listed by Warner (1995a section 6.7) as possible desynchronised polars.

The nova-like variable BK Lyn is an excellent match for an SU UMa star in superoutburst, and was identified as a superhumper by Skillman & Patterson (1993). Its spectra have shallow asymmetric lines (Skillman & Patterson 1993), it has an orbital period similar to an SU UMa star (1.7995 h: Ringwald et al. 1996), it has low-amplitude flickering (consistent with a bright disc) and a photometric period that exceeds the orbital period by $\sim 4.5\%$. The star seems to be an SU UMa star stuck in permanent outburst. The high $\dot{M}_2$ could be the result of an nova outburst: BK Lyn is possibly the remnant of Nova Lyn 101 AD (Hertzog 1986). The amplitude of the superhumps (0.027 mag) is small and the drift in the photometric period is less than $\dot{P}= 10^{-7}$, a factor of ~ 500 smaller than that typically shown by the superhumps in SU UMa stars. This star could represent the equilibrium that the SU UMa stars cannot achieve because of their short-lived outbursts.

H 0551-819 ('Tafelberg') is a superhumper which, during different observing seasons, has shown photometric periods both less than and exceeding its orbital period (Buckley et

al. 1993, Patterson 1995). Photometry from 1993 – 1995 (Patterson 1995) showed a persistent photometric modulation at 2.9518 h (taken to be the orbital period), together with a normal superhump (with a positive period excess) at 3.053 h in 1993. A negative superhump may also have been present in 1994–5 near 2.85 h, although the identification was not as secure as for the normal superhump. Interestingly, the star showed the corresponding beat period between the superhump and the orbital period in the light curve when the each of the superhumps were seen.

CN Ori shows superhump-like behaviour in *quiescence*. Photometric periods at 3.917 h and 3.828 h are reported by Schoembs (1982). Spectroscopic studies in quiescence show the 3.917 h period to be the orbital period. During outburst, the system shows asymmetric absorption lines which vary with a period of 3.7 ± 0.3 d (Mantel et al. 1987): this may be the beat period between the orbital and a superhump period, although not the superhump observed in quiescence!

V1159 Ori, a short recurrence time SU UMa star, has shown negative superhumps on the decline from normal eruptions. These are in addition to the normal superhumps it displays during superoutburst and the late superhumps it shows after superoutburst (Patterson et al. 1995). The negative superhumps are observed to last until quiescence and persist until the next normal outburst (at a diminished amplitude). The dwarf nova V503 Cyg also shows negative superhumps during quiescence and normal outbursts. Negative superhumps and the normal superhumps are, on occasion, present *simultaneously* in the light curve (Harvey et al. 1995).

1.2.3 Precessing accretion discs

It was Vogt (1982) who first suggested that the superhumps in dwarf novae could be due to prograde precession of an eccentric accretion disc around the white dwarf primary. The negative superhumps, with periods less than the orbital period, are thought to be caused by a retrograde precession of the line of nodes of the plane of the disc (i.e. the disc itself does not retrogress), and the disc is tilted with respect to the orbital plane.

1.2.3.1 Positive superhumps: the Tidal Resonance Instability model

Whitehurst (1988) discovered that the accretion discs in systems with small mass ratios are subject to a tidal resonance instability. In a particle simulation of the disc of Z Cha, the initially circular disc was transformed after ~ 1 d into a progradely precessing elliptical disc. Subsequent theoretical studies (Osaki 1989, Hirose & Osaki 1990, Whitehurst & King 1991, Molnar & Kobulnicky 1992, Lubow 1994 and Murray 1996) have refined and extended models of precessing non-circular discs. In these models, the mechanism that causes the superhumps is a periodic enhancement of tidal dissipation that occurs each time the orbiting secondary transits the disc's line of apisides. This will occur with a period that is slightly longer than the orbital period due to the prograde advance of the line of apisides. The superhump frequency is the lower precessional sideband of the orbital frequency, and its period P_s is given by

$$P_s = \frac{P_{pr} P_{orb}}{P_{pr} - P_{orb}}. \tag{1.12}$$

Whitehurst & King (1991) show that the superhump phenomenon can be explained in terms of the resonant behaviour of the accretion disc in the potential well of the secondary. Resonance occurs in the disc when the frequency of radial motion of a particle orbit in the disc is commensurate with the angular frequency of the secondary star. Small perturbations in a particle's orbit can be amplified because the particle will 'see' the secondary in the same position after each cycle. If the prograde apisidal precession frequency is ω_{pr}, the radial (epicyclic) frequency is $\omega - \omega_{pr}$, where ω is the mean angular frequency of the particle in the non-rotating frame. Resonance thus requires that

$$k(\omega - \omega_{pr}) = j(\omega - \Omega_{orb}) \tag{1.13}$$

where Ω_{orb} is the orbital frequency and j and k are positive integers. A j:k resonance appears close to a commensurability of the form j:$j-k$ between particle and orbital frequencies. The strength of a resonance is measured by its growth rate which goes as e^k, where e is the eccentricity of the particle orbit. The strongest resonances thus occur at j:$j-1$ commensurabilities, followed by j:$j-2$ and so on. To see which resonances occur in an accretion disc, we need to compare the radii of the resonant orbits near the

j:k resonance with the disc's tidal radius r_{max}, given by equation 1.3. The radius of the j:k resonance is close to

$$\frac{r_{jk}}{a} = \frac{(j-k)^{2/3}}{j^{2/3}(1+q)^{1/3}} \tag{1.14}$$

and a resonant orbit can exist only where $r_{jk} > r_{max}$. This places restrictions on q. The strongest resonances can only occur for very small mass ratios: $j = 2$, $k = 1$ requires $q \lesssim 0.025$, and even smaller mass ratios for larger j. For SU UMa stars $0.1 \lesssim q \lesssim 0.25$, so this cannot be the resonance that causes superhumps in SU UMa stars. For the next strongest ($k = 2$) resonances, the smallest radius is for $j = 3$. Larger k values give weaker resonances, and larger j values require more extreme mass ratios. The strongest possible resonance in the discs of SU UMa stars is thus at $j = 3$, $k = 2$. The 3:1 commensurable orbits are doubly-periodic in the rotating frame of the binary. For an accretion disc to be able to access r_{32}, the mass ratio of the system must satisfy $q \lesssim 0.22$ (Molnar & Kobulnicky 1992).

Figure 1.10 from Whitehurst (1994) shows a disc evolution simulation for a system with $q = 0.15$. The six frames show the development of a non-circular disc (in the binary frame) during a time of 72 P_{orb}. The primary is centred at the origin and the secondary at (-1,0). Two orbital periods after an initial burst of mass transfer, a circularized torus of gas has formed, the angular momentum of the material in the torus being equal to that of the initial mass transfer stream. The action of angular momentum transfer within the disc causes the initial torus of gas to spread out into an accretion disc (the physical details of this process are not understood but can be parameterized). The outward expansion of the disc is halted by tidal interaction with the secondary which removes angular momentum from the disc at the tidal limit (equation 1.3). In systems with small mass ratios, the outer parts of the orbit are unstable, and the 3:1 commensurability perturbs the particles in the outer parts of the disc. The onset of the development of the asymmetrical disc occurs at $\sim 32\, P_{orb}$ (figure 1.10(d)). The last two frames show the fully-fledged asymmetrical disc.

Warner (1995a) derives an expression relating the ratio of the precession and orbital periods to the mass ratio of the binary. To first order,

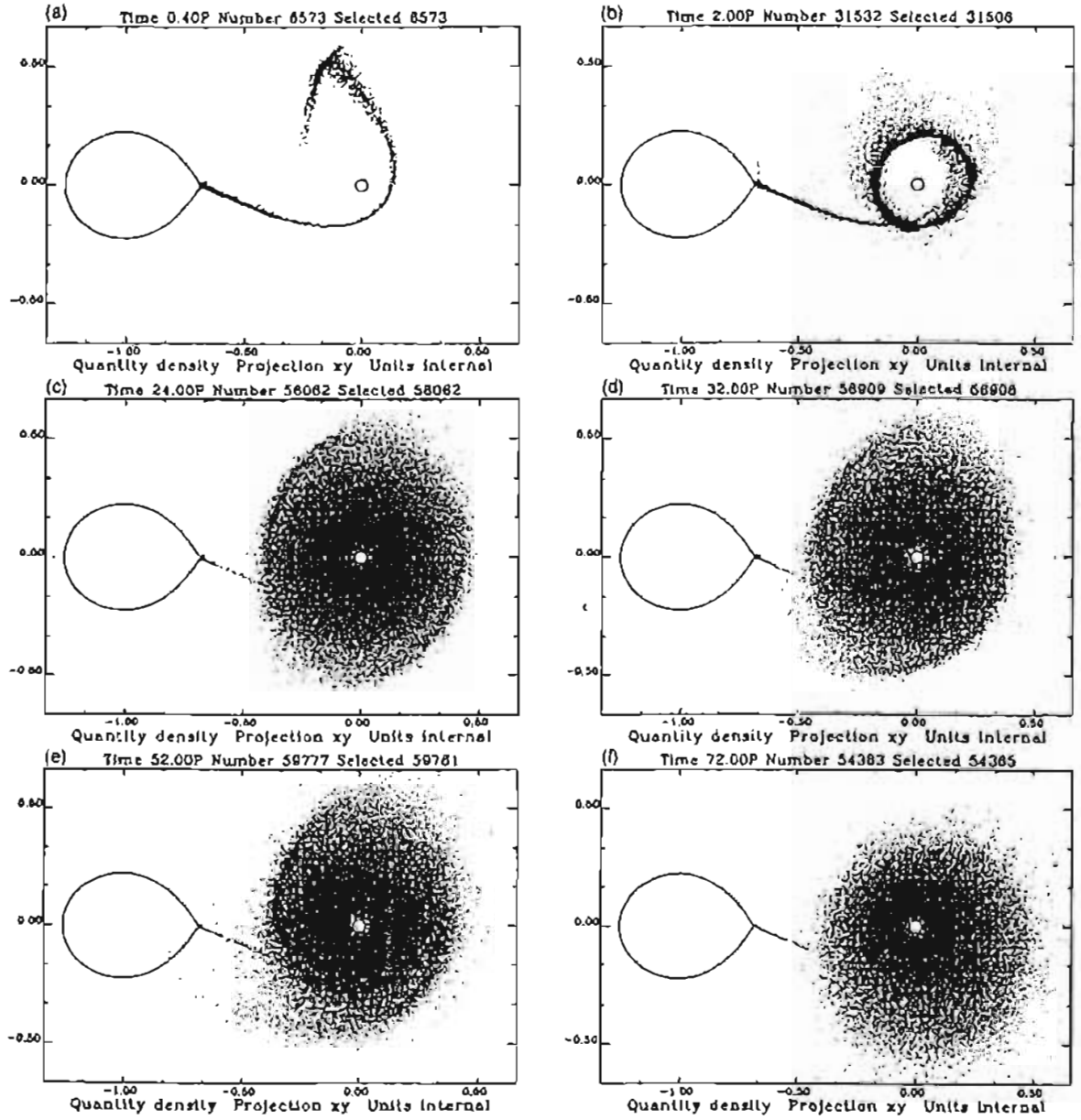

Figure 1.10: Disc evolution simulation for $q = 0.15$ in the binary frame. The first two frames show the inital formation of the disc. After 32 P_{orb} the effects of tidal resonance begin to produce a precessing, asymmetrical disc. From Whitehurst (1994).

$$\frac{P_{pr}}{P_{orb}} = A\frac{1+q}{q} \tag{1.15}$$

where $A = 3.85$ for $0.1 \lesssim q \lesssim 0.22$ and $A = 3.73$ for $q \gtrsim 0.05$. With the exceptions of the long recurrence time, large outburst amplitude systems such as WZ Sge, the precession periods in SU UMa dwarf novae are $P_{pr} \approx 2.2\,\mathrm{d}$.

Nova-likes and nova remnants with $P_{orb} \gtrsim 3\,\mathrm{h}$ will not have mass ratios as small as those of the SU UMa systems, yet several show photometric periods that exceed the orbital periods (e.g. MV Lyr, V603 Aql, V442 Oph). Using equations 1.14 and 1.7, a system with $q \gtrsim 0.3$ would have to have a disc radius greater than 90% of the primary's Roche lobe to access r_{32}. This is not in conflict with observation: the disc radii of eclipsing nova-likes and (in particular) nova remnants are large, and in several cases approach the size of the primary's Roche lobe (Harrop-Allin & Warner 1996). Note that there are no eclipsing or high-inclination systems in table 1.2: observational selection may have resulted in many non-P_{orb} periods being overlooked. V442 Oph may be a low- inclination analogue of the SW Sex stars (M. Still, private communication).

In SU UMa stars, the changing superhump period can be explained in terms of shrinkage of the disc (Warner 1995a section 3.6.6.3). Patterson et al. (1993) postulate that the drifting period in V603 Aql could arise from small changes in the outer radius of the disc.

Late superhumps may arise from bright spot brightness modulations (e.g. Osaki 1985, Whitehurst 1988). The distance between the secondary and the point of impact of the mass transfer stream on the disc varies because of the eccentric precessing disc. The position of the bright spot has a varying depth within the potential well of the primary, and the bright spot light is thus modulated at the superhump period. The effects of disc overflow may also be significant: part of the mass transfer stream flows over the face of the disc and continues until it impacts on the disc at a later time, creating a second bright spot in the vicinity of the point of closest approach to the primary (Lubow 1989). Variations in the amount of disc overflow could occur as a result varying disc rim height. There are problems with this model, the most important of which is that the eccentricity of the accretion disc in SU UMa stars may not be sufficiently large to modulate the bright

spot brightness at the amplitudes observed for late superhumps (e.g. van der Woerd et al. 1988, Hessman et al. 1992).

A precessing, non-circular disc can also account for the variable line asymmetries observed in superhumping systems. Theoretical radial velocity variations calculated using two-dimensional hydrodynamic simulations (Hirose & Osaki 1990, 1993) show variations in γ-velocity with the superhump beat period that are similar in phase and amplitude to observed γ-velocity variations.

1.2.3.2 Negative superhumps

Less is known about the mechanism that produces negative superhumps. The few CVs showing this effect have little in common. Unlike normal superhumps, negative superhumps seem to show no preference for shorter orbital periods and smaller mass ratios (e.g. CN Ori with $P_{orb} = 3.917\,\mathrm{h}$ and TV Col, with $P_{orb} = 5.487\,\mathrm{h}$). Negative superhump amplitudes are widely different from system to system: they range from less than 0.003 to 0.60 mag (Harvey et al. 1995).

Negative superhumps could be produced by a *retrogradely* precessing disc that is tilted with respect to the orbital plane. While the precession period of a progradely precessing, non-circular disc will not necessarily be observed in the light curve, a *tilted* disc may produce a brightness modulation at P_{pr} because of the varying aspect of the bright inner regions of the disc (in the higher inclination systems) and the changing inclination of the disc to the line of sight. A retrograde precession period of 4 d is seen in TV Col (Barrett, O'Donoghue & Warner 1988, Hellier 1993) and a 3.8 d period is seen in TT Ari (Udalski 1988). The mechanism that would produce the brightness variation that we see as a negative superhump is not known.

Devising a theory whereby a tilted disc is produced and maintained in a binary system is difficult. This is because unless viscosity is large enough to couple the annuli together each annulus in a Keplerian disc will precess with a different period, producing a twisted disc. Also, matter from the mass transfer stream has to be fed to the disc in such a way as

to maintain the tilt. Several mechanisms that could drive the disc out of the orbital plane have been proposed by Iping & Petterson (1991), but all involve very high luminosities (approaching the Eddington limit) or relativistic effects, neither of which are appropriate for CVs. Barrett, O'Donoghue & Warner (1988) propose a tilt-maintaining mechanism in which the mass transfer stream is initially forced out of the orbital plane because of channelling by magnetic fields on the secondary.

The precession period of a tilted, retrogradely precessing disc can be approximated by

$$\frac{P_{pr}}{P_{orb}} \approx 2.86 \frac{(1+q)^2}{q} \tag{1.16}$$

(Warner 1995a section 2.5.6).

In systems that show both negative and positive superhumps (e.g. V503 Cyg), the difference between the orbital period and the superhump period is smaller for the negative superhump than for the normal superhump. Comparing different systems, the period excess ϵ_{pos} for normal superhumps is usually larger than the difference between the orbital and the negative superhump periods ϵ_{neg} (see e.g. figure 17 in Patterson et al. 1992). Neverthless, ϵ_{pos} and ϵ_{neg} are similar, even though they originate from different mechanisms. This is because the time scales for non-circular precessing and tilted precessing discs are both governed by the same departure from a central potential (as felt by the particles in orbit around the primary).

1.3 The case for superhumps in the AM CVn stars

The idea that the photometric behaviour in the AM CVn stars could be due to tidal interactions between the outer disc and the secondary was first proposed by O'Donoghue & Kilkenny (1989). Systems that are good superhump candidates have (1) small mass ratios (smaller than about 0.22) and (2) high rates of mass transfer (comparable to that of an SU UMa dwarf nova in superoutburst: $\dot{M}_2 \sim 3 \times 10^{-9}$–$1 \times 10^{-8}\,M_\odot\,y^{-1}$).

The AM CVn stars have orbital periods even shorter than those of the SU UMa stars, and will thus have smaller mass ratios. To estimate the mass ratios in the AM CVn stars, we have to use the M_2–P_{orb} relation that is appropriate for degenerate secondaries (equation 1.9). For an orbital period of ~ 0.4 h, the mass of the secondary is $0.06\,M_\odot$. Taking $M_1 \approx 0.74$ (the average primary mass for nova-likes, Warner 1995a), q is approximately 0.08. Because of the small mass ratio, the disc of an AM CVn star can easily access the r_{32} radius. For $q = 0.08$, the tidal limitation radius of the disc is $0.56\,a$, whereas $r_{32}/a = 0.40$. The tidal resonance radius is only slightly larger than the *smallest* radius the disc can have. The minimum (circularization) radius r_r is given by equation 1.2; for $q = 0.08$, $r_r/a \approx 0.3$. Comparing equations 1.2 and 1.14, a system with $q \approx 0.01$ will have a *minimum* disc radius equal to the r_{32} radius (such a disc will also be able to access the much stronger 2:1 resonance).

The other requirement for superhumps, a high mass transfer rate, is certainly satisfied by AM CVn and EC 15330 (equation 1.10). CR Boo, V803 Cen and CP Eri are in a quasi-stable state where the mass transfer rate is comparable to that of AM CVn and EC 15330 in the high state, but in the low state may be insufficient to provide sufficient mass at r_{32} to maintain superhumps. GP Com has too low a mass transfer rate (and probably too small a disc) to produce permanent superhumps.

The optical flux gradients and broad-band colours (in the high state) of AM CVn stars are well-fitted by blackbody distributions with temperatures near 20 000 K. Partial helium ionisation occurs at a similar temperature, and would provide an efficient mechanism for driving pulsations. This argument has been used (e.g. by Provencal et al. 1995) to speculate that the white dwarf primary in AM CVn stars may be pulsating, and that the photometric variations can, in part, be accounted for by pulsation. However, the temperature estimates for the AM CVn stars refer to the colour temperatures of the *accretion discs* and not the primaries. Pulsations in an accretion disc show theselves as QPOs, because each annulus of the disc oscillates with its own frequency, and the pulsation manifests itself as a broad region of power. Pulsation cannot account for the complex photometric behaviour seen in the AM CVn stars.

The variable line asymmetries in AM CVn have obvious similarities to those seen in the

superoutbursting SU UMa stars. The drifts in radial velocity observed by O'Donoghue & Kilkenny (1989) in V803 Cen are due to drifts of the γ-velocity that occur over time scales of several hours. O'Donoghue & Kilkenny (1989) show that the long time scale drifts constrain the mechanisms that cause the asymmetry to be either

- deviations from axisymmetry of the light emitted by various parts of the disc – the asymmetry variations are then due to geometrical effects in a binary with an orbital period equal to the period of the line asymmetry variations.
- an intrinsic feature of the line profile in a disc with an axisymmetric brightness distribution – the asymmetry variations are then due to physical changes in the line-forming region.
- an asymmetrical brightness distribution in the disc which changes more slowly than the orbital period.

The first option cannot be correct, since a Roche lobe-filling helium secondary in a binary with an orbital period of several hours would have a mass of several solar masses. Such a star would produce easily-detectable radial velocity variations (which are not seen) and would be very luminous and dominate the spectrum, especially in the low states of CR Boo, V803 Cen and CP Eri. The second option requires a periodic fine-tuning of the electron density in the line-forming region around a value of 10^{17} cm^{-3}, which is implausible. The final option is the most probable, especially seeing as the hydrogen-rich counterparts of the AM CVn stars show similar behaviour. This conclusion points to a model in which tidal instabilities are the cause of both the photometric variations and the line asymmetry variations.

1.3.1 The predictions of the superhump model

The identification of the principal photometric period as a superhump period allows us, in principle, to determine the orbital periods of the AM CVn stars, and, through equation 1.15, their mass ratios. However, to use equation 1.12, we need to know the precession

period of the accretion disc, which will be the period of the line profile asymmetry variation. The precession period is known only for AM CVn, where the line profile asymmetries vary on a period of 13.38 h (Patterson, Halpern & Shambrook 1993). However, the precession period also reveals itself in *photometry* as fine structure accompanying the harmonic peaks (e.g. Provencal et al. 1995) — the inverse of the separation between the multiplet peaks is equal to the precession period. A way to identify the precession period in the other AM CVn stars would be to search for low-amplitude peaks on the high-frequency side of the harmonic peaks that are separated from the harmonic peaks by a constant amount. However, without WET data to reduce the aliasing in amplitude spectra of high-speed photometry, the identification of fine structure in an amplitude spectrum is difficult.

For AM CVn, the precession period is known, but what precisely is the principal photometric period? The commensurate periods in AM CVn are harmonics of 1051 s, but the power at this frequency is much weaker than that at the harmonics, and is often buried in the noise (e.g. Provencal et al. 1995). If the light curve is folded on 1051 s, the alternate minima and maxima are not equal, implying that there is some power at 1051 s (Patterson et al. 1992). The fact that the fine structure splitting is a constant 20.77 μHz for the lower as well as the higher harmonics, led Provencal et al. (1995) to insist that the periodic structure is not consistent with harmonics of a 1051 s period. Instead, they describe the photometric periods in terms of the dominant 525.6 s period. The absence of a substantial signal at the fundamental frequency is, however, atypical of the AM CVn stars: EC 15330, the star most similar to AM CVn, has a fundamental frequency of 1119 s with two harmonics. Looking to the hydrogen-rich systems for similar behaviour (i.e. power that is predominantly in the first harmonic of the superhump period) we notice the late superhumps, which are shifted by $\sim$ 0.5 of a superhump cycle with respect to the original superhumps. If the late superhump and superhump amplitudes were comparable, the light curve would be double-humped with the dominant power at the first harmonic. The light curve of the SU UMa star V1159 Ori in late superoutburst is distinctly double-humped (Patterson et al. 1995). At this stage, the light curve of V1159 Ori closely resembles that of AM CVn (see figure 1.11): this similarity was pointed out by O'Donoghue (1993). The problems with the late superhump mechanisms for the SU UMa stars outlined in section 1.2.3.1 are that the eccentricity of the accretion disc may

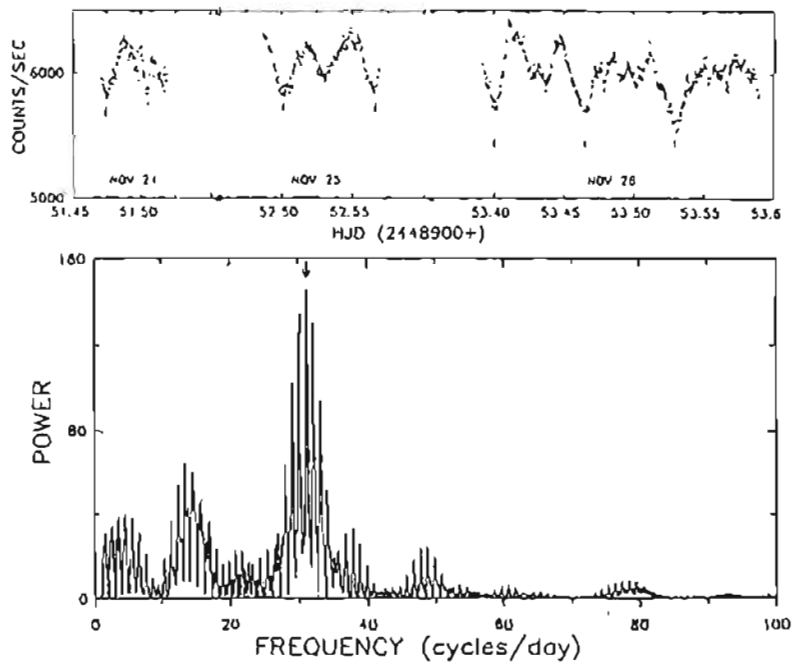

Figure 1.11: Light curve and the corresponding power spectrum of V1159 Ori in late superoutburst, from Patterson et al. (1995). The tick marks on the light curve indicate the minima separated by the superhump period. The dominant peak in the power spectrum is at a frequency corresponding precisely to the first harmonic of the superhump period. AM CVn shows a similarly double-humped light curve.

not be sufficient and the energetics of the bright spot are not large enough to produce the observed late superhump modulations. However, in SU UMa stars, $\dot{M}_2$ is relatively small compared with $\dot{M}_d$, whereas they are equal in AM CVn. Also, the small disc radius of AM CVn results in a more luminous bright spot (section 1.1.4.4) than is expected for a hydrogen-rich nova-like, which has a comparable $\dot{M}_2$. The bright spot in AM CVn might produce a late superhump with an amplitude comparable to that of the normal superhump, resulting in a double-humped light curve.

If the principal period is indeed 1051 s, the orbital period of AM CVn (equation 1.12) is 1028.77 ± 0.18 s (Patterson, Halpern & Shambrook 1993). There is a weak signal at the orbital frequency in figure 3 of Solheim et al. (1991) with an amplitude of 0.0012 mag. From equation 1.15, the mass ratio of AM CVn is 0.084. The variable 1490 s period in CR Boo is its superhump period, and the coherent 1471.4 s period is probably P_{orb}, implying

a mass ratio of 0.057. In addition, upper limits for the mass ratios of V803 Cen and EC 15330 can be found by using the observed upper limits on K_1: in V803 Cen $q \leq 0.043$ and EC 15330 $q \leq 0.066$. In GP Com, the observed $P_{orb} = 2790\,\mathrm{s}$ and $K_1 = 14.6\,\mathrm{km\,s^{-1}}$ yield $q = 0.039$ and $i \approx 30°$ (Warner 1995b). If the accretion disc in AM CVn fills $\sim 80\%$ of its Roche lobe (reasonable for nova-like variables with high mass transfer rates), the disc size is $\sim 6.0 \times 10^9\,\mathrm{cm}$.

Because these estimates of q are model-dependent, there is a possibility that the mass ratios in the AM CVn stars are sufficiently small for the discs to be able to access a higher resonance than the 3:2 resonance. To access the 2:1 resonance, a system would have to have $q \lesssim 0.025$.

The disc precession period for AM CVn is 13.38 h; are similar precession periods expected for the other AM CVn stars? If equation 1.9 is substituted into equation 1.15, we see that

$$P_{pr} = 200.5\, M_1 (1+q) {P_{orb}}^{2.274}\,(\mathrm{h}) \tag{1.17}$$

The $(1+q)$ factor is roughly constant (because q is small), and the precession period is thus proportional to ${M_1 P_{orb}}^{2.274}\,(\mathrm{h})$. If we assume that the primary masses are the same (which they are probably not), the beat period for CR Boo would be $\sim 30\,\mathrm{h}$. This compares well with the beat period between the periods identified as P_s and P_{orb}, which is $\sim 32\,\mathrm{h}$. Rough guesses for the other systems (using the photometric periods for P_{orb}) are 16 h for EC 15330, 37 h for V803 Cen and 43 h for CP Eri. In the SU UMa stars, there is a correlation between P_{pr} and P_{orb}, with scatter coming from the different primary masses (Warner 1995a equation 3.43). In the AM CVn stars we do not yet have enough empirical data to see a correlation between P_{orb} and P_{pr}, but a similar correlation may exist, with scatter coming from variations in M_1.

If the commensurate periods in the AM CVn stars are caused by a non-sinusoidal superhump, what are the non-commensurate periods? Patterson et al. (1993) postulate that the 1011 s period in AM CVn is a negative superhump. This would mean that, when the 1011 s period is present, the eccentric disc is tilted with respect to the orbital plane and has both regressing nodes and an advancing line of apisides. It would also mean that we

might see the beat period between the negative superhump and the orbital period (i.e. 16.5 ± 0.3 h) in the light curve. In addition, we might expect the absorption line widths to change if the disc tilt is large enough. Patterson, Halpern & Shambrook (1993) do not detect either line width changes or a photometric period at the 16.5 h period when the 1011 s period was present in the light curve. This sets a stringent upper limit of a few degrees to the amplitude of the tilt in the inner disc (where the highest velocities exist). A warped *outer* disc is not disallowed by these observations.

The 175 s period in V803 Cen could be a QPO arising in the accretion disc. Such periods are seen in a wide variety of CVs (including a number of SU UMa stars and nova-like variables: see table 8.2 in Warner 1995a) but are in general far less stable than the 175 s period appears to be (O'Donoghue & Kilkenny 1989). It is possible that V803 Cen has an intermediate polar structure, and that the 175 s is the spin period of the primary. This period is short enough that V803 Cen would most likely be a star like DQ Her, with little hard X-ray emission (Warner 1995a chapter 8).

Chapter 2

CCD Observations

Although the data presented in this study were taken from several rather diverse sources, all observations obtained specifically for this dissertation were acquired at the Sutherland observing station of the South African Astronomical Observatory, using the University of Cape Town high speed Wright CCD photometer. This chapter outlines CCDs in general and the UCT Wright camera in particular, discusses the structure and characteristics of these devices, and why CCDs have become the detector of choice for many astronomical applications.

2.1 The CCD detector

2.1.1 Structure and operation

The CCD has become extremely popular for astronomical applications because of its linearity, area imaging capabilities and high quantum efficiency. The CCD detector is a metal oxide semi-conductor solid state integrated circuit composed of a two-dimensional array of discrete electrodes (usually made of silicon). The electrodes are arranged on the CCD imaging surface in closely spaced columns that are separated by channels running perpendicular to the electrodes. The channels prevent any sideways movement of charge and are a few micrometres wide. In a three-phase CCD, a single pixel is defined by a set of three parallel electrodes and the two channels on either side. The readout section of

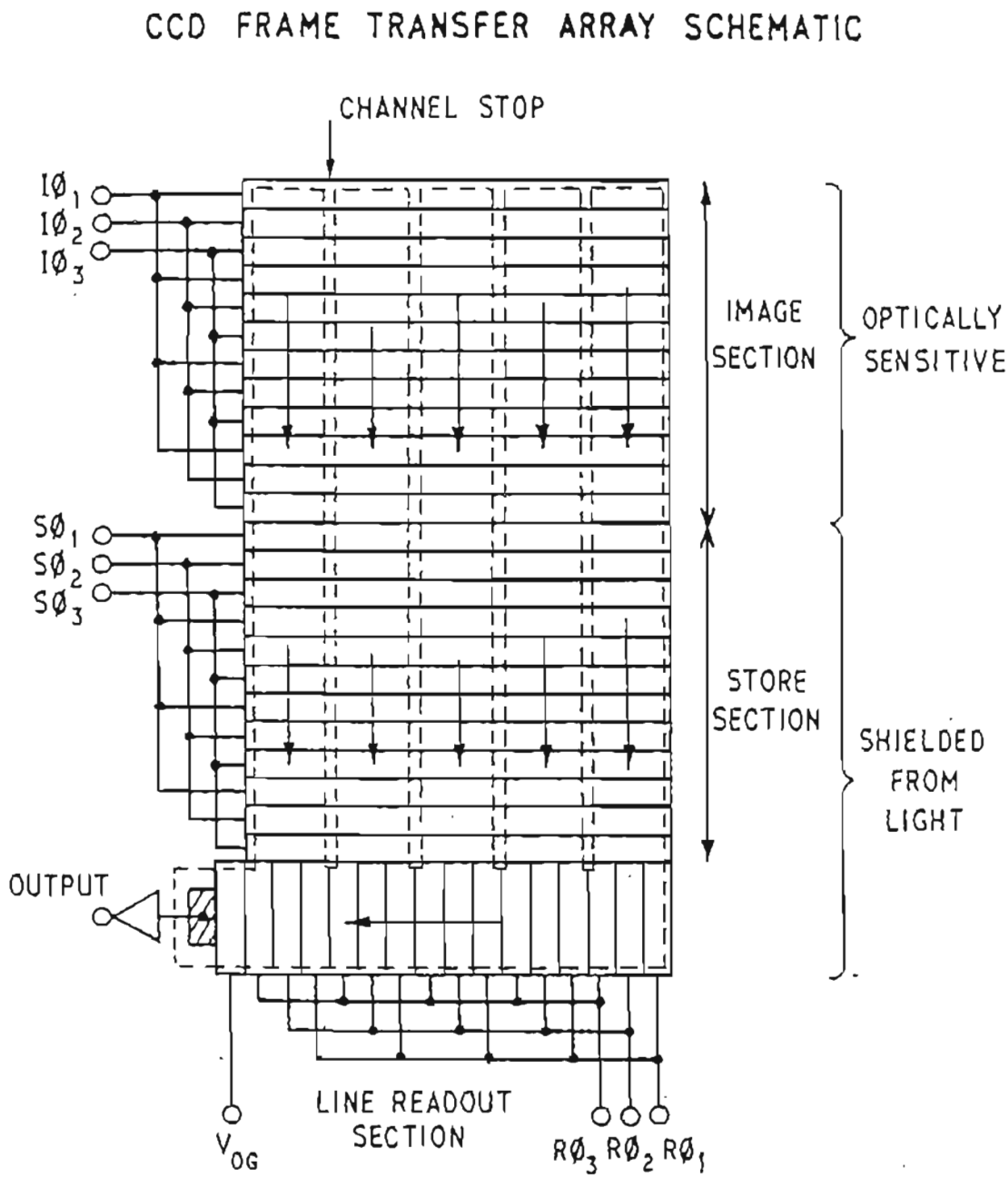

Figure 2.1: A schematic diagram of the UCT Wright frame transfer CCD. The main area of the device is divided into two regions, the image and the storage region, each with separate clock connections. Below the storage region is the output register (line readout) leading to the output amplifier.

the CCD is a single row of electrodes on one side of the chip running perpendicular to the electrodes which comprise the imaging area of the CCD. This row is the output register, which leads to an output amplifier (see figure 2.1).

During an exposure, one of each triplet of electrodes in a pixel is held at a positive voltage while the other two are held at ground level. This creates a potential well in each pixel which can accumulate negative charge. When a photon strikes the surface of the CCD array and is absorbed by the silicon, an electron is released from the valence band and promoted to the conduction band where its movement can be influenced by an electric field. The electron is attracted to the nearest potential well and stored there. At the same time, a hole is created by the removal of the electron; this hole is repelled from the potential well and vanishes through the silicon substrate. During an exposure electrons accumulate in each potential well; the total charge in each potential well is proportional to the number of photons incident on that pixel.

At the end of an exposure the two-dimensional charge distribution is read out. Each step of the readout involves changing the voltages applied to each electrode so that the potential wells move towards the output register, carrying the accumulated charge with them; this is called "clocking" the device. Each full clock cycle (three phases) will move the charge of each pixel to the adjacent pixel. Charge in the last row of electrodes before the output register is moved into the output register. The output register is then clocked repeatedly to move the potential wells and the charge they contain to the output amplifier.

As the charge in each pixel arrives at the output amplifier, it is transferred to a capacitor, producing a change in the voltage of the capacitor. This voltage change is measured by the camera electronics as an analogue signal and is then digitised to form the output signal. The final signal is represented in ADU (analogue-to-digital units); the number of ADU depends on the gain of the CCD. The Wright CCD was operated with a gain of 10 electrons per ADU.

The output signals are then sent to an acquisition system where the images can be displayed and stored (or reduced on-line). In the case of the UCT Wright camera, signals are sent from the CCD electronics module via a coaxial cable to a personal computer running

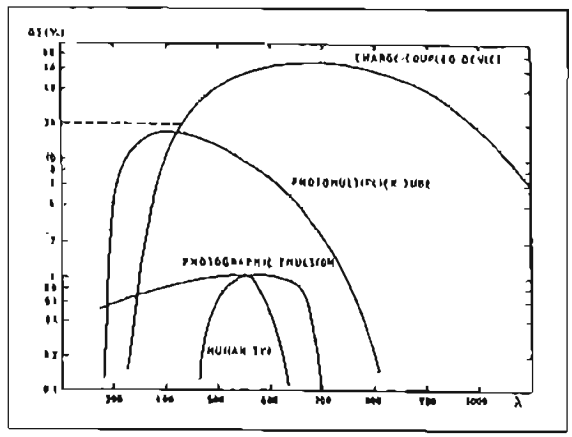

Figure 2.2: A comparison of the quantum efficiencies of CCDs and other detectors (from Sterken & Manfroid 1992)

the acquisition software. Each signal contains 16 bits of image data. The incoming frames are passed via an ethernet connection to a Sun workstation for storage. Preliminary reductions can be performed on the workstation, allowing the observer to monitor the data in near-real-time. The stored frames are reduced with care at a later stage (see section 2.2).

2.1.2 Characteristics

2.1.2.1 Quantum efficiency

The quantum efficiency (QE) of a detector is the ratio of the number of photons detected by the device to the number of incident photons, usually expressed as a percentage. The QE of the CCD detector exceeds that of both photomultipliers and photographic plates, as shown in figure 2.2. Peak efficiencies for CCDs can exceed 80%.

Because silicon is more transparent to light of longer wavelengths, red photons pass further into the silicon than light of shorter wavelengths. CCDs therefore have good red responses out to 1μ. CCDs are less sensitive to blue photons, which are readily absorbed in the electrodes covering the surface of the device. To improve the blue response of a

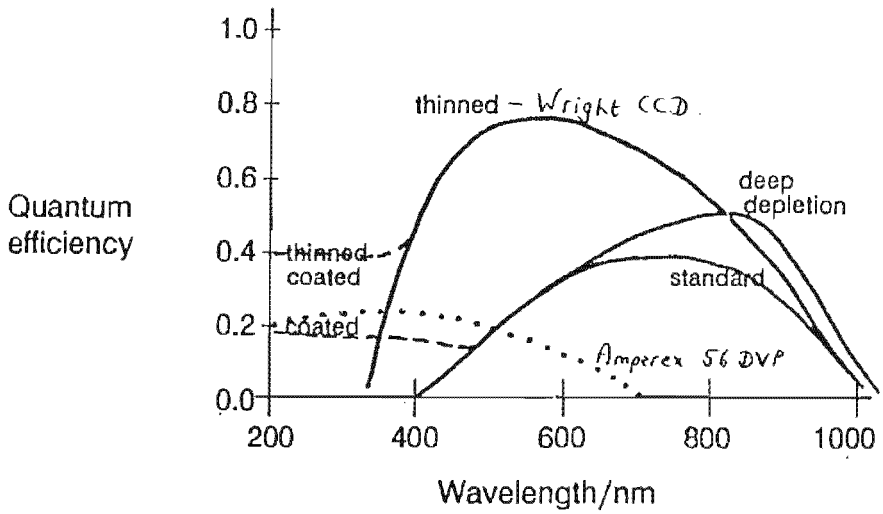

Figure 2.3: Quantum efficiency curves for various types of CCD. The quantum efficiency curve for the blue-sensitive Amperex 56 DVP tube on the University of Cape Town photometer is shown for comparison

CCD the chip can be thinned and used upside down so that the starlight falls on the back of the chip, a procedure called "back illuminaton". This extends the blue response to $\sim 3500\AA$. The UCT Wright CCD is a thinned, back-illuminated device. The blue response of a CCD can be extended further by coating the chip with a phosphor layer. The phosphor coating absorbs photons with wavelengths less than about $4200\AA$ and re-emits photons with wavelengths of around $5500\AA$; in this way the CCD's response can be extended to $\sim 2000\AA$. The result is a flat response throughout the B band (with a QE of $\sim 40\%$): a coated chip would thus not be a good choice for observing blue stars like CVs. Figure 2.3 compares the QEs of different types of CCD, showing typical values (the peak QE of the UCT Wright CCD is measured to be 68% at $5500\AA$).

2.1.2.2 Charge transfer efficiency

When charge is transferred across a CCD, not all the electrons in each pixel will advance as the potential well is moved. Residual charge from one pixel usually appears in the following pixel. However, poor charge transfer may affect an entire column, or, if

the efficiency is poor in the output register, rows will be affected. For the Wright CCD the charge transfer efficiency is given in the manufacturer's specifications as a 1% charge loss for a transfer from the diagonally opposed corner of the device to the output amplifier.

Possible causes of charge transfer inefficiency include a clocking frequency that is too high for the electrons to follow the moving potential wells, and impurities or defects in the device structure which prevent charges from being transferred to the next pixel. Such "charge traps" cause problems in certain (mainly older) CCD designs. The solution in these cases is to pre-flash the chip before an exposure so that the charge traps are filled and all charges above the pre-flash level are transferred efficiently. Charge trapping does not appear to be a problem with the Wright CCD.

2.1.3 Nonlinearity and saturation

A potential well on the CCD can hold only a certain amount of negative charge; the well will be able to hold electrons as long as their combined negative charge is smaller than the positive potential of the well. This maximum charge storage capacity is the *full well capacity* of the potential well. At high exposure levels, when the charge stored in a pixel approaches full well capacity, the response of the pixel becomes nonlinear. The nonlinear response of the well manifests itself as a drop in the quantum efficiency. In the Wright CCD this occurs at levels above $\sim 210\,000$ electrons per pixel.

When the charge stored in a pixel equals or exceeds the trapping potential of the well, the pixel becomes "saturated" and charge can spread up and down the CCD columns. Saturation in the Wright CCD occurs at $\sim$ 300000 electrons per pixel. In some CCD systems the saturation level is set, not by the trapping potential of the CCD pixels, but by the digitisation electronics; a signal larger than the largest number representable in the electronics will produce a saturated result.

2.1.4 Sources of noise

Several noise sources limit CCD performance. Photons behave according to Poisson statistics: the intrinsic noise in the signal is the square root of the number of electrons registered by the detector in a particular pixel. Poisson noise cannot be eliminated or reduced, it is intrinsic noise that is present in any measurement of a light source.

Thermally excited electrons in the silicon layer of the chip are indistinguishable from electrons excited by collisions with photons in the incident sky- and starlight. In the absence of light, thermal effects will give rise to a *dark current* I_d of the form

$$I_d = A\, e^{\frac{-B}{kT}} \tag{2.1}$$

where A and B are constants for the device, T is the device temperature and k the Boltzmann constant. Lowering the operating temperature of the device to an appropriate level will lower the dark current to a level where the dark current is small in comparison to other noise sources. The Wright camera is cooled by a 4 stage Peltier cooler which gives an operating temperature of $\sim$ 200K. At this temperature the dark current is typically 0.03 electrons per pixel per second, and is negligible for most imaging applications. Dark current is usually fairly uniform over the chip and can be represented as a single value for the whole detector, but CCDs sometimes display dark current spikes at pixels where the dark current is unusually high; this results in bright pixels in the image data which may be more troublesome than the dark current background.

A further type of noise is created by the transistors in the output amplifier. This is the *readout noise* which is present in each signal produced by the camera: the more pixels covered by a stellar image, the larger the readout noise. In observations of extremely faint sources one can use a focal reducer that concentrates the stellar image on only one pixel; in this way the readout noise for that image is reduced to that for one pixel. Readout noise is essentially an uncertainty in the number of ADU registered by the chip electronics and is a statistical deviation with a zero mean and a Gaussian distribution. The Wright CCD has a readout noise of less than 10 electrons RMS. Readout noise increases as the readout rate is increased.

Further uncertainty is introduced during the conversion of the output signal from analogue to digital. The size of this *digitisation noise* depends on the gain of the CCD and the type of analogue-to-digital converter used. A CCD gain of 10 electrons per ADU will yield an output signal of 1 ADU for 10 electrons; it will also yield 1 ADU for 19 electrons: the remaining 9 electrons are lost. As a result, the analogue-to-digital conversion process may throw away as much as 1 ADU per pixel in any integration.

In addition to all these noise sources, cosmic rays and other ionizing particles are a source of random noise that will be present on any CCD frame. The reduction software that extracts data from the CCD images must be able to deal with cosmic ray hits and distinguish them from stellar images.

2.1.5 Frame transfer CCDs

A conventional CCD is not the ideal detector for high speed photometry because the time taken to read out the chip creates a dead time between exposures. Increasing the speed of readout will increase the readout noise. However, *frame transfer* CCDs without shutters (often used in video devices) are ideally suited to high speed photometry.

In a frame transfer device, half the chip is masked and is used as an image store buffer while the other half is exposed to starlight (see figure 2.1). When the exposure is finished, charge from the exposed half of the chip is transferred rapidly to the storage half. The storage half is then read out by the CCD controller, amplified and digitised while the image half is collecting photons for the next frame. The transfer of charge from the image half to the storage half of the chip takes only a few milliseconds; during this time no shutter is used, but the faint star trails that result are undetectable in the background noise. In this way a frame transfer device can produce a series of images of a particular field with almost no dead time.

The time taken to read out the storage half of the chip, send the digitised signals to the acquisition computer and write the image to disk, sets the limit on how quickly successive frames can be taken, and thus determines the shortest integration time of the data.

The highest time resolution possible with the UCT Wright camera and its peripherals is about 10 seconds. Although it takes only $\sim$ 4s to read out the storage half of the CCD, the acquisition computer takes a total of 8 to 9 seconds to write this information to the Sun workstation; the time taken depends to a certain extent on how full the Sun's disk is. If the camera electronics send frames to the acquisition computer faster than the computer can write these frames to the Sun workstation, the whole system freezes. In practice the shortest time resolution for data produced by the UCT CCD system is 10s.

2.2 Data Reduction

CCD data reduction is a complex image-processing job which is the equivalent of the usual steps of sky subtraction and correction for atmospheric extinction in reductions of photometric data from a photomultiplier. The following description outlines the various steps in the reduction procedure for a typical CCD high speed photometry data set.

2.2.1 Debiasing

Because of the random nature of readout noise and Poisson noise from the sky and observed objects, it is possible that spurious negative values can be produced in the signal; these would cause problems during the analogue-to-digital conversion process. To avoid this, an electrical offset is applied to the CCD before readout by adding a constant amount of charge to each pixel. This level is the *bias* of the frame. Since the exact value of the offset is subject to some random variation, the bias has to be calculated for each frame individually. This is done by measuring the values in the overscan region of the chip. The overscan region does not correspond to a physical area of the chip but is measured by clocking the CCD further after the real charge distribution has been read out. The charge values in the overscan region are subject to the same instrumental effects experienced by the rest of the chip, apart from the exposure to sky- and starlight. To debias a CCD frame, the mean number of ADU per pixel for each row in the overscan region is calculated and a polynomial is fitted to these values. The polynomial is subtracted from each column on the imaging portion of the CCD.

2.2.2 Flat-fielding

It has been remarked that "the only uniform CCD is a dead CCD" (Charles Mackay) - although the response of each pixel in a CCD is linear, not all pixels have the same sensitivity. This results in a spatially non-uniform response across the chip which must be corrected before any attempt is made to extract data from a frame. This sensitivity variation can be due to manufacturing imperfections such as inhomogeneities in the substrate material, geometrical variations between pixels (including dust grains or any object projecting a shadow on the photosensitive surface), or mechanical stresses caused by the thinning process.

There are two ways in which sensitivity varies across the chip. Overall sensitivity gradients cause low frequency variations (as a function of, for example, substrate thickness) of the order of tens of percent, while smaller high frequency pixel-to-pixel variations ("granularity") cause variations of a few percent. To correct for these variations, each frame is divided by a correction image – the flat field – to obtain a frame with a spatially uniform response. Correct flat-fielding is crucial: flat-fielding errors cause the brightness of a star to depend on its position on the chip.

A flat field image is obtained by exposing the chip to a uniform light source such as the twilight or dawn sky in the same way that the scientific exposures are made. Usually, several flat field images are taken for each filter and an average of these images is used in the reductions. Sharp variations in the illumination (such as bright stars that are significantly brighter than the twilight or dawn sky background) should be avoided as they might be confused with the pixel-to-pixel granularity. The count rate per pixel in each individual flat field image should be fairly high so that its noise level is smaller than the granularity: in the case of the UCT Wright CCD, the total number of ADU per pixel in a flat field image was chosen to be between 12000 and 18000.

2.2.3 Data extraction

Once the bias has been subtracted from a CCD frame and the frame has been divided by the flat field image, information about the brightness of the objects on the frame can be extracted. Two methods are used: aperture photometry and profile fitting.

2.2.3.1 Aperture photometry

The total number of ADU in the image of an object is summed inside a software-defined aperture. Background subtraction is done by subtracting the modal value of the signal in the pixels in a comparison area. Because it is best to observe the background at symmetrical locations around the star in order to take into account any linear trend in the background brightness, the best option is to use an annulus around the star as the comparison area. The inner radius of this annulus is chosen to be sufficiently large to avoid the wings of the stellar image.

2.2.3.2 Profile fitting

Although a star is a point source, the atmosphere produces a seeing profile which is approximately Gaussian in its central part. The optical path followed by the starlight through the telescope further modifies the stellar image so that the real stellar brightness profile appearing on a CCD frame is an unknown time-, position- and signal-dependent function called the *point-spread-function* (PSF). The PSF represents the variation of the brightness of the image relative to the centroid of the image. Because of seeing variations and imperfect guiding, the PSF for stellar images may vary on a time scale comparable to the exposure time, and the PSF thus has to be calculated for each frame. Sometimes a single frame may require several different PSFs.

The PSF may be represented as an analytic function or as an empirical array of values determined from examining several images on the frame; the array is moved and scaled to fit any stellar image. Each of these approaches has its advantages. Although modelling an asymmetrical or irregular image with an analytic function may require many free pa-

rameters, this number of parameters will still be smaller than the number of pixels in an empirical PSF. The PSF width is usually a few pixels so that especially near the centre of the image, the pixel-to-pixel variations in irradiance are quite large. The analytical PSF is a better choice here because a profile can be fitted even if the image is not uniformly sampled. An empirical approximation may not represent the true profile of the stellar image. On the other hand, numerical integration of analytic distributions is usually more time-consuming than for empirical functions. The software used to reduce the CCD images for this dissertation makes use of an analytical PSF.

2.2.4 DoPHOT

The Wright camera produces CCD frames in FITS format (NASA Science Data Systems Standards Office, 1990). The software used to extract magnitudes from the FITS images was DoPHOT (see Schechter, Mateo & Saha 1993 for a more complete description). Several details in the description that follows apply specifically to the version of DoPHOT that is in use at UCT.

DoPHOT was originally intended for reducing observations of star clusters, and was designed to be able to cope with large numbers of objects with poorly sampled and oddly shaped PSFs on a single frame. However, because DoPHOT is fast and highly automated, it is also suited to the task of reducing the large sets of frames of a single field that comprise a high speed photometry run.

DoPHOT searches for objects on a CCD frame and provides positions, magnitudes (derived from profile fitting and aperture photometry) and crude classifications for these objects. The program adopts a model for each kind of object on the frame: each object is classified as a bright star, a faint star, a close pair of stars, a galaxy, a cosmic ray, or an object initially identified as a star but subsequently scrapped. A cosmic ray is modelled as a single high pixel, while stars and galaxies are modelled using analytic PSFs with a number of free parameters. The PSF used by DoPHOT is an elliptical Gaussian with power law wings:

$$I(x,y) = I_0\left(1 + z^2 + \frac{1}{2}\beta_4(z^2)^2 + \frac{1}{6}\beta_6(z^2)^3\right)^{-1} + I_s \tag{2.2}$$

where

$$z^2 = \left[\frac{1}{2}\left(\frac{x^2}{\sigma^2{}_x} + 2\sigma_{xy}xy + \frac{y^2}{\sigma^2{}_y}\right)\right] \tag{2.3}$$

and $x = (x' - x_0)$, $y = (y' - y_0)$. x' and y' are the coordinates of the current pixel. There are seven free parameters in this function: the shape parameters σ_x, σ_y and σ_{xy}; the object centre (x_0, y_0); the central intensity I_0 and the background intensity I_s. The profile fitting is done using a nonlinear least squares procedure by minimizing χ^2. Signal-to-noise based weighting is used for each pixel.

In high speed photometry, one is usually interested only in the target star and selected comparison stars as opposed to *all* the stars on a frame, and the approximate coordinates of the objects of interest can be specified beforehand. The program can then search for objects at the known positions of the target star and the comparison stars. Because of differential refraction through the atmosphere and flexure between the various components of the optical system on the telescope, the positions of objects on the frame tend to drift during the exposure, even if an autoguider is used throughout the run. The drift is usually $\sim$ 10 pixels, but depends on the hour angle and declination of the star and the length of the run. To ensure that DoPHOT is able to find the objects of interest despite the drift in star positions, a number of (square) windows are specified in which the program will search for an object. The user specifies the length of the side of the window and the approximate position of the centre of each object to be measured.

The program performs multiple scans of each frame, each succeeding scan being performed at a lower detection threshold. On the first pass, the program identifies the brightest pixel within the specified windows (bad pixels and any bright regions at the edges of the chip are specified beforehand and are excluded from the search). This number of ADU is assigned to the variable T_{max}. The lowest detection threshold, T_{min}, is set by the program or by the user: this is the number of ADU per pixel below which DoPHOT will not attempt to fit a star. The quantity $T_{max} - T_{min}$ is divided into a number of steps such that the

difference in intensity between successive steps is as close to a factor of two as possible. For example, if $T_{min} = 16$ and $T_{max} = 128$, the program, on its first pass, would identify, classify and fit all objects containing pixels 128 ADU above the local sky background. The appropriate model fitted for each object is subtracted from the image, producing a "working image". The second pass would search for objects with pixels greater than 64 ADU above the background, then 32 ADU, and finally 16 ADU. By choosing T_{min} appropriately, the user can ensure that the program will attempt to fit very faint objects. The data collected for this dissertation of CP Eri in its low state, for example, required values of T_{min} of only 6 or 7 ADU above the local background.

The advantage of repeated passes with successively smaller detection thresholds is fairly obvious for crowded frames: the procedure avoids the need for fitting several closely-spaced objects simultaneously. It is, however, best to operate in this mode even when the field is sparse, especially if any bright stars are present. If the program is searching for any pixel above a fairly low initial threshold, it will attempt to fit stars in the wings of a bright star if the pixels there have values greater than T_{min}. The program will thus take some time to identify the subraster of pixels where the stellar model can be fitted successfully. Operating the program using multiple passes ("crowded field mode") tends to minimize this problem and speeds up the reductions considerably. Nevertheless, measurements of bright stars can still be problematic. When an analytic function is fitted to a bright star, large residuals may remain after the profile is subtracted, especially where the bright star has broader wings than the analytic model. These bright pixels may, on subsequent passes, trigger the identification of false "phantom stars". The program usually recognises these phantom stars as false detections and classifies them as such in the output file, although occasionally they are classified as faint stars. In practice, one ignores the false faint objects surrounding a bright star once one is satisfied that the objects are not real.

After each pass through the working image all objects found on previous passes are once again fitted to obtain improved estimates of the parameters used in the analytic models. In this way the shape of a typical star on the frame is determined. Stars with sufficient signal-to-noise are fitted for 7 parameters: the object centre, the central intensity of the fitted profile, the background intensity, and σ_x, σ_y and σ_{xy} which define the shape of

the profile. Stars with central intensities less than a certain value C_{min} (which can be specified by the user) are fitted only for the sky background, the object centre and the central intensity, while adopting the current best estimates of the stellar shape parameters determined from the brighter stars.

All objects identified as stars and fitted with analytic functions of either 7 or 4 parameters, together with cosmic ray hits and spurious identifications where the program was not able to identify the object reliably, are listed in an output file ("sum file"). For each object, the file lists the object's classification, the fitted sky value, coordinates of the object centre, fitted central intensity from which the fit magnitude is obtained, shape parameters for the fit, background-corrected aperture intensity in ADU, sky aperture intensity, difference between the fit and aperture magnitudes and standard errors for the fit and aperture magnitudes. The header of each sum file contains information extracted from the header of the original FITS image and lists the frame number, object name, right ascension and declination and the sidereal and universal time at the beginning of the exposure. The time signal was obtained from the central time service at Sutherland which is a PC-based system locked to signals from a GPS receiver. The signal is distributed to each dome via an optical cable and is used by the acquisition computer and the encoder system for the telescope. The timing errors are no more than $1 - 2$ μs under normal conditions. Universal and sidereal times are calculated from the mean time.

The next step is to combine the information from the sum files into a single file containing information on the variation in brightness of the target and comparison stars as a function of time. The heliocentric Julian Date and airmass for each frame are calculated using the star's right ascension and declination, the latitude of the observatory, the date and UT at the beginning of each frame. The aperture intensities and central intensities of the fitted PSFs are used to calculate the aperture and fit magnitudes. These data are then written to a file containing the time series for the target and comparison stars.

The aperture photometry measurement in the sum file for each object represents the total number of ADU in a software-defined aperture, the diameter of which is several full widths at half maximum of the fitted profile for that object. The aperture magnitudes that appear in the final data file are obtained using

$$-2.5 \log \left(\frac{I}{t} \right) + C \tag{2.4}$$

where I is the (background-corrected) number of ADU in the aperture, t the integration time and C is a zero point determined by obtaining aperture photometry for a star of known magnitude. When observations are taken without a filter (as was usually the case), the V magnitude of the star is used to represent the "white light" magnitude. This is because the UCT Wright CCD has a response that can be described as a "broad V" response (Johnson V is centred on 5500$\AA$ and is about 1000$\AA$ wide at full width half maximum, while the Wright CCD response is also centred on 5500$\AA$ but is $\sim$ 5000$\AA$ FWHM). In photometric conditions this method produces results that are accurate to about a tenth of a magnitude. Because in general only *differential* magnitudes are considered in the analysis, placing the results on a standard system is not important.

The fit magnitude is calculated from the central intensity of the fitted stellar profile. For a given frame, the shape parameters σ_x, σ_y and σ_{xy} will be the same for all stars, so the height of the PSF should be a measure of the star's brightness relative to the comparison stars. In reality, because of seeing variations, the shape parameters calculated by DoPHOT vary from frame to frame. To calculate the fit magnitude the total volume under the PSF must be taken into account. The fit magnitude is calculated using

$$2.5 \log \left(\frac{Int \times \sqrt{\sigma^2{}_x} \times \sqrt{\sigma^2{}_y}}{t} \right) + C \tag{2.5}$$

where t is the exposure time, Int is the central intensity of the profile, C is a zero point and $\sqrt{\sigma^2{}_x} \times \sqrt{\sigma^2{}_y}$ is a measure of the volume under the profile. The zero point is calculated to bring the profile magnitudes into rough agreement with the aperture magnitudes. The systematic error in the fit magnitude is, as for the aperture magnitudes, about a tenth of a magnitude in photometric conditions.

Aperture magnitudes are generally noisier than magnitudes obtained by profile fitting because there is much more Poisson and readout noise from the sky inside an aperture than there is under a fitted profile. Thus only the fit magnitudes were considered for the high speed photometry runs. The aperture measurements were used for standard stars

used to calibrate the high speed photometry runs.

The term "data reduction" is particularly appropriate in this context. Each raw frame produced by the Wright camera is 0.247 Mb, and each bias-subtracted and flat-fielded frame contains 0.211 Mb. A high speed photometry run of 500 frames thus requires 123 Mb for the raw frames and 106 Mb for the bias-subtracted, flat-fielded frames. Each sum file produced by DoPHOT contains approximately 1.5 kb (depending on the number of stars listed), so the sum files for one 500 frame photometry run contain $\sim$ 0.75 Mb. The final data file containing the time series for the target and comparison stars contains only about 40 kb, a reduction of the original data by a factor of over three thousand!

2.3 Differential photometry

One of the great advantages of using a CCD as a detector for high speed photometry is that the images of many objects appear on a single frame, each of which is recorded in similar atmospheric conditions. Spatially, objects on a single frame are very close to each other (the Wright camera in frame transfer mode on the 1m telescope at Sutherland has a field of view of 1.2 by 1.4 arcminutes), so they have essentially the same zenith distance. Differential photometry involves comparing the target star to other comparison stars on the frame by differencing their magnitudes. Differencing removes (to first order) extinction variations and corrects any other variation (instrumental or atmospheric in origin) that is unrelated to the intrinsic variations of the target star. Differential photometry allows observations to be made through thin cloud, greatly increasing the number of usable observing nights. Although in bad weather one usually has to increase the exposure time to obtain a reasonable signal-to-noise ratio, this is offset by the large increase in the usable data that can be acquired. Differential CCD photometry allows good signal-to-noise measurements of faint stars to be made with small telescopes.

Although differential techniques remove the need to correct observations for atmospheric extinction, problems can arise where the target star and the comparison stars have very different colours, and second order extinction terms become important. CVs observed

away from the Galactic plane are unlikely to be sufficiently near a blue comparison star. At large airmasses, differential extinction occurs as the blue CV light is scattered more than redder light from the comparison stars. The target star thus fades faster than the comparison star at large airmasses. This produces low frequency noise in the final light curve.

2.4 CCDs versus photomultiplers

CCDs as detectors have several advantages over photomultipliers (PMTs), but are not superior in all respects. CCDs have higher quantum efficiencies than PMTs (see figure 2.2): whereas the peak QE for a photomultiplier is around 25%, peak efficiencies for CCDs can exceed 80%. CCDs provide simultaneous measurements of a target and comparison stars, making differential photometry possible. Also, the background is constantly monitored with a CCD; this enables more effective background subtraction. As a result, much fainter sources can be observed with a CCD using a particular telescope than is possible with a photomultipler. In CCD aperture photometry, one can choose vey small software-defined apertures of only a few arcseconds across, whereas photomultipler apertures have diameters of tens of arcseconds. The smaller the aperture, the less Poisson noise from the background is included with the signal.

In some cases, however, PMTs may still be a better choice of detector. They allow much shorter integration times and are thus a better choice in situations where very rapid sampling is necessary. Blue-sensitive PMTs have, in general, better blue responses than CCDs. The blue response of a CCD can be improved by thinning, back illumination and coating the chip, but this is an expensive and risky (in the case of thinning) business. Another advantage of a photomultipler photometer over a CCD photometer is that real-time results are easier to obtain at the telescope, allowing the observer to monitor the incoming data. In addition, the computational requirements for photomultiplier data acquisition, storage and reduction are modest in comparison to those for a CCD photometer. The output of a PMT photometer consists of a single number (say 16 bits) per integration, and the data from a week's observing can fit easily onto a 360 kb floppy

disk. On the other hand, each CCD frame readout produces hundreds or thousands of kilobytes, depending on the size of the chip. The UCT Wright camera in frame transfer mode produces almost a quarter of a megabyte per integration. During a night of a total of 10 hours of high speed photometry with an integration time of 10s, the acquisition system must be capable of storing almost a gigabyte of data, so that the images can be reduced at a later stage. CCD reductions, too, require substantial computing facilities.

For this study, the CCD photometer has several clear advantages over a PMT photometer. Because the aim of the study is to examine photometric periods of the order of a thousand seconds, a time resolution of higher than 10s is not necessary. The Wright CCD, being a back-illumunated, thinned device, has a good blue response and is appropriate for observing blue stars such as CVs. Furthermore, the sensitivity of the CCD, improved background subtraction and differential photometry, increase the quality of the data and make observations of very faint sources possible. Two light curves of CP Eri in the low state were obtained when the star was at 19.5 mag. GP Com, with a magnitude of about 16.5 and large airmasses (its declination is $+18°$; the latitude of Sutherland is $-33°$) was previously unobservable with the 1m telescope at Sutherland.

Chapter 3

Examples of hydrogen-rich superhumpers

3.1 Introduction

The superhump phenomenon was first identified in superoutbursting dwarf novae (Vogt 1974, Warner 1975). Normal and negative superhumps have subsequently been observed in a variety of other close binary systems: evidence for precessing accretion discs has been seen in "permanently erupting" nova-like variables and nova remnants such as BK Lyn (Skillman & Patterson 1993) and V603 Aql (Patterson et al. 1993); in low mass X-ray binaries (eg. V1405 Aql: Patterson et al. 1993); and magnetic CVs (eg. TV Col: Hellier, Mason & Mittaz 1991, Hellier 1993). See chapter 1 section 1.2.2 for a discussion of hydrogen-rich systems with multiple periodicities that are thought to be due to accretion disc precession.

In this chapter, observations of two hydrogen-rich superhumpers are presented. The aim is to demonstrate some of the observational properties of hydrogen-rich systems in which superhumps are believed to occur, in order to be able to draw comparisons with the helium-rich AM CVn stars. V442 Ophiuchi is a nova-like variable with a variable photometric period that differs from its spectroscopic (presumably orbital) period. TY PsA is an SU UMa dwarf nova which, during superoutburst, displays asymmetric absorption line profiles that vary in asymmetry on the beat period between the orbital period and

the superhump period.

3.2 Photometry of V442 Ophiuchi

3.2.1 Observational background

V442 Ophiuchi is a nova-like variable of the VY Scl subtype (Warner 1995a) with a visual magnitude range of 12.6 to 15.5. V442 Oph was identified by Szkody & Wade (1980) as a CV, based on its spectral properties, blue colour and flickering behaviour. The spectra showed He II λ4686Å and Hβ lines of comparable strength in the high state. Equivalent widths of 3.9Å for He II and 4.8Å for Hβ were measured by Williams (1983). In this regard, V442 Oph resembles V603 Aql (Williams 1983, Patterson et al. 1993); V603 Aql has, however, a much smaller range of variability than V442 Oph. The photometric and periodic behaviour of V442 Oph is strikingly similar to "Tafelberg", the optical counterpart of the hard X-ray source H 0551-819 (Buckley et al. 1993, Patterson 1995).

IUE spectra of V442 Oph show a lack of strong emission or absorption lines: this is typical of nova-like variables (Szkody & Shafter 1983). The UV spectra are similar to those of V603 Aql. The He II λ1640Å is surprisingly weak considering the He II λ4686Å strength. The ratio of the fluxes 1640/4686 is about 2.3 while recombination theory (Brocklehurst 1971) predicts a ratio of 1640/4686 = 7; this implies either a strange energy balance in the disc or a large variation in the disc between the time of the optical and the UV spectra.

Infra-red photometry (Szkody & Shafter 1983) shows variability with 30% of the points more than 2σ from the mean. The IR fluxes are consistent with an optically thick disc. The mass transfer rate is approximately $10^{-8}M_{\odot}y^{-1}$ which is in the the range of mass transfer rates deduced for nova-like variables, nova remnants and dwarf novae in outburst (Warner 1995a). V442 Oph has no significant circular polarisation and is thus not a polar with a strong magnetic field and synchronously rotating primary (Szkody & Shafter 1983).

Szkody & Shafter (1983) obtained a period of 3.367 $\pm$ 0.015h from Hα radial velocity variations; a consistent period was obtained from the radial velocities of He II λ4686Å.

A recent study by M.D. Still and R.C. Smith (private communication) finds three candidate spectroscopic periods from radial velocity variations of the sum of the Hβ and Hγ emission lines. The candidate periods are one cycle day^{-1} aliases of each other: 2.643 h, 2.971 h and 3.390 h. The favoured period is 2.971 ± 0.007 h from the Hβ core velocity and 2.969 ± 0.010 h from the He II λ4686Å. The 3.390 h period of Szkody & Shafter (1983) is probably the one cycle day^{-1} alias of this period.

The evidence from Still & Smith's recent study suggests that V442 Oph is a non-eclipsing analogue of the SW Sex stars (Thorstensen et al. 1991). It is interesting to note that SW Sex, which is an eclipsing system, shows no indications of multiple periodicities (i.e. a spectroscopic period which differs from the photometric period or periods). Warner (1995a) observes that no high-inclination, multiple period systems are yet known. It will be interesting to see, should an eclipsing AM CVn star ever be discovered, whether it displays the complex photometric behaviour of the lower-inclination AM CVn systems.

V603 Aql, a system very similar to V442 Oph, has shown both negative and positive superhumps, although not at the same time. The negative superhumps have dominated the lightcurve since 1992 (Patterson, private communication), and the positive superhumps were present in data from June to October 1991 (Patterson et al. 1993). H 0551-819 has also shown both positive and negative superhumps at different times (Patterson 1995). In this section, observations of V442 Oph from 1983 and 1995 are presented; the photometric period from 1983 is different from the 1995 period, and both these periods are less than the spectroscopic period, suggesting a negative superhump. In addition, there is evidence of dwarf nova oscillations (DNOs) in the 1995 high-speed photometry.

3.2.2 New observations

High speed photometry of V442 Oph was obtained in 1983 at Sutherland by Darragh O'Donoghue with the UCT photometer (Nather & Warner 1971) attached to the 0.75m reflector. Observations were taken without a filter; the S-11 cathode of the Amperex 56DVP photomultiplier yields a response corresponding to an effective wavelength close to that of Johnson B. A log of observations is given in table 3.1. The sky-subtracted

Table 3.1: Journal of observations: July, August 1983 high-speed photometry of V442 Oph

Run	Date (start)	$JD_{\odot}$ (2440000+)	Length (h)
S 3136	1983 July 8	5524.43013	0.9
S 3137	1983 July 8	5524.46759	1.8
S 3143	1983 July 9	5525.39999	3.3
S 3145	1983 July 10	5526.36064	0.9
S 3146	1983 July 10	5526.47268	1.1
S 3149	1983 July 11	5527.55471	5.1
S 3168	1983 August 8	5555.30644	3.5

observations were corrected for extinction using a mean extinction coefficient of 0.4. The mean intensity of the star during each run was subtracted from the data which were normalised by the same quantity to yeid a time series in units of fractional intensity. All observations were made with integration times of 5 s; these were subsequently binned to give a sampling time of 20 s to improve the signal-to-noise ratio.

An additional set of data was obtained by the writer in June and July 1995 using the UCT Wright CCD Camera (see chapter 2) on the 1m telescope at Sutherland. Table 3.2 is a journal of the observations. All exposure times were 10 s. The frames were reduced using the procedure described in chapter 2. Since the magnitudes calculated by the reduction software are subject to a systematic error of about 0.1 mag, the mean magnitude in each run was subtracted. The data presented are thus differential magnitudes from the mean magnitude for each run.

A rough estimate of the B and V magnitudes of V442 Oph was obtained on 28 July by comparing the count rates (i.e. number of ADU per second) with the nearby blue star HD 158661 at $\alpha_{1900} = 17^h28^m19^s$, $\delta_{1900} = -17°06'19''$: this star was chosen for standardisation purposes (instead of an E-region standard) because of its colour and its proximity to V442 Oph (to minimize extinction effects). HD 158661 was kindly measured by Fred Marang

Table 3.2: Log of observations: June, July 1995 high-speed photometry of V442 Oph

Run	Date (start)	$JD_{\odot}$ (2440000+)	Length (h)
A336	1995 June 2	9870.45050	3.8
A342	1995 June 3	9871.47103	3.7
A350	1995 July 25	9924.31508	3.9
A357	1995 July 27	9926.31731	3.9
A362	1995 July 28	9927.31620	4.1
A364	1995 July 29	9928.20977	5.5
A369	1995 July 30	9929.30439	4.7
A373	1995 July 31	9930.25983	5.2

with the 0.5m telescope at Sutherland on the same night that the filtered observations of V442 Oph were made. The results were $V = 8.197$ and $B = 8.380$. The estimates for V442 Oph were $B = 14.1$ and $V = 13.9$. As most of the observations made with the UCT Wright Camera were made without a filter, an estimate of the "white light" magnitude of V442 Oph was also made. This was done by assuming that the white light magnitude of HD 158661 is the same as its V magnitude – the Wright Camera CCD has a "broad V" response (see chapter 2 section 2.2.4). This rough method yielded a white light magnitude for V442 Oph of 13.8. The motivation for obtaining these rough estimates of the magnitudes of the star was to be able to monitor any long-term changes in the star's brightness.

3.2.3 The photometric periods

The 1983 observations in table 3.1 are shown in figure 3.1. They resemble the results of Szkody & Shafter (1983) and show rapid flickering and flare-like brightenings on a time scale of $\sim$ 15 min. The light curves in Szkody & Shafter (1983) cover less than two orbital periods and do not show the sinusoidal variation observed during the longer Sutherland runs.

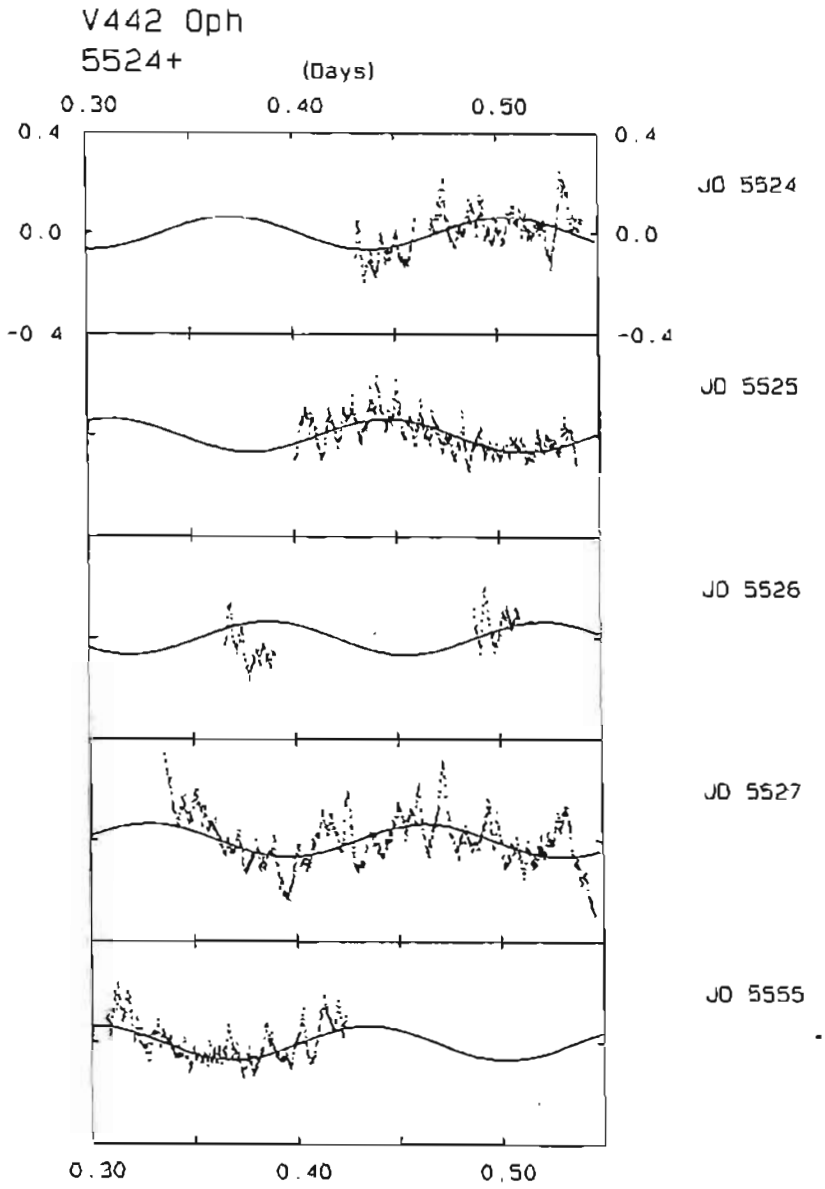

Figure 3.1: The high speed photometry of V442 Oph listed in table 3.1. The horizontal axis is in days (including the heliocentric correction) and the vertical axis is in units of fractional intensity. The sinusoidal fit is a non-linear least squares fit using the parameters for the second of the arrowed peaks in figure 3.3.

A Fourier amplitude spectrum of the July 1983 runs ($JD_{\odot}$ 2445524, 2445525 and 2445527) from 0.0 to 3.0 mHz is shown in figure 3.2a. There is no significant structure in the amplitude spectrum from 3.0 mHz to the Nyquist frequency. The highest peak in the spectrum occurs at $\sim 85.96\,\mu$Hz, and there are other power excesses from 0.12 – 0.24 mHz and at ~ 0.32 mHz, ~ 0.56 mHz and ~ 0.98 mHz with amplitudes about half that of the principal peak. The arrows in figure 3.2b show the 85.96 mHz peak and the positions of its first three harmonics: there is no obvious evidence for harmonic structure of this variation, although a first harmonic may be buried in the broad band of power at ~ 0.17 mHz.

A close-up of fig 3.2 around 0.1 mHz shows a broad excess of power at $\sim 90\,\mu$Hz (see figure 3.3). The three highest peaks, at 74.40, 85.89 and 97.55 μHz are one cycle per day aliases of each other, and have amplitudes of 0.057 ± 0.002, 0.063 ± 0.002 and 0.061 ± 0.002 mag, respectively. The superimposed sinusoid in figure 3.1 uses the parameters of the second of the three high-amplitude peaks: $P = 3.231 \pm 0.036$ h, $A = 0.063 \pm 0.002$ mag and $T_{max} = JD_{\odot}2445524.36532 \pm 0.00028$. The formal error of the non-linear least squares fit (0.002 h) is probably an underestimate of the true uncertainty because the photometric variation is not merely a sinusoid with random noise. The uncertainty of 0.036 h quoted above is obtained using the following rule of thumb: $\Delta P \approx \frac{P^2}{4T}$, where T is the timebase of the observations.

A Fourier transform of *all* the 1983 data, including the run from August 1983 which was taken 28 days after the other 4 runs, is shown in figure 3.3. There are two similar peaks (one cycle per day aliases of each other) with periods of 3.228 ± 0.004 and 2.845 ± 0.003 h and amplitudes of 0.066 ± 0.002 and 0.065 ± 0.002 (the second one cycle day^{-1} alias of the 3.228 h peak has a much smaller amplitude than the other two peaks : $A = 0.057 \pm 0.002$ mag).

The pattern of aliases in the amplitude spectrum in figure 3.3 is not consistent with the windowing of the light curve, and there is a distinct window pattern centred on 3.59 or 3.12 h. In order to investigate any underlying low-amplitude structure, the data were pre-whitened in turn by the frequencies of each of the arrowed peaks in figure 3.3 (it is not clear at the outset which of these aliases is the true principal frequency, as the alias pattern envelope does not match the spectral window function). The amplitude spec-

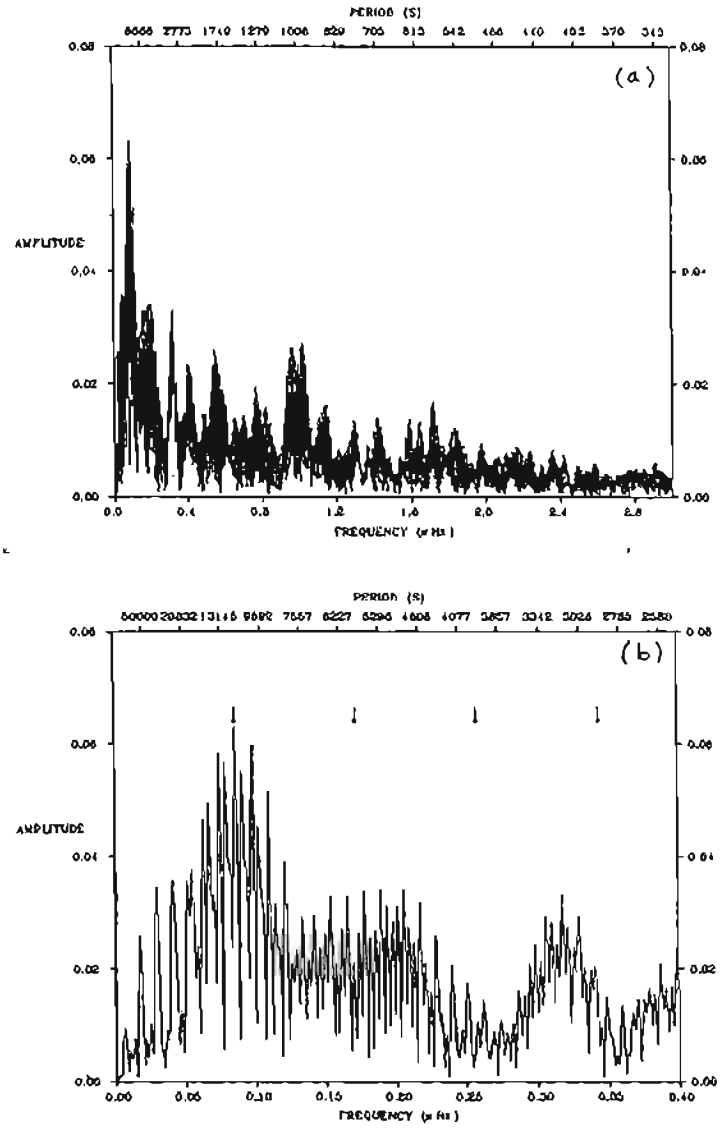

Figure 3.2: (a) Fourier amplitude spectrum of the July 1983 runs out to 3.0 mHz (there are no further features from 3.0 mHz to the Nyquist frequency). The highest peak is at 85.96 μHz. (b) The amplitude spectrum from 0.0 to 0.4 mHz. The arrows show the 85.96 μHz variation and the positions of its first three harmonics. There is no obvious harmonic structure for this frequency, although a first harmonic may be buried in the broad band of power at ~ 0.17 mHz.

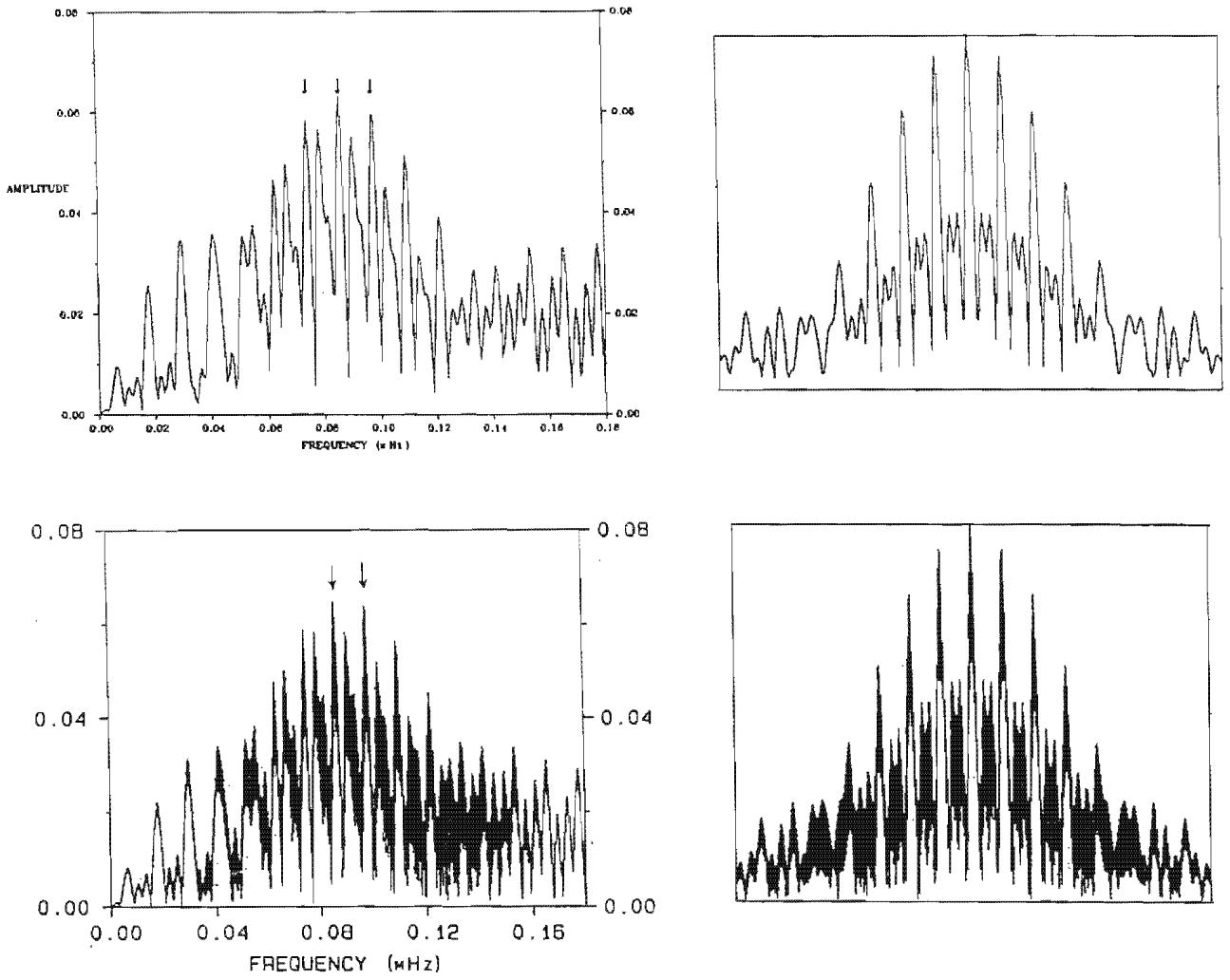

Figure 3.3: The Fourier amplitude spectrum of the 1983 V442 Oph data in the region of 0.1 mHz. (a) Amplitude spectrum of the July 1983 runs. The spectral window function is shown alongside. The arrows indicate the three 1 cycle per day aliases of similar amplitude, each of which could represent the true principal frequency. (b) Amplitude spectrum for *all* the 1983 data, including the run from August 1983 which was obtained 28 days after the July runs. The spectral window function is shown alongside. The two arrows indicate the two 1 cycle per day aliases which could represent the true principal frequency.

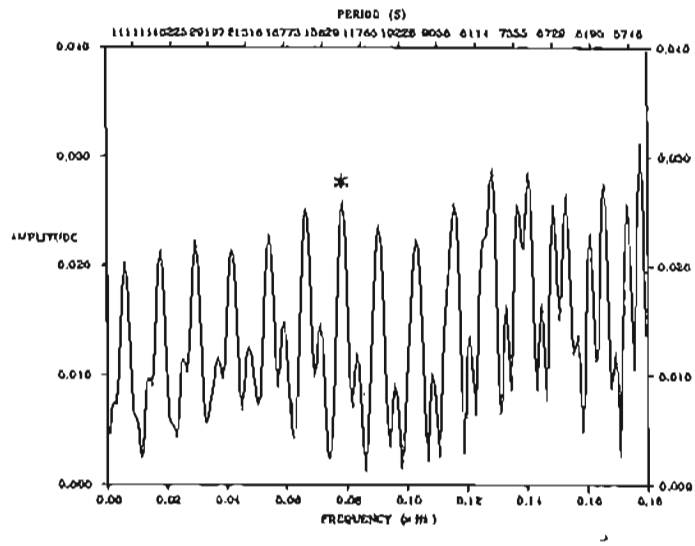

Figure 3.4: Amplitude spectra of runs S3136, S3137, S3143 and S3149 pre-whitened by the second of the three arrowed peaks in figure 3.3. No structure resembling the spectral window (left) is evident in the pre-whitened data. The asterisk marks the peak at $\sim 0.80\,\mathrm{mHz}$ that appears in figure 3.3 between the first two of the three arrowed alias peaks, but this figure shows that the $\sim 0.80\,\mathrm{mHz}$ peak is not significant.

trum was then re-calculated. The spectrum obtained after pre-whitening with the second of the three alias peaks is shown in figure 3.4. No variations (with an upper limit of 0.030 mag) appeared above the noise in the region of the original power excess. The peak at $\sim 0.08\,\mathrm{mHz}$ (marked with an asterisk in figure 3.4) appears in figure 3.3 between the first two arrowed peaks. If real, it has a period $\sim 3.55\,\mathrm{h}$ or its one cycle day^{-1} alias, but figure 3.4 shows that it is not significant. The distortion of the alias pattern envelope in figure 3.3a and b could be due to the flickering and flare-like features in the light curve: the varying amplitude of the flickering may be causing an overall amplitude modulation of the signal.

The 1995 light curves of table 3.2 are shown in figure 3.5. These also show a clear sinusoidal variation with superimposed flickering; the flickering time scale is similar to that of the 1983 data. The trailing ends of the last two runs ($\mathrm{JD}_\odot$ 2449929 and 2449930) are

probably due to differential extinction (at large airmass) with respect to the comparison stars that were used for the differential photometry.

The Fourier amplitude spectrum of the July 1995 observations from 0.0 to 0.4 mHz is shown in figure 3.6. As with the 1983 amplitude spectrum, there is a broad band of power around $\sim$ 0.1 mHz: the highest-amplitude peak is at 95.73 μHz. The amplitude spectrum is featureless from 0.4 mHz up to the Nyquist frequency apart from a low-amplitude peak at $\sim$ 0.04 Hz (see later). The first harmonic may be buried in the band of power at $\sim$ 0.19 mHz, and there is a suggestion of a power excess at the second harmonic, but apart from this there is no obvious harmonic structure for the peak frequency.

A close-up of figure 3.6 in the region of 0.1 mHz is shown in figure 3.7 together with its spectral window function. As with the 1983 observations, the pattern of aliases in the amplitude spectrum does not correspond in detail with the spectral window: the alias pattern is asymmetric and there are two high-amplitude peaks that could represent the true period. The larger peak is at 95.73 μHz: a non-linear least squares fit to all the data yields $P = 2.902 \pm 0.002$ h, $A = 0.080 \pm 0.002$ mag and $T_{max} = \mathrm{JD}_{\odot}2449870.49715 \pm 0.00044$. These parameters were used for the sinusoid fit in figure 3.5. The second high-amplitude peak in the amplitude spectrum (figure 3.7) is the 1 cycle day^{-1} alias of the 2.902 h period and corresponds to a period of 2.589 ± 0.002 h with an amplitude of 0.078 ± 0.002 mag.

The 1995 observations were pre-whitened by both the peak frequency and its high-amplitude one cycle day^{-1} alias to check for closely-spaced low-amplitude peaks that could produce the asymmetric alias pattern. The pre-whitened amplitude spectra show no significant structure in the region of the 0.1 mHz frequency (with an upper limit of 0.026 mag).

In neither figure 3.3 nor figure 3.7 is there any convincing sign of the spectroscopic frequency, 93.53 μHz.

The amplitude of the principal variation is greatly reduced in run A 364 ($\mathrm{JD}_{\odot}$ 2449928). An amplitude modulation like this suggests the presence of two closely-spaced, beating periods, although there is no evidence of a low-amplitude frequency near the principal

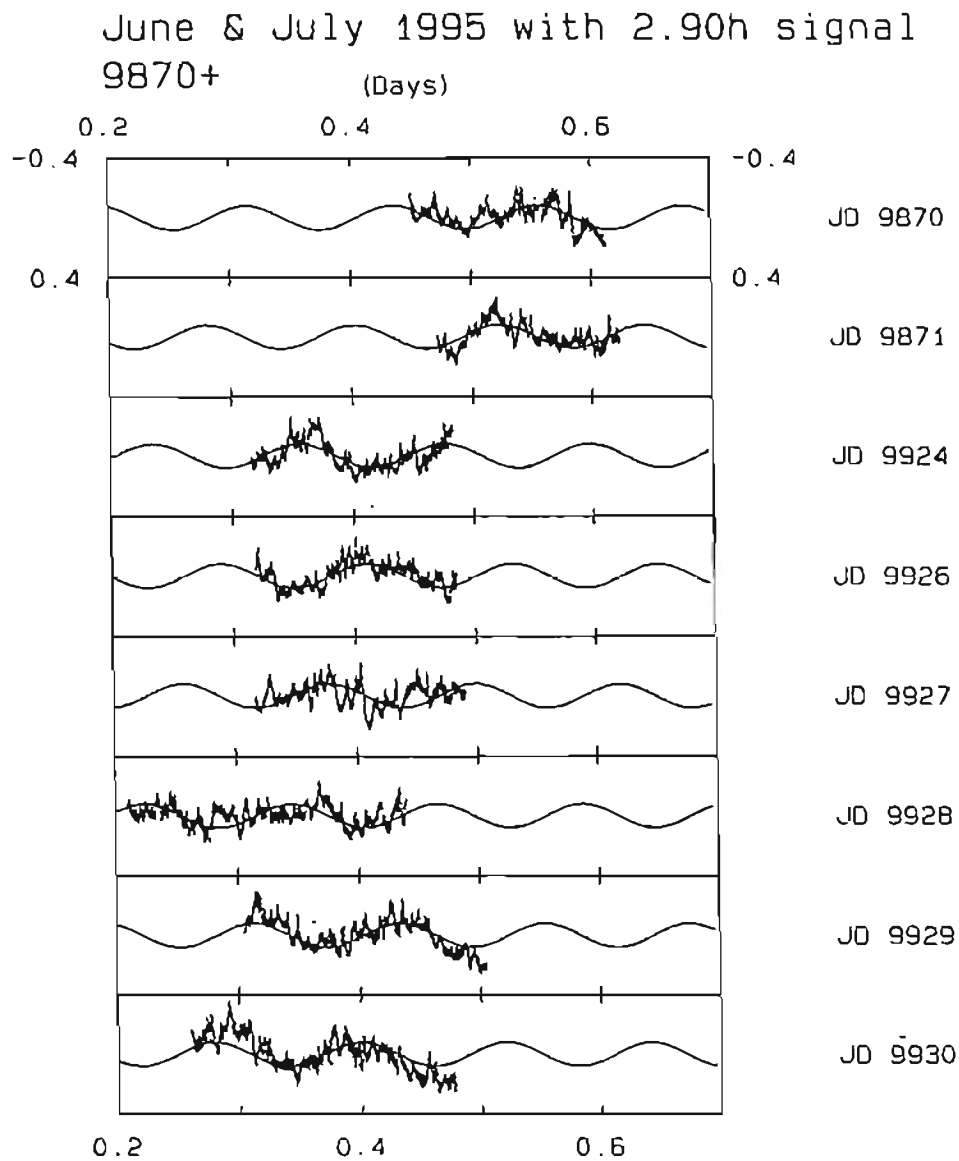

Figure 3.5: The high-speed photometry of V442 Oph listed in table 3.2. The vertical axis is in units of differential magnitudes from the mean (white light) magnitude for each run. The sinusoidal fit is a non-linear least squares fit to all the data using the parameters of the 2.902 h peak in figure 3.7.

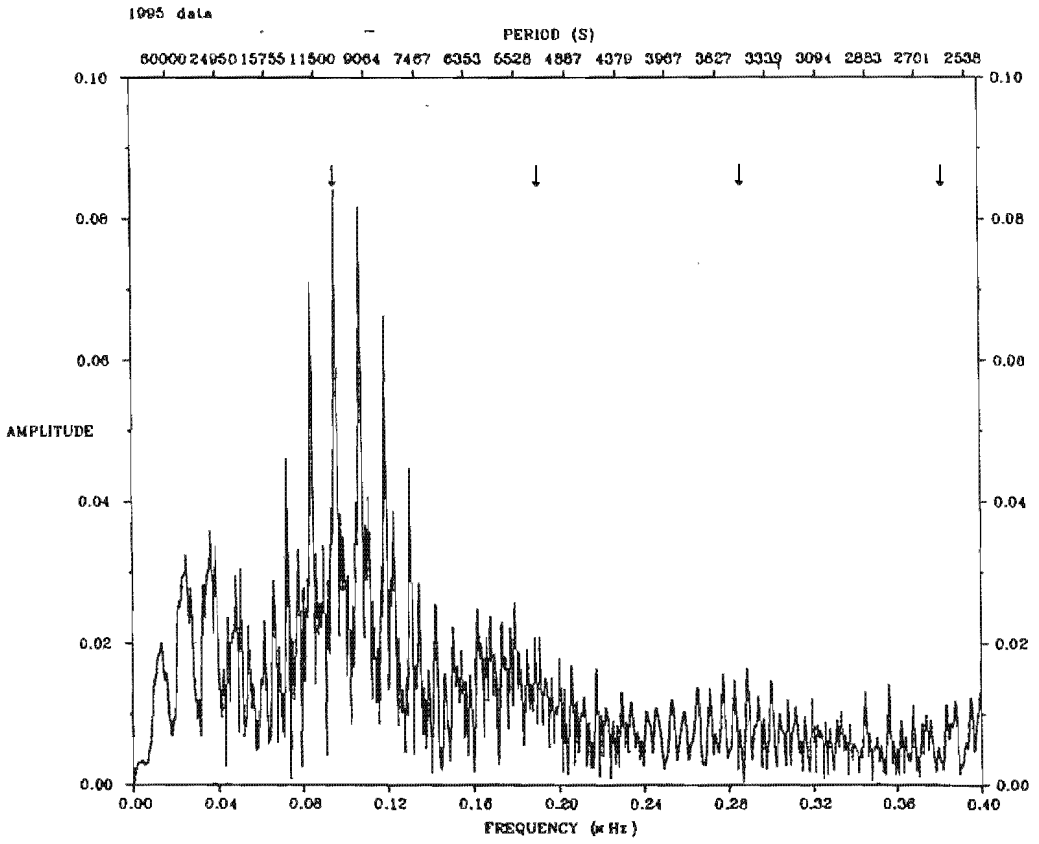

Figure 3.6: Fourier amplitude spectrum of the 1995 observations from 0.0 to 0.4 mHz showing the positions of the 95.73 μHz peak and its first three harmonics. Apart from the first harmonic which may be hiding in the broad band at $\sim$ 0.19 mHz and a suggestion of a power excess at the second harmonic, there is no obvious harmonic structure for the 95.73 μHz peak.

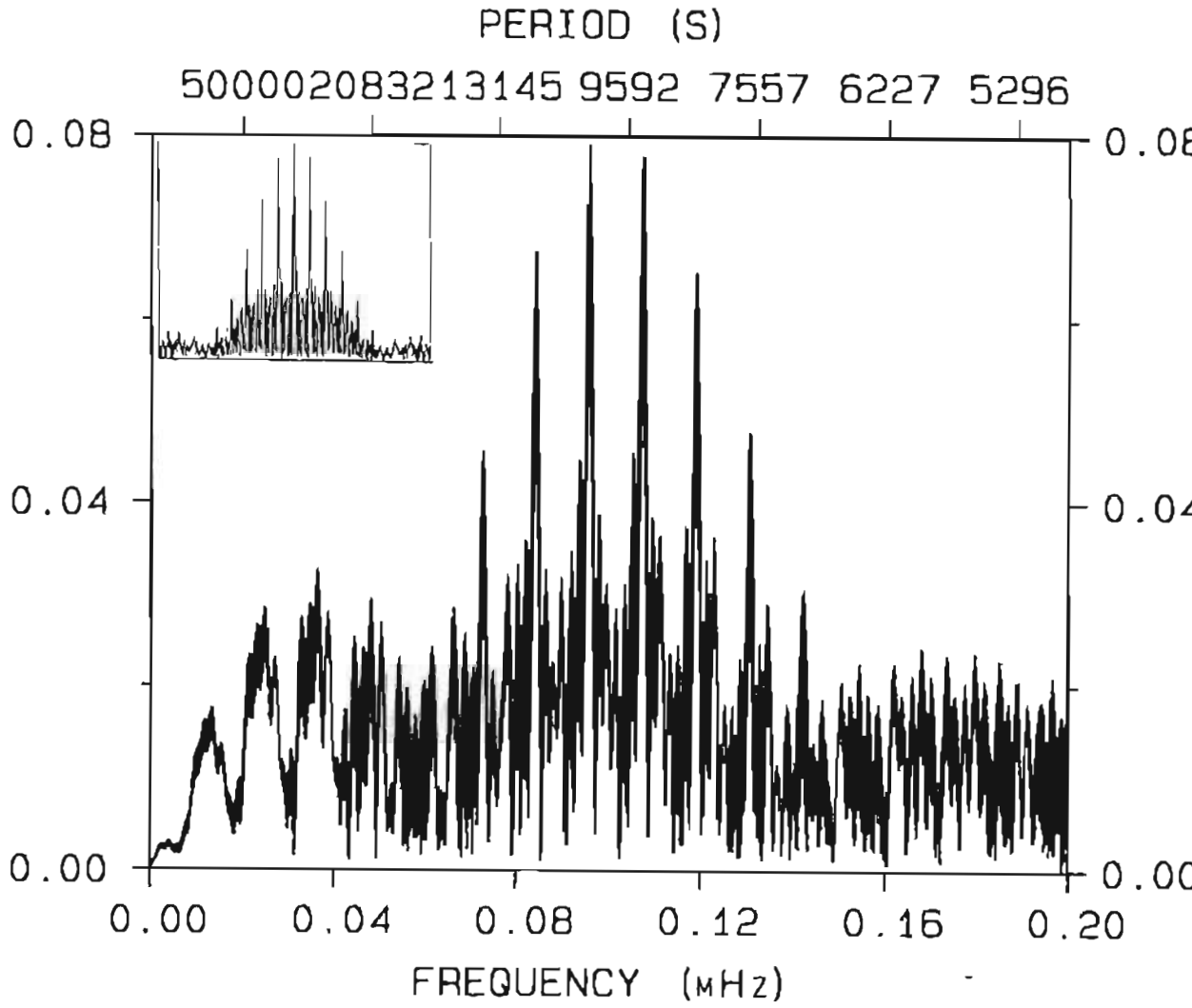

Figure 3.7: Fourier amplitude spectrum of the 1995 V442 Oph high-speed photometry in the region of 0.1 mHz. The spectral window function is shown as an inset. There are two high-amplitude peaks, either of which could represent the true principal frequency.

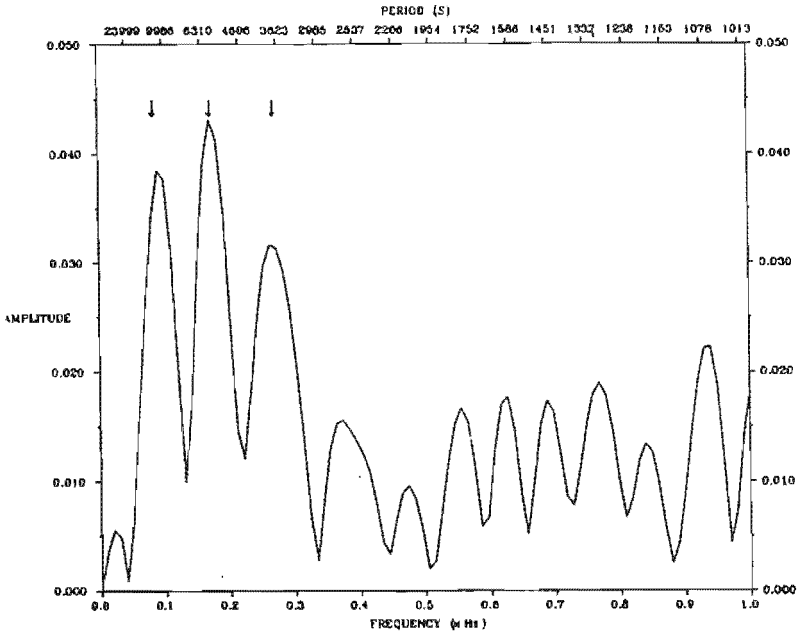

Figure 3.8: Fourier amplitude spectrum of run A364. The arrows mark the approximate positions of the principal variation from the other 1995 runs, together with its first two harmonics.

frequency in the pre-whitened spectrum. The amplitude spectrum of run A364 is shown in figure 3.8. The peak with the highest amplitude in figure 3.8 corresponds to a period of 5790 ± 100 s. This period is consistent with the first harmonic of the principal variation. A peak consistent with the third harmonic also appears in figure 3.8, showing that the harmonics of the principal variation strengthen occasionally in the light curve.

3.2.4 A negative superhump?

There are three (aliased) candidate periods from 1983 and two from 1995. It is likely that the correct periods are 2.845 ± 0.003 h from 1983 and 2.902 ± 0.002 h from 1995, as these are the two most similar periods from the two years. Observations of V442 made during 1995 from CTIO have yielded a "healthy" period of 8.271 ± 0.009 cycles day^{-1} or 2.902 ± 0.003 h (Patterson, private communication), confirming the 1995 identification. If the choice of principal frequency for the two years is correct, the photometric period changes significantly between 1983 and 1995, *and* is different to the spectroscopic period.

It is tempting to speculate that the photometric period is a negative superhump, and that the correct spectroscopic period is 2.970h, the one cycle day^{-1} alias of the period derived by Szkody & Shafter (1983).

Some support of this interpretation comes from the 1995 photometry: Patterson (private communication) has found a low-frequency variation with a period of 0.229 ± 0.009 cycles day^{-1}, i.e., 105 ± 4 h. This could be the precession period of a tilted disc with regressing nodes: the beat period between the 2.902 h period and the spectroscopic period, 2.970 h, is 126 ± 20 h. The precession period of a tilted disc would be visible in the photometry due to the varying visibility of, for instance, the central regions of the disc, or the variation of disc overflow by the mass transfer stream.

3.2.5 Dwarf nova oscillations

An interesting feature of the 1995 photometry is the presence of high-frequency peaks around ~ 0.04 Hz at very low amplitude in some, but not all, runs. The runs from one month show an excess of power at approximately the same frequency, but the location of the excess power changes from June to July. Aside from these low-amplitude peaks, the nightly amplitude spectra are featureless up to the Nyquist frequency.

Of the two June nights, a region of excess power appears in run A342 around 42.47 mHz with an amplitude of 0.003 mag: see figure 3.9. There is no (convincing) power excess at high frequencies in the previous night's run (A336). In the July runs, a low-amplitude, high-frequency power excess is seen clearly in three nights: runs A357, A369 and A373. The amplitude spectra of these three nights' data in the region of 39 mHz is shown in figure 3.10. The corresponding periods are 25.45 s, 25.57 s and 25.56 s. The amplitudes are variable from one run to the next: in run A357, $A \approx 2.9 \times 10^{-3}$ mag while in run A373, $A \approx 5.5 \times 10^{-3}$ mag. The complex structure of the peaks in the amplitude spectra might be caused by the fact that the periods are comparable to the integration time of 10 s (see the discussion by Warner & Brickhill 1978).

Low-amplitude, high-frequency brightness modulations with unstable periods were dis-

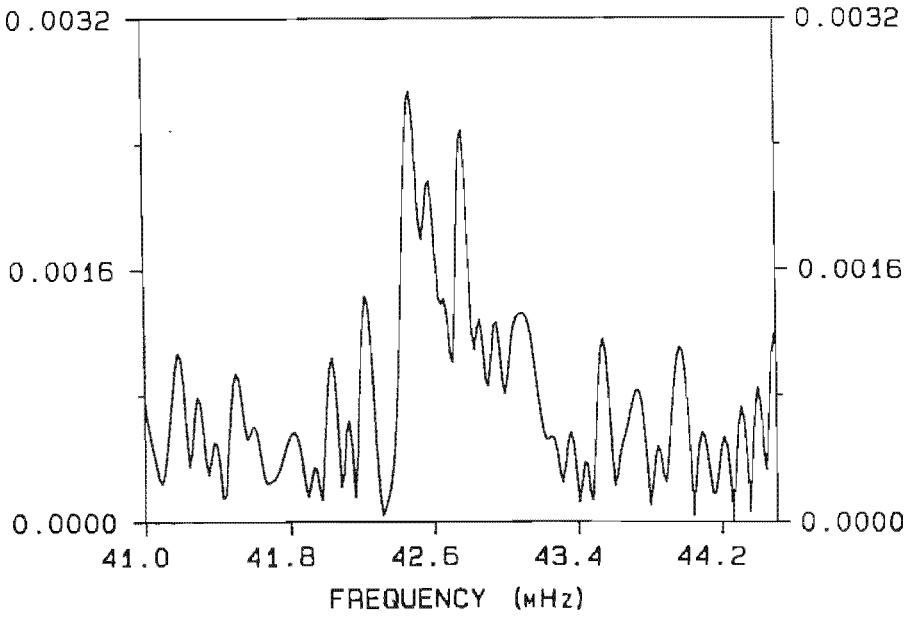

Figure 3.9: The high-frequency, low-amplitude power excess in run A342. The period corresponding to the highest peak is $\sim 23s$.

covered in outbursting dwarf novae (Warner & Robinson 1972) and termed "dwarf nova oscillations" (DNOs). DNOs were subsequently detected in several nova-like variables (see Warner 1995a, Table 8.4 for a list of CVs which show short-period optical oscillations). The oscillations are usually too low in amplitude to be seen in the light curve itself, and are only seen in power spectral analyses. In some dwarf novae, DNOs have never been observed (despite good observational coverage), while in others DNOs have been observed in one but not in other outbursts. DNOs have never been seen in dwarf novae in quiescence. VW Hyi (the best-studied superoutbursting dwarf nova) shows DNOs in the range 20 – 36 s which appear towards the end of normal and superoutbursts (for references see Warner 1995a). TY PsA has shown DNOs in both normal and superoutbursts (Warner, O'Donoghue & Wargau 1989). During one run taken during superoutburst, DNOs were visible in the light curve.

Nova-like variables in which DNOs have been detected have DNO periods in the range 19 – 32 s. DNOs are present in about half the observations of UX UMa (Warner 1995a). TT Ari, which has a similar orbital period (3.30 h) to that for V442 Oph (2.970 h), has

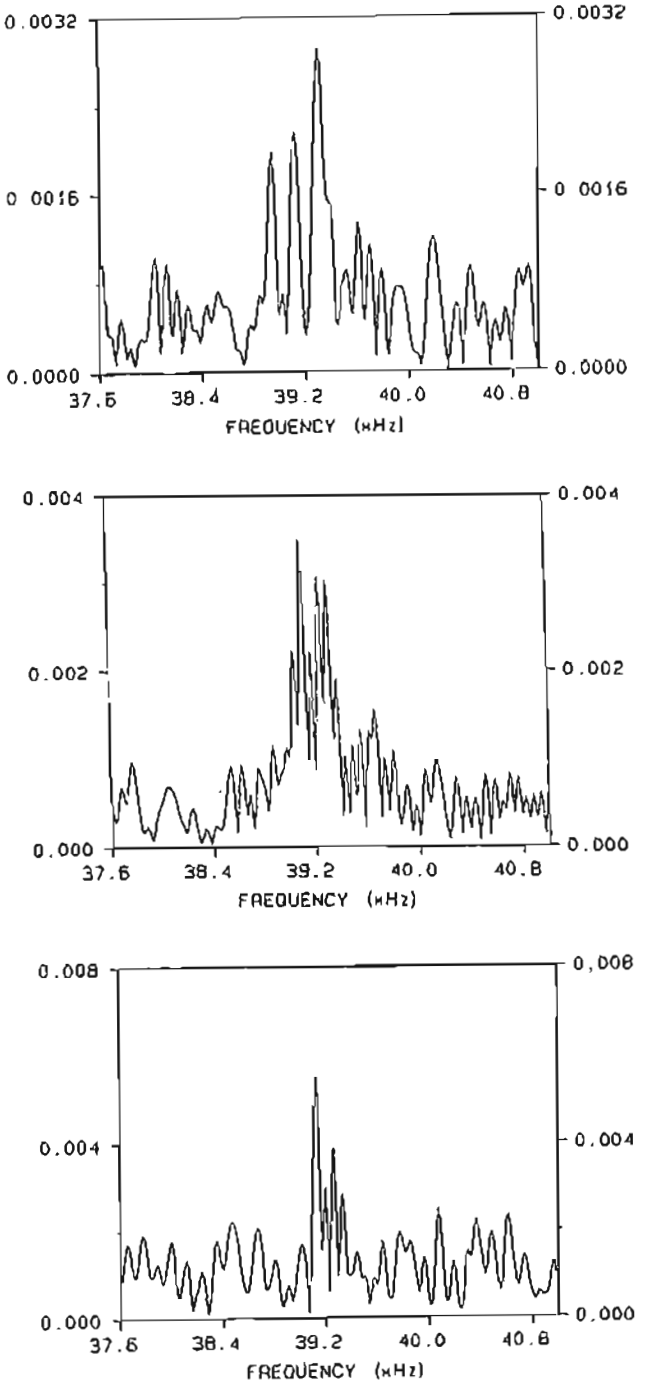

Figure 3.10: The excess high-frequency power in runs A357, A369 and A373. The frequency and amplitude of the peak varies from run to run.

quasi-periods of $\sim$ 12, $\sim$ 32 and $\sim$ 40s and shows negative superhumps (Udalski 1988, Patterson et al. 1993). By analogy, therefore, it is probable that the high-frequency power seen in V442 Oph is caused by DNOs. The DNOs are expected to be seen only in runs where the coherence of the oscillations is particularly high.

3.3 Spectroscopy of TY Piscis Austrini

3.3.1 Introduction

The spectra of the AM CVn stars differ from the spectra of DB white dwarfs in several respects (see chapter 1 section 1.1.4.3): the lines in the AM CVn stars are narrower and shallower than those in DB white dwarf spectra and occasionally show emission at He II λ4686Å. AM CVn stars also show heavier elements (N, Si, C) in their UV spectra, while the spectra of DB pulsators are largely featureless. The line profiles of AM CVn star spectra most closely resemble the line profiles seen in spectra of superoutbursting dwarf novae (O'Donoghue 1993, Patterson, Halpern & Shambrook 1993, Warner 1995a). This is probably the most compelling piece of evidence suggesting that similar mechanisms operate in AM CVn stars and in superhumping systems.

During the rise to outburst, the characteristic Balmer emission-line spectrum of a quiescent dwarf nova is gradually transformed into an absorption spectrum. Large variations in the γ-velocity of the broad absorption lines have been observed in TY PsA (Warner, O'Donoghue & Wargau 1989), TU Men and VW Hyi (for references see Warner 1995a). In these systems, the γ-velocities alternate between ~ -200 and $\sim 200\mathrm{km\,s^{-1}}$ on the beat period between the superhump and the orbital period. These apparent γ-velocity modulations are not caused by a real change in the motion of the system, but by the changing asymmetries of the absorption line profiles. Similar line profile asymmetry variations are observed in AM CVn (Patterson, Halpern & Shambrook 1993) and V803 Cen (O'Donoghue & Kilkenny 1989: see chapter 4).

In this section, spectra of the SU UMa dwarf nova TY PsA from Warner, O'Donoghue & Wargau (1989) are re-examined in an attempt to improve the estimate of the period

of variability of the line profile asymmetries. The aim is to see whether this period is consistent with the beat period between the orbital and superhump periods. If the asymmetries vary on the beat period, the case for superhumps in AM CVn stars would be more secure. In AM CVn the available evidence is strongly suggestive of a superhump interpretation, but is not definitively established. In addition, the orbital period of AM CVn is not observed directly but is derived from a beat with the line profile asymmetry period (Patterson, Halpern & Shambrook 1993). In TY PsA, however, the photometric modulations during superoutburst are superhumps (by definition!) and the identification of the orbital period in the photometry is fairly certain. The observation, therefore, of varying absorption line asymmetry on the beat period between the orbital and the superhump periods, supports the interpretation that we have adopted for AM CVn, i.e. that the principal photometric modulations in AM CVn are caused by the superhump mechanism that operates in SU UMa dwarf novae.

3.3.2 The orbital and superhump periods

Spectra and photometry of TY PsA in quiescence and superoutburst were obtained by Warner, O'Donoghue & Wargau (1989). Photometric observations at or near quiescence show rapid flickering and flare-like behaviour superimposed on an orbital modulation of brightness (see figure 3.11). The flickering behaviour in the light curves of TY PsA is similar to that of V442 Oph: in V442 Oph, however, the brightness modulation is a superhump, not an orbital modulation, and is more sinusoidal in shape. The dominant flickering time scale in TY PsA is $\sim 10\,\mathrm{min}$. Power spectra of the quiescent light curves of TY PsA yield an orbital period $P_{orb} = 2.016 \pm 0.002\,\mathrm{h}$. The first harmonic of the orbital period is also present with an amplitude about one-third of the orbital modulation (Warner, O'Donoghue & Wargau 1989). During the middle and late stages of a superoutburst in June 1984, superhumps were observed with a period $P_s = 2.103\,\mathrm{h}$. The beat period between P_{orb} and P_s is 2.022 d.

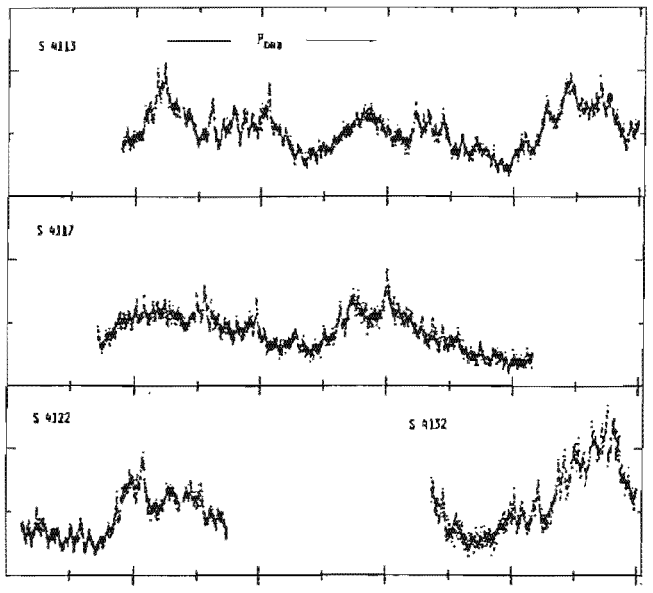

Figure 3.11: Light curves of TY PsA in quiescence from Warner, O'Donoghue & Wargau (1989). The flickering behaviour is similar to that of V442 Oph (figures 3.1 and 3.5), but in TY PsA is superimposed on an orbital modulation, whereas in V442 Oph the slow variations are a superhump modulation.

3.3.3 Line profile skewness variations

In superoutburst, the spectrum of TY PsA shows a blue continuum and broad, shallow Balmer absorption lines with central emission cores. The strength of the emission core weakens towards the higher members of the Balmer series. The line widths range from 4500km s^{-1} at Hϵ (full width at the continuum level) to 9000km s^{-1} at H$_\beta$. It was noted by Warner, O'Donoghue & Wargau (1989) that there were significant differences between the spectra from night to night: the emission cores in the broad absorption lines lie on alternate sides of the absorption troughs on consecutive nights. After removing the emission cores by fitting Gaussian profiles and subtracting them from the spectra, it was observed that the residual absorption profiles were strongly asymmetric, but that the extreme wings of the lines did not change from night to night. It was concluded that the observed changes in γ-velocity are due to changes in the line profiles and not the line

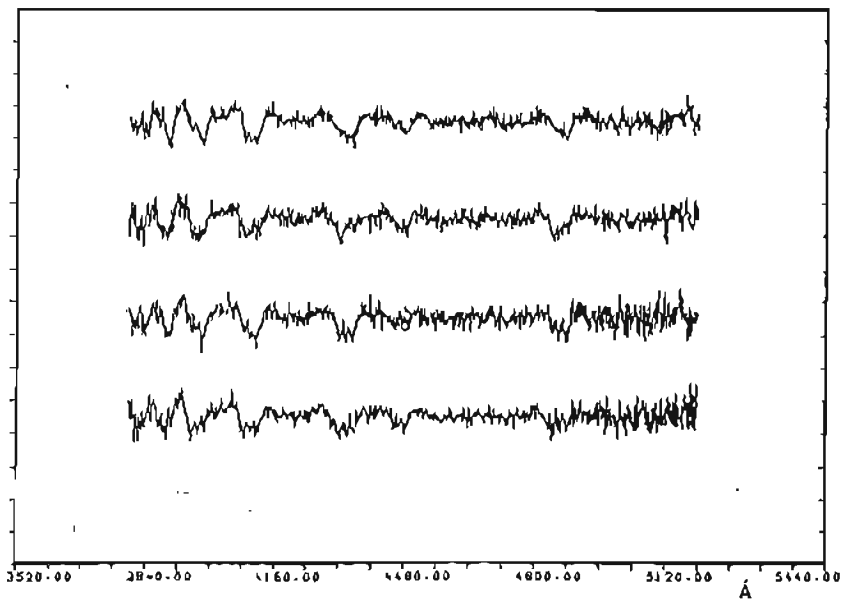

Figure 3.12: Normalised spectra of TY PsA on four consecutive nights during a superoutburst. The asymmetry of the absorption lines appears to vary on a period of $\sim$ 2 days, corresponding to the beat period between the orbital and the superhump periods. From Warner, O'Donoghue & Wargau (1989).

positions.

Figure 3.12 shows the mean normalised absorption spectra for four consecutive nights during the superoutburst (with the emission cores removed). It is clear that the asymmetries of the absorption lines change sense such that the lines are skewed to the right on the first and third nights, and to the left on the second and fourth nights. The period of variability (if the asymmetry variations are indeed periodic) appears to be $\sim$ 2 days.

In order to refine the estimate of the line profile asymmetry variability, the skewness (third moment) of the Balmer absorption lines was calculated using an approach similar to that of Patterson, Halpern & Shambrook (1993) in their study of the line profile variability in AM CVn. The wavelength-calibrated superoutburst spectra from Warner, O'Donoghue & Wargau (1989) were used: these were obtained on 1984 June 22 – 25 with the Reticon Photon Counting System and Unit Spectrograph on the 1.9 m telescope at Sutherland. The spectra are in sequences of eight 210 s exposures followed by a comparison Cu/Ar arc calibration spectrum; approximately 6 such sequences were obtained per night. Further

details of the reductions can be found in Warner, O'Donoghue & Wargau (1989). The analysis described below was performed using the Starlink DIPSO package (Howarth et al. 1995) as well as FORTRAN routines written specifically to calculate the third moment of the absorption lines.

First, the instrumental response was removed from the spectra. To do this, all 168 spectra from the four nights were summed and then smoothed using a Gaussian filter with $\sigma = 2$. The wavelength intervals free from any obvious spectral lines were identified by eye. Each individual spectrum was corrected by fitting a spline curve to the data in these wavelength intervals, and dividing the spectrum by this curve to yield a "flattened" spectrum with the continuum level at 1.0 (see figure 3.13).

The spectra were summed to give three spectra per night, each with a total integration time of about 1 h. The lines Hδ and Hϵ were chosen for the skewness analysis because the central emission components are weak: although the emission core can be removed from each line in turn before the third moment is calculated, this could introduce non-systematic changes to the line profile from spectrum to spectrum. Another way of avoiding the emission cores would be to calculate the third moment in the wings of the line. The disadvantage with this approach is that the skewness in the line wings is less pronounced than in the line cores.

The third moment S of each line is

$$S = \frac{\Sigma_i(\lambda_i - \lambda)^3(F_{cont} - F_i)}{\Sigma_i(F_{cont} - F_i)}. \tag{3.1}$$

The sum is taken over a particular wavelength interval around the line centre, λ_i is the wavelength of a point in that interval, F_i is the corresponding flux value, F_{cont} is the value of the continuum flux ($F_{cont} = 1$ for the normalised spectra), and λ is the rest wavelength of the line. The widths of the Hδ and Hϵ absorption lines (measured from the sum of all the superoutburst spectra) are 89 ± 2Å (measured at the continuum) for Hδ and 75 ± 4Å for Hϵ; these correspond to velocities of $\sim 3250\mathrm{km\,s^{-1}}$ and $\sim 2730\mathrm{km\,s^{-1}}$ from the line centre, respectively. The skewness of the lines was calculated in the interval

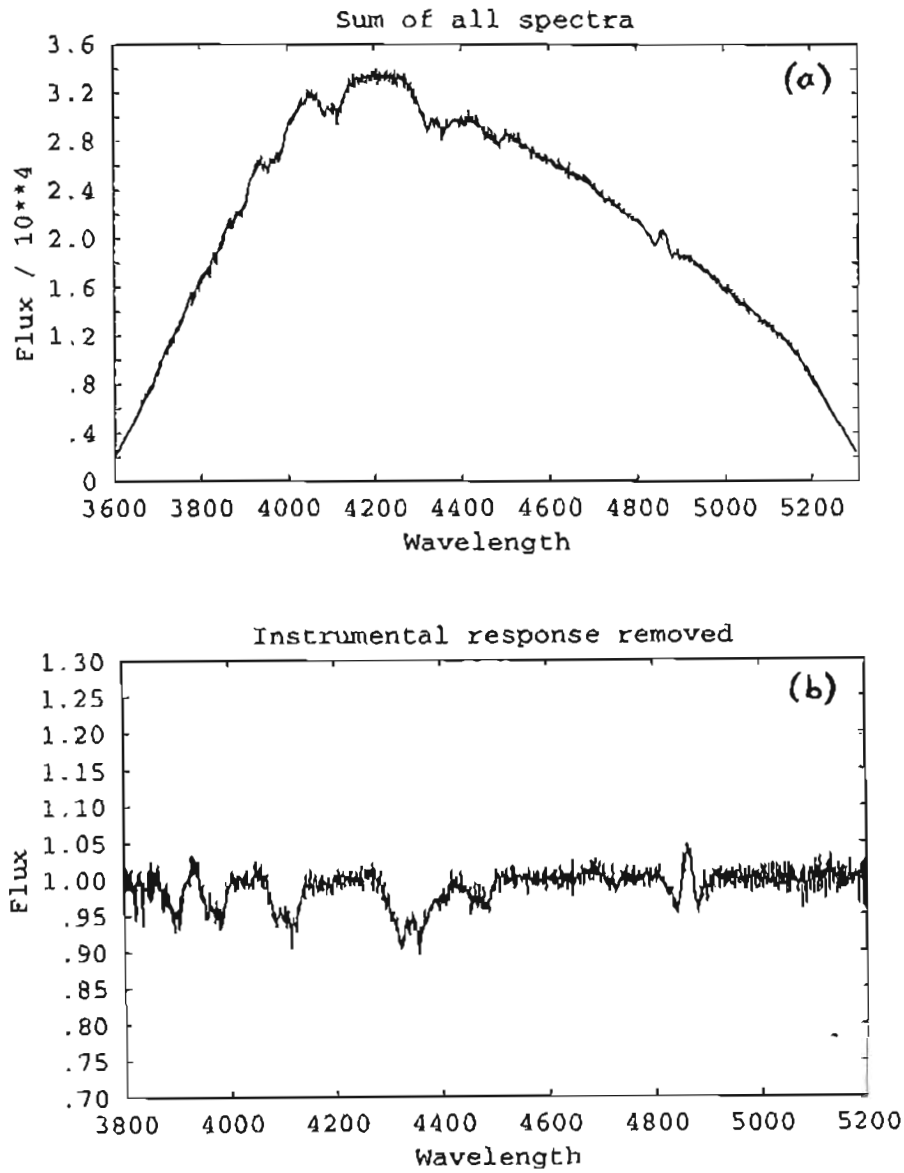

Figure 3.13: Sum of all the superoutburst spectra of TY PsA from Warner, O'Donoghue & Wargau (1989), (a) before the instrumental reponse is removed and (b) after the spectrum is divided by a spline curve fit to the continuum.

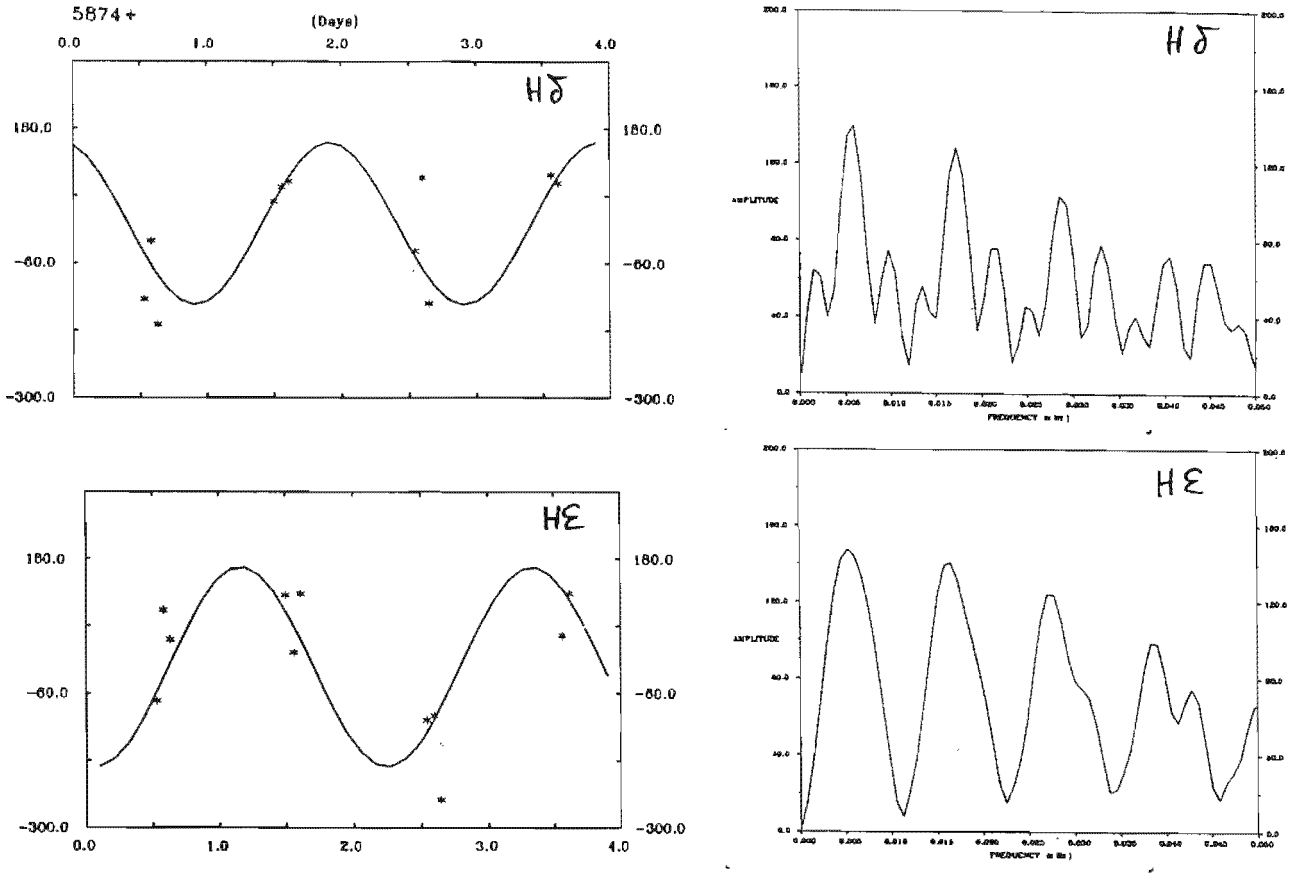

Figure 3.14: The changing skewness of the Hδ and Hϵ absorption lines together with the amplitude spectra for these variations. The best-fitting sinusoids are shown. The amplitude spectra of the two skewness time series indicate a period of 2.1 ± 3 d.

$|v| \leq 3250 \mathrm{km\,s^{-1}}$ for Hδ and $|v| \leq 2700 \mathrm{km\,s^{-1}}$ for Hϵ.

Figure 3.14 shows the changing skewness of the line cores together with non-linear least squares sinusoid fits to the skewness variations. The Fourier amplitude spectra of the skewness results for the two lines are shown alongside. The non-linear least squares fits give $P = 2.2 \pm 0.3$ d, $A = 180 \pm 80$ Å^3 and T_{max} =JD$_\odot$5875.16 $\pm$ 0.07 for Hϵ, and $P = 2.0 \pm 3$ d, $A = 150 \pm 90$ Å^3 and T_{max} =JD$_\odot$5873.91 $\pm$ 0.07 for Hδ.

Having obtained independent (but poor) estimates of the beat period of TY PsA from the spectroscopy, the results were coadded on the photometric beat period to verify that

the spectroscopic and photometric beat periods are compatible. Although only a small part of the beat cycle is covered by the spectra, the results (figure 3.15) obtained by folding the skewness data on a period of 2.022 d are reasonable. Because the beat period in most SU UMa stars is ~ 2.2 d, in order to get better coverage of a beat cycle it would require cooperative observing from opposite sides of the globe. A WET campaign would be feasible for systems such as RZ LMi which show very frequent superoutbursts.

Superhumps in the SU UMa dwarf novae are best understood as arising from tidal stresses in a precessing non-circular disc (see, for example, Warner 1995c). The similarity between the line profile variations in the spectra of superoutbursting dwarf novae and those of AM CVn is crucial evidence which supports the superhump model for the AM CVn stars.

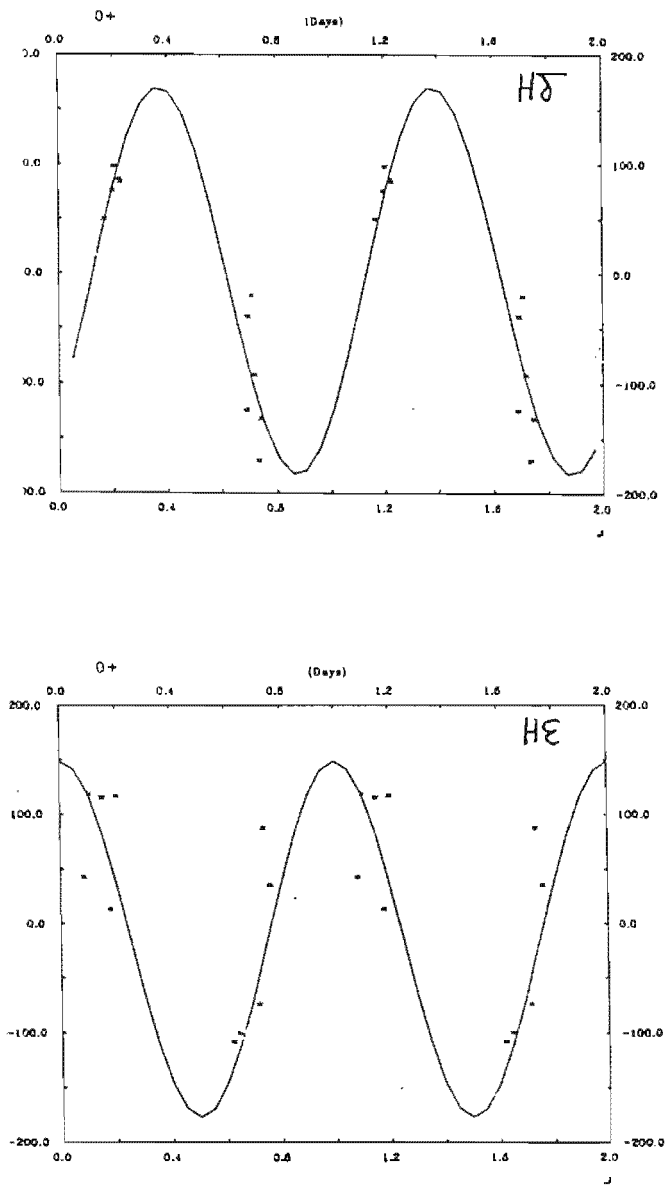

Figure 3.15: The skewness time series for Hϵ and Hδ coadded on the photometric beat period.

Chapter 4

V803 Centaurus

4.1 Introduction

During a photometric survey of a region around the galaxy NGC 5128, Elvius and Hall (1964) noticed a star on their survey plates with strong intensity variations and blue colours. Further investigation by Elvius (1975) revealed variations in V from 14th to 17th magnitude with no accompanying change in $B-V$, and spectra showing broad absorption lines of He I with intensities varying on a time scale of days. Westin (1980) confirmed the variations in the intensities of the He I lines, and showed a correlation between the line strengths and the object's brightness. In addition, large radial velocity variations of $\sim 400\,\mathrm{km\,s^{-1}}$ on a time scale of about a day were observed (see figure 4.1). In an attempt to account for the enigmatic properties of the star, Elvius (1975) and Westin (1980) compared the star to other hydrogen deficient stars such as the DB white dwarfs and the R CrB star MV Sgr. Elvius noted the similarity of the spectra of AE-1 to those of HZ 29 (AM CVn), but excluded the possibility of a close binary model due to the lack of evidence for rapid photometric variations in her observations.

AE-1 was given the variable star designation V803 Cen (Kholopov 1985), and identified as a possible IBWD candidate during a literature search conducted by E L Robinson. This prompted a search for short time scale variations similar to those seen in AM CVn and CR Boo (PG 1346+082). These were found by Kepler (1987) and studied by O'Donoghue, Menzies & Hill (1987), who identified a 1611 s periodicity in the light curve very similar

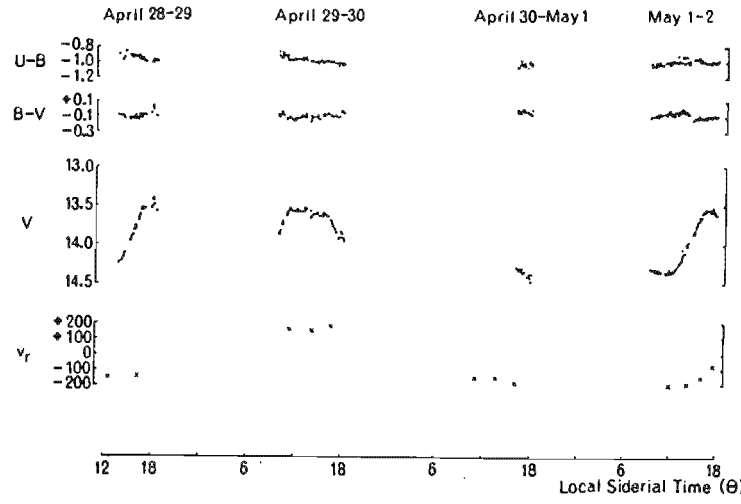

Figure 4.1: Photometric and radial velocity variations of V803 Cen from Westin (1980). There are large ~ 4 magnitude variations in V over the four day period, with no accompanying variations in $U-B$ or $B-V$. Large radial velocity variations with an amplitude of $\sim 400\,\mathrm{km\,s^{-1}}$ are present.

to the 1490 s period seen in PG 1346+082 (Wood et al. 1987). It was concluded that V803 Cen was indeed the same kind of object as PG 1346+082 and AM CVn, and an interacting binary white dwarf model was proposed.

Recent studies of V803 Cen have revealed a plethora of intriguing photometric and spectroscopic properties. The rapid photometric variability in V803 Cen is due to two basic periods: 1611 s and 175 s. The 1611 s variation has an amplitude of about 5%. In the high state ($V \sim 13.5$), up to eight harmonics of the 1611 s period are present in the light curve; the strength of the fundamental and its harmonics is variable from night to night (O'Donoghue, Menzies & Hill 1987). The 175 s period is close to, but not consistent with, the eighth harmonic of the 1611 s period. The 1611 s signal disappears from time to time: O'Donoghue, Menzies & Hill (1987) observed rapid variability during July 1986 when the star was at a mean magnitude of $B \sim 13.5$; the rapid variations were either absent or of considerably lower amplitude during the previous May, when the mean magnitude

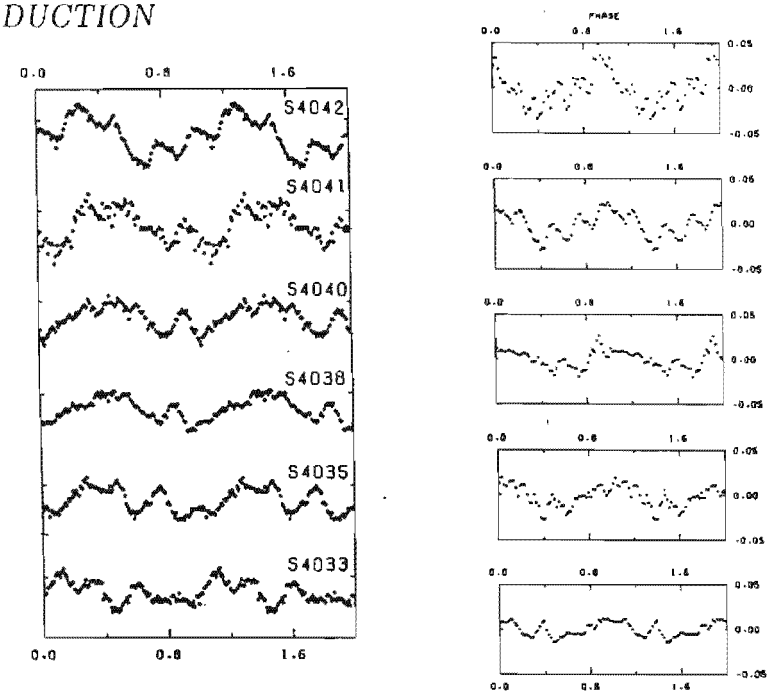

Figure 4.2: The variable photometric pulse shape of the 1611 s variation in V803 Cen from O'Donoghue, Menzies & Hill (1987) and O'Donoghue & Kilkenny (1989).

was $B \sim 14.0$. Similar behaviour has been seen in CR Boo: some high speed photometry runs show no rapid photometric variations exceeding 0.5%. The changing harmonic structure gives rise to a variable 1611 s pulse shape. Figure 4.2 shows two sequences of mean light curves from O'Donoghue, Menzies & Hill (1987) and O'Donoghue & Kilkenny (1989) folded on the principal period. There is a striking similarity between the pulse shapes in these two sequences (see the next section for a discussion). The photometric variations in both V803 Cen and CR Boo are most evident in the high state, implying a disc origin. There is no evidence for light from either of the component stars (O'Donoghue & Kilkenny 1989).

The 1611 s period was observed by O'Donoghue, Menzies & Hill (1987) to maintain coherence over a period of 4 days when the system was at $B \sim 13.4$, but when the system faded to $B \sim 15.4$, the coherency of the 1611 s period appeared to break down and a significant period change in the 175 s period was observed. An apparent correlation between the coherence of the photometric periods and changes in the overall brightness of the system is also observed in CR Boo, where the 1490 s period maintains coherence for

about a week, a time scale similar to the quasi-period of the large-amplitude luminosity variations observed in this system (Wood et al. 1987). The mean magnitude variations of V803 Cen are rather erratic, unlike those of CR Boo, which have a definite quasi-period of 4–5 days.

In the low state ($V \sim 17$), the amplitude of the 1611 s variation (in units of fractional intensity) is much smaller than in the high state; however, the *relative* amplitude could be comparable to that seen in the high state (O'Donoghue et al. 1990). Neither the harmonics of the 1611 s nor the 175 s period have been detected in the low state light curve. A tentative identification of flickering, the give-away signature of mass transfer, was made in Whole Earth Telescope data (O'Donoghue et al. 1990); flickering has also been observed in CR Boo in the low state (Wood et al. 1987). One of the WET runs in the low state (S4232) bears a strong resemblance to high speed photometry of GP Com due to the large amplitude, low frequency flickering behaviour: see for example run A341 of GP Com (chapter 5) where the flickering occurs on a time scale of ~ 5 min and has an amplitude of about 10%.

The high state spectra of V803 Cen show a blue continuum displaying only broad, shallow absorption lines of HeI (Elvius 1975, Westin 1980, Kepler et al. 1989, O'Donoghue & Kilkenny 1989). Possible detections of He II λ6560 Å (Kepler et al. 1989) and weak features at $\lambda\lambda$4625, 4673 Å (Westin 1980, O'Donoghue & Kilkenny 1989) have also been made in high state spectra. The absorption lines have full widths at half maximum of ~ 20 Å and are 10 - 20% deep: they are roughly twice as deep and narrow as those of AM CVn and CR Boo (it is probable that V803 Cen has a lower inclination than AM CVn and CR Boo). The line profiles show evidence of doubling, typical of lines formed in an accretion disc (O'Donoghue et al. 1990) and have decidedly asymmetrical profiles (O'Donoghue & Kilkenny 1989): see figure 4.4. There are large variations in the widths of the He I lines at a given wavelength, ruling out Doppler broadening as the dominant cause of line-broadening; the widths of the stronger lines appear to be consistent with Stark broadening in a $\log g = 6$ atmosphere, which is appropriate for the inner regions of an accretion disc around a white dwarf (O'Donoghue & Kilkenny 1989). The weakness of lines such as $\lambda\lambda$3889 & 4713 Å relative to a model of a $\log g = 6$ atmosphere indicate that non-LTE effects are very important in the line-forming region. The spectra of

V803 Cen display a flat He I decrement: this corresponds to the flat Balmer decrement seen in hydrogen-rich CVs (Warner 1995a) and indicates that the lines are optically thick (O'Donoghue & Kilkenny 1989).

As the system fades from high to low state, the strength of the He I lines decreases. At an intermediate state ($B \sim 15.4$) the spectrum is virtually featureless; the black body distribution which most closely matches the shape of the continuum has a temperature of 10 000 – 15 000 K (O'Donoghue, Menzies & Hill 1987). The low state spectrum of V803 Cen displays weak emission features of He I (O'Donoghue & Kilkenny 1989, O'Donoghue et al. 1990). The accretion disc appears to be the main source of optical light since, even in the low state, there is no sign of the Stark-broadened absorption lines that one would see from the DB primary (O'Donoghue & Kilkenny 1989).

IUE spectra of V803 Cen (Ulla & Solheim 1991) show lines of N IV, N V, Si III, Si IV and C IV which change from emission in the low state to absorption in the high state. The UV lines are generally deeper and more variable in equivalent width than in the optical; dramatic line variations are evident on a time scale of a few days. The UV absorption line widths are less than 10 Å, i.e., much narrower than in the optical. Radial velocities obtained from the ultra-violet lines are considerably larger than those found in the visible: N V, Si III, Si IV and C IV show variations from -1800 km s^{-1} to 1200 km s^{-1} (Ulla & Solheim 1991).

There is no periodic radial velocity variability in the range 400 - 10 000 s in the high state spectra; all variations have a stringent upper limit of 16 km s^{-1} (O'Donoghue & Kilkenny 1989). Specifically, no radial velocity variations have been detected at any of the photometric periods. However, variations in the asymmetry of the absorption lines on a time scale of hours are present (see figure 4.3), and there is a relative velocity shift of 70 km s^{-1} from one night to the next. The asymmetry variations produce a linear trend in radial velocity during each night: the radial velocities reported by Westin (1980) are apparently also due to the line asymmetry variations rather than real changes in the motion of the system from one night to the next. O'Donoghue & Kilkenny (1989) were the first to suggest a tidal origin for the varying line asymmetries and pointed out the similarities to the variable line asymmetries seen in the dwarf nova TY PsA in superoutburst (Warner,

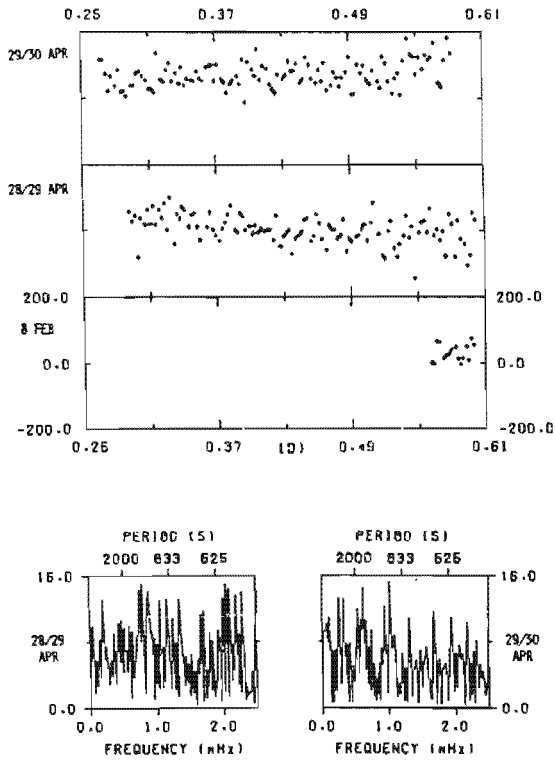

Figure 4.3: Radial velocities for V803 Cen on 28/29 and 29/30 April 1987 (from O'Donoghue & Kilkenny 1989). The lower two panels show power spectra of the radial velocities: no periodic variations with an amplitude exceeding $16\,\mathrm{km\,s^{-1}}$ were found in the frequency range 0.1-2.5 mHz. However, there are slow linear drifts in radial velocity during each night.

O'Donoghue & Wargau 1989).

The aim of this chapter is to re-examine both the photometric and spectroscopic data of O'Donoghue & Kilkenny (1989, hereafter OK89) to see whether the data are consistent with a non-circular precessing disc model. As discussed in Chapter 1, the most compelling evidence to support the model would be the presence of a definite period in the asymmetry of the He I absorption line profiles or in the radial velocity variations (the slow drifts in γ-velocity on a time scale of hours are caused by the changing asymmetry). The line profile asymmetry period is predicted to be ~ 37 h if the primary masses in AM CVn and V803 Cen are the same (see chapter 1 equation 1.17). The period of the line asymmetry

or radial velocity variations is the beat period between the 1611 s variation and the orbital period; the orbital period of the system could thus, in principle, be determined. We are at a disadvantage in that the line profile asymmetries seen in V803 Cen are smaller than those seen in AM CVn and CR Boo; also, the absorption lines are twice as narrow as those in AM CVn and CR Boo, making detection of periodic variations in the line asymmetry difficult.

In AM CVn, the beat period between the superhump and orbital periods can also be seen in the photometry (see chapter 1 section 1.1.4.2). In WET data, the harmonics of the unseen 1051 s fundamental have a multiplet structure in which smaller peaks appear on the high frequency side of the dominant peak (Provencal et al. 1995). The frequency difference between the dominant peak and the second component is 20.77 μHz; the inverse of this is the line profile skewness period. The photometric data in OK89 are single-site data. As a result, the alias patterns in the amplitude spectra prevent a clear identification of any low-amplitude peaks underlying or near the 1611 s period and its harmonics. Aliasing is a problem, since two photometric variations closely-spaced in frequency can produce overlapping alias patterns which create a spurious peak in the amplitude spectrum, leading to misidentifications. However, if the frequency difference between one of these low amplitude peaks and the nearby large-amplitude peak corresponds to a period determined from the line asymmetry or radial velocity variations in the spectroscopy, the correct low amplitude-peak might be identified as a member of a multiplet similar to those seen in the WET data of AM CVn.

4.2 Spectroscopy

Wavelength-calibrated spectra from OK89 were used to search for periodic variations in the absorption line profiles. The spectra were obtained on two successive nights (28/29 April and 29/30 April 1987) and comprise sequences of five 200 s exposures on V803 Cen followed by a 100 s Cu/Ar arc calibration spectrum. The details of the reductions can be found in OK89. Further analysis described below made use of the Starlink DIPSO package (Howarth et al. 1995), as well as FORTRAN routines written specifically to calculate

the absorption line asymmetries.

The first step was to remove the instrumental response from each spectrum. The placement of the continuum had to be indentical for each spectrum in order to avoid altering the line profile asymmetries in a non-systematic way. Firstly, all the spectra from both nights were summed and a Gaussian filter with $\sigma = 2$ was applied in order to make the identification of the continuum intervals easier. The continuum intervals were identified by inspection. Spline and third order polynomial fits were made to the continuum intervals, and the summed spectra were divided by the fits to produce the "flattened" spectra shown in figure 4.4. Because the spline fits to the continuum intervals produced an apparently better instrumental response correction, a spline fit was used for the subsequent analysis. For each spectrum, a spline curve was fitted to the continuum level in the previously determined intervals, and the spectrum was divided by the curve.

The individual (continuum-normalised) spectra were examined by eye for any obvious asymmetry variations in the absorption line profiles. Patterson, Halpern & Shambrook (1993) obtained spectra of AM CVn with an integration time of 1051 s in order to eliminate any modulations that may exist at this period. Unfortunately a similar approach could not be followed for V803 Cen: spectra were summed in groups of five, giving an effective integration time of 1000 s. The asymmetry calculations (see below) were also performed on groups of ten spectra in an attempt to reduce the scatter in the results. Following the approach of Patterson, Halpern & Shambrook (1993), four strong and unblended lines were selected: $\lambda\lambda$3705.3, 3819.7, 4387 and 4471.5 Å. The asymmetry of each line was calculated by determining the third moment S of each line (see equation 3.1). The mean magnitude of V803 Cen on each of the two nights of observation is $B \sim 13.3$; as the line depth is correlated with system luminosity, the line depths for the two nights are expected to be similar.

Patterson, Halpern & Shambrook (1993) calculated the asymmetry in the line core, which they defined to be $|v| < 1000\,\mathrm{km\,s^{-1}}$. Because the absorption lines in V803 Cen are roughly twice as deep and narrow as those in AM CVn, it was not clear at the outset in which velocity interval the asymmetry would be most obvious. Asymmetries for the four lines were thus calculated for five velocity intervals: $|v| < 500$, 750, 1 000, 1 500 and

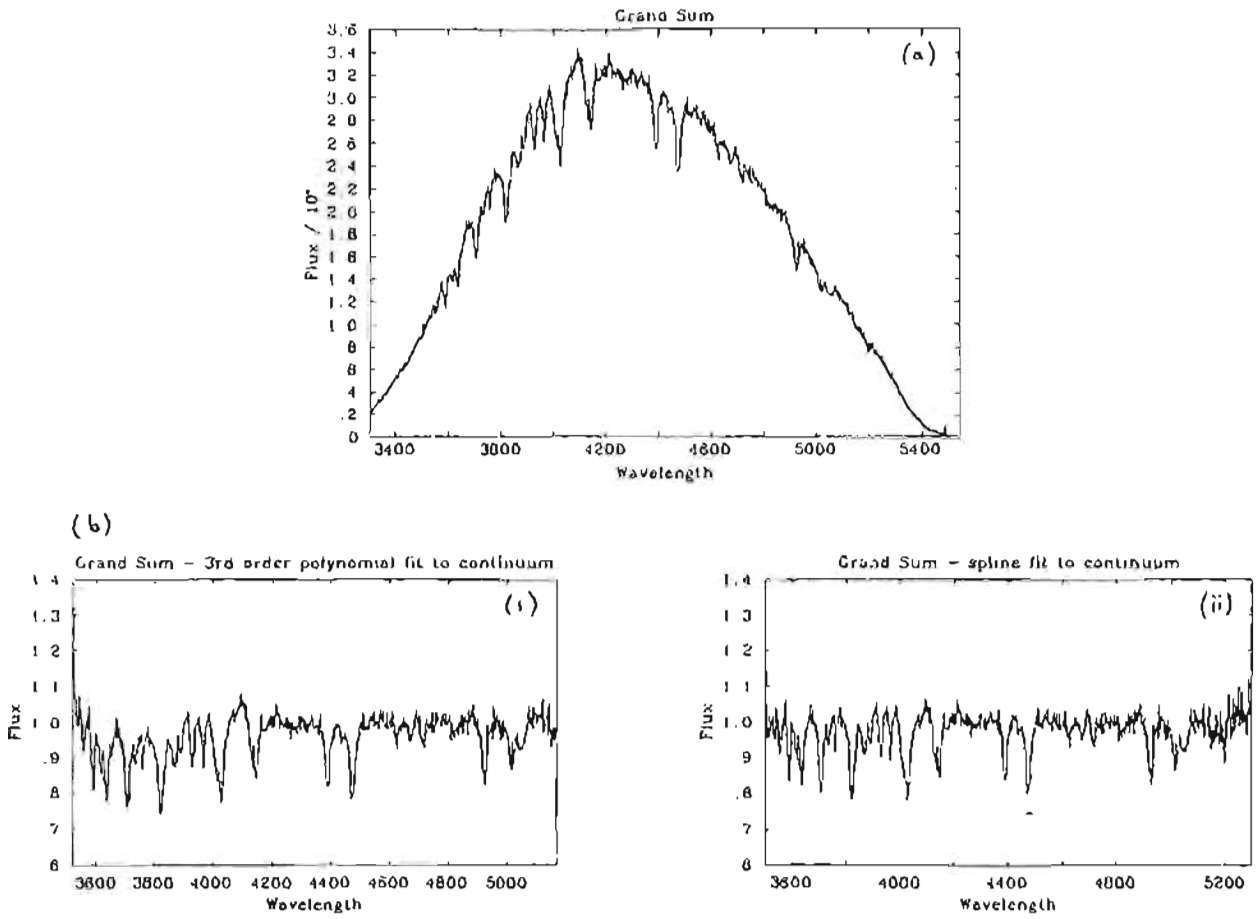

Figure 4.4: (a) The sum of the high state spectra of V803 Cen from O'Donoghue & Kilkenny (1989). The spectrum has a blue continuum and displays wide, shallow and asymmetric absorption lines of He I. (b) The summed spectrum after division by (i) a third order polynomial and (ii) spline fit in order to remove the instrumental response.

2000 km s^{-1} . Drifts in asymmetry were clearest in the groups of ten spectra and in the velocity interval $|v|$ <750 km s^{-1} : see figure 4.5. The trends in the asymmetry variations of e.g. λ4387.9 Å, where there appears to be a gradual decrease in the third moment during the first night and an increase during the second, have the same sense as the radial velocity drifts in figure 4 of OK89. Although we cannot guess a period for the skewness variations, it is clear that there is some asymmetry drift over a time scale of hours that is consistent with a model in which the accretion disc in V803 Cen is non-circular.

Because the variations in radial velocity track the changes in asymmetry, the period of variation in the line profile asymmetry might be discernable in the radial velocities. The radial velocity curve in figure 4.1 from Westin (1980) indicates a smooth variation from -200–200 km s^{-1} over four days. The period of variation (if a unique period exists) appears to be a sub-multiple of three days, since the curve has returned to its starting point after $\sim$ 3 d. The linear trends in radial velocity shown in Figure 4 of OK89 have a gradual slope of $\sim$ 20 km s^{-1} h^{-1}; this eliminates 9 h as a candidate radial velocity period (the duration of each of the runs in OK89 is $\sim$ 8 h).

The Fourier amplitude spectrum of the radial velocities from Westin is shown in figure 4.6. The periods in the amplitude spectrum were refined by a non-linear least squares fit. The highest peak in figure 4.6 corresponds to a period of 73 $\pm$ 2 h and an amplitude of 216 $\pm$ 15 km s^{-1} . The errors quoted are the formal errors of fit from the non-linear least squares fitting routine; the real errors are probably considerably larger due to the sparseness of the data. A more conservative error calculation gives an uncertainty of $\sim$ 14 h. The second highest peak corresponds to a period of 36 $\pm$ 2 h and the third to 18 $\pm$ 1 h (these are all sub-multiples of 3 d, as expected).

To check that the original data are adequately described by a sinusoid with the frequency of the first peak in figure 4.6, data were synthesised at the frequencies, amplitudes and phases of the first four peaks in figure 4.6 and sampled as the original radial velocity data. The amplitude spectra for these artificial data are shown in figure 4.7. The amplitude spectrum of the data synthesised using the parameters of the first peak in figure 4.6 corresponds most closely to the amplitude spectrum of the original data. Thus, a line profile variation with a period of 73 $\pm$ 2 h best fits the data of Westin (1980).

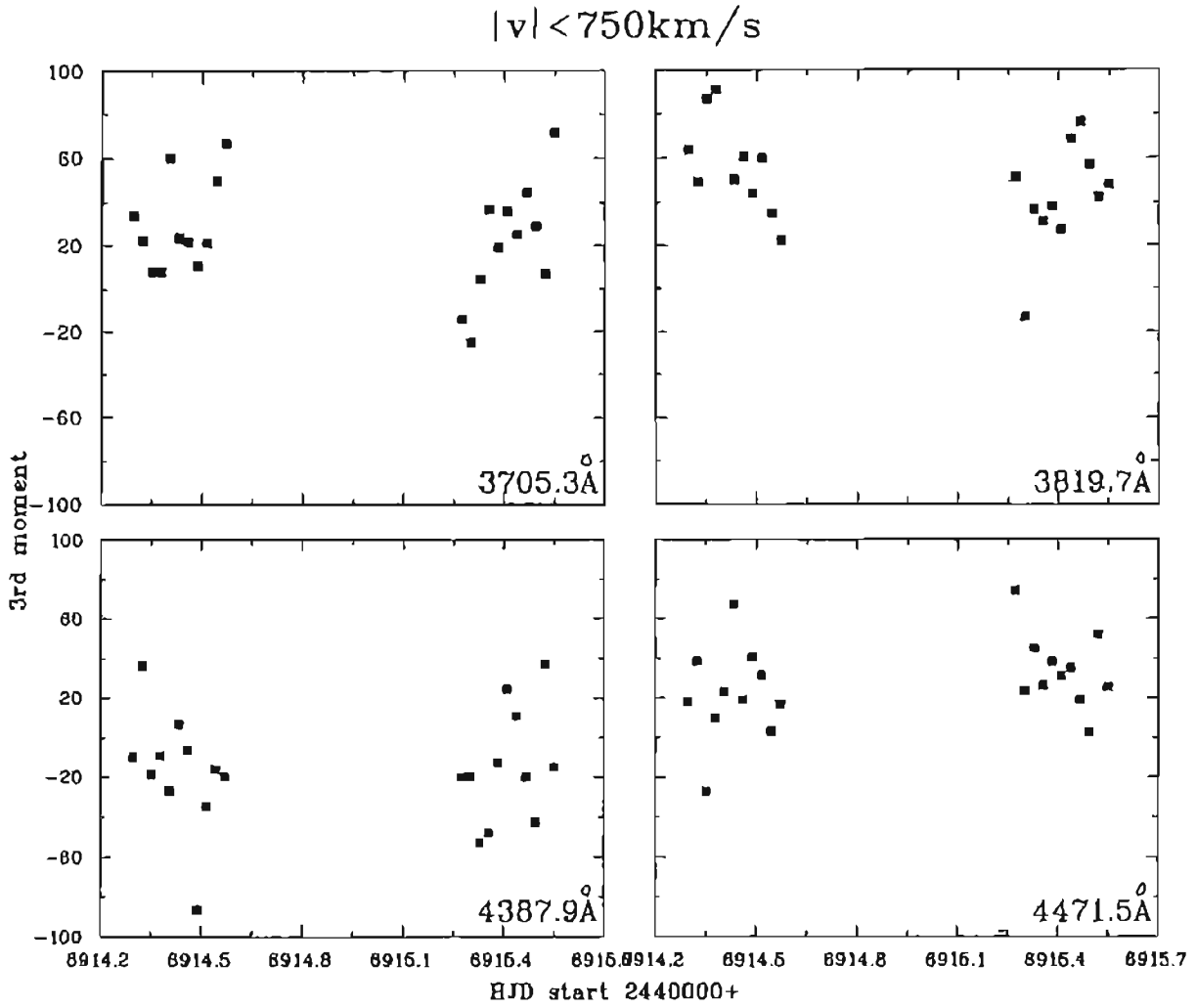

Figure 4.5: The variation in time of the asymmetry (third moment) for the lines λλ3705.3, 3819.7, 4387.9 & 4471.5 Å on the nights 28/29 April and 29/30 April 1987. Although a period of variation cannot be determined, the asymmetries display drifts which could be produced in an eccentric, progradely precessing disc.

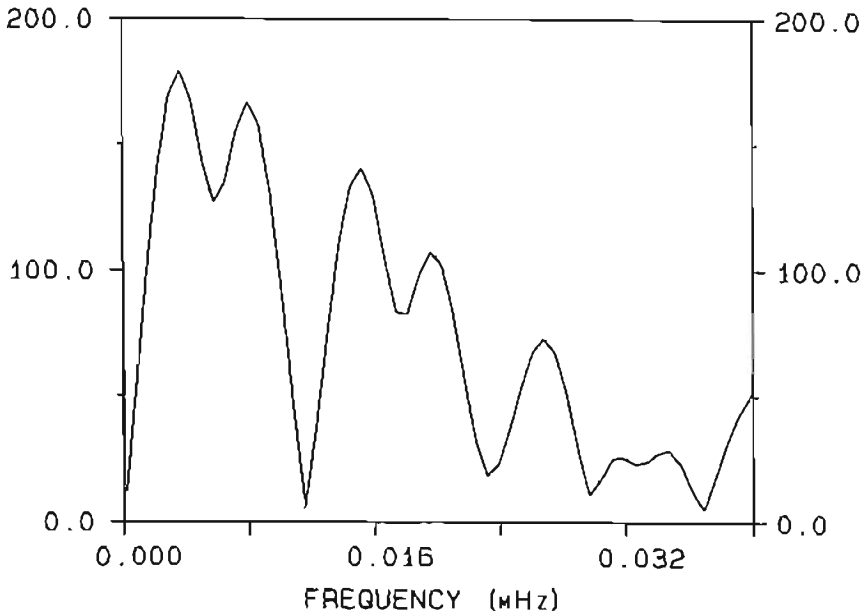

Figure 4.6: Fourier amplitude spectrum of the radial velocity variations from Westin (1980). The ordinate scale is in $\mathrm{km\,s^{-1}}$.

4.3 Photometry

The next step is to search the photometry for signs of fine structure as seen in the amplitude spectra of AM CVn (Provencal et al. 1995). The V803 Cen data consist of 43 h of high speed photometry obtained on 6 consecutive nights in April and May 1987, during which the star was in a high state with a mean B magnitude of 13.4 (see OK89 for details of the reduction procedure). The analysis described here (as is the case with most of the photometric analysis for this dissertation) was performed using the program EAGLE, written by Darragh O'Donoghue.

What is the magnitude of the fine structure splitting that might be expected in V803 Cen? In AM CVn, the radial velocity period (as well as the line profile asymmetry period) is the precession period of a non-circular disc, and represents the beat period between the superhump and the orbital variation. We expect the beat period of V803 Cen to be larger than that of AM CVn, because V803 Cen has a longer orbital period than AM CVn (see

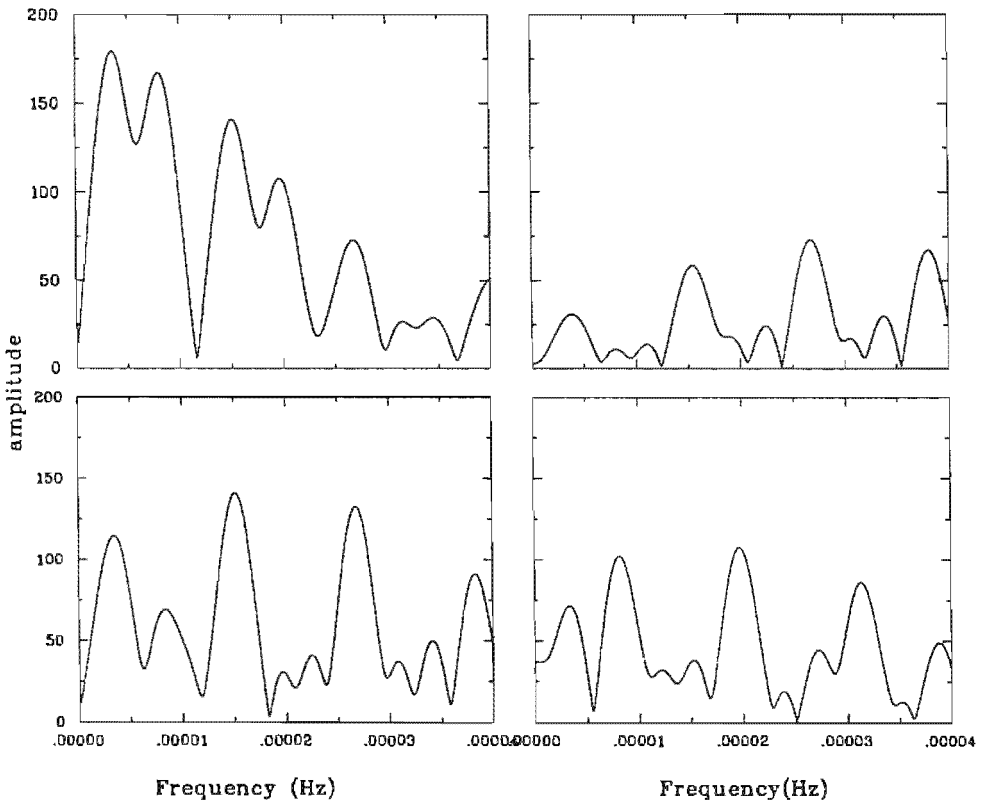

Figure 4.7: Fourier amplitude spectra of data synthesised at the frequencies, amplitudes and phases of the first four peaks in figure 4.6.

section 1.3.1). The principal variation in V803 Cen, 1613 s, is very similar to the 1051 s period of AM CVn and the 1490 s period in CR Boo, and probably represents a superhump period slightly in excess of the orbital period[1]. The precise values for the dominant variation are found by fitting a sinusoid of variable period, amplitude and phase to the data; this gives $P = 1613.0 \pm 0.3$ s, $A = 0.0069 \pm 0.0004$ (in units of fractional intensity) and T_{max} =JD$_{\odot}$6914.2444 $\pm$ 0.0005. These are *mean* values, because the 1613 s period shows amplitude and phase variability over the six nights. If we assume that the radial velocity period of 73 ± 2 h is the beat period between the orbital and the (mean) superhump period, the orbital period is 1603.1 ± 0.3 s. The orbital and superhump frequencies differ by 3.8 ± 0.1 μHz. If our model is correct, we can expect to find low-amplitude peaks separated from the harmonic peaks by this amount.

4.3.1 Mean light curves and pulse shape evolution

The complex pulse shapes (figure 4.2) are due to the 1613 s period and its harmonics. Although the 1613 s period derived from this set of observations differs by several standard deviations from the 1611 s period found in O'Donoghue, Menzies & Hill (1987), it is not clear that a real period change occurred from 1986 to 1987: due to the highly non-sinusoidal pulse shape, the formal errors of a non-linear least squares fit are an underestimate of the true uncertainty. Up to seven harmonics of the 1613 s variation are present in the nightly amplitude spectra. There are systematic changes in the amplitudes of the harmonic peaks (see figure 4.8). From bottom to top (i.e. chronological order) the power in the fundamental steadily grows, while the power in the first harmonic falls first and then grows. The power in the other harmonics also varies systematically.

The two sequences of mean light curves in figure 4.2 are very similar, and appear to follow the same chronological sequence. We can identify the following similar pairs: S4042 and S3882; S4041 and S3880; S4040 and S3879; S4035 and S3876. The combination of all the harmonics (and any unresolved components) creates a pattern in the mean light curve that drifts first one way and then the other, such that it appears to complete a full

[1]However, in AM CVn, the power at 1011 s is frequently as large as the power in the superhump harmonics. There may therefore be a system in which the dominant power is a *negative* superhump.

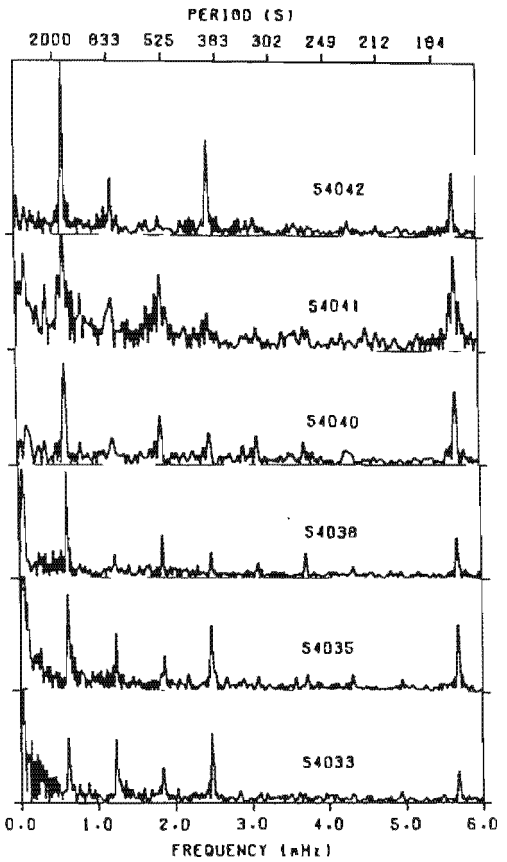

Figure 4.8: Nightly amplitude spectra of the six high speed photometry runs of V803 Cen in the high state (from O'Donoghue & Kilkenny 1989).

oscillation in about seven days.

4.3.2 Fine structure in the amplitude spectrum in the region of 1600 s

The cumulative amplitude spectrum of all six nights in the region of the principal frequency is shown in figure 4.9 together with the spectral window function. There are several low-amplitude peaks in the alias pattern that do not correspond to peaks in the spectral window function. In addition, the alias pattern envelope is not symmetrical: the alias peak on the high-frequency side of the principal peak has a greater amplitude than the alias peak on the low-frequency side. This may indicate the presence of nearby periods whose window patterns are entangled with that of the principal peak.

When the data are prewhitened by the 1613.0 s period and the amplitude spectrum is calculated for the residuals, the highest peak has $P = 1608.6 \pm 0.3$ s and $A = 0.0043 \pm 0.0004$. It can be seen from figure 4.9 that the peaks in the alias patterns of the 1613.0 s signal and those in the 1608.6 s signal overlap, implying that the two variations are *not resolved*. This means that the 1613.0 s peak in the full spectrum is not necessarily the correct frequency with which to pre-whiten the light curve to reveal the underlying structure: the peak in the original spectrum is pulled over slightly towards the lower-amplitude, unresolved component. In turn, this means that the 1608.6 s period is not properly determined. In the original spectrum, the one cycle day^{-1} alias of 1613.0 s near $\sim$ 1580 s has a higher amplitude than the alias peak on the low-frequency side. This could mean that the peak power of the unresolved frequency is at 1579.2 s, and that this period, not 1608.6 s, should be considered as the second strongest contributor of power (the value 1579.2 s is not well determined because of the blending with the main power).

Is the putative orbital period (as deduced from the radial velocity variations) present in the amplitude spectrum? When the 1613.0 s and 1608.6 s periods are subtracted from the light curve and the amplitude spectrum re-calculated, the dominant period is 1588.1 $\pm$ 0.3 s. The *fourth* highest amplitude peak in the 1600 s region belongs to a signal with $P = 1603.4 \pm 0.3$ s and $A = 0.0025 \pm 0.0004$ (marked with an arrow in the

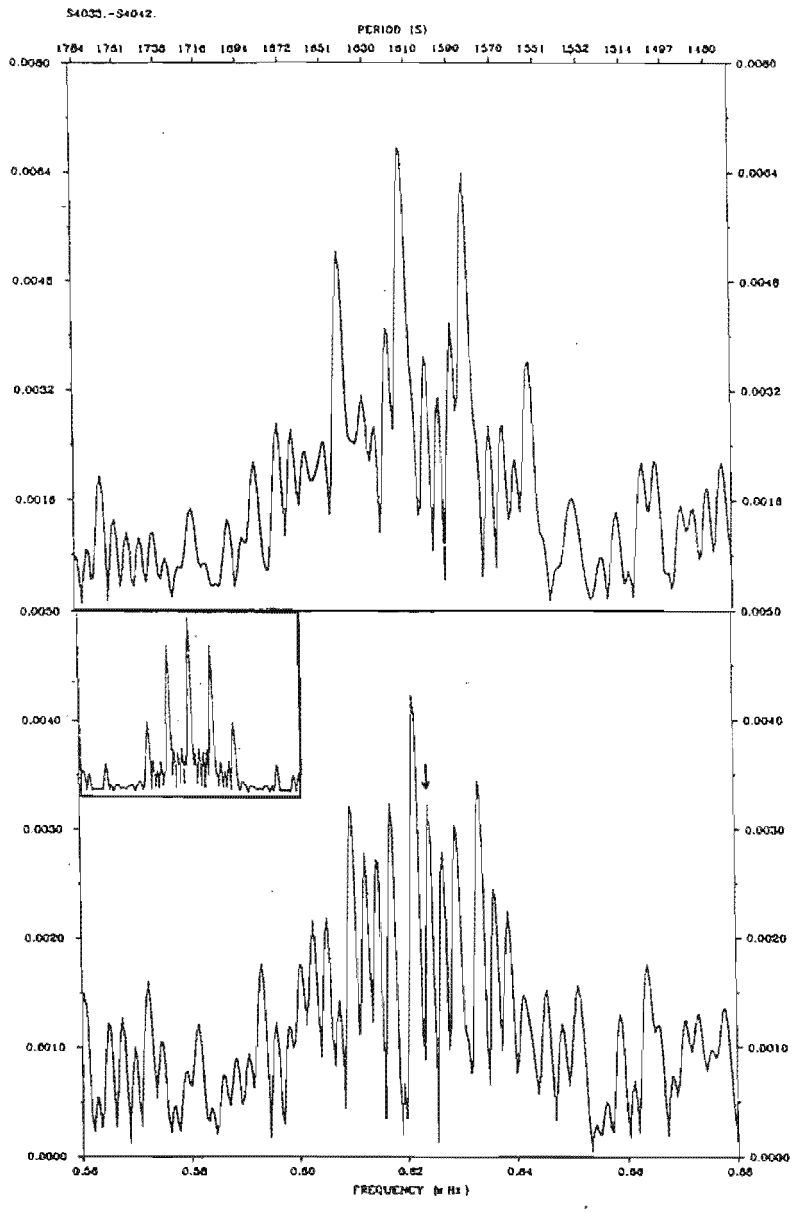

Figure 4.9: Amplitude spectra in the region of the principal 1613 s variation, and the amplitude spectrum of the data prewhitened by the principal frequency. The spectral window for the data is shown as an inset. The 1613 s period and its underlying signal are not resolved, since the peaks in their respective alias patterns overlap. The proposed orbital frequency is indicated by an arrow in the lower panel.

lower panel of figure 4.9. This period is consistent with the orbital period derived from the radial velocity data; its amplitude is approximately one third of that of the principal 1613.0 s signal.

Because the 1613.0 s and 1608.6 s signals are not resolved, an attempt was made to "clear up" the region around 1600 s by pre-whitening the original data by the putative orbital frequency, seeing as we have independent evidence that this signal is genuine. This done, the periods of the first and second highest contributors of power in the 1600 s region were calculated to be 1612.9 s and 1608.6 s (the formal errors are approximately 0.3 s). These are the best estimates of the two dominant periods that could be obtained from these data.

4.3.3 Fine structure near the harmonics of the 1613 s period

The amplitude spectrum was searched for fine structure in the region of the seven visible harmonics of the 1613 s period. The highest amplitude frequency for each of the seven harmonic peaks was calculated, and the data were prewhitened by this frequency. The amplitude spectrum was then re-calculated to identify the frequency with the next largest amplitude. This was repeated until all peaks significantly above the noise level were accounted for. The frequency differences between the principal peak and the nearby peaks were examined to see if there was any evidence for a constant frequency splitting (of 3.8 μHz, the difference between the proposed orbital and superhump frequencies, or any other constant amount). A low-amplitude peak with a splitting of 19.7μHz was found on the high frequency side of both the fundamental and the third harmonic peaks. The amplitudes of these peaks are $\sim$ 0.0014 in units of fractional intensity, about a fifth of the amplitude of the nearby principal peak. Apart from this, however, no constant frequency splittings between the harmonic peaks and nearby low-amplitude peaks were found.

4.3.4 Phase variations

OK89 observed a wandering in phase of the 1613 s period over $\sim$ 120° during the six nights of observation. The phases were calculated by fitting a sinusoid of $(1613)^{-1}$Hz to suc-

cessive overlapping sections of the data. Each section was approximately five cycles (i.e., 8060 s) long and the sections overlapped by 50%. Within each night's data, the intrinsic phase variations are much greater than the formal errors of fit: see figure 4.10. The third night in particular shows substantial phase variations during the run. The variations are due to both observational noise and noise intrinsic to the system – observational noise could include scintillation and photon noise, while system noise might include flickering that distorts the wave shape.

The phase variations appear to follow part of a sine curve which has a period longer than the observational baseline; with a bit of imagination one could propose a period of ~ 7 d. Interestingly, this is the period that was identified for the pulse shape evolution in the sequences of light curves in figure 4.2. Now, the beat period of 1613.0 s and 1608.6 s is approximately 6.8 d. It remains, however, to be seen whether the second strongest contributor of power in the 1600 s region of the amplitude spectrum is 1608.6 s, or its one cycle per day alias at 1579.2 s.

In an attempt to distinguish between the 1608.6 s and 1579.2 s signals, two sets of synthetic data were created. Each set is a superposition of two sinusoids of the form $A_1 \sin(\omega_1 t + \phi_1) + A_2 \sin(\omega_2 t + \phi_2)$. For one data set $\omega_1 = (1613.0)^{-1}$ Hz and $\omega_2 = (1608.6)^{-1}$ Hz, while the other has $\omega_1 = (1613.0)^{-1}$ Hz and $\omega_2 = (1579.2)^{-1}$ Hz. The amplitudes A_1 and A_2 are the amplitudes of the signals in the original data, as deduced from the amplitude spectra. The phases ϕ_1 and ϕ_2 are the phases of the signals in the original data. The idea is to see whether the phase variation observed in the real data can be duplicated by either or both sets of synthetic data.

The synthetic data were sampled as the real data and then fitted with a single sinusoid of variable frequency, phase and amplitude by non-linear least squares to determine the principal frequency for each synthetic data set. To calculate the variations in phase of the principal signal for each data set, a sinusoid of the appropriate frequency was fitted to successive sections of the data by least squares (as was done for the original data). The results are shown in figure 4.10. Because the synthesised data are noiseless, it is difficult to decide which of the two synthetic data sets produces a phase variation that is more like the original phase variation.

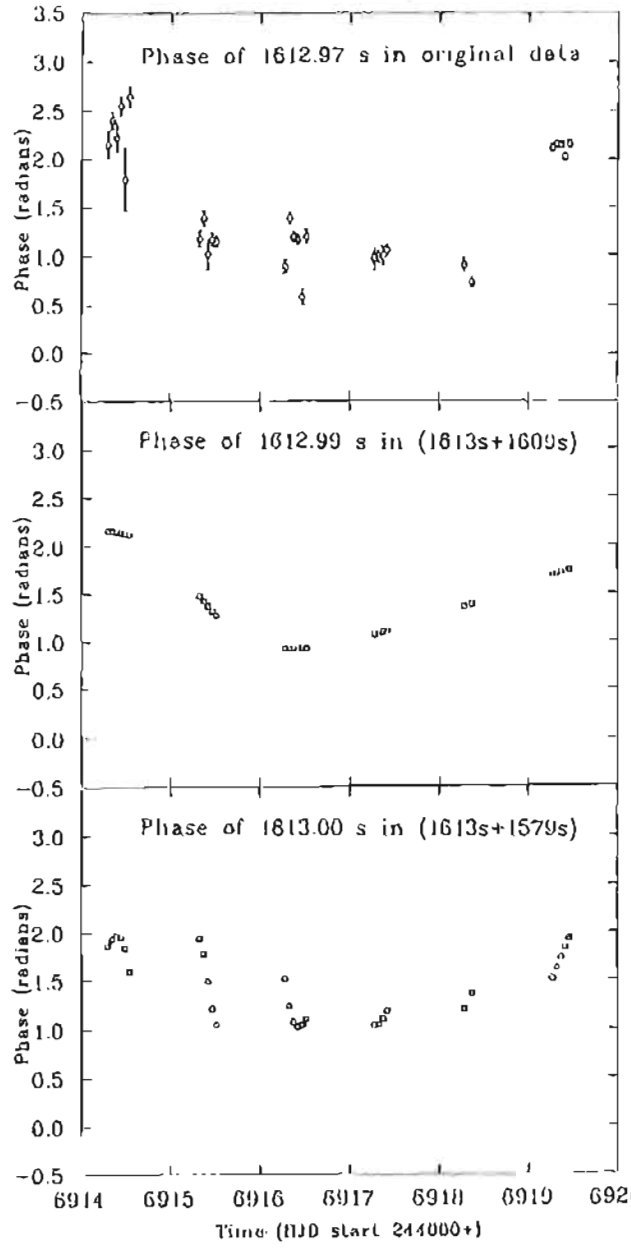

Figure 4.10: The phase of the 1613 s clock (a) in the original photometry and in two sets of synthetic data: (b) $\omega_1 = (1613.0)^{-1}$ Hz and $\omega_2 = (1608.6)^{-1}$ Hz, (c) $\omega_1 = (1613.0s)^{-1}$ Hz and $\omega_2 = (1579.2)^{-1}$ Hz.

To enable a more realistic comparison between the phases from the real and synthetic data, Gaussian noise with a zero mean and various standard deviations was added to the synthetic data. Figure 4.11 shows the two sets of synthetic data with increasing levels of added Gaussian noise. When noise with $\sigma = 0.03$ is added, both curves appear to be reasonable representations of the original data: one cannot exclude one or the other because of a rapid rise or descent seen in the original data, because such changes can be produced or nullified by the addition of noise.

4.4 Discussion

There are four signals in the region of the fundamental photometric variation that need to be accounted for. In addition, we have to choose between 1608.6 s and 1579.2 s as the second strongest contributor of power. The radial velocity period, together with the identification of 1613.0 s as a (normal) superhump, implies that the 1603.4 s signal is the orbital period. The precession period of the eccentric disc is thus 72 ± 3 h. What, then, are the 1608.6 s (or 1579.2 s) and 1588.0 s periods?

If we identify the 1579.2 s period as the second strongest contributor of power, we could postulate that it is a *negative superhump* period, as it is less than the orbital period. In this case, the regression period of the line of nodes of the tilted disc is ~ 29 h. This leaves the 1588.0 s signal to explain. The frequency difference between $(1588.0)^{-1}$ Hz and the negative superhump frequency is $3.5\,\mu$Hz, which is close to the prograde precession frequency of the eccentric disc. Despite this numerical coincidence, there is no obvious way of explaining the origin of the 1588.0 s period.

These speculations rest on the assumption that the radial velocity period is the beat period between a positive superhump and the orbital period. If it is not, the mechanisms producing the dominant power in the amplitude spectrum would be different from the ones suggested here.

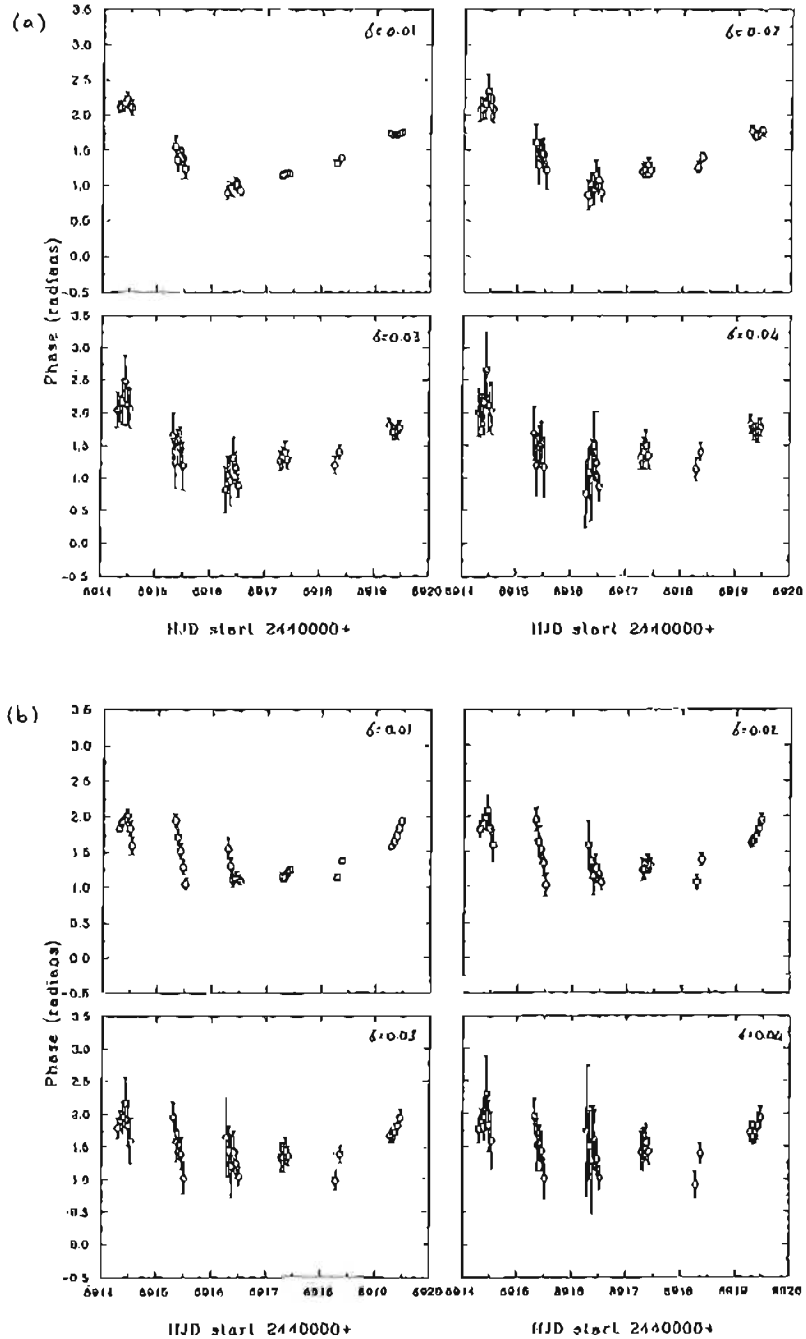

Figure 4.11: Variations in phase of a constant clock of 1613.0 s in the two sets of synthetic data where Gaussian noise of $\sigma = 0.01$, 0.02, 0.03 and 0.04 has been added: (a) superposition of 1613.0 s and 1608.6 s, (b) superposition of 1613.0 s and 1579.2 s.

There is a small possibility that the low-amplitude peaks found on the high frequency side of the fundamental and the third harmonics in the amplitude spectrum are multiplet components similar to those seen in AM CVn. The frequency difference between these low-amplitude peaks and the local principal peak is 19.7 μHz, corresponding to a beat period of 14.1 h. Interestingly, this beat period is approximately equal to the first harmonic of the proposed nodal regression period of $\sim$ 29 h (if we interpret the 1579.2 s period as a negative superhump). The 14.1 h beat period does not appear in the radial velocities. However, the radial velocity data coverage is neither extensive nor of very high quality; the data from Westin were tracings of photographic spectra and there are only three or four radial velocity data points for each of the four nights of observation.

Multi-site high speed photometry will probably be required to establish the presence or absence of fine structure in the high state amplitude spectra of V803 Cen. The differences in photometric behaviour during the high and low states would complicate the analysis, since the large-amplitude brightness variations introduce amplitude modulations into the analysis: the relative amplitude of any physical period in the data (that does not participate in the process causing the large-amplitude variations) will be modulated by the varying background. In addition, it has not been established whether the periodicities seen in the high state are produced by the same mechanism as those in the low state.

Spectral observations need to be obtained over a period of a week or more to refine the estimate of the radial velocity period presented above. All observations, however, need to be obtained when the star is in a high state. It is difficult to predict when this will occur, as the transitions between low and high state occur on an unpredictable time scale. To eliminate any possible variations of the line profiles on the principal period, the spectra should have integration times of 1613 s.

Chapter 5

GP Comae

5.1 Introduction

GP Com was first recorded by Giclas, Burnham & Thomas (1961) as a high proper motion star, G61-29. The spectrum of the star was found by Burbidge & Strittmatter (1971) to consist exclusively of broad helium emission lines; at the time, G61-29 was the only object known with a pure helium emission spectrum. The spectra showed exceptionally broad emission lines of He I with widths of $\sim$ 20Å at half maximum together with a weak emission feature at He II λ4686Å. The profiles of a number of lines were observed to display variable asymmetry with accompanying radial velocity changes. Photographic data from eight plates taken over 23 years suggested that the luminosity of the star had remained essentially constant to within $\sim$ 0.1 mag during that time. They rejected a binary model for the system on the grounds that, if their radial velocity changes were caused by binary motion in a system comprising a DB white dwarf and a main-sequence helium star, the main sequence companion would have to be extremely faint and have too low a mass to sustain helium fusion.

The similarity of the spectrum of G61-29 to that of AM CVn (with its helium *absorption* spectrum) prompted Warner (1971) to obtain high-speed photometry of G61-29 to search for periodic modulations such as those seen in AM CVn. The observations revealed the presence of rapid flickering, and it was suggested that G61-29 was a short-period, mass-transferring binary. Warner (1971) observed that G61-29 and AM CVn were probably

helium analogues of the hydrogen-rich CVs.

The unusual spectral properties of GP Com have been examined by Smak (1975), Lambert & Slovak (1981), Nather, Robinson & Stover (1981), Marsh, Horne & Rosen (1991) and Marsh et al. (1995). Smak (1975) showed that the lines can be separated into two basic components: a broad and variable double-humped line profile with a shallow central depression, and a narrow single-peaked stationary peak displaced ~ 1Å to the red of the centre of the broad component. Agreeing with Warner's (1971) mass-transferring binary interpretation, he proposed that the broad component originates in an accretion disc. The origin of the narrow central component of the He I lines is uncertain. Nather, Robinson & Stover (1981) proposed that the narrow component is produced in an external shell — similar features are found in the spectra of old novae such as DQ Her. Nather, Robinson & Stover (1981) detected what appeared to be nebulosity around GP Com on Palomar Sky Survey plates, and postulated that this was a shell that had been ejected from the star in the recent past. Stover (1983) showed that the apparent nebulosity is in fact a grouping of faint background stars that do not share GP Com's proper motion, and are therefore unrelated to the object.

The first detection of an element other than helium in GP Com was made by Lambert & Slovak (1981) when N V λ1240Å was detected in an IUE spectrum. Emission lines of N I, N II, O I and Ne I were discovered in the near infrared by Marsh, Horne & Rosen (1991), together with a possible detection of Mg II. By modelling the spectrum as emission from a uniform, optically thin slab of gas in LTE, they deduced that nitrogen is highly over-abundant in GP Com relative to both carbon and oxygen (compared to solar values), and that all hydrogen originally present has been converted to helium. There are also under-abundances of a factor of ~ 1000 of calcium, silicon and iron, relative to a solar composition. The accretion disc thus has the rather exotic composition of 99.7% helium and 0.3% nitrogen by number.

Time-resolved ultraviolet spectra of GP Com taken with the Hubble Space Telescope (Marsh et al. 1995) show dramatic variability in the dominant N V emission line: three large flares, roughly equally-spaced in time, were observed during a total of 13h of observation. Flaring behaviour of this kind has not yet been seen in non-magnetic CVs. Marsh et

al. (1995) suggest that the flaring observed in GP Com may be a result of rapidly variable outflows from the system or of irradiation of the accretion disc. An emission line in the flare spectrum at λ1550Å was identified as C IV, the first evidence for carbon in GP Com.

GP Com has a significant X-ray flux and has been unambiguously detected by ROSAT in both the hard (0.52–2.4 keV) and soft (0.11–0.4 keV) bands. The count rates in each of these bands are 0.528 ± 0.010 counts s^{-1} and 0.267 ± 0.007 counts s^{-1} respectively. Assuming a distance of 165 pc (Ulla 1994), the X-ray luminosity is in the range 1.91×10^{30}–5.52×10^{31} erg s^{-1} (Ulla 1995). The derived X-ray luminosity for GP Com is at least an order of magnitude greater than that of AM CVn, CR Boo and V803 Cen (Ulla 1995; see also chapter 1 section 1.1.4.2). The X-ray light curve of GP Com (Beuermann & Thomas 1993) is very similar to that for low mass transfer rate systems like SU UMa (Warner 1995a).

The hard X-ray flux is expected to be high in systems with low accretion rates ($\sim \dot{M} \lesssim 2 \times 10^{-10} M_\odot\, y^{-1}$) (Patterson & Raymond 1985). In Marsh, Horne & Rosen's (1991) model, the mass transfer rate through the disc in GP Com is $\sim 5 \times 10^{-12} M_\odot\, y^{-1}$. Warner (1995b) obtains a theoretical estimate of $\approx 1 \times 10^{-11} M_\odot\, y^{-1}$ for the rate of mass transfer from the secondary. These values are lower than typical values of the mass transfer rate from the secondary for dwarf novae (e.g. Z Cha has $\dot{M} \approx 3 \times 10^{-11} M_\odot\, y^{-1}$, Wood et al. 1986; and IP Peg with $\dot{M} \approx 2 \times 10^{-10} M_\odot\, y^{-1}$, Marsh 1988).

Evidence that GP Com might undergo dwarf nova-like outbursts comes from Marsh, Horne & Rosen (1991) who found that the spectrum was best fitted by a temperature of ~ 11000 K. This is less than the critical temperature $T_{crit} \approx 12500$ K above which helium accretion discs are stable (Smak 1982, Warner 1995a). One of GP Com's closest relatives among the hydrogen-rich CVs is the SU UMa star WZ Sge, which has a very long superoutburst recurrence time (~ 30 years), a hard X-ray luminosity of 4.0×10^{31} erg s^{-1} in the range 0.2 – 4.0 keV and a mass transfer rate of $\lesssim 5 \times 10^{-12} M_\odot\, y^{-1}$ (Patterson & Raymond 1985). Although no outburst has been observed in GP Com, the observational coverage is too sparse to exclude occasional brief outbursts (Warner 1995a, 1995b).

GP Com is the "odd man out" of the AM CVn stars. It distinguishes itself by being the

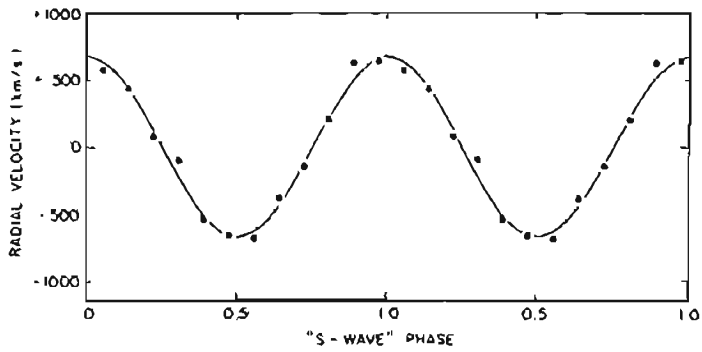

Figure 5.1: The radial velocities of the 'S'-wave variation in GP Com as a function of orbital phase. From Nather, Robinson & Stover (1981).

only AM CVn system in which the orbital period is observed directly (it could be argued that the 1028s orbital period of AM CVn obtained by Patterson, Halpern & Shambrook (1993) is model-dependent). Its binary nature was established by Nather, Robinson & Stover (1981) who showed that the narrow emission line component in the triple-peaked optical emission lines moves between the two outer peaks with a period of 46.5 minutes (see figure 5.1). By analogy with the 'S'-waves in CVs (see, for example, Honeycutt, Schlegel & Kaitchuck 1987), Nather, Robinson & Stover (1981) identified the moving component with the bright spot where the mass transfer stream hits the accretion disc. Ultraviolet counterparts of the optical 'S'-wave are observed in HST spectra (Marsh et al. 1995). The ultraviolet 'S'-wave is seen in N IV, C IV, N I λ1493Å and a line at λ1335Å which may be C II λ1335Å. The 46.5 min period is confirmed by the X-ray light curve (Beuermann & Thomas 1993). GP Com has the longest orbital period of the known AM CVn stars: the orbital period of four of the six is not well-established, but under the superhump model, their principal photometric (superhump) periods differ from the orbital periods by a few percent.

GP Com also distinguishes itself by being the only AM CVn star which is permanently in a low state: it has displayed a strong emission line spectrum on every occasion it has been observed. The emission lines in its spectrum are far stronger than the emission lines seen

in the low state spectra of V803 Cen (O'Donoghue et al. 1990) and CR Boo (Wood et al. 1987). GP Com does not show the complex periodic photometric behaviour of the other stars; the light curve is dominated by flickering and does not show consistent orbital or superhump-like variations. However, a variation with a period consistent with the orbital period does occasionally appear in the light curve. In figure 3 of Warner (1972) the light curve shows four humps with a period of about 44 ± 3 min and an amplitude with a fractional intensity of 0.09. This variation is not present in other light curves in Warner (1972). Simultaneous multi-colour high-speed photometry over two nights obtained by Provencal (1994) shows quasi-periodic variations in all colour bands; the character of the variations differs from band to band. The power spectra of the data are dominated by broad power excesses at low frequencies, presumably due to transparency variations that were incompletely removed during the reduction process. Each of the U, B, V and R power spectra shows a broad power excess in the region of the 46.5 min orbital period, but the power is clearly not that of a single frequency and indicates that the brightness modulations in GP Com on that time scale are not constant in frequency or amplitude.

The evidence from previous photometric observations of GP Com suggests that modulations in the region of the orbital period are *occasionally* present in the light curve. The aim of this chapter is to present a high-speed photometry data set taken over a period of five months. The idea is to see if are any repeatable periodicities in the GP Com light curve during this time, and in particular, to see whether an orbital modulation could be detected in any of the runs.

5.2 Observations

High-speed photometry of GP Com was obtained during March, May, June and July for a total of $\sim$ 33h using the UCT Wright CCD on the 1m telescope at Sutherland. Table 5.1 is a journal of the observations. All frames were obtained without a filter. During the first seven runs, frames were obtained at the highest time resolution permitted by the cloud and seeing conditions. For subsequent runs, the exposure time was increased to 60s in an attempt to reduce the high-frequency flickering noise, once it had been established that

there were no coherent or consistent rapid periodicities in the light curve. Because GP Com is at a high Galactic latitude ($b \approx 80°$) and is in a sparse field, no nearby blue stars were found within 1.5 arcminutes of GP Com. As a result, several of the light curves show pronounced differential extinction effects where the blue light of GP Com was scattered more than the redder light of the comparison stars. Differential extinction effects can be seen most clearly in the July runs, where the airmass had increased to almost three atmospheres by the end of each run (GP Com has a declination of $\approx +18°$, while the latitude of Sutherland is $\sim 33°$ south).

Two nearby stars were used for the differential photometry. Unfortunately, there were no nearby comparison stars with a greater white light count rate than GP Com. During the reductions of the CCD frames, therefore, GP Com was the only star on each frame that was classified as "bright" by DoPhot and awarded a seven parameter fit to its point-spread-function (see chapter 2 section 2.2.4). The point-spread-function for each frame was thus defined by a star with $V \approx 16.0$, and the profile fitting for the two fainter comparison stars was of correspondingly poor quality. In addition, because the signal-to-noise for the fainter stars was greater than that for GP Com, the differencing techniques used in the reductions (see chapter 2 section 2.3) resulted in a slightly increased signal-to-noise level for the GP Com light curve. Despite these sources of noise, however, it must be pointed out that without the CCD detector and the profile-fitting and differencing techniques used in the reductions, GP Com is not observable with the 1m telescope at Sutherland.

Estimates of V, B and the "white light" magnitude (see chapter 2 section 2.2.4) of GP Com were made on July 28 before run A361. The comparison star used was HD117624 at $\alpha_{1900} = 13^h28^m55^s$, $\delta_{1900} = +17°49'30''$ which was measured on the 0.5 m telescope at Sutherland to have $V = 8.352$ and $B = 8.642$. The mean of three filtered measurements of GP Com (taken over a period of approximately 10 min) before run A361 yielded $B = 15.9$ and $V = 16.0$. Assuming that the "white light" magnitude of HD117624 is the same as its V magnitude, the mean white light magnitude for GP Com during run A361 is 16.3.

Table 5.1: Journal of observations: March, May, June, July 1995 high-speed photometry of GP Com.

Run	Date (start)	$JD_{\odot}2440000+$	Length (h)	Exposure time (s)
A062	1995 March 4	9780.48695	3.9	20
A068	1995 March 5	9781.48502	1.5	20
A071	1995 March 6	9782.51287	3.4	20
A329	1995 May 31	9869.23875	4.5	20
A335	1995 June 1	9870.21680	5.2	15
A341	1995 June 2	9871.21324	5.4	15
A345	1995 June 3	9872.23816	2.7	20
A349	1995 July 25	9924.20556	2.1	60
A356	1995 July 27	9926.20431	2.1	60
A361	1995 July 28	9927.21221	2.0	60

5.3 Results

The data in table 5.1 are shown in figure 5.2. The light curves show flickering on a time scale of $\sim 15 - 20$ min superimposed on low-frequency variations with amplitudes of ~ 0.05 mag. The runs were searched individually for any significant periodicities, and then combined into groups of closely-spaced runs (A062 + A068 + A071; A329 + A335 + A341 + A345; A349 + A356 + A361). No repeatable periods were found from night to night or month to month, confirming the results of Provencal (1994). As no rapid variations were found, the data were all binned to 60 s resolution to improve the signal-to-noise ratio.

The low-frequency variations were examined by calculating a Fourier amplitude spectrum for each monthly group and identifying the highest peak in the range 0.0 - 0.2 mHz. The amplitude spectra are shown in figure 5.3. In each case there is a broad power excess in the amplitude spectrum at low frequencies, indicating that there could be an underlying clock in this region that is not maintaining good coherence within each group of runs. A non-linear least squares sinusoid with the frequency corresponding to the highest

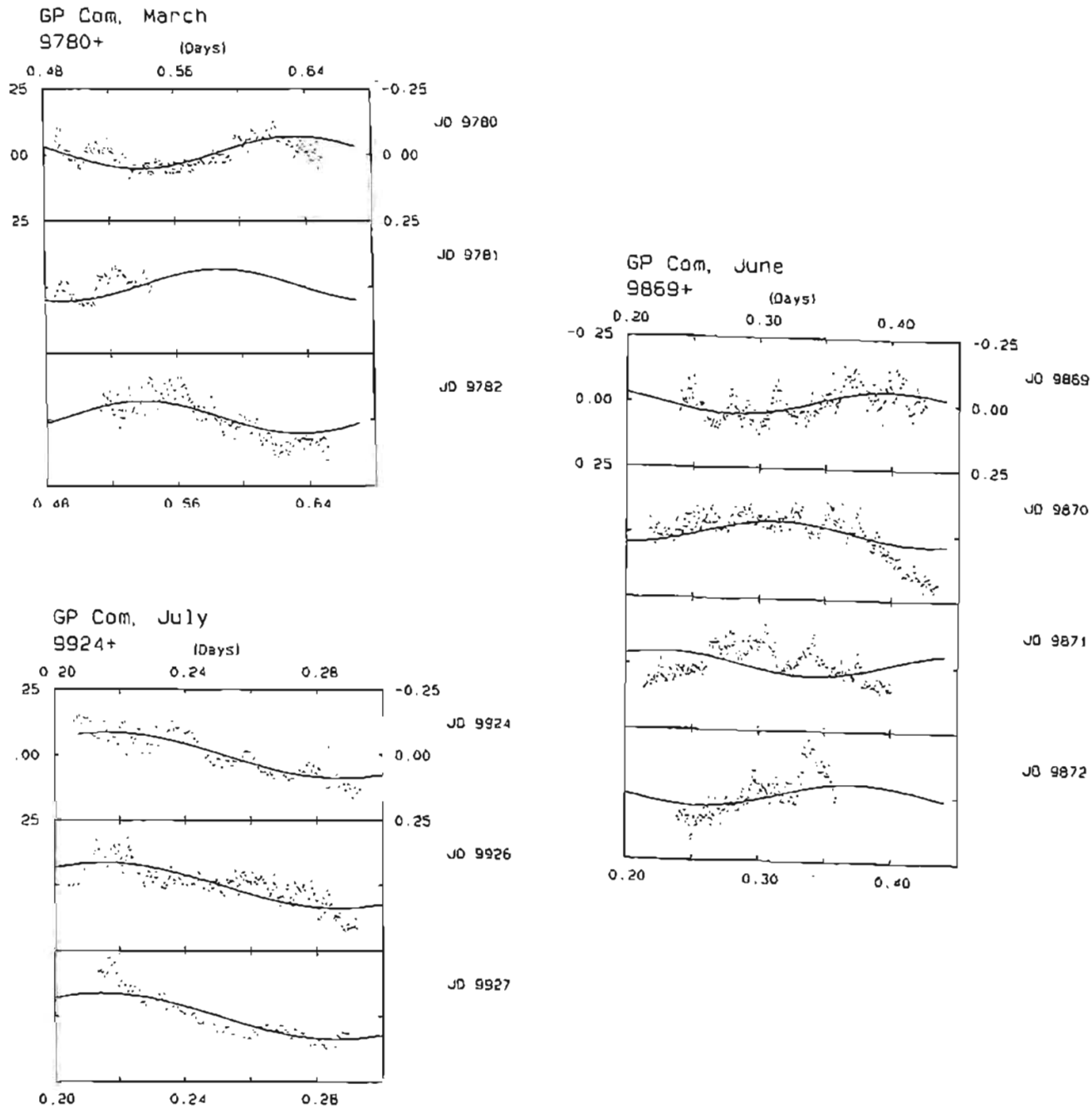

Figure 5.2: High-speed photometry of GP Com listed in table 5.1. The light curves show flickering superimposed on slow, low-frequency modulations. The superimposed sinusoids are non-linear least squares fits to each monthly group of runs.

peak in the range 0.0 – 0.2 mHz was fitted to each group of runs; the results are shown in figure 5.2. The period obtained for the March runs is 4.57 h with an amplitude of 0.060 ± 0.003 mag. This sinusoid appears to be a good fit to the data, but seeing as the period obtained is longer than the longest run in this group, the period could be due to the windowing of the light curve. This is also the case for the best-fit low-frequency period for the June runs (A329, A335, A341 and A345). The least squares sinusoid for the June runs is a bad fit to A341, implying that the low-frequency variation in these runs is not well represented by a unique period and differs from night to night. The period obtained by the non-linear least squares fit is 5.49 ± 0.08 h with an amplitude of 0.045 ± 0.004 mag; because this period is longer than the longest June run, it is not clear whether this result has any significance. The low-frequency variation in the July runs is almost certainly due to differential extinction: the period obtained is 3.44 h, which is almost exactly seven cycles per day. The three runs were taken at approximately the same time each night, and the star would have been affected by differential extinction to the same degree at the same time of day. This creates an apparently coherent periodicity that is not intrinsic to the star, and explains the appearance of the amplitude spectrum of the July runs, which is suggestive of a coherent period with a series of harmonics.

In an effort to suppress the low-frequency variations (which are probably not intrinsic to the star), the data were detrended using a two-point difference filter. The amplitude spectra of the filtered data from each group of runs are shown in figure 5.4. In the May/June group of runs, there is an excess of power around 0.37 mHz corresponding to a period of $\sim$ 45.5 min, but the band is broad and does not represent a coherent period with a stable amplitude. There are no pronounced power excesses near the orbital frequency in the March and the July runs.

If an intermittent variation is present in the light curve, calculating an amplitude spectrum of a group of runs may result in a dilution of the the power at that frequency. To investigate whether there is intermittent power at or near the orbital period, therefore, amplitude spectra were calculated for each run separately (once the data had been binned into 60s integrations). Excess power appears in the region of 0.36 mHz in runs A062, A329, A341, A345 and A349 with an amplitude and frequency that changes from run to run. In two of the runs, A329 and A341, the power excess is quite pronounced (see figure 5.5). To

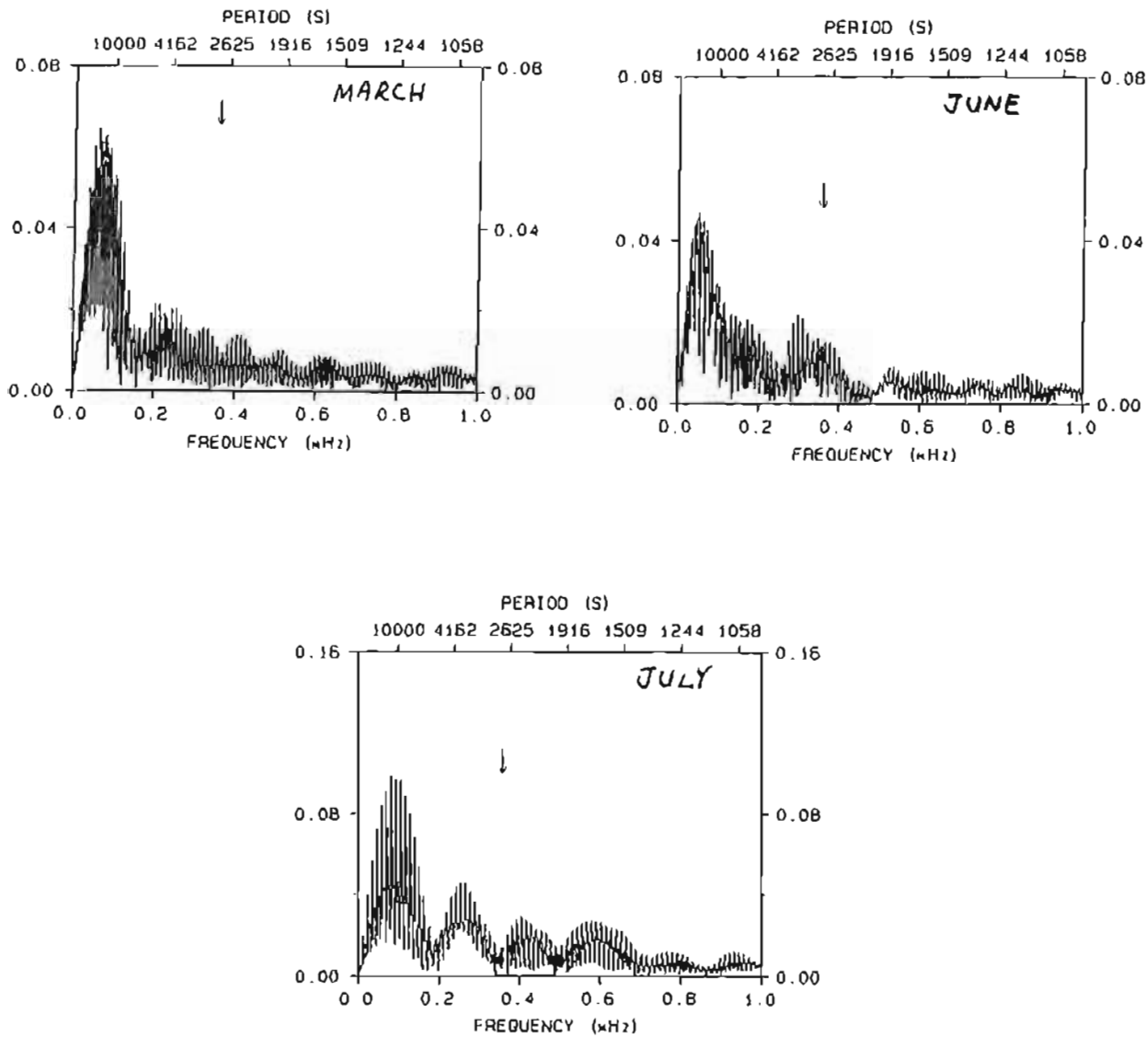

Figure 5.3: Fourier amplitude spectra of the three monthly groups of closely-spaced high-speed photometry runs (see table 5.1). The spectra are dominated by a broad band of power around 0.08 mHz. The arrow shows the location of the orbital frequency from Nather, Robinson & Stover (1981).

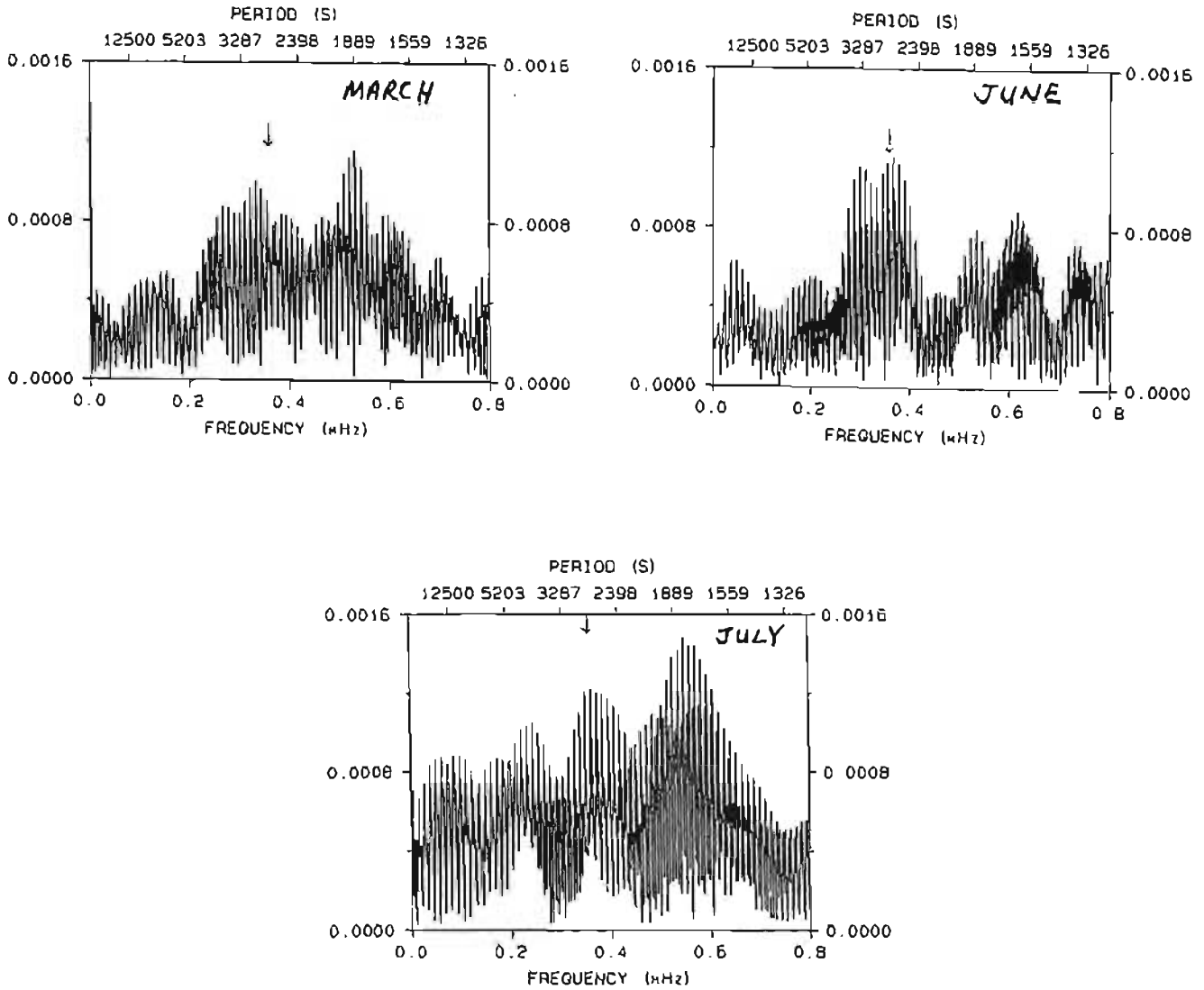

Figure 5.4: Amplitude spectra of the data after applying a two-point difference filter to surpress the low-frequency variations. The three panels are amplitude spectra of each of the three monthly groups of runs. The arrow marks the orbital frequency of GP Com.

check whether the power excess is an artifact caused by the window pattern of the low-frequency variations (which have much larger amplitudes than the peaks near 0.36 mHz), artificial signals with the frequencies and amplitudes of the low-frequency variations for each run were created and were sampled as the original data. The amplitude spectra of these artificial sinusoids are shown alongside the amplitude spectra of A329 and A341 in figure 5.5. The excess of power between 0.3 and 0.4 mHz in the two runs is not part of the window pattern of the low-frequency variation.

The periods, amplitudes and time of minima for the 0.36 mHz power excess in run A329 are $P = 44.4 \pm 2.0$ min, $A = 0.034 \pm 0.003$ mag and T_{min} =JD$_\odot$2449869.2341 $\pm$ 0.0047, and in run A341 are $P = 49.7 \pm 2.3$ min, $A = 0.033 \pm 0.005$ mag and T_{min} =JD$_\odot$2449871.2199 $\pm$ 0.0022. The uncertainties in these periods are large because the period determination has been made from only $\sim$ 5 h of observation in each case. The light curves are shown in figure 5.6 with the best non-linear least squares fit to the $\sim$ 46 min periods. The data have been pre-whitened by the dominant low frequency variation in each case: $\sim$ 312 min in A329 and $\sim$ 249 min in A341.

5.4 Conclusions and speculations

There is suggestive evidence of intermittent structure in the light curve of GP Com that produces excess power on a time scale similar to that of the orbital period. During runs A329 and A341 (which are separated by two days) the excess power near the orbital frequency is fairly pronounced. When the group of four runs which include A329 and A341 are filtered using a high-pass two-point difference filter, the amplitude spectrum of the data show a power excess with a peak frequency corresponding to the orbital frequency. The peak, however, does not represent a stable, coherent period of constant amplitude.

The intermittent variation is unlikely to be an orbital modulation, because any signal of orbital origin would maintain coherence on very long time scales. The observed variations do not maintain a constant frequency or amplitude on even a nightly basis. It could be argued that the $\sim$ 46 min variations found in A329 and A341 (and at a lower amplitude in

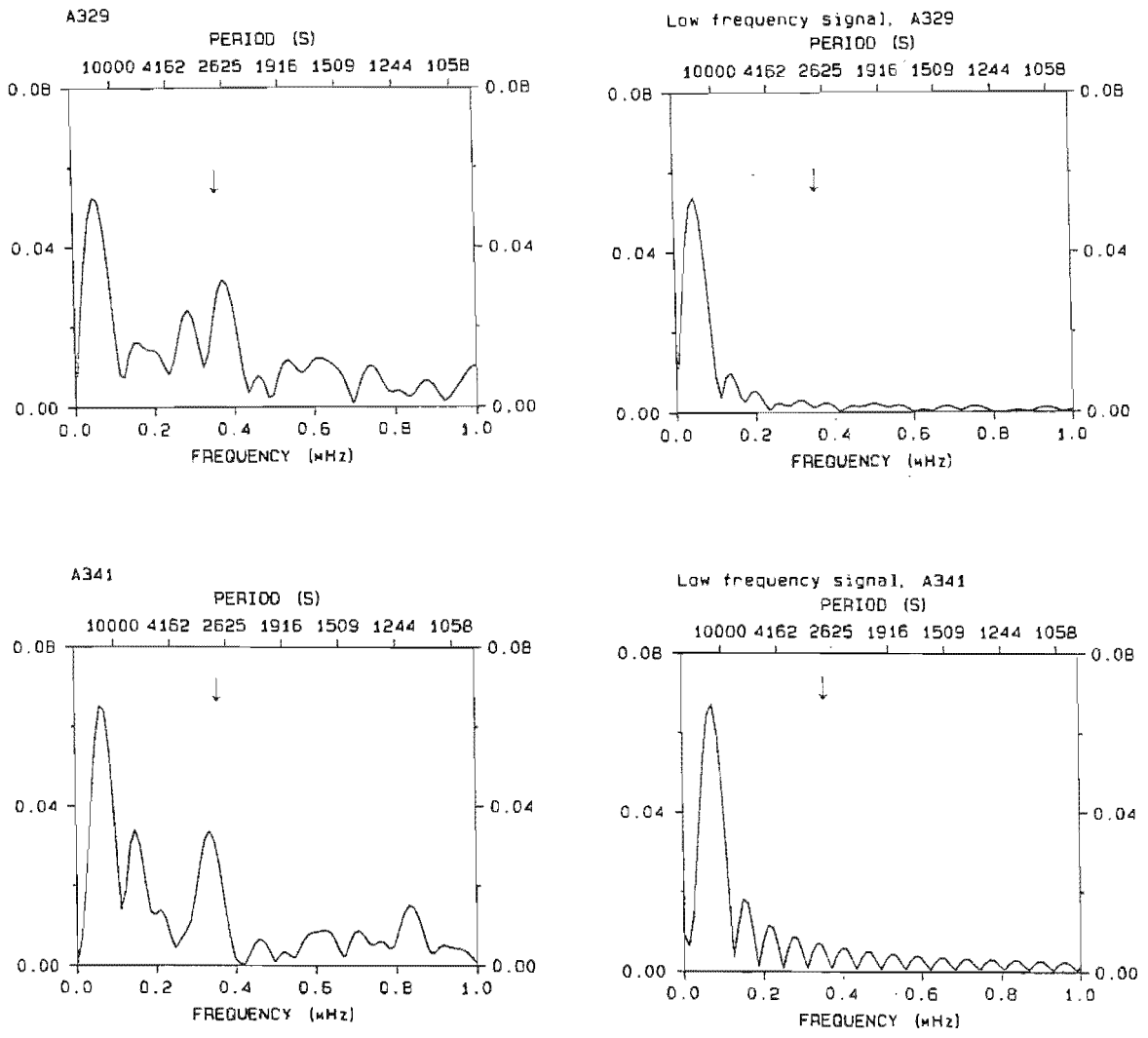

Figure 5.5: Amplitude spectra for runs A329 (top) and A341, showing an excess of power around 0.36 mHz. The accompanying amplitude spectra are spectra of an artificial signal with the period and amplitude of the dominant low-frequency variation in each run: the power excess in the photometry is not an artifact caused by the window pattern of the low-frequency variation. The arrows mark the location of the orbital frequency of GP Com.

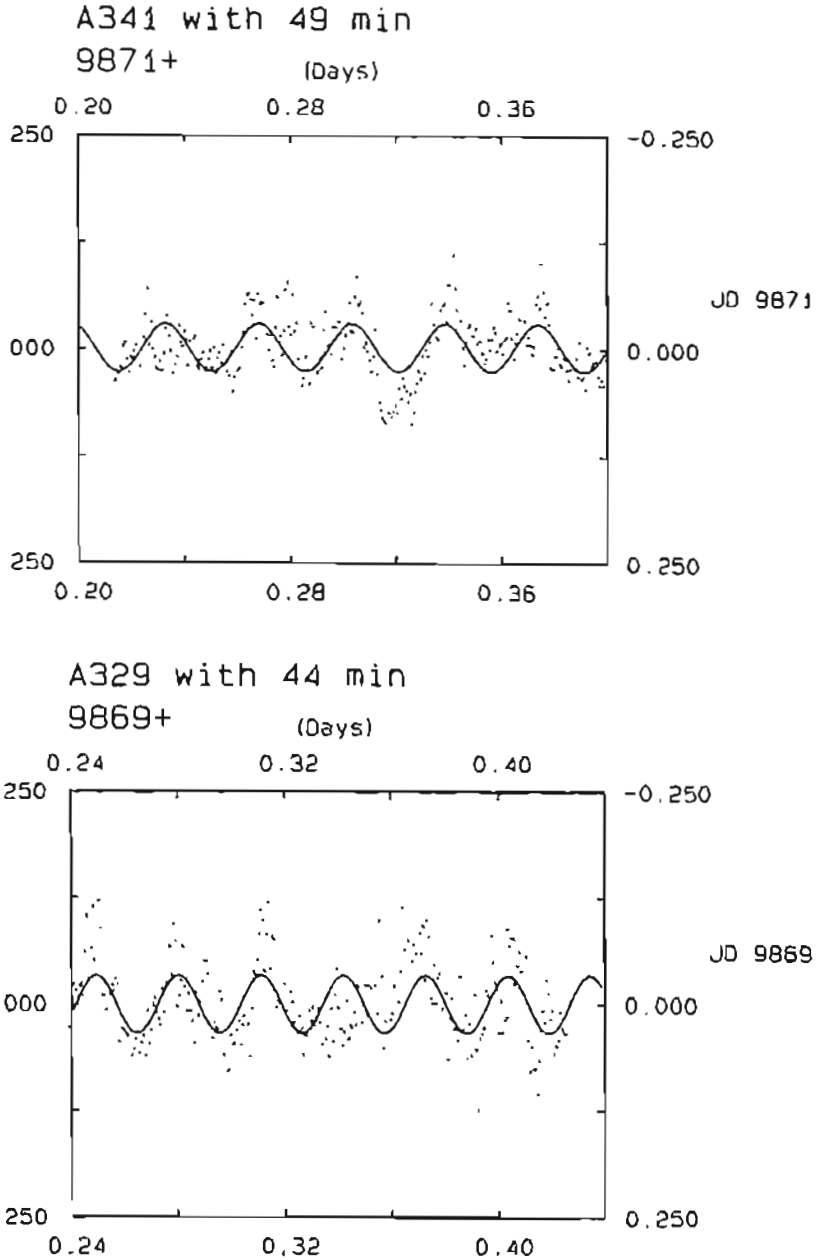

Figure 5.6: Runs A329 and A341, showing the intermittent ~ 46 min modulations. The dominant low-frequency variations (~ 312 min in A329 and ~ 249 min in A341) have been removed from the light curve in each case.

A062, A071 and A349) are merely stochastic variations, and that it was by chance that a periods similar to the orbital period appeared in the light curve on a few nights. However, the flickering in the light curve is on a time scale of $\sim$ 15 – 20 min, much shorter than the observed intermittent modulations. Also, the $\sim$ 46 min variation has been seen in previous observations (Warner 1972), where four humps with a period close to the orbital period are present in a light curve obtained on February 17, 1972. If the intermittent $\sim$ 46 min modulation has its origin in the disc, what is the mechanism producing the brightness variation, and what causes the modulation to appear one day and disappear the next, changing period as it does so? Given the very low mass transfer rate from the secondary in GP Com, the disc is expected to be very small, and it is possible that the disc radius never acheives the r_{32} resonance radius (see chapter 1 section 1.2.3.1). If this is the case, superhumps will not be produced. However, if the disc radius changes (due to, perhaps, fluctuations in the mass transfer rate from the secondary) on a viscous time scale, the particles in the outer disc may occasionally access the 3:1 resonance and produce superhump-like behaviour which would disappear as the disc shrinks back inside r_{32}. Because the disc is small, the viscous time scale is expected to be short. To initiate disc precession, however, a high mass density is required in the vicinity of r_{32}. To acheive this, the system would probably need to undergo an outburst: the angular momentum of the material accreting onto the primary would be carried outwards by the mass in the outer disc, causing the disc radius to increase and tidal interactions to begin.

It is possible that GP Com has a magnetic primary and perhaps a disrupted inner disk. Its hard X-ray flux is certainly larger than that of AM CVn, and is very similar in magnitude to the intermediate polars TV Col, YY Dra, GK Per and AO Psc in the range 0.2–4 keV (Patterson & Raymond 1985).

Chapter 6

CP Eridanus

6.1 Introduction

CP Eri was identified by Luyten & Haro (1959) as a high Galactic latitude blue star with large brightness variations. The star was observed at a magnitude of $V = 17.8$ by Szkody et al. (1989). During the 2.7 h of monitoring the star brightened by 0.2 mag and displayed flickering behaviour with amplitudes of 0.2 – 0.4 mag but showed no evidence of periodic brightness modulations. Short-period variations were discovered by Howell et al. (1991) when the star was at a magnitude of $V = 19.7$. Modulations in V with a period of 29.5 ± 1.5 min and amplitude of $0.1 - 0.2$ mag were observed, as well as a strong harmonic at 13.6 ± 1.5 min. Not suspecting CP Eri to be a helium-rich object, they pronounced the 29.5 min period too short to be an orbital period and proposed an intermediate polar model for CP Eri (the shortest observed orbital period for a CV with normal hydrogen-rich composition is $\sim$ 75 min (Warner 1995a), while the theoretical $P_{orb,min}$ for helium-rich cataclysmics is $\sim$ 13 min (Iben & Tutukov 1991)).

A spectroscopic and photometric study by Abbott et al. (1992) revealed an absence of hydrogen in CP Eri and confirmed the presence of short-period variations. Light curves obtained when the star was at $V = 16.5$ showed a photometric period of 1724 ± 4 s with a complex and variable harmonic structure. No other periodicities were detected in the data. Spectra of CP Eri show broad, shallow absorption lines of He I at $\lambda\lambda$4921, 5015 and 5876 Å in the high state ($V \sim 16.5$) and are almost featureless, apart from weak

emission features of He I at $\lambda\lambda$5015 and 5876 Å, when the star is in the low state. The spectroscopic and photometric properties of CP Eri are thus very similar to those of V803 Cen and CR Boo, and CP Eri was classified by Abbott et al. (1992) as an IBWD, the fifth to be identified, and the third to show large-amplitude brightness variations.

Further photometric observations of CP Eri from 1991 obtained by Provencal (1994) show interesting differences between the photometric behaviour in the high and low states. In the high state, the power spectrum is dominated by a band of power with the largest peak at 1700 ± 2 s (the uncertainty quoted here is an estimate obtained using the "rule of thumb" described in chapter 3). The asymmetric alias pattern suggests the presence of other low-amplitude, unresolved periodicities in the region of 1700 s, or could be evidence that the 1700 s period is not a perfect clock. Seven harmonics of the dominant period are present in the high state power spectra. The low state power spectrum shows two peaks corresponding to 1715 ± 2 s and a harmonic at 850.4 ± 0.4 s. Interestingly, the 850.4 s period differs significantly from the value expected for the first harmonic of 1715 s, corresponding instead to the first harmonic of the dominant period in the high state data, 1700 s.

The gross photometric behaviour of CP Eri is very similar to that of CR Boo, although CR Boo has a larger difference in magnitude between the high and the low state ($\sim$ 5 mag) than CP Eri ($\sim$ 3.5 mag). WET data of CR Boo has revealed two principal periods, a variable period of $\sim$ 1490 s and a coherent period of 1471.4 s (Provencal 1994): these two periods could represent a superhump and an orbital period, respectively (Warner 1995b). The dominant features of low state power spectra of CR Boo are the coherent 1471.4 s period with its first harmonic (Provencal 1994). The 1493 s period is also present in low state data at about half the amplitude of the 1471.4 s period. Now, CP Eri also shows one principal variation and one harmonic in the low state. It could be that the principal variation in the low state is the orbital period. The remaining large-amplitude system, V803 Cen, does not mimic the behaviour of CP Boo and CP Eri in the low state. The 1613 s period appears in combinations of low state runs, and no harmonic structure is present. V803 Cen is, however, at a lower inclination than CR Boo (O'Donoghue & Kilkenny 1989, Warner 1995b); this may somehow account for the differences in the low state power spectra (a more in-depth spectroscopic analysis of CP Eri is necessary to

estimate its inclination). There is an inverse dependence of the amplitudes of the principal variations in CP Eri (measured in units of fractional intensity) with the overall brightness of the system, suggesting that we are observing a constant source against a variable background. Similar behaviour is seen in CR Boo (Provencal 1994) and V803 Cen (O'Donoghue et al. 1989).

New observations of CP Eri were obtained in both the low and high state in order to investigate whether the photometric periods differ between the high and low state, and to observe the varying harmonic structure and amplitude changes. The aim of this chapter is also to compare the periods obtained in the new data with those obtained by other authors to see whether there is evidence that the photometric periods in CP Eri are not maintaining strict coherence, and are therefore consistent with a superhump model.

6.2 Observations

High-speed photometry of CP Eri was obtained during July and August 1995 using the UCT Wright CCD on the 1 m telescope at Sutherland; see table 6.1 for a journal of observations. All observations were taken without a filter. The first set of observations was obtained on five consecutive nights during which the star was in a high state and faded by ~ 0.2 mag per night; by the fifth night the star had faded a further 1.5 mag and appeared well on its way to a low state. The exposure time for the first two high state runs ($JD_{\odot}2449928$ and 2449929) was 30 s. On the following night conditions were poor, but observations persisted. The exposure times were increased to 100 s in order to accumulate sufficient photons despite the 1 mag extinction by thick cirrus clouds. The data from the following two nights (JD 2449931 and 2449932) were very kindly obtained by Dr. David Buckley using the SAAO Tek 4 CCD on the 1 m telescope (after some persistent petitioning by the author, who by that stage had completed her alotted seven observing nights on the 1 m telescope). Exposure times were 40 s per frame for the first run and 60 s per frame for the second. The exposures are separated by a dead time of ~ 12 s. Low state data were obtained on two consecutive nights towards the end of August; exposure times were 120 s per frame for both runs.

Table 6.1: Journal of observations: July, August 1995 high-speed photometry of CP Eri

Run	Date (start)	$JD_\odot$ (2440000+)	Length (h)	Exposure time (s)	Mean "white light" magnitude
A366	1995 July 30	9928.60862	1.9	30	16.2
A371	1995 July 31	9929.58591	2.5	30	16.3
A375	1995 August 1	9930.58431	2.4	100	16.5
A322a	1995 August 2	9931.61283	1.7	40	16.6
A322b	1995 August 3	9932.60082	2.0	60	18.0
A389	1995 August 28	9957.55010	2.9	120	19.8
A392	1995 August 29	9958.54779	2.9	120	19.9

Because CP Eri is in a sparse field, only two comparison stars were present on each frame, one $\sim 1'$ north east of CP Eri, and the other $\sim 0.5'$ north. These two stars were used for the differential photometry to produce the time series in figures 6.1 and 6.2. The star HD 20572 at $\alpha_{1900} = 03^h15^m54^s$, $\delta_{1900} = -09°54'58''$, was observed for standardisation purposes in unfiltered ("white") light on 28 July. To determine an approximate "white light" magnitude for CP Eri, it was assumed that the true unfiltered magnitude of HD 20572 corresponded to its magnitude in V of 7.86 (see chapter 2 section 2.2.4 for a justification of this assumption). The count rates for CP Eri were corrected for extinction by cloud by comparing them to the count rates of a comparison star $\sim 1'$ north east of CP Eri which appeared on all the frames. The white light magnitude of CP Eri was then calculated by comparing the cloud-corrected count rate with the white light count rate of HD 20572. The results are listed in table 6.1. The magnitude range from low to high state is comparable to that listed in Downes & Shara (1993), who give the range of CP Eri in V as 16.7 - 19.7.

6.3 Pulse shapes, phases and periods

The first five runs in table 6.1 are shown in figure 6.1. The light curves in the high state (first four panels of figure 6.1) show prominent pulses with complex superhump-like shapes. The shape and amplitude of the pulses change from night to night. A non-linear least squares sinusoid fit to the data from nights one to four, superimposed on the data from all five nights, is shown in figure 6.1. On the fifth night, when the white light magnitude had fallen to 18.0, the phase of the principal variation changed by $\sim 180°$ and the light curve developed secondary, lower amplitude humps which are in phase with the principal period of the preceding four nights. The low state light curves are shown in figure 6.2. Again, prominent pulses are observed; the pulse shape changes from the first to the second night of observation. The amplitude of the pulses, in *magnitudes*, is over twice the amplitude of the corresponding variations in the high state.

The periods, phases and amplitudes of the principal variation in each night were calculated so that the mean light curve at the principal period could be calculated for each night. The periods, amplitudes and times of the first pulse minima in each run, are listed in table 6.2 [1]. A direct comparison of the periods obtained from the Fourier amplitude spectra for each night is not possible because of the large errors. For a period of 1700 s, the uncertainty in the period of a noisy signal obtained from a time-series 3 h long, is about 70 s.

All but one of the periods listed in table 6.2 are consistent with a single period. The fundamental ~ 1720 s period is not present in run A332b, when the star was in an intermediate state. The principal period obtained for this run is consistent with the first harmonic of the ~ 1720 s period. It could be that the period doubling is due to the development of the secondary peaks on the falling sides of the previous pulse shapes. The growth of this secondary feature is reminiscent of late superhumps (chapter 1 section 1.2.3.1). The first harmonic of ~ 1720 s would dominate if the normal and the late superhump had comparable amplitudes (cf. V1159 Ori in late superoutburst, and AM CVn, with its missing 1051 s fundamental period — see chapter 1).

[1] The time of the first maximum in each run is given by $T_{max} = -\frac{\phi}{2\pi}P + T_0$, where P is the period and ϕ the phase of the least squares fit (in days) and T_0 is the $JD_\odot$ of the start of the run.

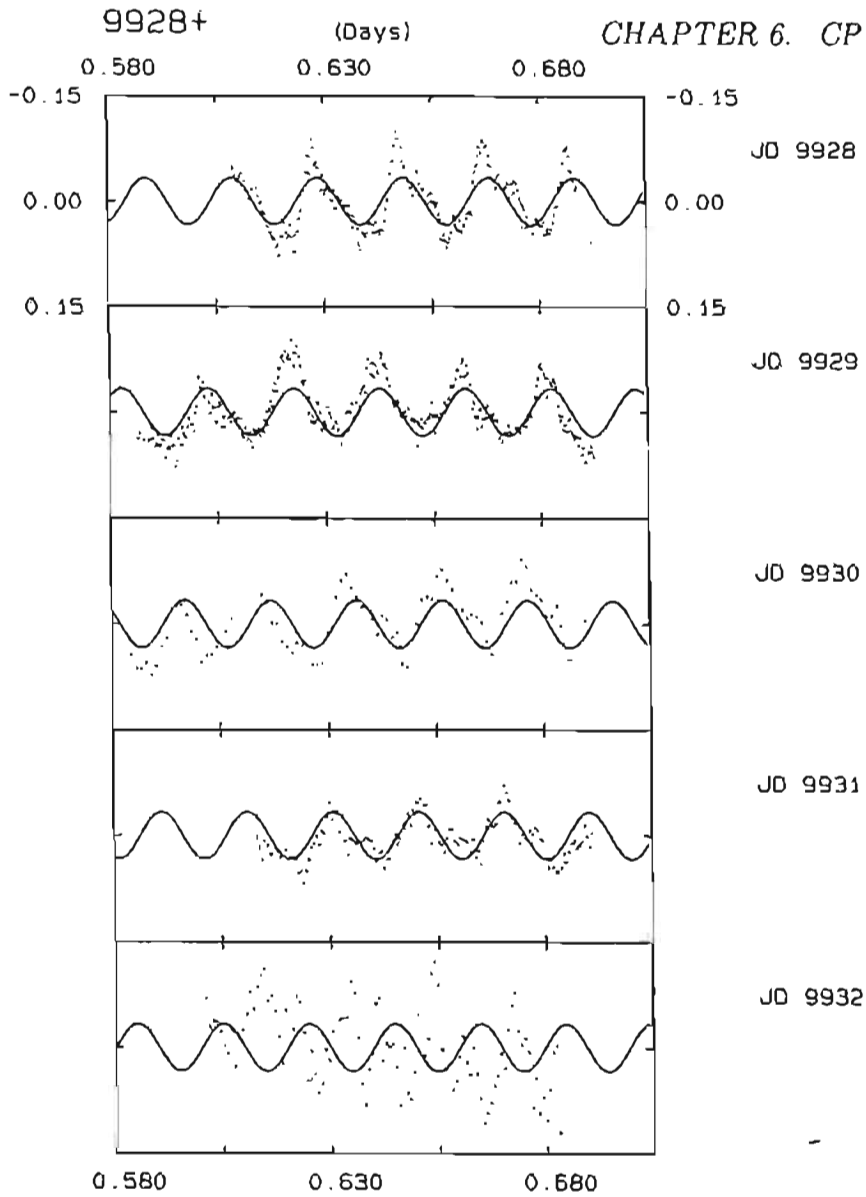

Figure 6.1: High-speed photometry of CP Eri obtained on five consecutive nights in July and August 1995, showing the transition from a high state to an intermediate state. The mean brightness of the system fell by 3.7 mag during these 5 nights. The sinusoidal fit is a non-linear least squares fit to data from the first four runs; in the fifth run, the pulse shape develops a double-peaked structure with the larger of the two peaks 180° out of phase with the principal period from the previous four runs; the smaller of the two peaks appears to be in phase with the principal variation from the previous four runs. This is reminiscent of the late superhumps seen in SU UMa dwarf novae.

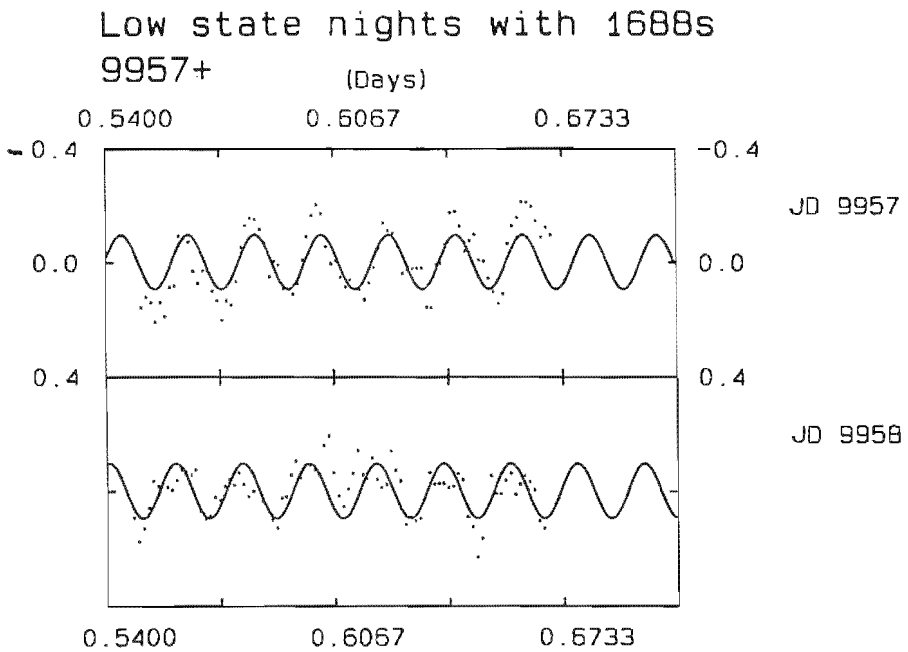

Figure 6.2: High-speed photometry of CP Eri in the low state obtained in August 1995 when the star was at a "white light" magnitude of 19.8. The sinusoidal fit is a non-linear least squares fit to both runs.

Mean light curves for each run were obtained by folding on the periods in table 6.2, with phase 0.0 corresponding to the pulse minimum. The period used for run A332b was twice its 870 s principal period, i.e. the data were folded on 1740 s, to show the double-humped shape. Figure 6.3 shows the mean light curve for run A366 together with the phase-binned light curve of the SU UMa dwarf nova TV Crv obtained towards the end of a superoutburst (Howell et al. 1996): the similarity is compelling. Figure 6.4 shows the mean light curves for the remaining runs. The pulse shape for the first low state run is similar to that of run A375.

To see whether the period of the principal variation in the high state is different to that for the low state, Fourier amplitude spectra were calculated for *pairs* of runs. In this

Table 6.2: Periods, amplitudes and times of minima for the nightly principal variation in CP Eri.

Run	Mean magnitude	Period (s)	Amplitude (mag)	T_{min} ($JD_\odot$)
A366	16.2	1700 ± 100	0.048 ± 0.002	9928.61908 ± 0.00026
A371	16.3	1690 ± 70	0.043 ± 0.002	9929.59259 ± 0.00012
A375	16.5	1740 ± 70	0.041 ± 0.004	9930.58510 ± 0.00071
A332a	16.6	1780 ± 70	0.041 ± 0.009	9931.62011 ± 0.00137
A332b	18.0	870 ± 30	0.036 ± 0.006	9932.57931 ± 0.00176
A389	19.8	1730 ± 70	0.129 ± 0.010	9957.55324 ± 0.00051
A392	19.9	1700 ± 70	0.069 ± 0.009	9958.54987 ± 0.00088

Table 6.3: Values of the ~ 1720 s period for pairs of nights in the high and low state of CP Eri.

Runs	Period (s)	Amplitude (mag)	T_{min} ($JD_\odot$)
A366 & A371	1715 ± 8	0.045 ± 0.001	9928.61915 ± 0.00015
A371 & A375	1718 ± 8	0.042 ± 0.002	9929.59291 ± 0.00043
A375 & A332a	1720 ± 8	0.041 ± 0.006	9930.58570 ± 0.00045
A389 & A392	1721 ± 8	0.096 ± 0.007	9957.55443 ± 0.00034

way the uncertainties become sufficiently small to allow comparisons to be made between the high and low state data, as well as to previously reported periods. The ~ 1720 s periods obtained for pairs of runs (excluding run A322b, where the 1720 s variation has disappeared and is replaced by its first harmonic) are listed in table 6.3.

The periods obtained for pairs of high state runs *and* the pair of low state runs in table 6.3 are consistent with being a single period of ~ 1720 s. This result is in agreement with the period obtained by Abbott et al. (1992) who obtained 1724 ± 4 s when the star was at $V = 16.5$. The low state period of 1715 ± 2 s from Provencal (1994) agrees with the low

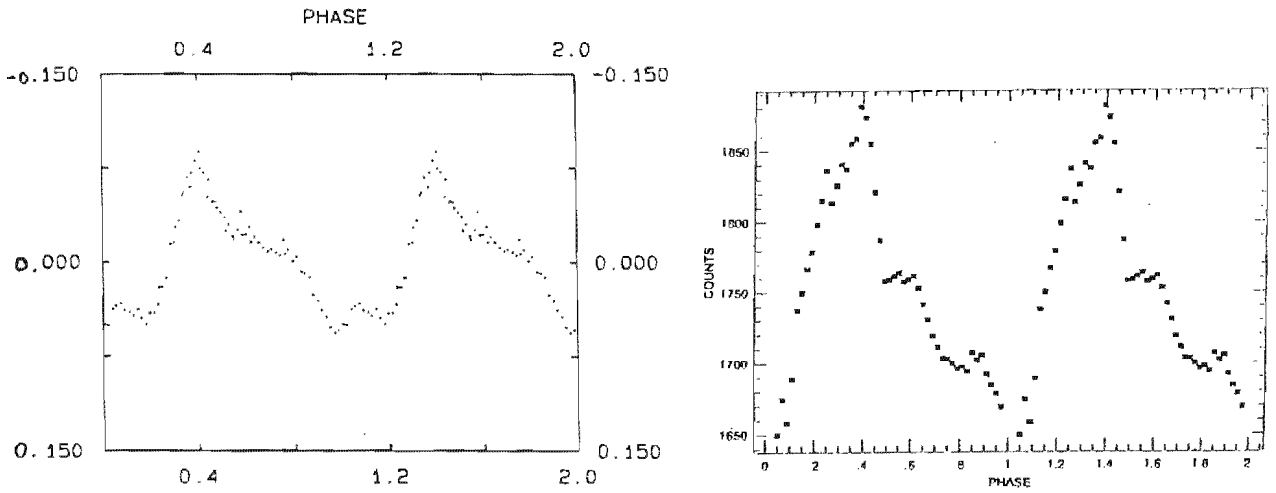

Figure 6.3: The mean light curve for CP Eri in the high state (run A366), compared to the mean light curve of the SU UMa dwarf nova TV Crv in late superoutburst (from Howell et al. 1996). The horizontal scale for the CP Eri pulse shape is in phase, chosen so that phase 0 corresponds to the minimum of a sinusoid fitted to the pulse by least squares.

state period of 1721 ± 8 s. Despite the apparent stability of the periods in table 6.3, the phase of the principal period tends to wander during each run. This can be seen when a sinusoid with the appropriate parameters is superimposed on the data. Figure 6.5 shows runs A371 and A375 with their best non-linear least squares sinusoid. A single period is an inadequate description of the fundamental variation. The phase of the high state light curve also drifts relative to the best sinusoid fit for the four nights (see figure 6.1).

To examine how the phase of the $\sim$ 1718 s period varies over runs A366, A371, A375, A322a and A322b, the best period for all four high state runs (see later), 1718 s, was fitted to overlapping sections of the data by least squares, and the phase of the best period in each section was calculated. The length of each section was three cycles of the 1718 s variation, with an overlap of 50%. The period used for run A332b was 870 s, because this

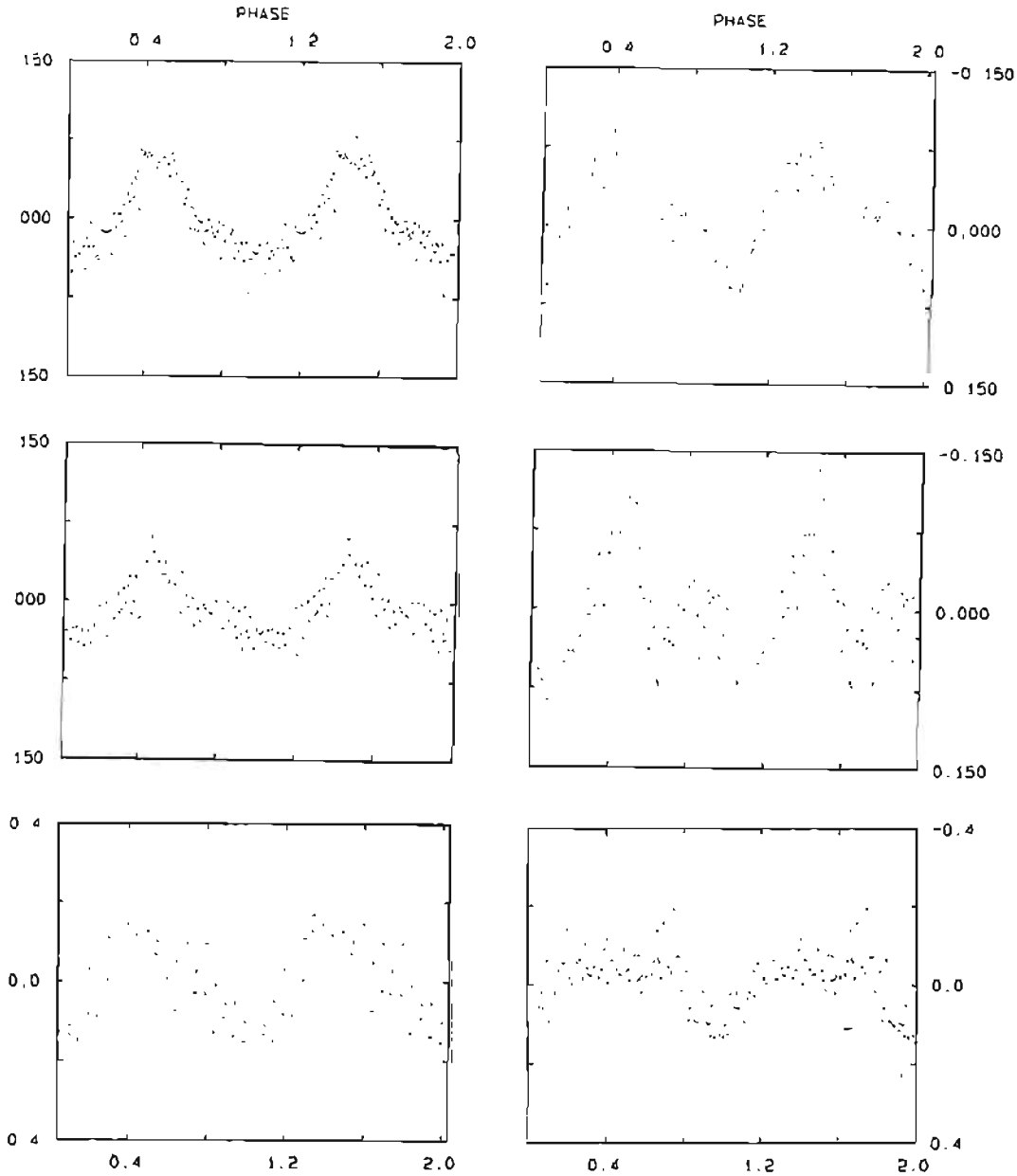

Figure 6.4: Mean light curves for runs A371, A375, A332a, A332b, A389 and A392. The mean pulse shape for the intermediate state run, A332b, has a double-humped shape; this could be due to the development of the secondary peaks on the falling sides of the high state pulse shapes. The mean light curves from the two low state runs are shown in the last panel. The amplitude of the pulse (in magnitudes) is almost twice as large for the low state runs as for the high state runs.

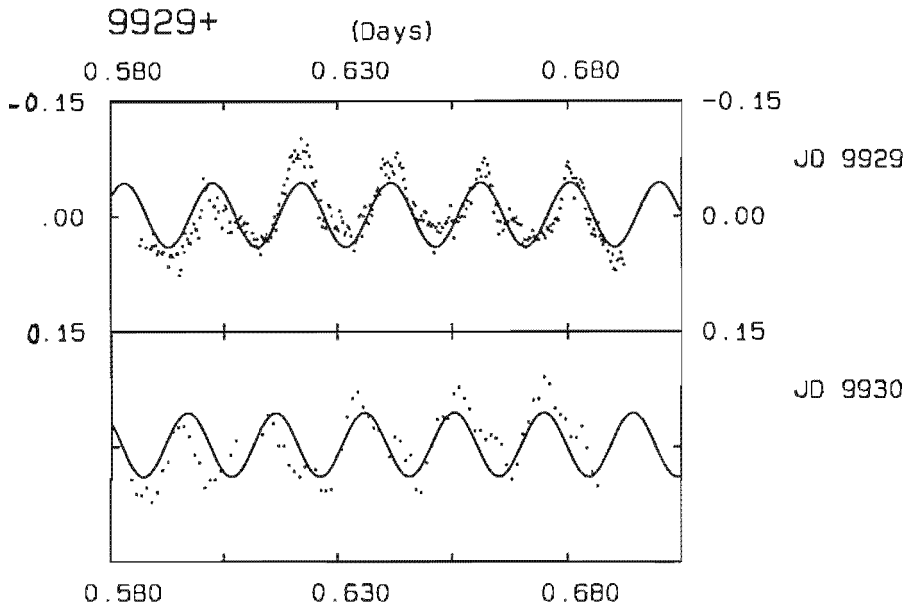

Figure 6.5: Runs A371 and A375 with a sinusoidal fit to the 1717 s period, showing the wanderings in phase of the fundamental variation.

is the period that appears to keep phase with the 1718 s fundamental of the previous four nights. The resulting phases for the principal variation during the first five nights are shown in figure 6.6. During each run there is phase "jitter" of up to 0.2 cycles, and there is a smooth variation in the mean phase for each run (resembling part of a sinusoid) from one run to the next, with the phase of the 870 s period in run A332b continuing the trend.

Figure 6.7 is a Fourier amplitude spectrum of runs A366, A371, A375 and A332a and shows a fundamental variation and two harmonics; the third harmonic is probably present at low amplitude. If further harmonics are present then their amplitudes are lower than about 0.005 mag. There are no other significant features above the noise level up to the Nyquist frequency. By contrast, both Abbott et al. (1992) and Provencal (1994) observed up to seven harmonics of the $\sim$ 1720 s period. The highest peak in the region of the fundamental corresponds to a period of 1718 ± 2 s with an amplitude of 0.043 ± 0.002 mag. The time of the first minimum is $JD_{\odot}2449928.61797 \pm 0.00023$. The period differs by 9σ from Provencal's (1994) high state period of 1700 ± 2 s.

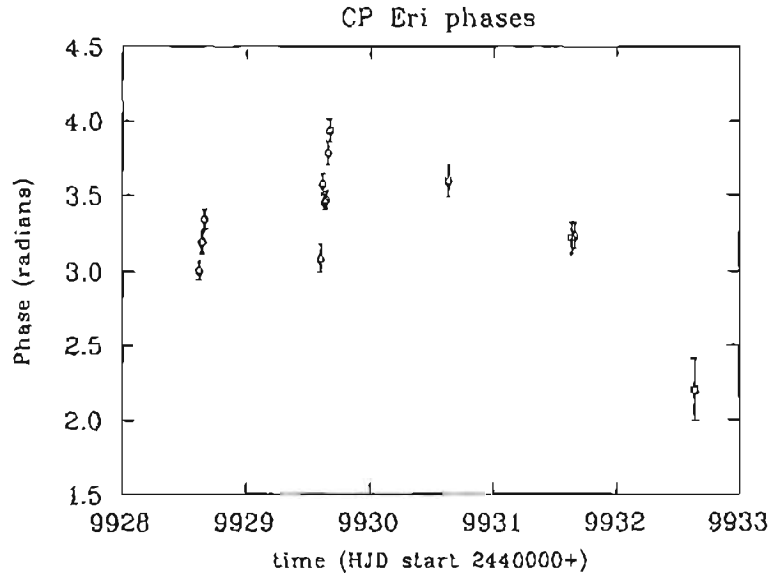

Figure 6.6: Phase of the 1718 s variation during A366 – A332a together with the phase of the 870 s variation in run A332b. The points are grouped into runs and have $\pm 1\sigma$ error bars. There is an ambiguity of 2π in each point.

A close-up of the amplitude spectrum in the region of the fundamental and the first two harmonics, together with the spectral window function, is shown in figure 6.8. The structure surrounding the fundamental and its harmonics is not identical to the alias pattern; the bulge on the high frequency side of the fundamental and the first harmonic could indicate a nearby low-amplitude signal. In order to expose these low-amplitude signals, however, the correct peak in the window pattern of the principal variation has to be identified so that the data can be pre-whitened by this frequency. The Fourier transform will identify the peak in the window pattern with the highest amplitude, and because the amplitudes of the peaks in the principal variation's window pattern are slightly distorted by the low-amplitude component, the peak with the highest amplitude could well be an alias of the true frequency. Identifying the correct frequency with which to pre-whiten the light curve to reveal the low-amplitude structure is therefore not simply a matter of using the frequency identified by the Fourier transform as having the highest amplitude.

To check whether the principal period in the high state data is indeed 1718 ± 2 s, and that

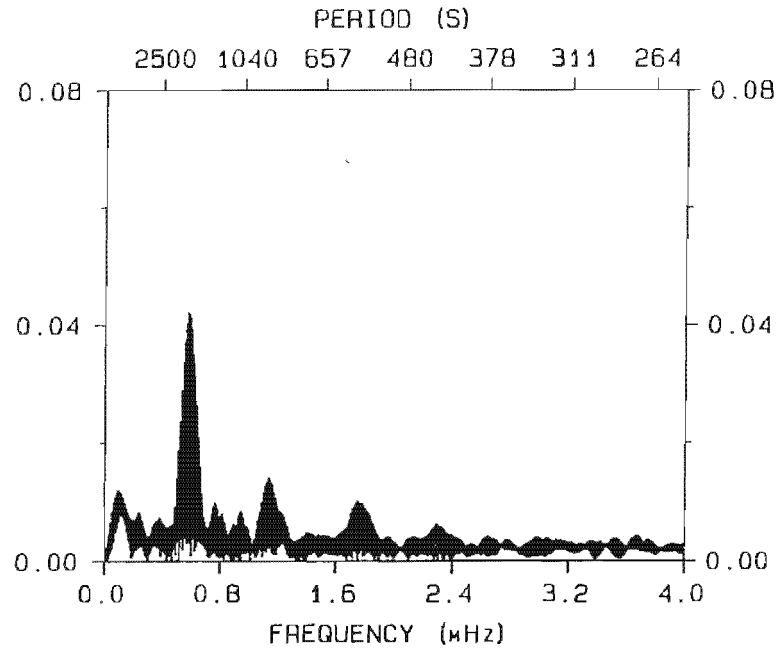

Figure 6.7: Fourier amplitude spectrum for the high state runs (A366, A371, A375 and A332a). A fundamental variation with a period of 1718 s and two harmonics are present above the noise. A third harmonic may be present at low amplitude.

this is the correct period to remove from the light curve in order to reveal the underlying structure, the following method was used. First, the envelope of the low-amplitude variation was sketched onto the amplitude spectrum by hand. The amplitude difference between this envelope and the principal variation envelope was then measured for each of the alias peaks, and the peak with the largest amplitude difference was identified. The frequency corresponding to this peak (in this case, 5.706×10^{-4} Hz) is the initial guess for the frequency of the principal variation. This frequency was then used to pre-whiten the data. The peak frequency in the amplitude spectrum of the pre-whitened data is 6.304×10^{-4} Hz. This frequency is an initial guess for the frequency of the low-amplitude signal. The original data are then pre-whitened by this frequency. The highest peak in the resulting window pattern should then be a good estimate of the true principal frequency. Using this method with 6.304×10^{-4} Hz for the frequency of the low-amplitude signal, the result obtained for the principal frequency is 5.822×10^{-4} Hz, i.e. the original result of 1718 s. This process was repeated for several choices of the initial guess for the principal frequency (including both one cycle day^{-1} and both two cycle day^{-1}

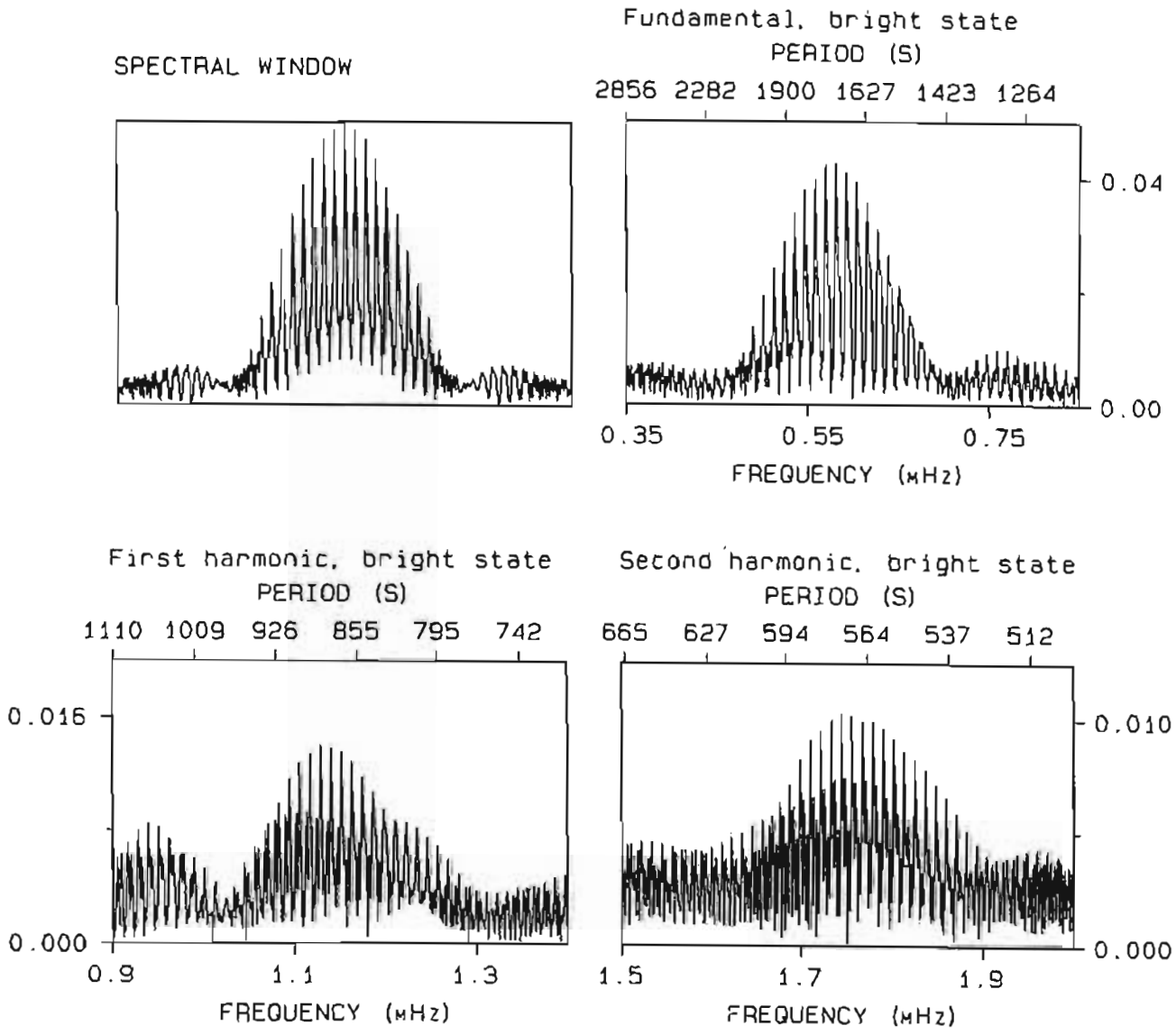

Figure 6.8: Amplitude spectra of the high state data in the region of the fundamental, first and second harmonics. The spectral window is shown on the top left. In all three peaks, the surrounding alias structure suggests the presence of low-amplitude signals.

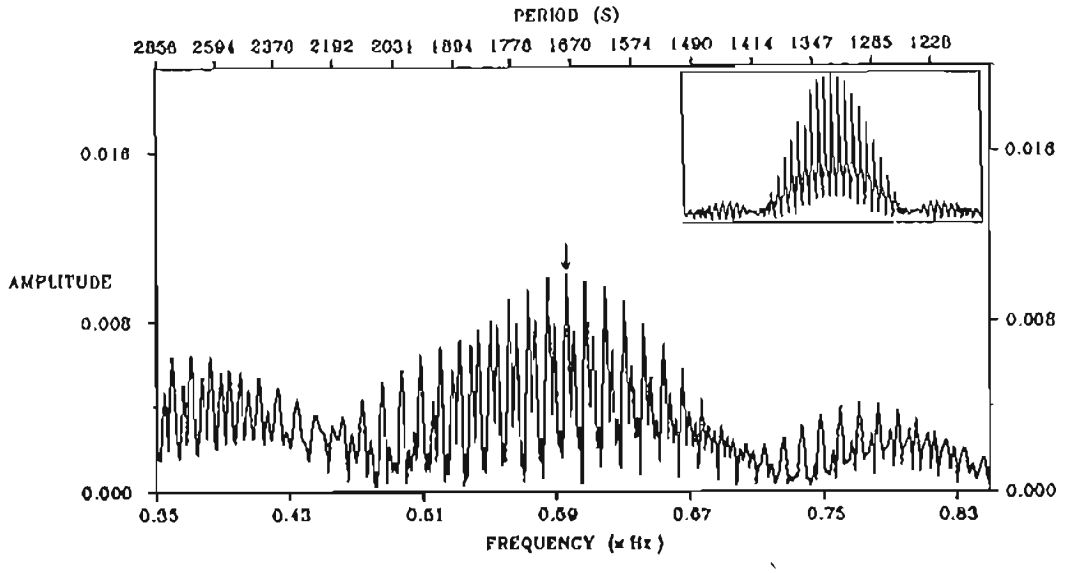

Figure 6.9: Amplitude spectrum of the high state data pre-whitened by the 1718 s signal. The arrow shows the highest peak, corresponding to a period of 1677 s. The spectral window is shown as an inset.

aliases of the 1718 s signal), and the result was a frequency of $(1718\,\mathrm{s})^{-1}$ (to the nearest 0.5 s) in each case. This strengthens our confidence that 1718 s is the true principal period.

Assuming that 1718 s is the correct high state fundamental period, an attempt can be made to determine the period of the nearby low-amplitude signal. The amplitude spectrum obtained after pre-whitening the light curve by $(1718\,\mathrm{s})^{-1}$ is shown in figure 6.9. The peak in the pre-whitened spectrum corresponds to a period of 1677 ± 2 s with $A = 0.010 \pm 0.002$ mag. This period should be treated with scepticism, however, because the result obtained for the low-frequency peak is strongly dependent on the choice of the pre-whitening frequency. For instance, if 5.938×10^{-4} Hz (a one cycle day^{-1} alias of the 1718 s signal) is chosen as the pre-whitening frequency, the period obtained for the low-amplitude signal is 1709 ± 2 s.

The period and amplitude of the first harmonic in the high state data are 867 ± 1 s and 0.014 ± 0.002 mag. This period is probably an alias of the correct first harmonic which

is expected at $\approx 859\,\mathrm{s}$; the distortion of the window pattern is due to the neighbouring low-amplitude modulations. The second harmonic peak has $P = 573.2 \pm 0.3\,\mathrm{s}$ and $A = 0.011 \pm 0.003\,\mathrm{mag}$.

The amplitude spectra of CP Eri (figures 6.7 and 6.10) appear to show low-amplitude coherent oscillations in addition to the principal variations and their harmonics: these appear as small window patterns just above the noise level. However, these features are probably artefacts caused by the stochastic variations in brightness that are present on a variety of time scales in AM CVn stars (and in all CVs). Amplitude spectra of finite data sets containing stochastic variations will show non-white noise, but the maxima and minima of the variations will not, in general, repeat from one run to the next. If data from only a few nights are added together and an amplitude spectrum calculated, power excesses in a certain region from one run can by chance by re-enforced by a power excess in that region from another run. This produces a broad hump in the cumulative amplitude spectrum that mimics the window pattern of a low-amplitude coherent variation. If one adds more runs and re-calculates the amplitude spectrum, the power excesses will probably be diluted, resulting in an excess barely above the (much lower) noise. Of course, if true coherent signals are present only occasionally, their amplitudes will also be diluted if many runs are added together. This effect is described in Warner & Cropper (1984) in their study of V1223 Sgr, an intermediate polar.

The amplitude spectrum of the low state data (figure 6.10) shows a fundamental variation with only one (convincing) harmonic (note that *amplitude* spectra appear to have greater noise relative to the coherent signal than *power* spectra, where the peak amplitudes are the square of the amplitudes shown here). The peaks at frequencies lower than the suspected fundamental at $\sim 0.6\,\mathrm{mHz}$ could be due to differential extinction, stochastic variations intrinsic to the star, or differential transparency variations (which should, however, be minimized by using a CCD with its differencing capabilities). The periods corresponding to these frequencies are comparable to the length of the runs, and the resulting "red noise" is present in many amplitude spectra. It is, as a result, very difficult to detect periods of $\sim 3 - 4\,\mathrm{h}$ in CVs and other rapidly varying stars, because the nightly observational baselines are often approximately this length.

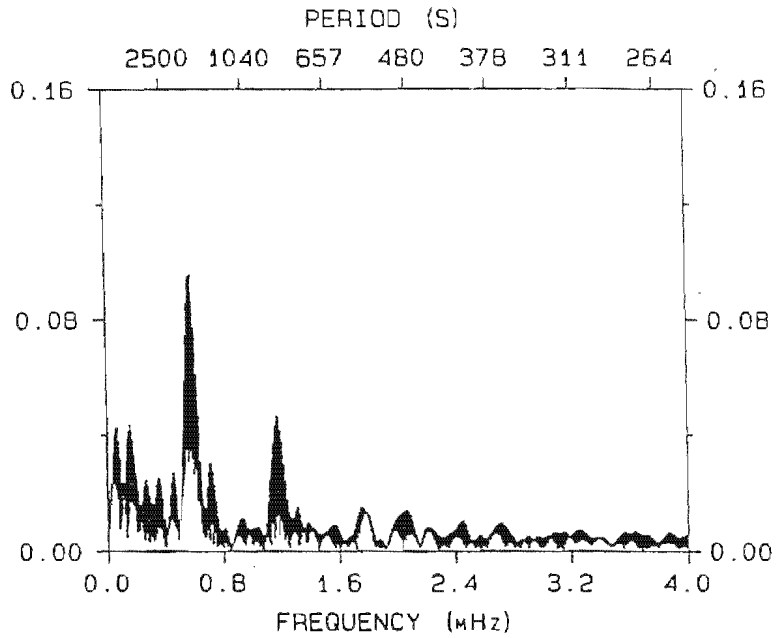

Figure 6.10: Fourier amplitude spectrum for the low state runs (A389 and A392). A fundamental variation at ~ 1720 s is present, together with its first harmonic.

The period obtained using a non-linear least squares sinusoid fit to both low state nights, is 1721 ± 7 s, with an amplitude of 0.098 ± 0.007 mag. The time of the first minimum is $JD_{\odot}2449957.55338 \pm 0.00035$. The period obtained for the first harmonic is 858 ± 2 s, with $A = 0.046 \pm 0.009$ and T_{min} =$JD_{\odot}2449957.54630 \pm 0.00051$. A close-up of the amplitude spectrum in the region of the fundamental and the first harmonic, together with its window function, is shown in figure 6.11. Unlike the window patterns for the variations in the high state (figure 6.8), the low state peaks are consistent with the windowing of the light curve.

There is an inverse dependence between the amplitude (in magnitudes) of the principal variation and the overall magnitude of the star. Similar amplitude changes are observed in CR Boo (Provencal 1994) and are suggestive of an (approximately) constant source seen against a varying background. To investigate how the amplitude of the principal variation of CP Eri changes as the system fades to a low state, the amplitudes of the 1718 s period were determined in overlapping sections of the high state data using least squares (similar to the way in which the phases figure 6.6 were obtained). The amplitudes were converted from magnitudes to intensities (in ADU/s) by calculating the fractional

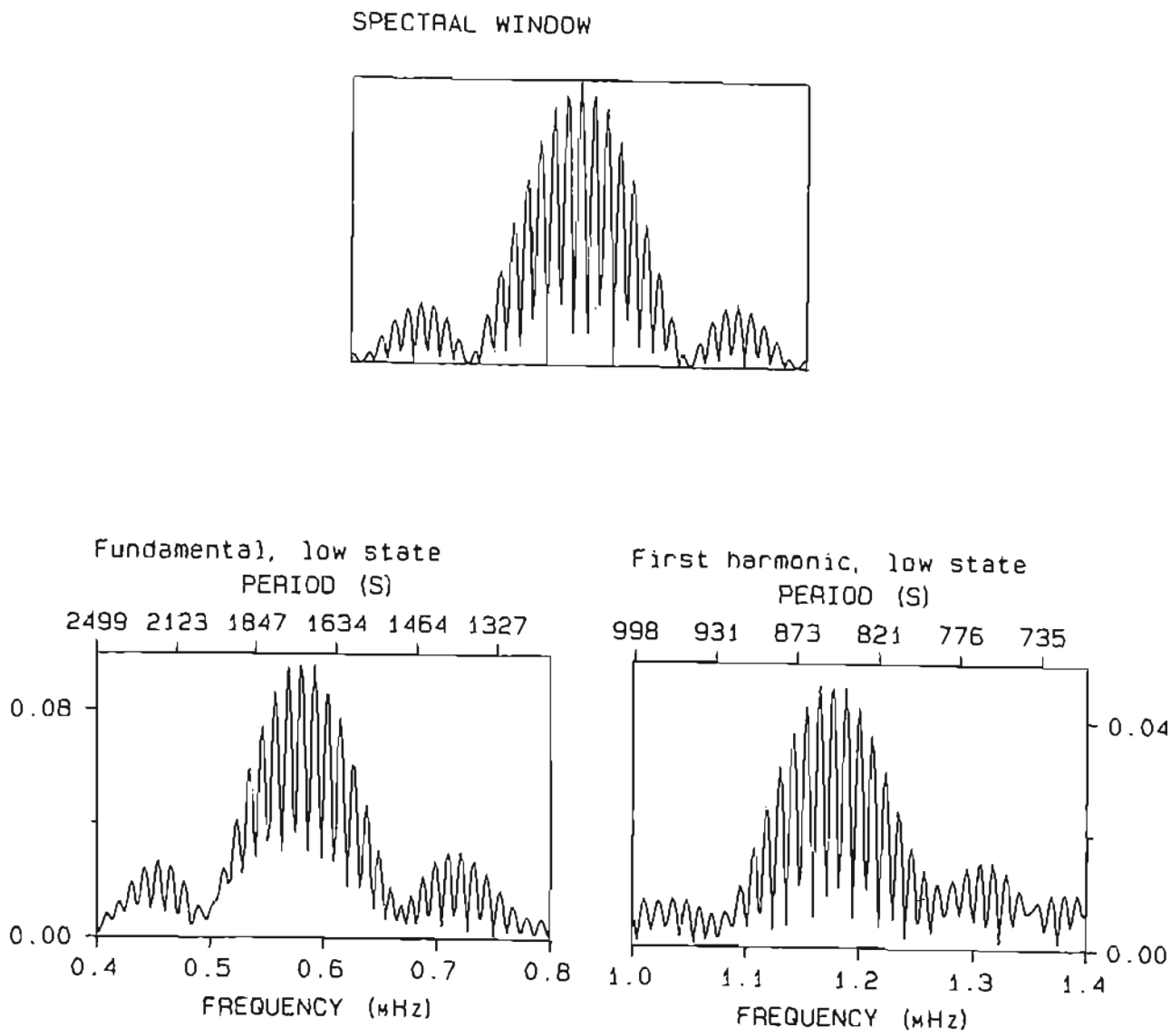

Figure 6.11: Amplitude spectra of the low state data in the region of the fundamental variation and its first harmonic, together with the corresponding spectral window. Unlike the high state data, these variations are consistent with the windowing of the light curve.

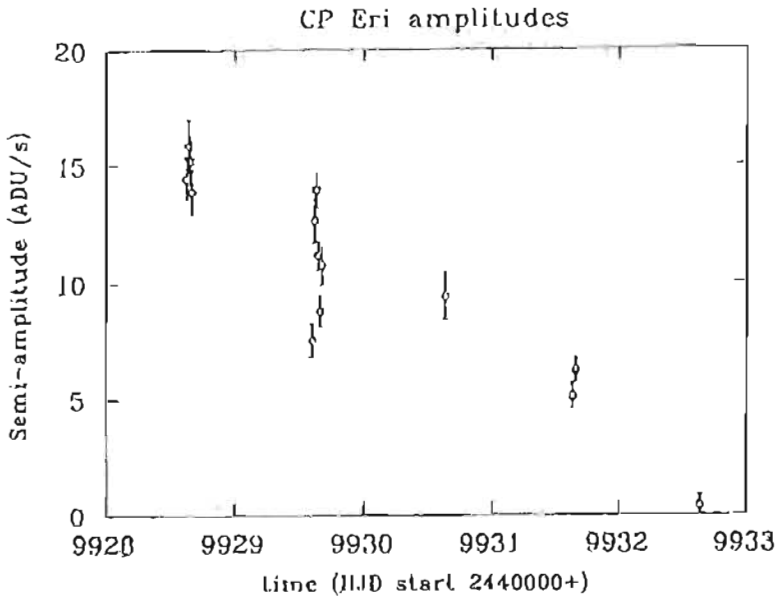

Figure 6.12: Amplitudes (in ADU/s) of the 1718s variation in runs A366, A371, A375 and A332a, together with the amplitude of the 870s variation in run A332b. Although the *relative* amplitude of the 1718s variation is larger in the low state than in the high state, the absolute amplitude in ADU/s decreases.

intensities of each amplitude and then multiplying these fractional intensities by the mean intensity in ADU/s for each run. The mean intensity for each run (corrected for extinction and cloud) was obtained using the mean white light magnitudes from the differential photometry together with the V magnitude and the white light count rate for a standard star. The amplitudes are shown in figure 6.12.

The amplitude of the principal modulation (in ADU/s) decreases as the system fades, but the *relative* amplitude (in magnitudes) of the photometric modulations is larger in the low than in the high state. This implies that, as the system becomes fainter, the amplitude of the modulations also decreases, but not as fast as the background, i.e. the actual amplitude decays on a *slower* time scale than does the system brightness.

6.4 Discussion

Although we do not have sufficient data (i.e. sufficiently small uncertainties) to distinguish between the period of the fundamental 1718 s modulation in the high state and the 1720 s period in the low state, there is evidence that the two modulations are different phenomena. Whereas the peaks in the low state amplitude spectra are consistent with the spectral window function, the high state amplitude spectra peaks show neighbouring low-amplitude structures which distort the alias pattern envelope. During the transition from high to low state (run A322b), the 1718 s period is no longer the dominant modulation, and is replaced by a modulation at 870 ± 30 s, consistent with the first harmonic of either the low or the high state fundamental variation. The 870 s variation has a similar phase to the 1718 s period of the previous four nights and its amplitude continues the trend established by the 1718 s amplitudes of the preceding high state runs (figure 6.12). The development of structures in the light curve towards the end of an outburst that are shifted by 0.5 in phase with respect to the original variations is reminiscent of the late superhumps seen in superoutbursting dwarf novae.

It is not clear whether the 1718 s signal survives through the transition and is the same signal observed in the low state. The obvious way to resolve this uncertainty would be to obtain high-speed photometry of the star each night from its maximum brightness until its minimum brightness at $V \approx 19.8$, and to see whether the 1718 s period can be phased from high to low state. It seems likely that the low state principal variation is similar to that seen in CR Boo, where a fundamental variation appears with a single harmonic. This is precisely what is seen in figure 6.10. It is tempting, therefore, to speculate that the low state period in CP Eri represents a coherent orbital period (like the 1471.4 s period in CR Boo), and that the principal variation in the high state is a superhump. More data will be required to refine the value of the low state period and to test its coherence. The observations of CP Eri by Provencal (1994) show a photometric period in the high state that is *greater* than the low state period. If the low state period is an orbital variation, the high state variation in these observations is a *negative* superhump.

The structure of the fundamental and harmonics in the high state suggests nearby periodicities; an estimate of the period of the low-amplitude signal near the fundamental

yields 1677 s. We are hoping to find two periods — one a superhump and the other an orbital modulation, if our model is correct — with a beat period of ~ 1 day, by analogy with CR Boo and AM CVn (Solheim et al. 1991, Provencal 1994). In AM CVn, the orbital period and the superhump have a beat period of 13.38 h; in CR Boo, the variable 1490 s variation and the coherent 1471.4 s variation have a beat period of ~ 32 h. The beat period between 1677 s and 1718 s is ~ 19 h. However, if the orbital period and its first harmonic dominate the low state light curve, the orbital period should be consistent with the period obtained for the two low state runs A389 and A392, i.e. 1721 ± 7 s.

It is probable, however, that the beat period between the orbital and the superhump periods in CP Eri is much longer than that for AM CVn. If the brightness modulations in the AM CVn stars are indeed superhumps, we can estimate approximate values for their orbital periods. CP Eri has a much longer period (~ 1720 s) than AM CVn (1028 s: Patterson, Halpern & Shambrook 1993). Because the ratio P_{orb}/P_s is expected to increase towards unity as P_{orb} increases (see chapter 1), the difference between P_{orb} and P_s will be smaller for CP Eri than for all the other AM CVn systems, with the exception of GP Com. The beat period of CP Eri will thus be longer than that for the other absorption-line AM CVn systems. If the primary masses in CP Eri and AM CVn are the same, the beat period expected for CP Eri is ~ 43 h (see chapter 1).

The precise nature of the "outbursts" seen in V803 Cen, CR Boo and CP Eri has not been established. The eruptions from the low state are very similar to dwarf novae outbursts: in CR Boo, the rise and decay times for the eruptions from $V \approx 18.0$ are in agreement with predictions for helium discs (Warner 1995a). In addition, we have observed late superhump-like features in CP Eri as it fades from a high state to a low state. However, the amplitude of the photometric modulations in CP Eri decreases more slowly than the background during the transition to a low state. This is in contrast to the superhump amplitude changes in superoutbursting SU UMa stars. For example, during the plateau of a superoutburst in V1159 Ori (Patterson et al. 1995), the fractional intensity of the superhump modulation decreased from 0.107 at the start of the plateau phase to 0.038 at the end of the plateau phase, 6 days later. This corresponds to a magnitude change of 1.7 mag. During this time the background light decreased by only 0.5 mag. In CR Boo (Provencal 1994), V803 Cen (O'Donoghue, Menzies & Hill 1987) and CP Eri (this study),

the fractional intensities of the photometric variations *increase* as the system fades to a low state. This suggests that a different physical process is occurring in CP Eri, CR Boo and V803 Cen to modulate the background light. Differences between the AM CVn stars and the SU UMa stars might be expected because, during the fall to quiescence in SU UMa stars, the eccentricity of the accretion disc decreases as the disc is drained of mass. In the AM CVn stars, the decline to a low state is a result of falling $\dot{M}_2$, and the disc may be more stable as the system fades to a low state than the disc of an SU UMa star as it declines to quiescence after a superoutburst.

Chapter 7

EC 15330-1403

7.1 Introduction

EC 15330-1403 was identified in the Edinburgh-Cape Survey (Stobie et al. 1992 and references therein) and is the most recently-discovered of the AM CVn stars. The EC Survey is a search for high galactic latitude, ultra-violet excess stars in the southern hemisphere and is the southern sky counterpart of the northern Palomar-Green survey (Green et al. 1986). The EC survey is potentially a rich source of blue stars such as AM CVn stars and other CVs.

Spectra of EC 15330 obtained in 1989 by O'Donoghue et al. (1994) resemble those of AM CVn (Patterson et al. 1992), and are similar to those of V803 Cen (O'Donoghue & Kilkenny 1989), CP Eri (Abbott et al. 1992) and CR Boo (Wood et al. 1987) in their high states. The main features in the EC 15330 spectrum are the broad shallow absorption lines of He I: λ4471 Å and λ4387 Å are weakly present, and a blend of λ4026 Å with λ4009 Å and λ4016 Å is the strongest feature in the spectrum. Neither the Balmer lines nor He II λ4686 Å are seen.

38 h of high-speed photometry (O'Donoghue et al. 1994) obtained in February and May 1993 show a prominent variation at 1119 s with an amplitude of $\sim$ 2%. The first harmonic at 559.5 s is present with an amplitude of $\sim$ 1.3%, and a weak second harmonic is also observed. Apart from the fundamental 1119 s variation and its first two harmonics,

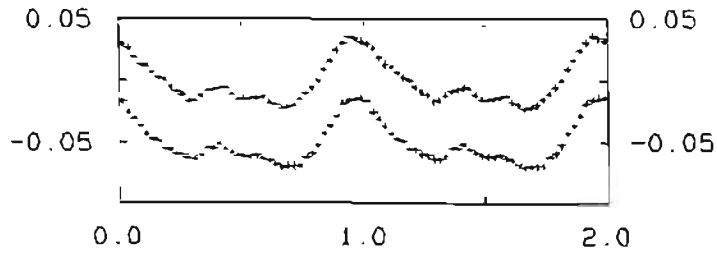

Figure 7.1: The pulse shape of the 1119 s period during February and May 1993 (from O'Donoghue et al. 1994). The horizontal scale is in phase and the vertical in units of fractional intensity. There are subtle changes in the pulse shape during this time, but in comparison to e.g. V803 Cen and CP Eri, the mean light curve is very stable.

no non-commensurate periods have been detected in EC 15330. This is in contrast to AM CVn, with its variable-amplitude 1011 s period (e.g. Solheim et al. 1991, Patterson, Halpern & Shambrook 1993), V803 Cen (175 s: O'Donoghue & Kilkenny 1989) and CR Boo (1471.4 s: Provencal 1994).

Mean light curves of EC 15330 folded on the 1119 s period consist of a principal maximum at phase 0.0 and weaker secondary peaks around phase 0.5 (O'Donoghue et al. 1994). Warner (private communication) has observed that the small-scale structure around phase 0.5 occurs at exactly one fifth of the principal frequency, and indicates the presence of a fourth harmonic in the light curve. The Fourier amplitude spectra of the corresponding data show a definite peak at the position of the fourth harmonic, although the amplitude of the peak is not higher than the surrounding noise. The pulse shape is very stable over a period of four months; however, there are some subtle changes in the mean light curves around phase 0.5 during this time (see figure 7.1 which is taken from O'Donoghue et al. 1994). The stability of the mean pulse shape is in contrast to the night to night variability of the pulse shapes of CP Eri (chapter 6) and V803 Cen (O'Donoghue, Menzies & Hill 1987, O'Donoghue & Kilkenny 1989, see also chapter 4).

No variations in radial velocity or line profile changes in the range 300 – 3000 s have been

found in time-resolved spectroscopy (O'Donoghue et al. 1994). In particular, an upper limit of $20\,\mathrm{km\,s^{-1}}$ has been established for radial velocity variations at the 1119 s period. A search for line profile variations similar to the 13.38 h variation observed in AM CVn (Patterson, Halpern & Shambrook 1993) yielded inconclusive results due to the weakness of the He I lines. Evidence for asymmetry in the profile of λ4143 Å was observed in some spectra (O'Donoghue et al. 1994), but no systematic changes in the line skewness were evident. An intensive study is needed (when the lines are stronger) to determine whether there is periodic variability in the asymmetry of the line profiles.

Of the AM CVn stars, EC 15330-1403 is the most similar to AM CVn itself. Like AM CVn, EC 15330 remains at an approximately constant mean brightness ($V \approx 13.7$) and does not show large-magnitude variations such as those seen in CR Boo, V803 Cen and CP Eri. Its photometric periods are similar to those of AM CVn. In the classification scheme of Warner (1995a), both AM CVn and EC 15330 are classified as helium analogues of the H-rich nova-like variables with bright, optically thick discs, and are permanently in a high state with high rates of mass transfer from the secondary ($\sim 3.9 \times 10^{-9} \mathrm{M_\odot y^{-1}}$).

One respect in which EC 15330 and AM CVn differ is the power at the fundamental frequency. In AM CVn, the photometric variations are harmonics of a 1051 s fundamental, but the amplitude of this variation is much smaller than the those of the harmonic peaks and the signal is often not detected. This has led Provencal et al. (1995) to argue that the photometric variations in AM CVn are not simply harmonics of 1051 s but arise via a more complex mechanism. EC 15330, which is very similar to AM CVn in most other respects, shows power at the fundamental frequency and two harmonics (as do CR Boo, V803 Cen and CP Eri in the high state). This suggests that AM CVn is an exceptional case and that the absence of power at the fundamental frequency is not a general property of the AM CVn stars (see the discussion in chapter 1 section 1.3.1).

The results obtained by O'Donoghue et al. (1994) for the fundamental period are 1118.9 ± 0.1 s for February 1993 and 1119.0 ± 0.2 s in May 1993. The similarity between these two periods suggests that, if the 1119 s period is not constant (it is not expected to be, by analogy with the 1051 s period in AM CVn), the changes in period are very gentle and it may be possible to track the changes in the fundamental signal over longer periods

Table 7.1: Journal of observations: August 1995 high-speed photometry of EC 15330-1403

Run	Date (start)	$JD_{\odot}$ (2440000+)	Length (h)	Exposure time (s)	Mean "white light" magnitude
A382	1995 August 25	9955.21018	2.0	10	13.3
A386	1995 August 27	9956.20448	2.3	10	13.4
A390	1995 August 28	9958.20858	1.7	10	13.4

of time. To explore this idea, new high-speed photometry of EC 15330 was obtained in August 1995 and compared to a more extensive set of photometry obtained earlier in 1995 at the Centre for Basement Astrophysics, Tucson.

7.2 Observations

High-speed photometry of EC 15330-1403 was obtained in August 1995 using the UCT Wright CCD on the 1 m telescope at Sutherland. Table 7.1 is a journal of the observations. The exposure time for all three runs was 10 s, and the observations were made without a filter. The mean white light magnitude of EC 15330 for each run was estimated by comparing the mean count rate of EC 15330 to that of an equatorial standard. The second of the three runs (A386) shows pronounced differential extinction towards the end of the run, implying that the two comparison stars used for the differential photometry have redder colours than EC 15330. The data were reduced according to the procedure described in chapter 2.

A second data set comprising eight runs was obtained in May, June and July 1995 using the robotic telescope at the Centre for Basement Astrophysics, Tucson (see Harvey et al. 1995 for a description of the system), and was kindly made available to the writer by Joe Patterson. A journal of these runs is given in table 7.2. The exposure time was 2 min for each run, and the frames are separated by a dead time of ~ 12 s.

Table 7.2: Journal of observations: May, June and July 1995 high-speed photometry of EC 15330-1403 from CBA West.

Run	Date (start)	$JD_\odot$ (2440000+)	Length (h)
J9861	1995 May 24	9861.65130	6.9
J9862	1995 May 25	9862.65951	6.9
J9863	1995 May 26	9863.64575	6.9
J9864	1995 May 27	9864.70603	4.9
J9867	1995 May 30	9867.66221	6.3
J9893	1995 June 25	9893.68832	1.4
J9925	1995 July 27	9925.65471	2.9
J9926	1995 July 28	9926.65503	2.7

7.3 Results

The runs in table 7.1 are shown in figure 7.2. The light curves resemble those in O'Donoghue et al. (1994) and show prominent non-sinusoidal variations with sharp peaks and rounder minima which occasionally contain small secondary peaks. The peak-to-peak amplitude of the pulses is $\sim$ 10% and the secondary peaks have amplitudes of about 6% peak-to-peak. The best-fit sinusoid for all three nights is shown; the parameters for the sinusoidal fit are listed in table 7.4. The CBA runs are shown in figure 7.3.

Fourier amplitude spectra were calculated for each run in turn to check for any changes in the periodic structure from night to night. The fundamental frequency and its first harmonic are present in every spectrum; the second harmonic is visible at low amplitude in three of the eleven runs. Apart from the $\sim$ 1119 s variation and two harmonics, there is no further structure above the noise in the nightly amplitude spectra. The periods and amplitudes of the fundamental $\sim$ 1119 s variation and its first harmonic (P_0, A_0, P_1 and A_1) obtained from the nightly amplitude spectra are listed in table 7.3. The values obtained for the fundamental period are consistent with being a single period, as are those for the first harmonic. The mean amplitude for the fundamental is 0.020 ± 0.002 and that

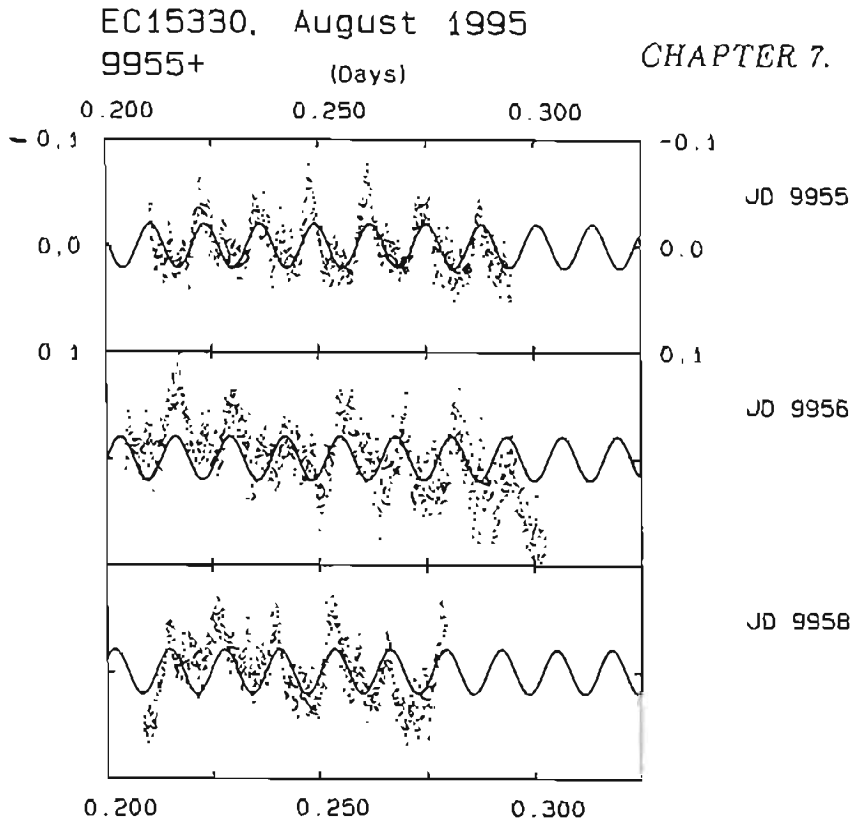

Figure 7.2: High-speed photometry of EC 15330 obtained at Sutherland during August 1995. The vertical axis is in units of differential magnitudes from the mean white light magnitude during each run. The best-fitting sinusoid is shown.

for the first harmonic is 0.014 ± 0.003. The August runs (which have the highest time resolution: 10 s) were searched in the range 0.005 – 0.05 Hz for quasi-periodic oscillations such as the $\sim$ 26 s oscillation observed occasionally in AM CVn (Patterson et al. 1992). There was no structure above the noise in the amplitude spectra at these high frequencies.

The runs were divided into monthly groups (see table 7.4) and the period of the principal variation and times of the first maximum for each group were determined. These periods and pulse timings were used to construct mean light curves for the individual runs (the periods in table 7.3 cannot be used because the nightly periods are very inaccurate and do not produce the best pulse shape). This was done by folding each run into 50 phase bins on the appropriate principal period. As there were no obvious differences in the pulse shape from night to night, the mean pulse shape for each monthly group was calculated.

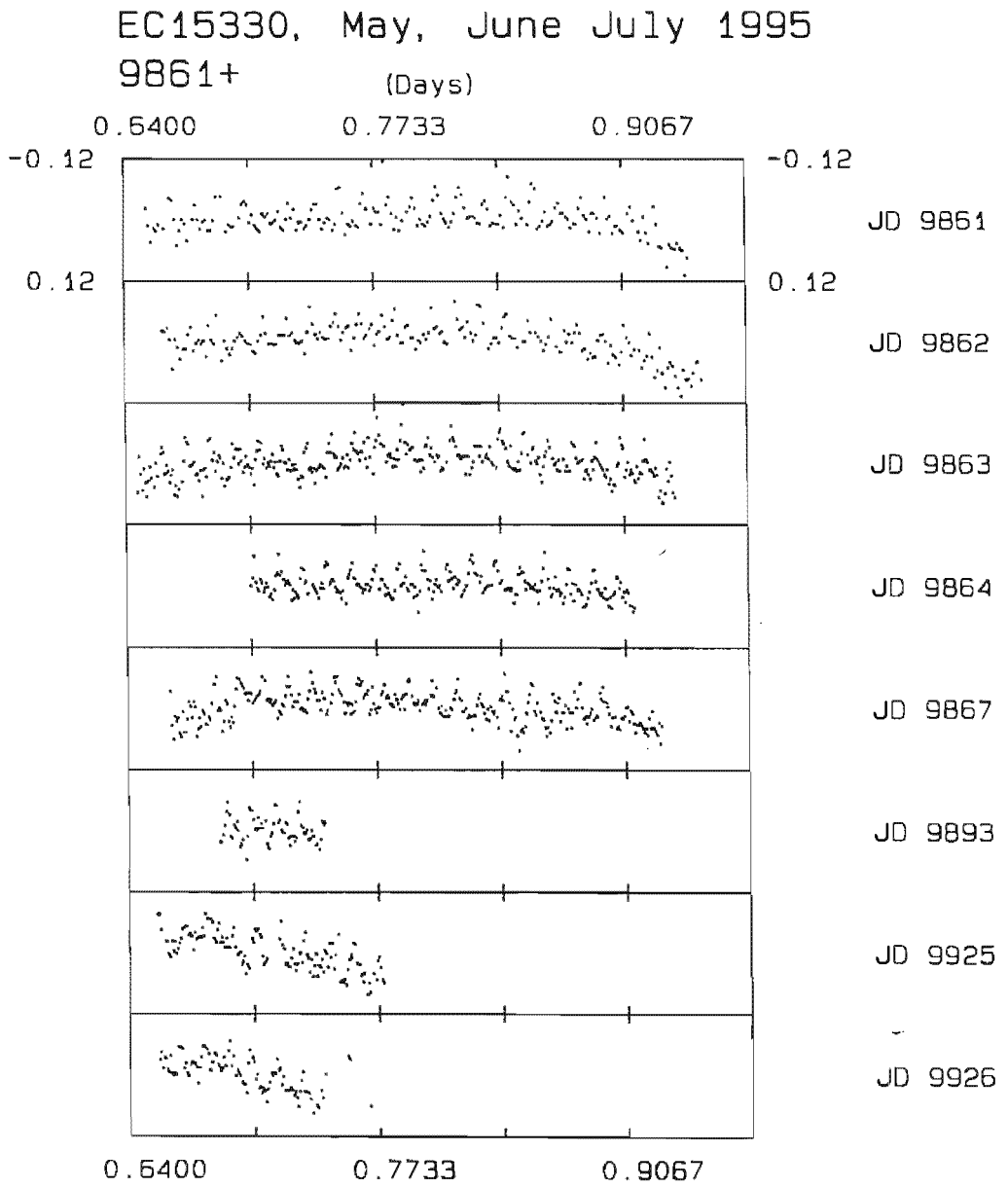

Figure 7.3: High-speed photometry listed in table 7.2. These observations were made at the Centre for Basement Astrophysics in Tucson and were very kindly made available by Joe Patterson. The vertical axis is in differential magnitudes from the mean V magnitude for each run.

Table 7.3: Periods and amplitudes of the principal variations in each run.

Run	P_0 (s)	A_0 (mag)	P_1 (s)	A_1 (mag)	Comments
J9861	1118 ± 13	0.021 ± 0.003	561 ± 3	0.016 ± 0.003	No 2nd harmonic
J9862	1119 ± 13	0.015 ± 0.003	558 ± 3	0.015 ± 0.003	No 2nd harmonic
J9863	1121 ± 13	0.020 ± 0.002	558 ± 3	0.014 ± 0.002	2nd harmonic: $A = 0.007 \pm 0.002$
J9864	1120 ± 18	0.020 ± 0.002	559 ± 4	0.014 ± 0.002	2nd harmonic: $A = 0.006 \pm 0.002$
J9867	1120 ± 14	0.022 ± 0.002	561 ± 4	0.013 ± 0.002	No 2nd harmonic
J9893	1117 ± 62	0.021 ± 0.003	560 ± 16	0.019 ± 0.003	2nd harmonic: $A = 0.010 \pm 0.004$
J9925	1130 ± 31	0.021 ± 0.004	558 ± 7	0.012 ± 0.004	No 2nd harmonic
J9926	1124 ± 33	0.018 ± 0.004	567 ± 8	0.010 ± 0.004	No 2nd harmonic
A382	1115 ± 43	0.023 ± 0.003	558 ± 11	0.013 ± 0.001	No 2nd harmonic
A386	1110 ± 37	0.022 ± 0.001	566 ± 10	0.010 ± 0.002	No 2nd harmonic
A390	1087 ± 48	0.022 ± 0.001	562 ± 13	0.016 ± 0.002	No 2nd harmonic

As was the case with the 1993 observations (O'Donoghue et al. 1994), the mean light curve appears very stable on a time scale of months. The pulse shapes for the monthly groups of data, and for all the runs together, are shown in figure 7.4. The low-amplitude structure around phase 0.5 occurs at 0.2 of the principal period, as was the case with the mean light curves from O'Donoghue et al. (1994), implying the presence of a fourth harmonic of the principal period.

The fundamental period in the August runs is clearly not the same as that obtained for the CBA runs and is incompatible with the results of O'Donoghue et al. (1994). The period obtained from *all* the CBA runs is 1118.9 ± 0.6 s: if this period is force-fit to the August runs by least squares, the amplitude obtained is 0.017 ± 0.001. This is considerably smaller than the amplitude of 1114 s in the August runs ($A = 0.022 \pm 0.001$). Also, folding the August light curves on 1118.9 s results in very noisy and badly-defined pulse shapes. Because of the different periods there is a suspicion that there is a period and/or a phase shift in the Sutherland runs relative to the ephemeris for the three months of CBA data. To identify the offending run(s), an ephemeris was calculated using the pulse timings and

Table 7.4: Periods, amplitudes and times of first maximum for the $\sim$ 1119 s period in monthly groups of runs, and in all the runs.

Group of runs	Period (s)	Amplitude (mag)	T_{max} ($JD_{\odot}$2440000+)
J9861 - J9864, J9867	1118.9 ± 0.5	0.020 ± 0.001	9861.65168 ± 0.00010
J9893, J9925, J9926	1119.8 ± 0.2	0.022 ± 0.002	9893.69335 ± 0.00032
a382, a386, a390	1114 ± 1	0.022 ± 0.001	9955.20409 ± 0.00024
all runs	1118.95 ± 0.04	0.018 ± 0.001	9861.65178 ± 0.00007

Table 7.5: Cycle counts and timings for pulse maxima of the 1118.9 s period

Run	cycle count	$JD_{\odot}$ (2440000+)	Error in timing
J9861	0	9861.651205	0.000253
	11	9861.793861	0.000313
J9862	78	9862.661794	0.000377
	89	9862.803964	0.000329
J9863	154	9863.646408	0.000201
	165	9863.789011	0.000214
J9864	236	9864.708445	0.000159
	243	9864.798947	0.000209
J9867	464	9867.660675	0.000179
	474	9867.790322	0.000210
J9893	2474	9893.693316	0.000321
J9925	4942	9925.655841	0.000236
J9926	5019	9926.653419	0.000286
a382	7224	9955.209782	0.000084
a386	7301	9956.204022	0.000105
a390	7456	9958.214383	0.000136

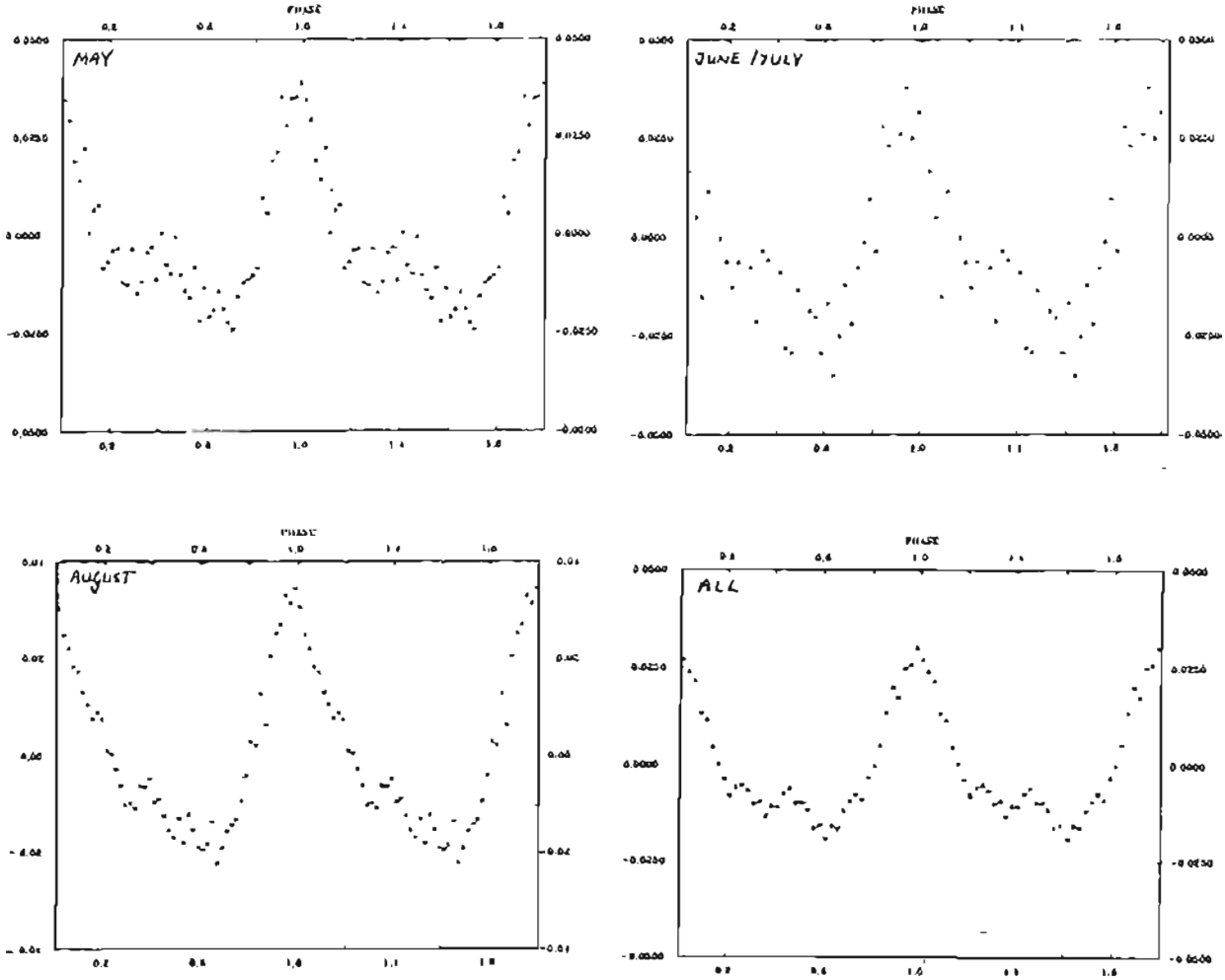

Figure 7.4: Pulse shapes of the 1119 s period for each monthly group of runs, and for all the runs together. The horizonal scale is in phase, calculated so that phase 0 corresponds to the maximum of a sinusoid fitted to the light curve by least squares. The periods and the times of first maximum are listed in table 7.4.

corresponding cycle numbers listed in table 7.5. The timings for the pulse maxima were calculated by fitting a least squares sinusoid with a period of 1118.9 s (the principal period of the CBA runs) to each run in turn, and calculating the time of the first maximum in the run using the phase of the fitted sinusoid. The longer runs were divided into two and the fit was performed separately for the second half of the run. The ephemeris for the pulse maxima is

$$T_{max} = (2449861.65177 \pm 0.00027) + (0.012950924 \pm 0.000000072)\, E \qquad (7.1)$$

The $O - C$ diagram is shown in figure 7.5. Apart from one wayward point (which belongs to run A386, the second of the Sutherland runs), the $O - C$ values are scattered about 0.0 with a spread of $\sigma = 0.07$ cycles (approximately 73 s). The errors shown in the figure are the uncertainties in the observed pulse arrival times. Because of the fairly close clustering of the $O - C$ values for all the other runs, the timings for run A386 are subject to some suspicion. However, it is not clear whether the inconsistency is due to a period change in the star or an artificial error introduced by the acquisition system. The apparent error is 0.23 of the phase of the principal variation, or 257 s, which is not an obvious amount (e.g. 4 min). No obvious timing errors were reported by other observers at Sutherland on the night of 26 August, so the error is unlikely to be caused by the central time service from the GPS receiver. It could be that the period in the star itself is changing on this short time scale. However, because of the stability of the principal period in the CBA runs and in the runs from 1993 in O'Donoghue et al. (1994), we suspect that the inconsistency is not due to the star.

We now move on to a discussion of the detailed structure in the amplitude spectra for the 1995 EC 15330 observations, bearing in mind that the timings for the second Sutherland run are suspect. O'Donoghue et al. (1994) drew attention to several alias patterns in their amplitude spectrum with amplitudes comparable to that of the second harmonic (see figure 7.6). Small 'satellite' peaks were observed at $\sim$ 1.03 mHz, $\sim$ 1.36 mHz and $\sim$ 1.91 mHz. These low-amplitude signals were present in the May 1993 observations but not in the runs from February 1993, and O'Donoghue et al. (1994) suggest that these peaks be searched for in future data sets. The $\sim$ 1.03 mHz and $\sim$ 1.91 mHz peaks are separated from the fundamental and first harmonic peaks by 0.143 ± 0.003 mHz (measured

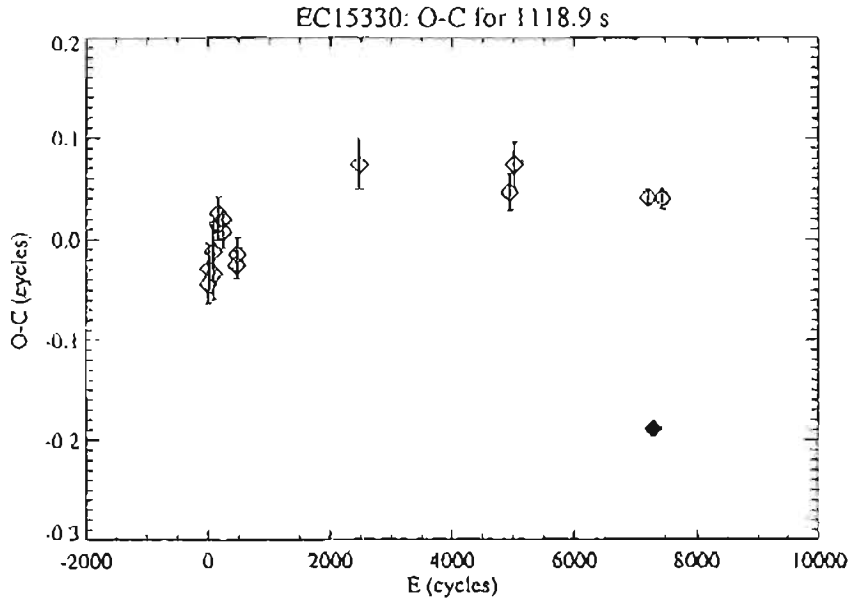

Figure 7.5: $O-C$ diagram of the timings of the pulse maxima with respect to a period of 1118.9 s. The $O-C$ result for run A386 (solid diamond) is much larger than those for the other 10 runs.

from the published amplitude spectrum). This is reminiscent of the fine structure seen in AM CVn spectra, but the spacing is much larger than the 22.7 μHz splitting observed in AM CVn. The beat period corresponding to a frequency splitting of 0.143 mHz is ≈ 1.94 h. In addition to the ~ 1.03 mHz and ~ 1.91 mHz satellite peaks, the fundamental and the first harmonic are accompanied by a second pair of low-amplitude components separated from the harmonic peaks by 0.065 ± 0.003 mHz; the beat period implied by this frequency splitting is ≈ 4.27 h.

The group of five May 1995 CBA runs offers the best hope for finding detailed structure near the fundamental and first harmonic. This is because the May runs are both long (with an average length of over six hours) and closely-spaced (four of the five runs were obtained on consecutive nights). The advantage of long runs is that the window pattern of a period in the data will be narrow and have few alias peaks to choose from (the width of the window pattern is a measure of the length of the runs) and the close spacing of the runs results in simpler alias structure within the window pattern.

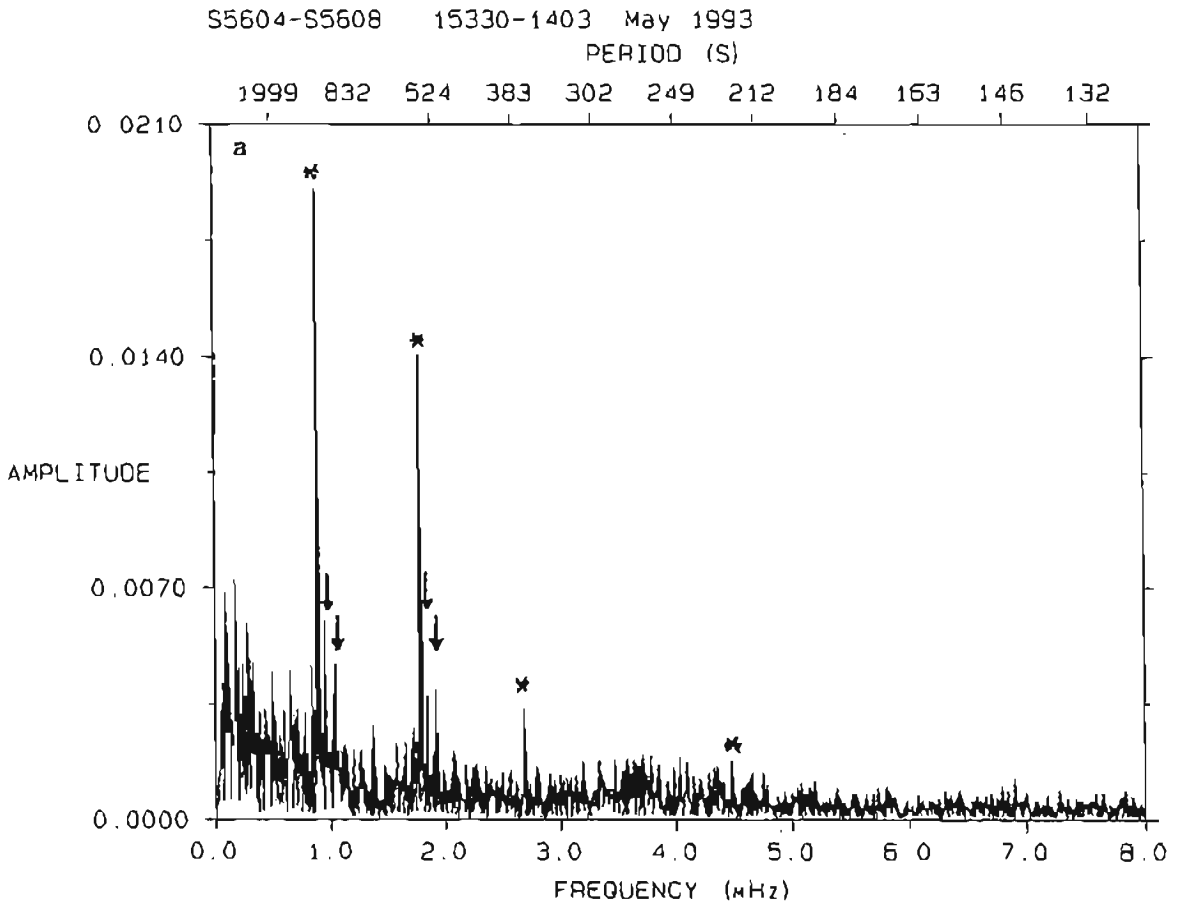

Figure 7.6: Fourier amplitude spectrum from O'Donoghue et al. (1994). The lower arrows indicate the 'satellite' peaks with a frequency difference of ~ 0.13 mHz from the main peaks; the upper arrows show the peaks separated from the harmonic peaks by ~ 0.05 mHz. The fundamental variation and the first, second and fourth harmonics are indicated by asterisks.

Figure 7.7 shows the amplitude spectrum for the May CBA runs up to the Nyquist frequency. The power at low frequencies may be due to differential extinction and other second order low-frequency trends that remain after the data are de-trended by subtracting a straight line. The main features are the fundamental variation and its first harmonic. The second harmonic is weakly present with an amplitude of about 0.003 mag. A broad peak consistent with the third harmonic also appears with an amplitude of ~ 0.002 mag. Unfortunately, because of the time resolution of the CBA data, the presence of the fourth harmonic (present at low amplitude in the Sutherland data) cannot be confirmed in the CBA observations.

Figure 7.8 shows close-ups of the regions surrounding the fundamental variation and the first harmonic. The values for the period, amplitude and time of first maximum of the fundamental in the May 1995 runs are listed in table 7.4; the results for the first harmonic are $P = 559.5 \pm 0.2$ s, $A = 0.014 \pm 0.001$ mag and $T_{max} = \mathrm{JD}_{\odot} 9861.65123 \pm 0.00008$. In both cases, the alias pattern matches the spectral window function fairly closely. The arrows in figure 7.8 indicate the approximate positions of the low-amplitude fine structure observed in figure 7.6. There is no obvious structure at the positions of the arrows on the high-frequency side of the fundamental, but there are two peaks on the high-frequency side of the first harmonic in the region of the second arrow that do not have counterparts on the low-frequency side, and are thus not part of the spectral window.

To check whether there is significant structure beneath the alias patterns of the harmonic peaks, the observations were pre-whitened by the fundamental and the first harmonic frequencies, and the amplitude spectra were re-calculated (see figure 7.9). The low-amplitude window pattern revealed near the position of the fundamental frequency is barely above the noise level and is probably not significant. Apart from a definite peak at the second of the two arrows for the first harmonic, there is no significant structure in the pre-whitened spectra. This tentative identification of a satellite peak for the first harmonic should be treated with caution, however, because the observed peak is barely above the noise level, and the *precise* frequencies of the satellite peaks in figure 7.6 are not known. Also, the amplitude of the peak at the second arrow is approximately 0.0020 mag, less than half the amplitude of the corresponding peak in figure 7.6, i.e. 0.042 mag (the vertical scale

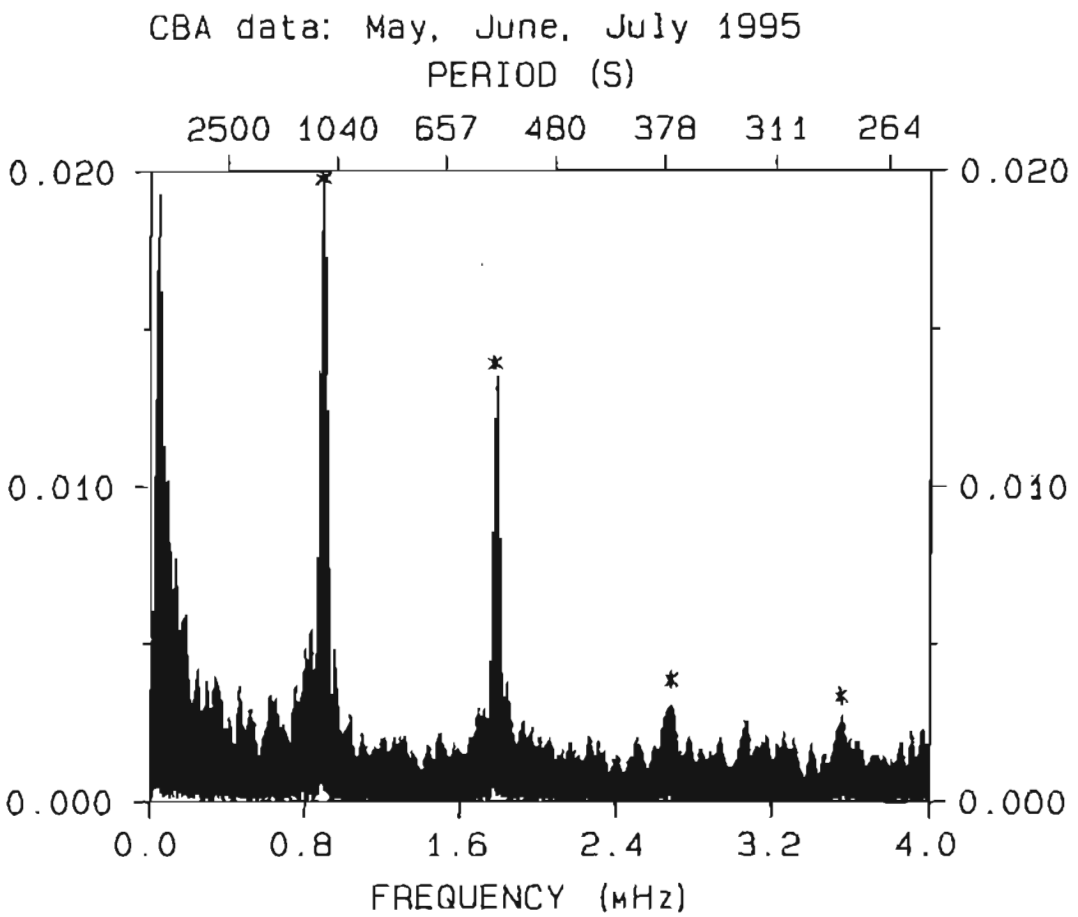

Figure 7.7: Fourier amplitude spectrum for the five CBA runs from May 1995 up to the Nyquist frequency. Apart from the low-frequency noise, the main features are the fundamental and the first harmonic; the second and third harmonics may also be present at low amplitude. The asterisks mark the positions of the fundamental and first three harmonics.

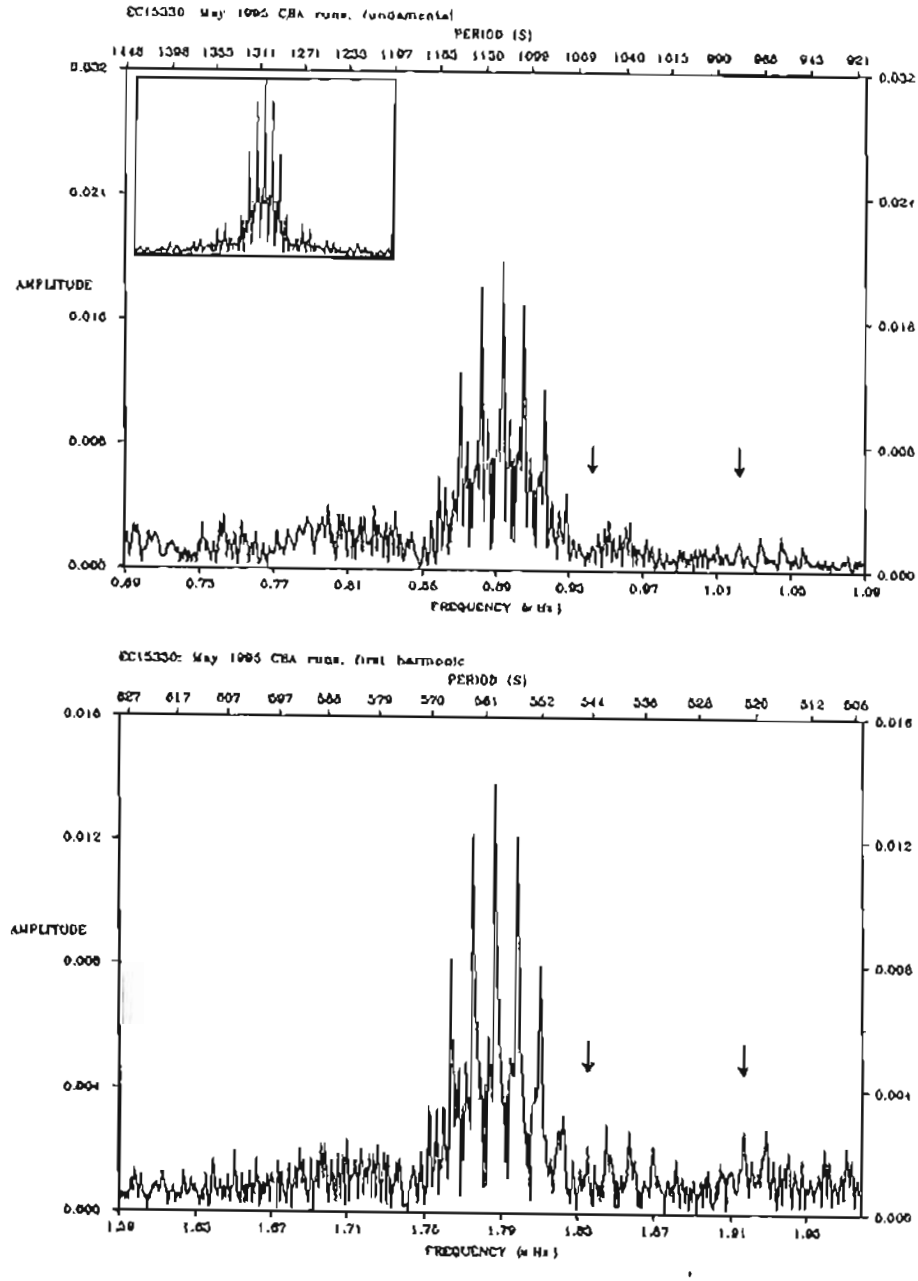

Figure 7.8: The fundamental and the first harmonic of figure 7.7 on a larger scale. The spectral window function is shown as an inset. The arrows mark the approximate positions of the satellite peaks seen in figure 7.6. The structure on the high-frequency side of the first harmonic at the position of the second arrow is not part of the spectral window.

in figure 7.6 is in units of fractional intensity).

The two remaining groups of runs (June/July 1995 and August 1995) were examined in the same way for evidence of fine structure and for signals underlying the fundamental and the first harmonic. No signals corresponding to the fine structure in figure 7.6 was observed.

7.4 Discussion

The fine structure present in figure 7.6 is not obvious in the 1995 observations, and although there is a peak consistent with the second of the two satellite peaks for the first harmonic, it occurs at a much lower amplitude than the peak in figure 7.6. O'Donoghue et al. (1994) point out that the low-amplitude peaks at $\sim 1.03\,\mathrm{mHz}$, $\sim 1.36\,\mathrm{mHz}$ and $\sim 1.91\,\mathrm{mHz}$ do not appear in their observations from February 1993. If the satellite peaks in figure 7.6 are the same phenomenon as seen in power spectra of AM CVn, the frequency splitting between the principal peak and the low-amplitude peak would represent the beat period between the orbital and a superhump period. There is a possibility of beating between an orbital period and a *negative* superhump, or between a positive and a negative superhump. If both superhumps are present in the star at the same time, and both have a train of harmonics, the splitting between the harmonic peaks of the positive and negative superhumps will increase with the harmonic index. This is not what is observed here: the splitting between the satellite peaks and the harmonic peaks appears to be a constant amount (although this will require verification, as the numbers quoted here were measured from a published spectrum). A constant frequency difference between harmonic peaks and satellite peaks would then be a similar phenomenon to the multiplet structure seen at the harmonic peaks of AM CVn, where the $20.77\,\mu\mathrm{Hz}$ splitting corresponds to the beat period between a normal superhump and the orbital period. If this is the case in EC 15330, the two pairs of satellite peaks give us candidate beat periods of 1.94 h and 4.27 h. According to the discussion in chapter 1 section 1.3.1, the beat period is proportional to $M_1 P_{orb}^{2.274}(\mathrm{h})$. If we assume that M_1 is the same in AM CVn and EC 15330 (there is no evidence that this should be the case, however), then EC 15330 should have

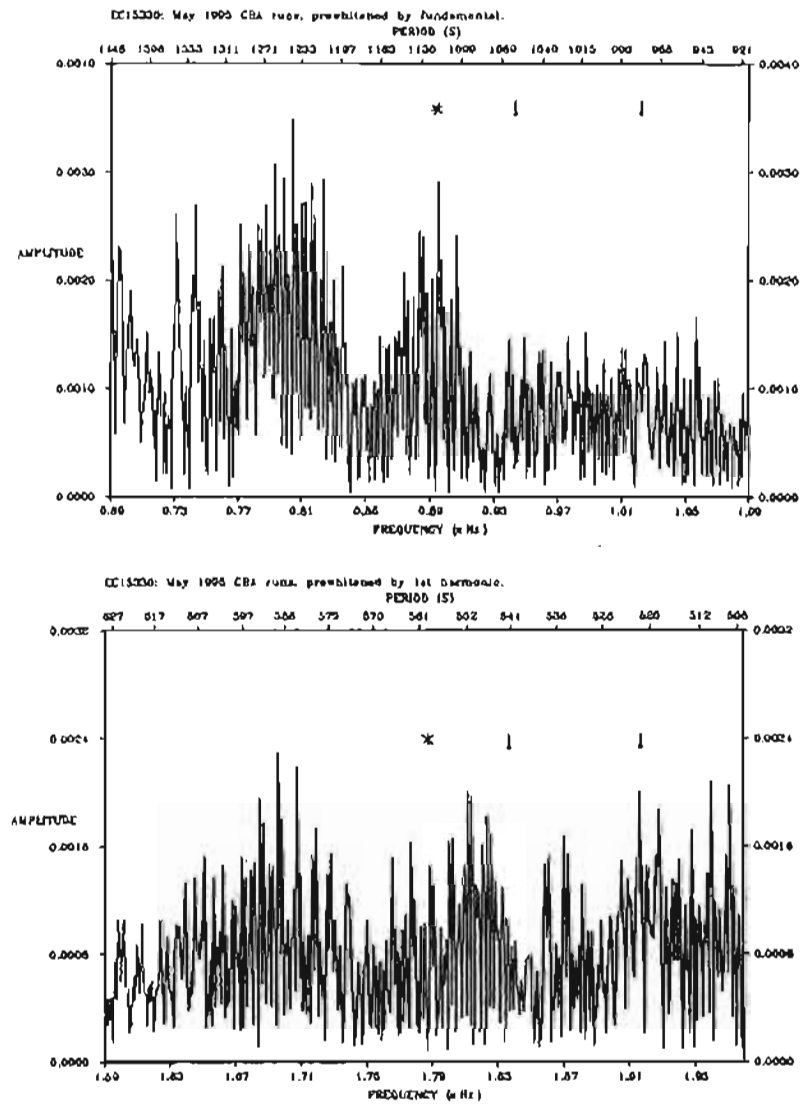

Figure 7.9: Amplitude spectra of the May 1995 CBA observations in the region of the fundamental (top) and first harmonic, pre-whitened by the harmonic peaks. The asterisks mark the positions of the (removed) fundamental and the first harmonic peaks. The arrows indicate the approximate positions of the satellite peaks in figure 7.6. Apart from a definite peak at the second of the two arrows for the first harmonic, there is no obvious structure corresponding to the peaks observed in figure 7.6.

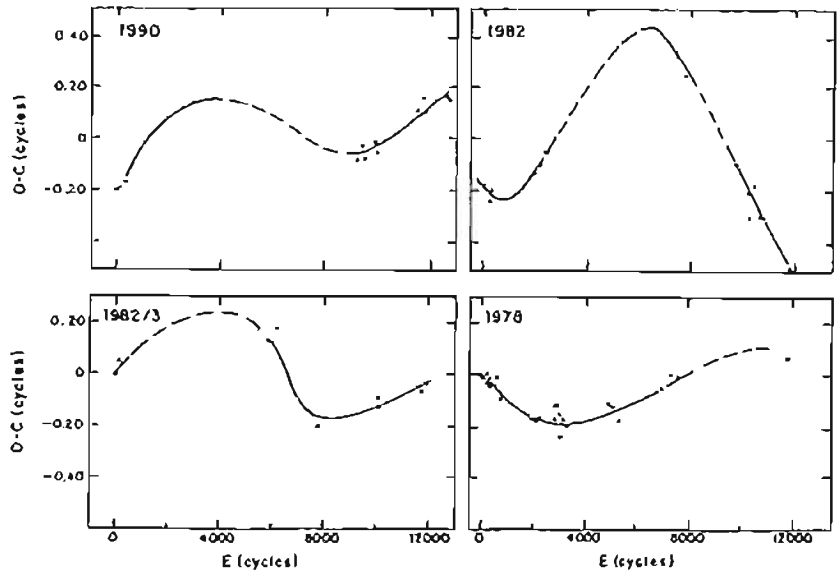

Figure 7.10: $O-C$ diagrams of AM CVn with respect to a mean period of 1051.2 s (from Patterson et al. 1993). The dashed lines indicate uncertain cycle count. The wanderings of O-C in EC 15330 during 1995 (figure 7.5) are similar to these changes, although the baseline of observation for EC 15330 is only 5 months.

a beat period of approximately 16 h. If the mass of the primary in EC 15330 is smaller than that of AM CVn, the predicted beat period would be less than this.

The results from O'Donoghue et al. (1994) and the CBA observations from early 1995 suggest that the changes in the 1119 s period are modest, with drifts of approximately 0.1 cycles over four months. Although there is no conclusive evidence that the discrepant point in figure 7.5 does not represent a period change in the star itself, there are several reasons for suspecting an artificial cause. The value of $O-C$ from A386 is over 5σ from the results for the other runs. In addition, the $O-C$ values from the preceding and following nights (runs A382 and A390) are virtually identical. It is unlikely that the photometric period in EC 15330, which until then had been fairly stable, would change so drastically on a time scale less than a day, and then return just as rapidly to its starting point. If we ignore the point from run A386, we see that the fundamental period of EC 15330 is definitely changing over the four month period; however, the changes are small enough to

allow an unambiguous cycle count during this time. The gentle changes are comparable to, but smaller than those observed in AM CVn. Figure 7.10 shows $O-C$ diagrams of AM CVn during four seasons of densely-spaced observation, with respect to the mean period of 1051.2 s (taken from Patterson et al. 1993). The principal period in AM CVn shows wanderings of ~ 0.4 cycles on a time scale of ~ 5 months. The period drifts observed in EC 15330, the many similarities to AM CVn, and the fact that EC 15330 is likely to have a small mass ratio (the radial velocity variations are not measurable), all strongly suggest that the 1119 s period is a superhump caused by periodic stressing of the outer edge of a non-circular accretion disc.

Chapter 8

Discussion

8.1 Summary

Superhumps are seen in a variety of CVs, including SU UMa dwarf novae in superoutburst, Z Cam dwarf novae, nova-likes and nova remnants, and intermediate polars. Superhumps are thought to be caused by accretion disc precession. Normal superhumps are caused by periodic enhancements of tidal dissipation in the outer regions of an eccentric, progradely precessing disc. Prograde disc precession is expected to be possible only for systems with mass ratios less than ~ 0.22 and for high rates of mass transfer through the disc ($\dot{M}_d \sim 3 \times 10^{-9}$–$1 \times 10^{-8}\,M_\odot y^{-1}$). Negative superhumps are thought to be caused by tilted discs with regressing nodes, although the precise mechanism that modulates the system brightness at the negative superhump period has not been identified.

The AM CVn stars form the end of a mass ratio sequence among CVs along which tidal effects become increasingly obvious. Spectroscopic and photometric similarities between the AM CVn stars and SU UMa stars in superoutburst suggest that the AM CVn stars possess precessing accretion discs, and that their photometric variations are consistent with a superhump interpretation. The one exception, GP Com, probably has too low a mass transfer rate to maintain a precessing eccentric disc.

Summarized below are the principal conclusions of this work.

1. Hydrogen-rich superhumpers

   - Nova-like variables and nova remnants with orbital periods below $\sim 2\,\mathrm{h}$ are good superhump candidates because they are likely to have both small mass ratios and high rates of mass transfer. Several nova remnants that have been put forward as superhump candidates (due to discrepancies between their spectroscopic and photometric or polarimetric periods) may, however, be desynchronised polars.
   - V442 Oph has a variable photometric period that is less than its spectroscopic period; the photometric period is probably a negative superhump. In general, the superhump shows power only at the fundamental frequency; however, in one run, the first and second harmonics of the superhump frequency were present.
   - Dwarf nova oscillations with periods around $\sim 25.5\,\mathrm{s}$ were detected in V442 Oph in observations from July 1995.
   - Spectra of TY PsA in superoutburst show line profile asymmetries that vary with a period that is consistent with the beat period between the superhump and the orbital period.

2. V803 Cen

   - The absorption lines in time-resolved spectra (from O'Donoghue & Kilkenny 1989) show variations in skewness which are consistent with accretion disc precession. However, a unique period could not be determined.
   - Radial velocity measurements reported in Westin (1980) vary with a period of $73 \pm 2\,\mathrm{h}$. If the principal period in the photometry, $1613.0 \pm 0.3\,\mathrm{s}$, is a (normal) superhump, the radial velocity period implies an orbital period of $1603.1 \pm 0.3\,\mathrm{s}$.
   - One of the more fascinating things about V803 Cen is the almost identical sequence of pulse shapes reported in O'Donoghue, Menzies & Hill (1987) and O'Donoghue & Kilkenny (1989). The combination of the harmonics (and any unresolved multiplet components) in the light curve creates a pattern that seems to drift first one way and then the other as one looks at mean light curves, night by night. Comparing the sequences of mean light curves from

1987 and 1988, the pulse shape evolution appears to be periodic with a period of about seven days. A more extensive data set is required to investigate this possibility.

- An amplitude spectrum in the region of the principal period shows an intricate web of closely-spaced periods. If the 1613.0 s period is removed from the data, the signal with the largest amplitude is at 1608.4 s: the alias pattern of this signal and that of the 1613.0 s period are not resolved. This implies that the values of both the 1613.0 s and the 1608.4 s signals are not properly determined. Because of the asymmetric shape of the alias pattern in the original power spectrum, it could be that the second strongest contributor of power is not 1608.6 s, but its one cycle per day alias at 1579.2 s.
- A signal with a period of 1603.4 ± 0.3 s is present with an amplitude of approximately one third of the principal 1613.0 s period. The period of this signal is consistent with the orbital period predicted by the radial velocity variation. This signal has the fourth largest amplitude in the region of 1613 s. The third largest amplitude signal has a period of 1588.0 s.
- The phase variation of the 1613.0 s period in the original photometry is similar to the phase variation of the principal period in synthetic data composed of a superposition of two sinusoids, one with the parameters of the 1613.0 s variation, and the other with the parameters of the 1608.4 s variation. We cannot choose between the 1608.6 s variation and its one cycle per day alias at 1579.2 s because the phase variation of the principal period in synthetic data using the parameters of the 1613.0 s and the 1579.2 s signals, is an equally good imitation of the phase variation in the original data. The beat period between 1613.0 s and 1608.6 s, however, corresponds to the period proposed for the pulse shape changes.
- If the second strongest contributor of power is 1579.2 s, we could speculate that this is a negative superhump, as its period is less than the orbital period. This leaves the 1588.0 s period unaccounted for.

3. GP Com

- The light curves of GP Com obtained over a baseline of five months are dom-

inated by flickering on a time scale of $\sim$ 15 – 20 min, superimposed on low-frequency variations with amplitudes of $\sim$ 0.05 mag.

- Amplitude spectra of individual runs show a broad power excess at low frequencies. The low-frequency variations are not consistent with a single period, and may be due to the windowing of the light curve, or due to differential extinction.
- Excess power appears in the region of the orbital frequency on several nights, with an amplitude and frequency that changes from night to night. On two nights, the power excess is quite pronounced. There is thus evidence of intermittent structure in the light curve that produces excess power on a time scale similar to that of the orbital period.

4. CP Eri

- The mean high state light curve is very similar to those of SU UMa stars in superoutburst. The high state amplitude spectrum shows a principal variation with a period of 1718 ± 2 s together with three harmonics. The detailed structure of the peaks in the amplitude spectrum suggests the presence of nearby low-amplitude signals.
- The low state amplitude spectrum shows a fundamental variation at 1721 ± 7 s together with one harmonic. The alias patterns of these signals are consistent with the spectral window function, suggesting that the low state modulation has a constant frequency, amplitude and phase during the two nights of low state observation.
- During the transition to a low state, the light curve develops secondary features displaced from the original maxima by $\sim$ 0.5 cycles, reminiscent of late superhumps seen in SU UMa stars. The light curve assumes a double-peaked shape with the dominant power in the first harmonic of the principal high state period.
- There is an inverse dependence between the amplitude (in magnitudes) of the principal variation and the overall magnitude of the star, although the *intensity* of the modulations decreases as the star fades to a low state.

- The superhump amplitude decreases more slowly than the background system light. This is in contrast to SU UMa stars, where the superhump amplitudes decay on a faster time scale than the system light.

5. **EC 15330-1403**

   - Amplitude spectra of data from May, June, July and August 1995 show a fundamental variation at $\sim 1119\,\mathrm{s}$ together with up to three harmonics.
   - One run obtained in August shows timings of pulse maxima which do not agree with timings from the other runs. It is unlikely that the apparent period change is intrinsic to the star, since the timings from nights immediately preceding and immediately following the discrepant run were consistent with the period obtained from the previous runs.
   - Apart from one discrepant run, the values of $O - C$ calculated with respect to an ephemeris for the pulse maxima show a scatter of $\sigma = 0.07$ cycles over the five month baseline. During this time, the gentle changes in the 1119 s period are sufficiently small to allow an unambiguous cycle count.
   - Amplitude spectra of the runs from May 1995 were searched for fine structure. Apart from a low-amplitude peak which was observed at a frequency similar to that of a peak seen in the amplitude spectrum from O'Donoghue et al. (1994), no obvious constant frequency splittings were observed.

8.2 Models and speculations

As yet, no model has been proposed to explain why the fine structure splitting in amplitude spectra of AM CVn is (a) precisely the inverse of the absorption line skewness period; (b) is a *constant* quantity and (c) most obvious on the *high-frequency* side of the harmonic peaks. The correspondence between the inverse of the fine structure splitting and the disc precession period is unlikely to be mere coincidence, and it is probable that the disc precession is somehow responsible for the asymmetrical multiplet structure.

The fact that the fine structure spacing is a constant quantity for different harmonics has caused some consternation. This is because in, for example, pulsating stars, fine structure

in an amplitude spectrum is often caused by closely-spaced oscillation modes. If each of these modes has a non-sinusoidal shape, the fundamental of each mode will be accompanied by a train of harmonics. For each mode, the amplitude spectrum will show peaks at twice, thrice etc. times the fundamental frequency. The splitting observed between the first harmonics of the various modes will thus be larger than the splitting observed between the fundamental frequencies. The splitting increases with harmonic number. This is not what is observed in AM CVn, and has led Marsh (1994) and Provencal et al. (1995) to declare that the constant $20.77\,\mu$Hz splitting is inconsistent with the hypothesis that the periodicities observed in AM CVn are harmonics of an unseen fundamental. There is nothing preventing the *principal peaks* in each multiplet from being harmonics, but the fine structure must arise in a different way.

We also require that the small multiplet peaks be more prominent on the high-frequency side of the local principal peak. This means that the frequency splitting cannot simply be due to amplitude modulation of the local principal signal, as this would yield two sidebands with equal amplitudes, one on each side of the principal peak. Is there a way in which one can obtain the constant frequency splitting seen in AM CVn which is consistent with what we know about the system, i.e. that it is a very compact binary with a bright disc?

8.2.1 The "Reflection" Model

A model that can explain many of the properties of the fine structure in the AM CVn amplitude spectrum has been proposed by Brian Warner (private communication). If the superhump light is emitted directly from the accretion disc and has a non-sinusoidal profile, we will observe a fundamental variation with a train of harmonics (the fundamental is missing from AM CVn). In addition, suppose that the secondary is reflecting some of the superhump light to us. If the secondary were fixed in the inertial frame, we would not notice the reflected light because the delay between the arrival of the disc light and the reflected light is too small. However, as the secondary moves in the binary orbit, its reflecting area (as seen by the observer) varies, both on the orbital period because only one half of the secondary is illuminated by the disc, and at twice the orbital period because

the secondary is Roche-lobe shaped and has the same reflecting area when it is side-on to the line of sight (this occurs twice per orbit). Hence, we should see the superhump harmonic train modulated both at P_{orb} and $\frac{1}{2}P_{orb}$.

If we write the superhump expressed as a sum of Fourier components (ignoring any phase information) as

$$A\cos(\omega_0 t) + B\cos(2\omega_0 t) + C\cos(3\omega_0 t) + D\cos(4\omega_0 t) + \ldots \tag{8.1}$$

(where ω_0 is the fundamental superhump frequency) we will see peaks in the amplitude spectrum at ω_0, $2\omega_0$, $3\omega_0$, ...We need to multiply the harmonic train by $\alpha\cos(\Omega t) + \beta\cos(2\Omega t)$, where Ω is the orbital frequency:

$$[\alpha\cos(\Omega t) + \beta\cos(2\Omega t)]\,[A\cos(\omega_0 t) + B\cos(2\omega_0 t) + C\cos(3\omega_0 t) + D\cos(4\omega_0 t)\ldots] \tag{8.2}$$

This gives a series of terms, each of which contains the product of two cosines. Applying the rule

$$\frac{1}{2}(\cos\theta + \cos\phi) = \cos\left(\frac{\theta+\phi}{2}\right)\cos\left(\frac{\theta-\phi}{2}\right) \tag{8.3}$$

yields a Fourier sum of the form

$$\begin{aligned}
&\frac{\alpha A}{2}[\cos(\Omega+\omega_0)t + \cos(\Omega-\omega_0)t] + \frac{\beta A}{2}[\cos(2\Omega+\omega_0)t + \cos(2\Omega-\omega_0)t] \\
&+\frac{\alpha B}{2}[\cos(\Omega+2\omega_0)t + \cos(\Omega-2\omega_0)t] + \frac{\beta B}{2}[\cos(2\Omega+2\omega_0)t + \cos(2\Omega-2\omega_0)t] \\
&+\frac{\alpha C}{2}[\cos(\Omega+3\omega_0)t + \cos(\Omega-3\omega_0)t] + \frac{\beta C}{2}[\cos(2\Omega+3\omega_0)t + \cos(2\Omega-3\omega_0)t]\ldots
\end{aligned} \tag{8.4}$$

so we expect peaks in the amplitude spectrum at

$$\begin{array}{llll} \Omega+\omega_0, & \Omega-\omega_0, & 2\Omega+\omega_0, & 2\Omega-\omega_0 \\ \Omega+2\omega_0, & \Omega-2\omega_0, & 2\Omega+2\omega_0, & 2\Omega-2\omega_0 \\ \Omega+3\omega_0, & \Omega-3\omega_0, & 2\Omega+3\omega_0, & 2\Omega-3\omega_0, \ldots \end{array}$$

and so on. The $\Omega+\omega_0$ and $\Omega-\omega_0$ components will have the same amplitude, as will the $2\Omega+\omega_0$ and $2\Omega-\omega_0$ components, etc. It can be seen that the peaks that will have the same power are not in the same part of the amplitude spectrum. The fine structure at a particular frequency does not come from modulations of the local principal frequency but comes from beats between modulations in *other parts of the spectrum*. For example, the combinations $(\Omega+2\omega_0)$ and $(\Omega-2\omega_0)$ of the orbital frequency and the first superhump harmonic in AM CVn, give components at 347.9 s and 1074.6 s. These two components will have similar amplitudes, and not the components on either side of the 350.4 s second harmonic. If the noise is different in the region of 347.9 s and 1074.6 s, the amplitudes of the two components will differ. In general, because of the way the fine structure peaks are formed in the various combinations of frequencies, it is not unlikely that they have detectable amplitudes only on the high-frequency side of the harmonic peaks. This will happen if only the first few combinations of the harmonics with P_{orb} and $\frac{1}{2}P_{orb}$ appear.

This model can be used to explain the absence of low-amplitude structure at the fundamental and the first harmonic in the low state amplitude spectrum of CP Eri. In the high state, the disc is sufficiently large and massive to produce superhump light which is reflected by the secondary, producing fine structure that appears in the amplitude spectrum as closely-spaced modes near the superhump fundamental and its harmonics. In the low state, although the system light is still dominated by disc emission, it may be that the disc radius is smaller than the tidal resonance radius r_{32} and superhumps are not produced. All we see, therefore, is a brightness modulation at the orbital period and at half the orbital period (i.e. the factor in the second set of square brackets in equation 8.2 disappears). Low state amplitude spectra of CR Boo, too, show only a fundamental and one harmonic peak: both of these periodicities maintain a constant phase, amplitude and frequency on a time scale of weeks. In the low state of V803 Cen, the photometric variations are at a very reduced amplitude, although a signal near 1611 s was detected in combinations of runs (O'Donoghue et al. 1990). We know that V803 Cen is at a lower inclination than AM CVn and CR Boo (O'Donoghue & Kilkenny 1989), so this may account for the differences.

We would expect fine structure in the amplitude spectra of SU UMa stars in superoutburst, since it is likely that the secondary reflects the superhump light to us in the way described above for the AM CVn stars. There is evidence that such a reflection effect operates during superoutbursts: during the first 12 d of the 1978 superoutburst of WZ Sge, for instance, a prominent orbital hump was visible, and Smak (1993) shows that this can be adequately understood as arising from the irradiated surface of the secondary. However, the intensity of the reflection in the AM CVn stars should be higher than in the SU UMa systems because the secondary is so very close to the disc. There are no very long high speed photometry runs available for SU UMa stars in superoutburst, and the superhump period drifts quite rapidly during superoutburst. In addition, the orbital periods of the SU UMa stars are much longer than those of the AM CVn stars, and it might be difficult to detect the very low-amplitude signals that we can see in AM CVn, where there are more superhump cycles per night.

The hydrogen-rich permanent superhumpers (such as BK Lyn) appear to be in an equilibrium state that is not attained by the SU UMa stars during their short-lived superoutbursts. The pulse shapes of the permanent superhumpers are usually more simple than those of a superoutbursting SU UMa star (although V442 Oph has shown intermittent harmonic structure). Now, the AM CVn stars, which are also supposedly in an equilibrium state (AM CVn and EC 15330 all the time, and CR Boo, V803 Cen and CP Eri during their high states), show complex pulse shapes that are very similar to those of the SU UMa stars. Why is this? Some differences between the hydrogen-rich permanent superhumpers and the AM CVn stars are expected because of the smaller discs and hence the greater energetics of the bright spot in AM CVn stars. In AM CVn itself, the double-humped light curve may be due to an equally bright superhump light source and a *late* superhump, caused by modulations in the bright spot emission, or variable disc overflow.

8.3 Future work

Whole Earth Telescope observations are the best tool to use to unravel the complex photometric behaviour of the AM CVn stars. Frequency splitting from the harmonic peaks has only been observed clearly in AM CVn itself, and it is not yet certain whether the other stars show multiplet structure in their amplitude spectra. WET observations of CR Boo and V803 Cen are difficult to analyse and interpret because of the different photometric behaviour in the high and low states. EC 15330 may be a good target, as it is the system most like AM CVn itself. In addition, WET observations of SU UMa stars in superoutburst would reveal whether they, too, show fine structure in their amplitude spectra. Because the disc precession period of most SU UMa stars is $\sim 2.2\,\mathrm{d}$, multi-longitude observations are necessary to give good coverage of the beat cycle. With the recent discovery of systems such as V1159 Ori and RZ LMi, which show very frequent superoutbursts, Whole Earth Telescope coverage of superoutbursts has become more feasible.

There is a distinct lack of long-term light curves for the large-amplitude AM CVn stars. Unfortunately, the stars with the least coverage are (as is usually the case) the fainter stars: even in its high state, CP Eri (at $V \approx 16.7$) is far beyond the range of most amateur astronomers. From the sparse data that are available, it appears that the behaviour of V803 Cen is more erratic than CR Boo (O'Donoghue & Kilkenny 1989). It could be that, as an AM CVn star evolves towards longer orbital periods, the system spends increasingly less time in the high state. Unfortunately we have neither the theoretical models (of irradiation-modulated mass transfer in helium-rich systems) nor the observational data to test this hypothesis. It might be worth examining plate archives to see whether GP Com has undergone an outburst in the past: if it is the helium-rich analogue of SU UMa stars such as WZ Sge, it is expected to show outbursts with a recurrence time of decades.

Spectroscopic campaigns similar to that of Patterson, Halpern & Shambrook (1993) should be carried out for the remaining absorption-line AM CVn stars to search for evidence of disc precession. EC 15330 is the obvious target, as it is most similar to AM CVn, and the parallels between it and AM CVn should be more numerous than for the other stars. An attempt by O'Donoghue et al. (1994) to search for line profile asymmetries in EC 15330

failed because of the weakness of the lines. Time-resolved spectroscopy of the system should be obtained when the lines are stronger; however, there is no way we have of predicting *when* the lines will be stronger. CR Boo in the high state, with line widths and depths and variable profiles like those of AM CVn, would be a good target.

Does every system that displays superhumps, display line profile asymmetries varying on the beat period between the superhump and orbital period? This is an open problem. Patterson, Halpern & Shambrook (1993) suggest that all absorption line superhumpers will show line profile asymmetry and/or γ-velocity variations on the beat period between the superhump and the orbital period. What of the emission line systems? Some stars may only show emission lines when the disc radius is less than r_{32} (this is the case for many SU UMa stars in quiescence). Other emission line systems, such as V603 Aql, show permanent (normal) superhumps: there should be a spectroscopic signature of the precessing disc (assuming the lines are Doppler-broadened in the accretion disc). It could be that the V/R ratio is variable in the line *core*, where motion in the outer accretion disc should be most obvious.

Because of the extreme mass ratios in AM CVn stars, the radial velocity variations of lines from the primary are very small. However, any spectral feature originating in the *secondary* would have a huge radial velocity with an amplitude of $\sim 500 \sin i \,\mathrm{km\,s^{-1}}$ or more over the binary orbit. If such a feature could be identified in low state spectra of CR Boo, V803 Cen or CP Eri, the orbital period of the system would be easy to determine.

References

Abbott T.C., Robinson E.L., Hill G.J., Haswell C.A., 1992, ApJ, 399, 680

Arp H., 1994, A&A, 288, 738

Bailey J.A., 1981, MNRAS, 197, 31

Barrett P.E., O'Donoghue D., Warner B., 1988, MNRAS, 233, 759

Becker R.H., 1981, ApJ., 251, 626

Berriman G., 1984, MNRAS, 210, 223

Berriman G., Beattie D.H., Gatley I., Lee T.J., Mochnacki S.W., Szkody P., 1983, MNRAS, 204, 1105

Beuerman K., Thomas H.-C., 1993, Adv. Sp. Res., 13 115

Bianchini A., Friedjung M., Sabbadin F., 1985, IBVS no. 2650

Brocklehurst M., 1972, MNRAS, 157, 211

Bruch A., 1982, PASP, 94, 916

Buckley D.A.H., Remillard R., Tuhoy I., Warner B., Sullivan D.J., 1993, MNRAS, 265, 926

Burbidge E.M., Strittmatter P.A., 1971, ApJ, 170, L39

Burbidge G., Burbidge M., Hoyle F., 1967, ApJ, 147, 1219

Cannizzo J.K., 1993, in Wheeler J.C., ed., Accretion Discs in Compact Stellar Systems,

World Sci. Publ. Co., Singapore, p.6

Chanmugam G., 1987, A & SS, 130, 53

Cowley A.P., Crampton D., Hutchings J.B., Marlborough J.M., 1975, ApJ, 195, 413

Crawford J.A., Kraft R.P., 1956, ApJ, 123, 44

Cropper M., 1986, MNRAS, 222, 225

Cropper M., Mukai K., Mason K.O., Smale A.P., Charles P.A., Mittaz J.P.D., Machin G., Hassall B.J.M., Callanan P.J., Naylor T., van Paradijs J., 1990, MNRAS, 245, 760

Dhillon V.S., Marsh T.R., 1995, MNRAS, 275, 89

Diaz M.P., Steiner J.E., 1989, ApJ, 339, L41

Downes R.A., Shara M.M., 1993, PASP, 105, 127

Eggen O.J., Greenstein J.L., 1965, ApJ, 141, 83

Eggleton P.P., 1983, ApJ, 268, 368

Elvius A., 1975, A&A, 44, 117

Elvius A., Hall J.S., 1964, Lowell Obs. Bull., 6, 123

Faulkner J., Flannery B.P., Warner B., 1972, ApJ, 175, L79

Frank J., King A.R., Raine D.J., 1985, Accretion Power in Astrophysics, Cambridge University Press.
refitem Gallagher J.S., Code A.D, 1974, ApJ, 189, 303

Giclas H.L., Burnham R., Thomas N.G., 1961, Lowell Obs. Bull. no. 112, 61

Green R.F, Schmidt M., Liebert J., 1986, ApJS, 61, 305

Greenstein J.L., Matthews M.S., 1957, ApJ, 126, 14

Haefner R., Schoembs R., Vogt N., 1979, A&A, 77, 7

Harrop-Allin M.K., Warner B., 1996, 279, 219

Harvey D., Skillman D.R., Patterson J., Ringwald F.A., 1995, PASP, 107, 551

Hellier C., 1993, MNRAS, 264, 132

Hellier C., Mason K.M., Mittaz J.P.D., 1991, MNRAS, 248, 5P

Hertzog K.P., 1986, Observatory, 106, 38

Hessman F.V., Hopp U., 1990, A&A, 228, 387

Hessman F.V., Mantel K.H., Barwig H., Schoembs R., 1992, A&A, 263, 147

Hirose M., Osaki Y., 1990, PASJ, 42, 135

Hirose M., Osaki Y., 1993, PASJ, 45, 595

Honeycutt R.K., Schlegel E.M., Kaitchuck R.H., 1987, ApJS, 65, 451

Horne K., 1985a, MNRAS, 213, 129

Horne K., 1985b, Interacting Binaries, ed Eggleton P.P., Pringle J.P., Reidel, Dordrecht, p327

Horne K., Wood J.H., Stiening R.F., 1991, ApJ378, 271

Howarth I.D., Murray J., Mills D., Berry D.S., 1995, DIPSO: A friendly spectrum analysis program, Starlink User Note 50, Rutherford Appleton Laboratory

Howell S.B., Szkody P., Kreidl T.J., Dobrzycka D., 1991, PASP, 103, 300

Howell S.B., Reyes A.R., Ashley R., Harrop-Allin M.K., Warner B., *Photometric superoutburst observations of the short period dwarf nova TV Corvi*, submitted to MNRAS

Howell S.B., Szkody P., Cannizzo J.K., 1995, ApJ, 439, 337

Humason M.L., Zwicky F., 1947, ApJ, 105, 85

Iben I., Tutukov A.V., 1991, ApJ, 370, 615

Iping R.C., Petterson J.A., 1990, A&A, 239, 221

Joy A.H., 1954a, PASP, 66, 5

Joy A.H., 1954b, ApJ, 120, 377

Kepler S.O., 1987, IAU Circ. no. 4332

Kepler S.O., Steiner J.E., Jablonski F., 1989, IAU Symp. no. 114, p.443

Kholopov P.N., 1985, GCVS, 4th ed., Astr. Council of Acad. Sci., USSR, Moscow

Kopal Z., 1959, Close Binary Systems, Chapman & Hall, London.

Kraft R.P., 1962, ApJ, 135, 408

Kraft R.P., 1964, ApJ, 139, 457

Krzeminski W., 1972, Acta Astr., 22, 387

Krzeminski W., Kraft R.P., 1964, ApJ, 140, 921

la Dous C., 1991, A & A, 252, 100

Lambert D.L., Slovak M.H., 1981, PASP, 93, 477

Lemm K., Patterson J., Thomas G., Skillman D.R., 1993, PASP, 105, 1120

Linnell A.P., 1949, Sky & Tel., 8, 166

Livio M., Shankar A., Truran J.W., 1988, ApJ, 330, 264

Livio M., Pringle J.E., 1994, ApJ, 427, 956

Lubow S.H., 1989, Ap J, 340, 1064

Lubow S.H., 1994, ApJ, 432, 224

Luyten W.J., Haro G., 1959, PASP, 71, 469

Malmquist K.G., 1936, Stockholm Ann., 12, pt. 7

Mantel K.H., Barwig H., Haefner R., Schoembs R., 1987, A&SS, 131, 501

Marsh T.R., 1988, MNRAS, 231, 1117

Marsh T.R., 1994, Newsletter on analysis of astronomical spectra, no.21, p.45

Marsh T.R., Horne K., Rosen S., 1991, ApJ, 366, 535

Marsh T.R., Wood J.H., Horne K., Lambert D., 1995, MNRAS, 274, 452

Meintjies P.J., Raubenheimer B.C., de Jager O.C., Brink C., Nel H.I., North A.R., van Urk G., Visser B., 1992, ApJ, 401, 325

Moehler S., Richtler T., de Boer K.S., Dettmar R.J., Heber U., 1990, A&AS, 86, 53

Molnar L.A., Kobulnicky H.A., 1992, ApJ, 392, 678

Murray J.R., 1996, *SPH simulations of tidally unstable accretion discs in cataclysmic variables*, submitted to MNRAS

NASA Science Data Systems Standards Office, 1990, Flexible Image Transport System (FITS)

Nather R.E., 1989, in Wegner G., ed, White Dwarfs, IAU Colloq. no. 114, p.109

Nather R.E., Warner B., 1971, MNRAS, 152, 209

Nather R.E., Robinson E.L., Stover R.J., 1981, ApJ, 244, 269

Naylor T., Charles P.A., Hassall B.J.M., Bath G.T., Berriman G., Warner B., Bailey J., Reinsch K., 1987, MNRAS, 229, 183

O'Donoghue D., 1990, MNRAS, 246, 29

O'Donoghue D., 1993, Baltic Astron., 2, 459

O'Donoghue D., Menzies J.W., Hill P.W., 1987, MNRAS, 227, 347

O'Donoghue D., Kilkenny D., 1989, MNRAS, 236, 319

O'Donoghue D., Warner B., Wargau W., Grauer A.D., 1989, MNRAS, 240, 41

O'Donoghue D., Wargau W., Warner B., Kilkenny D., Martinez P., Kanaan A., Kepler S.O., Henry G., Winget D.E., Clemens J.C., Grauer A.D., 1990, MNRAS, 245, 140

O'Donoghue D., Kilkenny D., Chen A.L., Stobie R.S., Koen C., Warner B., Lawson W.A., 1994, MNRAS, 271, 910

Osaki Y., 1985, A&A 144, 369

Osaki Y., 1989, PASJ, 41, 1005

Paczynski B., 1971, Ann. Rev. Astr. Astrophys., 9, 183

Patterson J., 1979, ApJ, 231, 789

Patterson J., 1995, PASP, 107, 657

Patterson J., Skillman D.R., 1994, PASP, 106, 1141

Patterson J., Nather R.E., Robinson E.L., Handler F., 1979, ApJ, 232, 819

Patterson J., Halpern J., Shambrook A., 1993, ApJ, 419, 803

Patterson J., Jablonski F., Koen C., O'Donoghue D., Skillman D.R., 1995, PASP, 107, 1183

Patterson J., Raymond J.C., 1985, ApJ, 292, 535

Patterson J., Sterner E., Halpern J.P., Raymond J.C., 1992, ApJ, 384, 234

Patterson J., Thomas G., Skillman D.R., Diaz M., 1993, ApJSS, 86, 235

Pollacco D.L., Bell S.A., 1994, MNRAS, 267, 452

Provencal J.L., 1994, Ph.D. thesis, University of Texas at Austin

Provencal J.L. et al., 1991, in Vauclair, G.& Sion, E., eds., White Dwarfs, Kluwer, Dordrecht, p.449

Provencal J.L., Winget D.E., Nather R.E., Robinson E.L., Solheim J.E., Clemens J.C., Bradley P.A., Kleinmann S.J., Kanaan A., Claver C.F., Hansen C.J, Marar T.M.K., Seetha S., Ashoka B.N., Leibowitz E.M., Meistas E.G., Bruvold A., Vauclair G., Dolez N., Chevreton M., Barstow M.A., Sansom A.E., Tweedy R.W., Fontaine G., Bergeron P., Kepler S.O., Wood M.A., Grauer A.D., 1995, Ap.J., 445, 927

Povenda A., Allen C., Parrao L., 1982, ApJ, 258, 589

Ramseyer T.F., 1994, ApJ, 425, 243

Rappaport, S., Joss P.C., Verbunt F., 1983, ApJ, 275, 713

Ringwald F.A., Thorstensen J.R., Honeycutt R.K., Robertson J.W., 1996, MNRAS, 278, 125

Robinson E.L., Faulkner J., 1975, ApJ, 200, L33

Rutten R.G.M., Dhillon V.S., Horne K., Kulkers E., van Paradjis J., 1993, Nature, 362, 518

Sahade J., Wood F.B., 1978, Interacting Binary Stars, Pergamon Press, Oxford

Savonije G.J., de Kool M., van den Heuvel E.P.J., 1986 A & A, 155, 51

Schaefer B.E., Landolt A.U., Vogt N., Buckley D.A.H., Warner B., Walker A.R., Bond H.E., 1992, ApJS, 81, 321

Schechter P.L., Mateo M., Saha A., 1993, PASP, 105, 1342

Schlegel E.M., Barrett P.E., de Jager O.C., Chanmugam G., Hunter S., Mattox J., 1995, ApJ, 439, 322

Schoembs R., 1982, A&A, 115, 190

Schoembs R., 1986, A&A, 158, 233

Schoembs R., Vogt N., 1980, A&A, 91, 25

Shafter A.W., Robinson E.L., Crampton D., Warner B., Prestage R.M., 1990, ApJ, 354, 708

Skillman D.R., Patterson J., 1993, ApJ, 417, 298

Skillman D.R., Patterson J., Thorstensen J.R., 1995, PASP, 107, 545

Smak J., 1967, Acta Astr., 17, 255

Smak J., 1975, Acta Astr., 25, 227

Smak J., 1982, Acta Astr., 32, 213

Smak J., 1983, Acta Astr., 33, 333

Smak J., 1993, Acta Astr., 43, 121

Solheim J.E., Emanuelsen P.I., Vauclair G., Dolez N., Chevreton M., Barstow M., Sansom A.E., Tweedy R.W., Kepler S.O., Kanaan A., Fontaine G., Bergeron P., Grauer A.D., Provencal J.L., Winget D.E., Nather R.E., Bradley P.A., Claver C.E., Clemens J.C., Kleinman S.J., Hine B.P., Marar T.M.K., Seetha S., Ashoka B.N., Leibowitz E.M., Mazeh T., 1991, White Dwarfs, ed. Vauclair G., Sion E., Kluwer, Dordrecht, p.431

Sterken C., Manfroid J., 1992, Astronomical Photometry – A Guide, Kluwer Academic, Dordrecht

Stobie R.S., Chen A., O'Donoghue D., Kilkenny D., 1992, Variable Stars and Galaxies, ed Warner B., ASP Conf 30, 87

Stockman H.S., Schmidt G.D., Lamb D.Q., 1988, ApJ, 332, 282

Stover R.J., 1983, PASP, 95, 18

Szkody P., Shafter A.W., 1983, PASP, 95, 509

Szkody P., Wade R.A., 1980, PASP, 92, 806

Szkody P., Howell S.B., Mateo M., Kreidl T.J.N., 1989, PASP, 101, 899

Thorstensen J.R., Ringwald F.A., Wade R.A., Schmidt G.D., Norsworthy J.E., 1991, AJ, 102, 272

Tuohy I.R., Remillard R.A., Bradt H.V., Brissenden R.J.V., 1990, ApJ, 359, 204

Tutukov A., Yungelson L., 1995, *Double-degenerate semidetatched binaries with helium secondaries*, submitted to MNRAS

Udalski, A., 1988, Acta Astr., 38, 315

Udalski A., 1990, AJ, 100, 226

Ulla A.M., Solheim J.E., 1991, in Vauclair G., Sion E., eds, White Dwarfs, Kluwer, Dordrecht, p.441

Ulla A.M., 1994, Space Sci. Rev., 67, 241

Ulla A.M., 1995, A&A, 301, 469

van Amerongen S., Bovenschen H., van Paradijs J., 1987, MNRAS, 229, 245

van der Woerd H., van Paradijs J., 1987, MNRAS, 224, 271

van der Woerd H., van der Klis M., van Paradijs J., Beuermann K., Motch C., 1988, ApJ, 330, 911

Verbunt F., Rappaport S., 1988, ApJ, 332, 193

Visvanathan N., Wickramasinghe D.T., 1979, Nature, 281, 47

Vogt N., 1974, A&A, 36, 369

Vogt N., 1982, ApJ, 252, 653

Vogt N., 1983, A&A, 118, 95

Vogt N., Barrera L.H., Barwig H., Mantel K.H., 1990, in Mauche C.W., ed., Accretion-powered compact binaries, Cambridge University Press, Cambridge, 391

Walker M.F., 1954, PASP, 66, 230

Wampler E.J., 1967, ApJ, 149, L101

Warner B., 1971, PASP, 83, 817

Warner B., 1972, MNRAS, 159, 315

Warner B., 1975, MNRAS, 170, 219

Warner B., 1985, MNRAS, 217, 1P

Warner B., 1995a, Cataclysmic Variable Stars, Cambridge University Press, Cambridge

Warner B., 1995b, A & SS, 225, 249

Warner B., 1995c, A & SS, 226, 187

Warner B., 1995d, A & SS, 230, 83

Warner B., Robinson E.L., 1972, Nature. Phys. Sci., 239, 2

Warner B., Brickhill A.J., 1978, MNRAS, 182, 777

Warner B., Cropper M.S., 1984, MNRAS, 206, 261

Warner B., O'Donoghue D., 1988, MNRAS, 233, 705

Warner B., O'Donoghue D., Wargau W., 1989, MNRAS, 238, 73

Westin B.A.M., 1980, A&A, 81, 74

Whitehurst R., 1988, MNRAS, 232, 35

Whitehurst R., 1994, MNRAS, 266, 35

Whitehurst R., King A., 1991, MNRAS, 249, 25

Williams G.A., 1983, ApJS, 53, 523

Winget D.E., 1988, in eds. Christensen-Dalsgaard J., Frandsen S., Advances in helio- and asteroseismology, Dordrecht, p. 305

Winget D.E., Robinson E.L., Nather R.E., Fontaine G., 1982, ApJ, 262, L11

Wood J.H., Horne K., Berriman G., Wade R.A., O'Donoghue D., Warner B., 1986, MNRAS, 219, 629

Wood J.H., Horne K., Berriman G., Wade R.A., 1989, ApJ, 341, 974

Wood M.A., Winget D.E., Nather R.E., Hessman F.V., Liebert J., Kurtz D.W., Wesemael F., Wegner G., 1987, ApJ, 313, 757

Wu K., Wickramasinghe D.T., Warner B., 1995, PASA, 12, 60

Acknowledgements

Many people are to be thanked for providing me with the incentive to complete this dissertation. I would like to thank my supervisor Professor Brian Warner for introducing me to cataclysmic variables and for sharing his encyclopaedic knowledge on all subjects from fossil-collecting to classical music and back again. I am also grateful to Brian Warner for writing *Cataclysmic Variables*, aka. The Grand Repository of All Higher Knowledge, which is referenced 48 times in this dissertation. My sincere thanks go also to Darragh O'Donoghue, for allowing me to use his time-series analysis program EAGLE, for all the assistance and instruction in using said program, and for answering my questions even at the busiest of times. Thanks go to Darragh, too, for the Wright CCD camera, a marvellous instrument without which this dissertation would not have been possible.

I acknowledge the financial support of a UCT Research Associateship and an FRD Masters Scholarship during this period of study.

A big thank you to David Buckley for obtaining those crucial last two runs of CP Eri in August when the star was FINALLY in a high state and I had come to the end of my observing week. Thanks also go to Dave Kilkenny and Fred Marang for observing the HD stars that were used as standards for GP Com, V442 Oph and CP Eri. In the Astronomy department at UCT, thanks go to Penny Dobbie for her unremitting optimism and for typing my numerous application forms; to Patrick and Yuri for the lunches at the UCT Club and the cans of coke, and Richard Ashley for reminding me to appreciate what I have.

My thanks also go to Professor Keith Horne for allowing me to use to use the facilities in the Department of Physics and Astronomy during my "sabbatical" at the University of

St. Andrews during January and February 1995.

The final chapters of the dissertation were written at Mullard Space Science Laboratory: my thanks go to my Ph.D. supervisor Mark Cropper for his encouragement and for allowing me to work on my Masters writeup as opposed to my Ph.D! Thanks are also due to Encarni, Kerry, Mat, Lee and Steve for their humour and support, and for not killing me for persistently hogging the nice p.c. in the student office.

To Chris: without your love and encouragement, much more than just this dissertation would have been impossible.

I am eternally grateful to my parents for their continuing enthusiasm, support, encouragement and financial help through what has been a rather complicated and difficult time.